Pharmacology & Regulation of Slo2 and Slo3 Potassium Channels

David Charles Wrighton

Submitted in accordance with the requirements for the degree of Doctor of Philosophy

The University of Leeds
Institute of Membrane and Systems Biology

September 2011

The Candidate confirms that the work submitted is their own and that appropriate credit has been given where reference has been made to the work of others

TO
HOLDEN CAULFIELD
(Catcher in the Rye)
On the grounds that
had he read Comic
Books,
he might have had a
happier youth.

Charles Francis Wrighton
(1948-1990)

Acknowledgements

Firstly, I'd like to thank my supervisor Dr. Jon Lippiat for his support over the past four years of my PhD. I'd also like to thank Jon for the encouragement and assistance to follow my own research path. Had it not been for the freedom of study that Jon allowed to me, this body of work would be vastly different.

I'd like to thank Dr. Chris Cockcroft for his years of support and guidance with various techniques and for his comments and help in the writing of this thesis in particular curbing the occasional excesses and lapses of archaism and colloquialism. I'd also like to thank Matt McArdle for his help proofreading various chapters.

Thanks must of course go to Tim Munsey, not only because without him the ion channel labs would grind to a halt, but also for his help with the oocyte work. I also have to thank Tim for reigniting my interest in photography, which has led to many varied discussions and provided me with innumerate distractions from my lab work.

I must also thank the other PhD students that have provided solace and encouragement at lunch and in the pub throughout the four years in Leeds, (in no particular order); Amy Taylor, Nicola Clarke, Rebecca Caygill, Martin Fisher, Paul Bowles, Mandeep Dhillon, Miriam Walden, Steve Parsons, Yasser Majeed, Gareth Rosbrook and Georgina Cox.

I'd also like to thank my girlfriend Louise Daniels, without her love and support I doubt if this body of work would ever have been completed and for putting up with me throughout the PhD process. Lastly I'd like to thank my mum and step dad for their continuous support through the eight long years of university.

Abstract

Large-conductance-Ca^{2+}-activated potassium Slo1 channels are well characterised members of the Slo channel family. The other members, Slo3 and Slo2.χ, are less characterised and their physiological roles are elusive. Little is known of the pH-sensitive Slo3 channel, aside from a role regulating Ca^{2+} influx through CatSper channels during capacitation in spermatozoa. This thesis aims to investigate mSlo3 pharmacology and determine if mSlo3-EST's encode novel isoforms. Na^{+}-activated Slo2.χ channels (Slo2.1/Slo2.2) are thought to mediate adaptation of neuronal action potential firing rate and slow afterhyperpolarisations following repetitive firing. We aim to characterise hSlo2.2a currents and their bithionol sensitivity, an activator of a rat isoform.

Mutation of the conserved phenylalanine in the S6-domain (mSlo3-F304/hSlo1-F380) to tyrosine has similar effects on Slo channels, namely a negative shift in the voltage-dependence of activation and an increase in membrane conductance. mSlo3 pharmacology matches the I_{KSper} profile and suggests roles for mSlo3 as a pharmacological target in infertility treatment. This work identified a novel splice-variant of mSlo3; CV562866 lacks transmembrane domains and is more widely expressed than mSlo3. CV562866 protein is expressed *in vivo*, and contains the nominal RCK2 domain. CV562866 affects functional expression of mSlo3 and mSlo1 channels in *Xenopus* oocytes, decreasing and increasing expression respectively.

This study examined the hSlo2.2a channel characteristics, which unlike the previously reported rSlo2.2a channel, mediates a non-rectifying K^{+} current. Bithionol activates hSlo2.2a channels with an EC_{50} of 1.29±0.12μM and activation was Na^{+} co-operative. We found a candidate bithionol binding site in the C-terminal domain near the "Cl^{-} bowl". Due to toxicity of hSlo2.1 expression; determination of the bithionol selectivity of Slo2.χ channels was unattainable. *In vivo,* Slo2.χ channels act as a background K^{+} conductance, activated by a variety of conditions, stabilising the resting membrane potential of the cell. This study suggests Slo2.χ are viable pharmacological targets for treatment of inflammatory pain.

Table of Contents

Table of Figures

Chapter I

Chapter III

Chapter IV

Chapter V

Table of Tables

List of Abbreviations

4-AP	4-aminopyridine
8Br-cAMP	8-Bromoadenosine 3',5'-cyclic monophosphate
ADP	Adenosine diphosphate
AMPA	2-amino-3-(5-methyl-3-oxo-1,2- oxazol-4-yl)propanoic acid
ATP	Adenosine-5'-triphosphate
cAMP	Cyclic adenosine monophosphate
C_{cell}	Cell capacitance
cDNA	Complementary DNA
CHO	Chinese Hamster Ovary
cRNA	Complementary RNA
CV	CV562866 DNA Sequence
CV	CV562866 Protein
dCTP	Deoxycytidine triphosphate
dGTP	Deoxyguanosine triphosphate
DMSO	Dimethyl Sulfoxide
DRG	Dorsal Root Gangilion
dTTP	Deoxythymidine triphosphate
E2	17β-estradiol
EC_{50}	Half maximal effective concentration
EDTA	Ethylenediaminetetraacetic acid
EGFP	Enhanced GFP
E_K	Equlibrium constant for K^+
ENaC	Epithelial sodium channel
EST	Expressed Sequence Tag
FMRP	Fragile X mental retardation protein
GDH	Glutamate Dehydrogenase Enzyme
GFP	Green Flourescent Protein
GqPCR	Gαq-protein coupled receptors
hEAG	Human K^+ voltage-gated channel, subfamily H (eag-related)
HEK	Human Embronic Kidney
HEPES	4-(2-hydroxyethyl)-1-piperazineethanesulfonic acid
hERG	human *ether-a-go-go*-related gene K^+ channel
I/V	Current/Voltage
IC_{50}	Half maximal inhibitory concentration
IHC	Immunohistochemical
IK_{Sper}	K^+ channel of Sperm
ISH	*In-situ* hybridisation
K_{ATP}	ATP-sensitive K^+ channel
Kir	Inwardly rectifying K^+ channel
K_{Na}	Na^+ activated K^+ channel
KO	Knock Out
Kv	Voltage gated K^+ channel

MC13	chimaeric mSlo3 with residues 1-181 substituted with Slo1
MNTB	Medial Nucleus of Trapezoid Body
NAD^+	Nicotinamide adenine dinucleotide
$NADP^+$	Nicotinamide adenine dinucleotide phosphate
NFA	Niflumic acid
NPo	Number of openings
ORF	Open Reading Frame
PBS	Phosphate buffered saline
PCR	Polymerase Chain Reaction
PIP2	Phosphatidylinositol-4,5-bisphosphate
PKA	Protein kinase A
PKC	Protein kinase C
PLC	Phospholipase C
PMA	Phorbol 12-myristate 13-acetate
Po	Probable openings
PSD-95	Postsynaptic density-95
RACE	Rapid Amplification of cDNA Ends
RCK	Regulator of K^+ Conductance
RFP	Red Flourescent Protein
RMP	Resting membrane potential
RT-PCR	Real time PCR
RVD	Regualtory volume decrease
SACY	Soluble adenylyl cyclase
sAHP	slow afterhyperpolarisation
SDS	Sodium dodecyl sulfate
SUR	Sulfonylurea receptor
TAE	Tris-acetate-EDTA Buffer
TEA	Tetraethylammonium
TEMED	Tetramethylethylenediamine
TM	Transmembrane
TRIS	Tris(hydroxymethyl)aminomethane
VSD	Voltage Sensor Domain

Chapter I: Introduction

1.1 Introduction to potassium channels

1.1.1 General Introduction

Potassium (K^+) channels are the largest and most diverse super-family of highly selective ion channels, and form a selective pathway for K^+ ions to rapidly traverse the cell membrane. Due to the physiological asymmetric gradient of [K^+] across the cell membrane, created by the Na^+/K^+-ATPase pump, a Nernstian equilibrium potential (E_K) is generated, this potential is generally ≈ -90 mV in excitable cells. Activation of K^+ channels allows the efflux of K^+ ions from the cell resulting in hyperpolarisation of the membrane to near E_K, and away from the "threshold" potential at which the voltage gated Na^+ channels open (Hille, 2001). In excitable cells, like neurons, there are two functions of K^+ channels; repolarising the membrane after action potential firing and modulating the resistance to change via maintenance of the membrane potential with zero current flux (resting membrane potential). K^+ channels affect not only the overall excitability of the cellular membrane but also can affect the duration, shape and rate of action potentials (Hille, 2001). K^+ channels are generally grouped according to the pore forming alpha subunit topology. The three classes are the six transmembrane domain (like the voltage gated K^+ (Kv) channels), the four transmembrane two pore and the two transmembrane inward rectifying subunits. Within these structural classes there are sub-families that are classified by channel function and structure. The focus of this thesis is devoted to the Slo channel sub-family, which are members of the six transmembrane (TM) K^+ channel family, which have a distinctive large single channel-conductance.

1.1.2 Generalised Structural Features of Six Transmembrane K^+ channels

1.1.2.1 Pore Domain

The definitive feature of K^+ selective channels is the conserved signature sequence of TXXTXG[Y/F]G (where X can be any amino acid) that forms the K^+ selective filter of the ion conducting pore (Heginbotham *et al.*, 1994; Doyle *et al.*, 1998). The filter is located within a long extracellular loop between two TM domains, which partially re-enters the membrane. Mutagenesis of these conserved residues and the Y to F variant have been shown to lower the K^+ selectivity of the channel (Heginbotham *et al.*, 1994). Determination of the

crystal structure of KcsA, a two TM bacterial K^+ channel α-subunit, at 2 Å demonstrated the mechanism of channel selectivity for K^+ ions over smaller ions like Na^+. This structure showed that the K^+ ion is held in a square antiprism of eight water molecules in the intracellular vestibule, maintained in position by the negative charged amino acids at the base of the pore helices. This is mimicked by the carbonyl oxygen atoms within the selectivity filter, compensating for the energetic cost of dehydration of the K^+ ions (Figure 1.1). Smaller ions such as Na^+ have differing hydration distances and thus are not able to coordinate with the carbonyl groups to form the correct orientations required to pass through the filter. This selectivity is re-enforced in a low K^+ environment by the collapse of the selectivity filter (Zhou *et al.*, 2001; MacKinnon, 2004).

1.1.2.2 Voltage Sensor

Many of the six TM K^+ channel family are gated by voltage, the voltage sensor domain (VSD) is generally composed of the S1-S4 TM domains that contain a high density of charged residues that can respond to changes in TM potential. In particular the S4 TM domain contains a high density of positively charged arginine residues. However, there is still some contention as to the dynamics of voltage sensor activation in voltage gated K^+ channels. There are currently two theories; firstly the "paddle model" which suggests that the S3-S4 of the VSD is moved across/through part of the lipid bilayer in response to a change in voltage (Jiang *et al.*, 2003; Tao *et al.*, 2010). The second model suggests that instead of the large movement suggested by the first model, the S4 helix movement is limited. This model suggests that in response to voltage, the S4 undergoes a significant rotation and tilting within the membrane causing an upward movement, allowing the channel gate to move and allow the flux of ions through the selectivity filter (Bezanilla, 2000; Chanda *et al.*, 2005; Posson *et al.*, 2005).

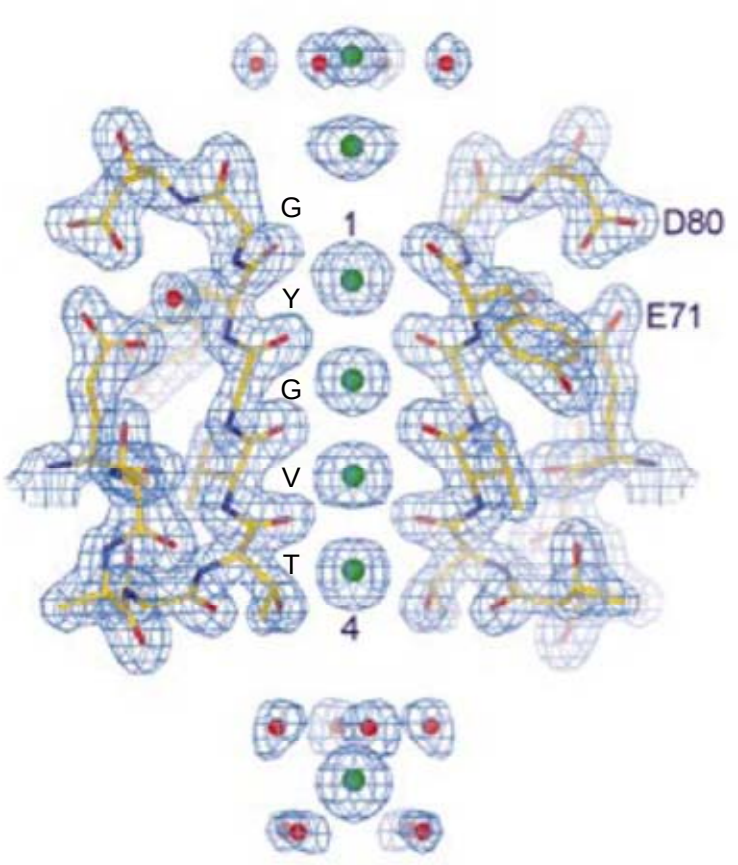

Figure 1.1 The selectivity filter of the K^+ channel pore. Electron density map of the K^+ selectivity filter from the 2Å crystal structure of the KcsA K^+ channel. The conserved selectivity filter sequence is overlaid on the crystal structure to show the positions of these residues. The selectivity filter is visualised with K^+ ions (green spheres) along the ion pathway, and water molecules (red spheres) in the vicinity. K^+ ions are shown both dehydrated in positions 1-4 along the filter but also hydrated in the inner and outer vestibule. Modified from Y. Zhou *et al*. (2001).

1.2 Slo1 channels

1.2.1. Discovery of a large conductance Ca^{2+} activated K^+ current

The Slo channel sub-family was first discovered by the convergence of two independent lines of research, electrophysiological studies of cellular membrane ion currents and *Drosophila melanogaster* neurogenetics. The first observation of the channel was a distinctive outward K^+ current in snail neurons, with dual dependence on Ca^{2+} influx and depolarisation of the membrane for activation (Meech, 1974; Meech & Standen, 1975). The distinctive large unitary conductances recorded by the newly-developed patch clamp technique, led to the nomenclature "big" potassium (BK_{Ca}) channels or the pseudonym "Maxi-K" channels being attributed to these channels. Separately, a *D. melanogaster* mutant, *slowpoke (slo)* was identified, this mutant exhibited a highly lethargic phenotype and under ether anaesthesia this mutant displayed a similar but less extreme leg-shaking behaviour to *Shaker* mutants (a Kv1 channel mutation). Voltage clamp recordings of the dorsal longitudinal flight muscles, showed an abolition of the Ca^{2+} dependent element of the outward K^+ current. This result demonstrated that the *slo* locus was the gene that encoded the BK channel protein (Elkins *et al.*, 1986). Identification of the *slo* gene and subsequent cDNA sequence analysis predicted a protein (dSlo1), with resemblance to the Shaker (Kv1) α-subunit. The mammalian ortholog of the protein, mSlo1, was isolated using *D. melanogaster slo* cDNA probes against mouse brain and skeletal muscle cDNA libraries, and successfully expressed in a *Xenopus* oocyte expression system. The resulting macroscopic currents corresponded to activation of a Ca^{2+} activated K^+ channel with a unitary conductance of 260 pS in symmetrical (160 mM) K^+, in contrast Kv1.1 (the mammalian Shaker ortholog) has a unitary conductance of approximately 10 pS (Butler *et al.*, 1993).

1.2.2 Structure of the Slo1 α-subunit

The Slo1 α-subunit has a similar structure to the Kv α-subunit, six TM segments (S1- S6), with the channel pore located between S5-S6 and a S4 domain with a series of three regularly spaced basic residues (Meera *et al.*, 1997; Ma *et al.*, 2006) (Figure 1.2.B). However, amongst the six TM K^+ channel family, the Slo channel sub-family is unique due to the presence of an extra TM domain termed S0. The presence of this additional domain causes the N-terminus of these subunits to be extracellular rather than intracellular (Meera *et*

al., 1997). This S0 domain is essential for interactions of the Slo1 α-subunits with the Sloβ subunits (Wu *et al.*, 2009), and correct trafficking to the cell surface (Liu *et al.*, 2008). The Slo1 α-subunit also has a large cytoplasmic tail consisting of two paired domains S7-S8 and S9-S10 (Meera *et al.*, 1997). These paired domains form a tandem arrangement of non-identical "regulator of K^+ conductance" (RCK) domain architecture in the large C-terminus tail that provides most of the physiological modulatory sites. Recent structural studies have confirmed that like other RCK containing channels; an octomeric gating ring is formed consisting of a tetramer with each subunit containing two RCK domains. This tetramer is found in close proximity to the TM ion conduction pore, and potentially forming a cytoplasmic ion conduction pathway for ions moving through the channel (Yuan *et al.*, 2010; Wu *et al.*, 2010). The RCK domains are thought to undergo ligand dependent conformational changes that alter the kinetics of the transition between the open/closed states of the channel activation gate (Yuan *et al.*, 2010; Wu *et al.*, 2010). The Ca^{2+} sensitivity of the channel is conferred by two distinct sites in the C-terminal tail, D362, D367 and M513, in the RCK1 (S7-S8) structure are critical for the high-affinity Ca^{2+} sensitivity. The second site is the "calcium bowl", located in the RCK2 (S9-10) domain. This is formed from five consecutive negatively charged aspartates (D894–D898) (Yusifov *et al.*, 2008). The RCK1 and RCK2 domains are linked by an unstructured linker sequence that cannot be resolved in the crystal structure (Yuan *et al.*, 2010). This linker region is known to contain at least three known sites for alternative splicing of the Slo1 α-subunit (Tseng-Crank *et al.*, 1994) and the linker length has been shown to affect channel activity with shorter lengths reducing channel activity (Lee *et al.*, 2009).

1.2.3 Formation of the Slo1 Channel

The tetrameric nature of the Slo1 channel was first ascertained using co-injection of the extracellular tetraethylammonium (TEA) - insensitive dSlo1 α-subunit mutant (Y308V) with the wildtype dSlo1 cRNA in *Xenopus* oocytes. This experiment demonstrated unitary currents with four discrete amplitudes in the presence of 3 mM TEA; these four amplitudes corresponded to inhibitions of approximately 80%, 55%, 25% and 10% at + 40 mV (Shen *et al.*, 1994). More recent investigations have shown that the tetramerisation in Slo1 is mediated by a conserved intracellular domain (BK-T1) located between the S6 TM domain and the S7 C-terminal domain (Quirk & Reinhart, 2001).

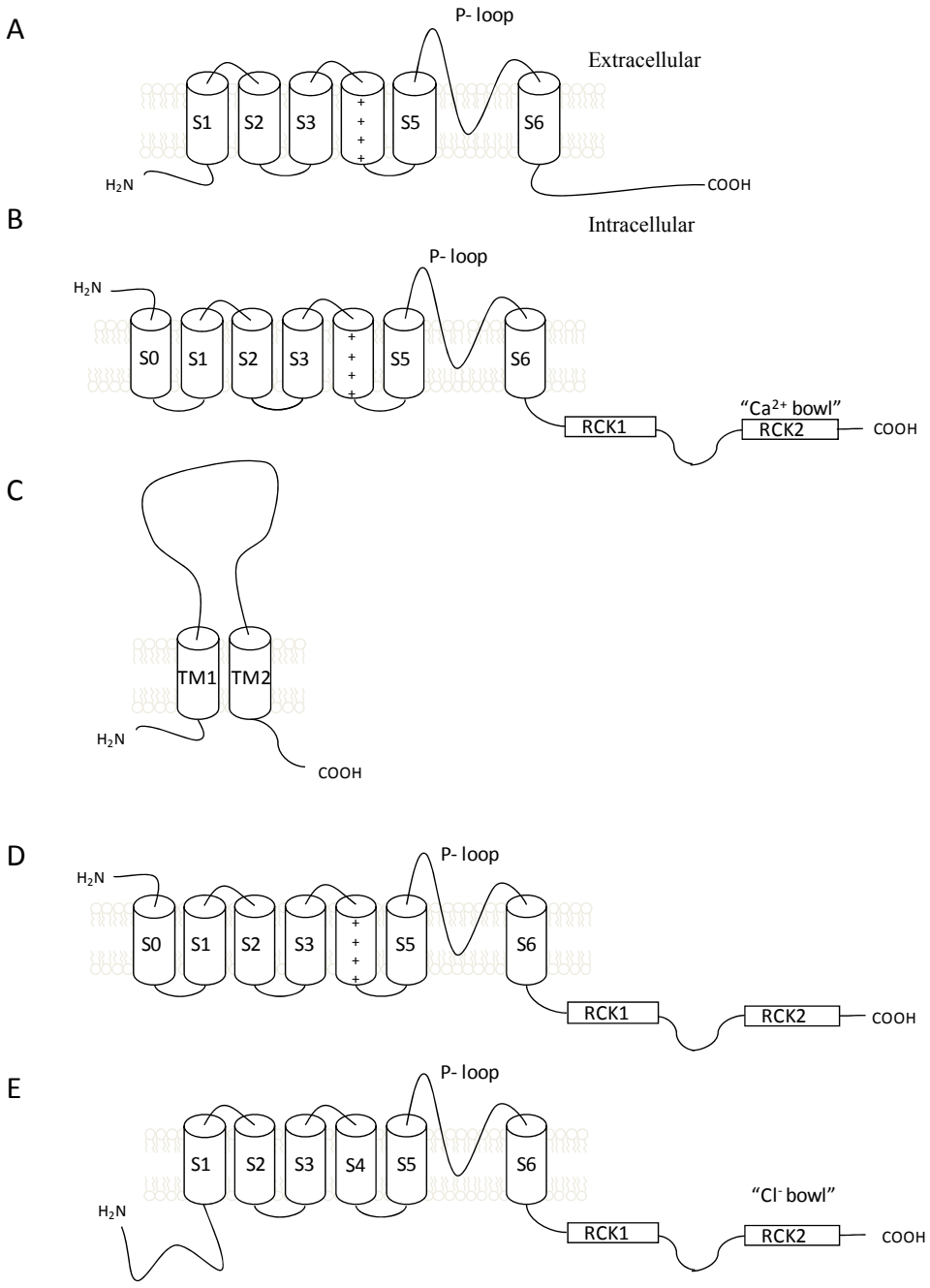

Figure 1.2 Schematic of the topology of six transmembrane K^+ channel α-subunits. The general topology of a Kv channel is shown in (A), with the six TM domains, and the pore forming P-loop. Slo α-subunits have a distinctive large carboxy-tail, which contains the sites required for sensing cytostolic factors, such as the calcium bowl in Slo1 (B). The carboxy-tail also contains the unifying structures for the Slo family, the two RCK domains separated by a non-conserved linker. Non-pore forming modulatory Sloβ subunits (C), however, have a general structure of two TM domains with intracellular N and C-terminal domains. Slo1 (B) and Slo3 (D) are also distinctive from Kv (A) and Slo2.χ (E) subunits due to an extra TM domain S0, which leads to an extracellular N-terminus and allows interaction with Sloβ subunits. The weak voltage sensitivity of Slo2.χ (E) can be explained by the lack of positive residues in the S4 domain in comparison with the other subtypes.

1.2.4 Physiological relevance of Slo1

The Slo1 channel has a large range of physiological relevance due to the ubiquitous expression in cells and tissues throughout the body. In vascular smooth muscle, Slo1 channels have been shown to regulate contractility and cause vasodilatation due to rises in $[Ca^{2+}]_i$ and depolarisation (Nelson *et al.*, 1995; Brenner *et al.*, 2000; Sausbier *et al.*, 2005). In bladder smooth muscle, disruption of Slo1 function by toxins or knock out (KO) of the Slo1 α-subunit results in an increase action potential size and frequency causing an overactive bladder and incontinence (Petkov *et al.*, 2001; Hashitani & Brading, 2003; Meredith *et al.*, 2004). Due to the large conductance of this channel, Slo1 channels also play a crucial role in the regulation of neuronal excitability in the central nervous system. In cerebellar and hippocampal neurons, the Slo1 α-subunit has been shown to localise to the presynaptic terminals and axons of the neurons (Knaus *et al.*, 1996; Misonou *et al.*, 2006; Sausbier *et al.*, 2006). Slo1 α-subunits have been found to co-localise with voltage gated Ca^{2+} channels in neurons, allowing Slo1 channels to contribute to the after-hyperpolarisation observed after an action potential that closes the voltage gated Ca^{2+} channels (Grunnet & Kaufmann, 2004; Berkefeld *et al.*, 2006). Thus Slo1 channels play a vital role in controlling synaptic transmission and the after-hyperpolarisation; allowing control of spike frequency adaptation (Raffaelli *et al.*, 2004; Gu *et al.*, 2007).

1.2.5 Modulation by Sloβ subunits

Slo1 channel inherent function is not only modulated through splice variation of the Slo1 α-subunit, but also by expression with the four modulatory Sloβ subunits (Sloβ1-4). Tissue specific expression of Sloβ subunits underlies many of the differences reported in Slo1 channel characteristics and thus their diverse roles in differing cell types. Sloβ subunits have a general structure of two TM domains with intracellular N and C-terminal domains and are unable to form a distinct channel as they lack a pore loop (Figure 1.2.C) (Knaus *et al.*, 1994). Sloβ subunits are thought to physically interact through the S0 and S1/2 domains of the Slo1 α-subunit (Wu *et al.*, 2009). Sloβ1 subunits were first observed by co-immunoprecipitation with the Slo1 α-subunit from bovine tracheal smooth muscle (Knaus *et al.*, 1994). Co-expression of Slo1/β1 in HEK cells generates currents that are activated at lower $[Ca^{2+}]_i$ compared with solitary expression of Slo1 α-subunit. These currents also display slower rates of deactivation and reduced iberiotoxin sensitivity. Sloβ1 expression in smooth muscle therefore produces Slo1 channels that can be activated under physiological conditions (Lippiat *et al.*, 2003).

Sloβ2 subunits are unique amongst the Sloβ subunits, as they cause N-type inactivation of Slo1 currents. This inactivation is due to the "ball" formed by the first 19 residues of N-terminus of the Sloβ2; inactivation can be relieved by intracellular application of trypsin (Wallner *et al.*, 1999; Lippiat *et al.*, 2003). Removal of the inactivation ball by trypsin application revealed that the voltage and $[Ca^{2+}]_i$ dependence of currents was similar to Slo1/β1 (Lippiat *et al.*, 2003). The Sloβ3 subunit was first proposed to cause N-type inactivation of Slo1/β3 currents like the Sloβ2 subunit (Xia *et al.*, 1999), however analysis of the sequence alignments determined that this original study was actually using the hSloβ2 subunit. Studies of the Sloβ3 subunit did find that two of the four splice variants (Sloβ3a and Sloβ3c) did cause partial N-type inactivation. However, whilst the time constant for inactivation was the same as for Sloβ2 subunits the fractional inactivation of the currents was reduced. The Sloβ3b subunit was found to confer a small component of very fast inactivation causing the appearance of an apparent inward rectification of currents (Uebele *et al.*, 2000). These inactivating Sloβ subunits mediate the inactivating Slo1 channels that are observed in adrenal cromaffin cells and pyramidal neurons of the hippocampus (Lippiat *et al.*, 2003). The Sloβ3d isoform causes no inactivation, and does not appear to affect the $[Ca^{2+}]_i$ or voltage range of activation (Uebele *et al.*, 2000; Lippiat *et al.*, 2003).

The Sloβ4 subunit, which is expressed predominantly in neuronal tissues, confers insensitivity to iberiotoxin and charybdotoxin to the Slo1/β4 channel complex (Lippiat *et al.*, 2003). Slo1/β4 channels in HEK cells have decreased sensitivity to voltage, $[Ca^{2+}]_i$ and slowed activation rates (Weiger *et al.*, 2000). The Sloβ4 subunit has been associated with epilepsy and dyskinesia; KO of the Sloβ4 subunit shifts the activation of Slo1 channels back to the normal physiological range, thus increasing the channel's contribution to action potential repolarization and increasing firing rates (Brenner *et al.*, 2005; Petrik *et al.*, 2011).

1.3 Slo3 channels

1.3.1 Introduction to Slo3 channels

With the advent of cDNA libraries and DNA sequence analysis, the next reported member of the Slo channel subfamily was identified in mouse cDNA via an expressed sequence tag (EST) from a promyelocytic WEHI-3 cell line with homology to the C-terminal "tail" of mSlo1. However, all of the isolated cDNA sequences from the WEHI-3 cell line were found truncated or incorrectly spliced. PCR analysis of a variety of tissues led to the discovery of the *Slo3* encoded channel, mSlo3. Expression of mSlo3 cDNA was found to be highly restricted solely to spermatozoa and testis.

Hydrophilicity plots of the mSlo3 and mSlo1 sequences indicated that like mSlo1, the mSlo3 structure has 11 domains, S0 through S10. Akin to mSlo1, these can be split into the "core" (S0-S8) domain, which includes the TM domains (S0-S6) and the start of the intracellular C-terminus (S7-S8), and "tail" domains (S9-S10) (Figure 1.2.D). The mSlo1 and mSlo3 sequences have highest similarity in the "core" domain (S0-S8) sharing 56% sequence identity. The orthologues mSlo1 and dSlo1 share 62% identity through this "core" region. The "tail" domains (S9-S10), however, are more divergent and have only 39% identity between mSlo3 and mSlo1 sequences. The channels also differ in their physiological modulation; mSlo3 channels, when expressed in *Xenopus* oocytes, were found to be modulated by internal pH, with channel activation at low $[H^+]$ and voltage. Unlike mSlo1 channels which are modulated by Ca^{2+} and voltage. mSlo3 channels displayed a lower unitary conductance (106 pS) in symmetrical K^+ (160 mM) compared to mSlo1 channels. mSlo3 channels have a GFG sequence motif in the selectivity filter of the pore, rather than the GYG sequence motif observed in the mSlo1 sequence. This results in mSlo3 channels having a reduced selectivity for K^+ over Na^+ ($P_K/P_{Na} \approx 5$) compared to mSlo1($P_K/P_{Na} > 50$) (Schreiber *et al.*, 1998).

1.3.2 Slo3 channel properties

1.3.2.1 Endogenous Activators

The original study noted that the mSlo3 channel had a short mean open time and a low open probability at physiological voltages (Schreiber *et al.*, 1998). Further studies have attempted to better define the links between voltage or pH and activation of the Slo3 channel. Slo3 activation by high pH was found to be the major determinant of the open probability (P_o), this effect of pH on channel conductance, was found to be largely voltage independent (Zhang *et al.*, 2006*b*). Estimates of Slo3 conductance at negative potentials predicted that Slo3 channel gating has weak intrinsic voltage dependence. This is believed to be due to a weaker coupling of the voltage sensor to the channel activation gate. This is possibly dependent on a more restricted motion through the membrane, in comparison to the Slo1 voltage sensor (Zhang *et al.*, 2006*a*). The weak voltage dependence of mSlo3 activation is exemplified by the requirement for a non-physiological range of positive voltages to activate the channel. Previous studies of mSlo3 have also shown that currents fail to reach a measurable G_{Max} plateau in macroscopic patches pulled from oocytes at voltages up to +300 mV (Zhang *et al.*, 2006*a*; Tang *et al.*, 2010*b*). Chimaeras made between the divergent mSlo3 and bovine Slo3 (bSlo3) orthologues have suggested regions outside the S0-S6 TM domains influence the voltage dependence of channel activation, in oocytes. bSlo3 currents differ from mSlo3 currents by having a faster activation time constant (τ), more negative voltage range of activation, a higher selectivity for K^+ (P_K/P_{Na} = 10) and are less sensitive to high pH. Using chimaeras, a region in the RCK1 of mSlo3, when replaced with the bSlo3 sequence, was found to shift the voltage sensitivity to bSlo3 levels. This chimaera also conferred the mSlo3 currents with the characteristic faster τ of bSlo3 currents. Interestingly the inverse chimaera in bSlo3 did not shift the voltage activation to the more positive potential of mSlo3. This suggests that in bSlo3 there are other structural components that determine the voltage range of activation. As the region in the distal half of the mSlo3 RCK1 contains two histidine residues, which are not present in bSlo3, these residues were mutated to test if these contribute to the reduced bSlo3 sensitivity to high pH. It was found that mutation of these two residues did not confer the reduced sensitivity to high pH to mSlo3 currents. Thus it appears that in mSlo3 the RCK1 domain may influence the coupling of the voltage sensor to the channel pore (Santi *et al.*, 2009).

The dependence of channel activity on pH implicates a role for a "pH sensor" mechanism that directs gating in an allosteric manner, similar to Ca^{2+} regulation of Slo1, rather than effects on ion permeation (Zhang *et al.*, 2006*a*). Activation of Slo3 was found to be limited to the range pH 7.4 - 9, illustrated in Figure 1.3. pH 9 is not a known physiological limit to

channel activation, as at pH values higher than 9, patch stability could not be maintained. Analysis of the effects of pH on P_o of the channel suggested that multiple protonation sites exist on the Slo3 C-terminus tail (Zhang *et al.*, 2006*a*). Interestingly, analysis of the activation and deactivation time courses of macroscopic currents exposed fast and slow exponential components. This suggested that there were two distinct inter-converting channel populations that are in differing kinetic states. Increasing pH was found to affect the amplitude of activation; whilst the time course of activation remained constant. This finding suggested a shift between populations was dependent on the level of protonation of the Slo3 channel (Zhang *et al.*, 2006*a*). An expectation of their theory is that the distinct populations would each have a discrete steady state P_o, however this was not observed in their analysis of single channel traces (Zhang *et al.*, 2006*b*). One curious aspect of the fast component of channel deactivation is the minimal dependence on pH. Therefore it was proposed that the fast deactivation of Slo3 represents a novel closing process that may be unrelated to the closing of the Slo3 S6 helix (Zhang *et al.*, 2006*a*). However this was not observed in single channel traces which exhibit a rapid opening and closing that prevented simple definition of a unitary current level. Thus it was concluded that there is insufficient evidence to determine the effects of pH on the gating steps controlling Slo3 activation time course (Zhang *et al.*, 2006*b*).

The structural determinants of the pH sensitivity have not been well defined. What little is known is predominantly due to production of chimaeras between Slo1 and Slo3. Studies of these chimaeras have focused on the effects on the Slo1 channel properties in contrast with wild type Slo1 (Xia *et al.*, 2004). One of these chimaeras was an exchange between Slo1 and Slo3 of the entire post S6 inner helix C-terminal cytosolic domain. When the Slo3 C-terminus was fused to the pore domain of Slo1, the resulting chimaera displayed regulation by pH (Xia *et al.*, 2004). However, little current activation at + 300 mV was observed at pH 7.4 in the chimaera; whereas in Slo3 activation at + 300 mV was observed from as low as pH 6.0. This difference in characteristics was shown to be due to differences in pore domain and cytosolic regulatory domain interactions being differentially effective at gating the channel dependent on the pore domain (Xia *et al.*, 2004). Another study, investigating the structural determinants of carbon monoxide sensitivity in Slo1, made a more restricted chimaera in which the C-terminal tail of the hSlo1 protein was replaced only with the S9–S10 module, equivalent to the "Ca^{2+} bowl" of Slo1, of mSlo3. The activity of this chimaera was not dependent upon intracellular pH. This observation suggests that the S9–S10 module (RCK2) of mSlo3 is not the pH sensor (Williams *et al.*, 2008).

The mSlo3 channel has also been shown to be modulated by cAMP and PIP_2 levels (Martínez-López *et al.*, 2009; Tang *et al.*, 2010*a*). When ooctyes injected with mSlo3 mRNA were treated using forskolin and a phosphodiesterase inhibitor (IMBX), to increase cAMP levels, mSlo3 currents increased. This increase could be inhibited if oocytes were preincubated with H-89, an inhibitor of cAMP dependent kinases (PKA). This suggests that the cAMP increase of mSlo3 current is dependent on phosphorylation (Martínez-López *et al.*, 2009). PIP_2 depletion has been shown to inhibit mSlo3 currents in oocytes. PIP_2 is thought to act through electrostatic interactions with two amino acids, K320 and K329, which are located on the C-terminus in the linker region between S6 and RCK1. Mutation of these two lysines to uncharged asparagine, individually or in tandem, increased the EC_{50} values for DiC_8-PIP_2, a soluble homologue of PIP_2, on mSlo3 currents (Tang *et al.*, 2010*a*).

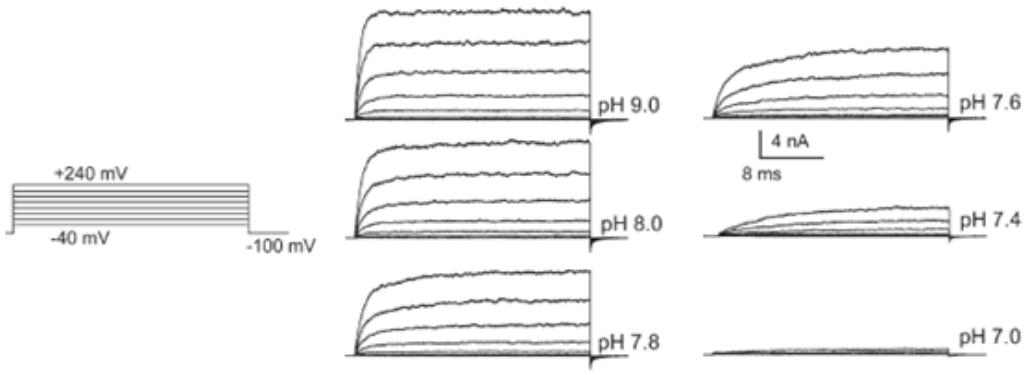

Figure 1.3 pH dependence of activation of mSlo3 macroscopic currents expressed in oocytes. Currents recorded from oocytes showing increased pH results in increased amplitude and speed of activation for a given voltage over the range -40 to +240 mV. Modified from X. Zhang, X. Zeng & Lingle (2006).

1.3.2.2 Expression Profile

Unlike the ubiquitously expressed Slo1 α-subunit, Slo3 α-subunit expression appears to be highly restricted. PCR and northern blot analysis of a variety of tissues found that expression of full length mSlo3 cDNA was restricted to tissue isolated from testes. This seems contrary to the initial detection of an expressed sequence tag (EST), from the mouse promyelocytic WEHI-3 lympocyte cell line, with homology to the C-terminal "tail" of mSlo1. However all of the isolated cDNA sequences from the WEHI-3 cell line were found to be truncated or incorrectly spliced. *In situ* hybridisation probing of seminiferous tubules found a high level of hybridisation to the mSlo3 probe in more mature spermatocytes (those closest to the lumen). However, the study did acknowledge that the techniques used could not exclude restricted expression within tissues or low level expression (Schreiber *et al.*, 1998).

1.3.2.3 Pharmacology

The pharmacology of mSlo3 differs from mSlo1; mSlo3 is largely insensitive to extracellular TEA with an IC_{50} of 49 mM in comparison to block of mSlo1 which has an IC_{50} of 0.14mM (Schreiber *et al.*, 1998). This difference in TEA sensitivity is due to the lack of a tyrosine (Y294) on the S5 linker region. When this site is mutated in Slo1 the mutant results in mSlo3 levels of inhibition (Tang *et al.*, 2010*b*). Most of the mSlo3 pharmacology was performed on a chimaeric mSlo3 α-subunit (MC13), which has residues 1-181 substituted from the mSlo1 α-subunit. This chimaera was used because whilst the expression in oocytes was increased, the basic gating properties were unchanged. Like mSlo3, MC13 currents are insensitive to the scorpion toxins, iberiotoxin and charybdotoxin, the "classical" Slo1 inhibitors.

In contrast to extracellular TEA application where MC13 has a lower sensitivity than Slo1, MC13 currents were ≈25 times more sensitive to cytosolic TEA than mSlo1 currents. This value, however, is estimated as none of the blocking schemes fitted to the data with high fidelity. Thus the study was unable to firmly conclude the affinity at 0 mV of TEA to MC13. The MC13 chimaera was also tested against the non specific K^+ channel inhibitors, 4-aminopyridine (4-AP) and quinidine. Blockade of MC13 by 4-AP was negligible when applied to the extracellular side of the membrane but potent with intracellular application. This was suggested to be due to low permeation of 4-AP across the membrane at pH 7.0, as at this pH only ≈ 0.6% of 4-AP remains uncharged and thus able to cross the membrane. Quinidine block of MC13 was proposed to be due to the protonated form binding with a higher affinity to the closed state of the channel. However, the study acknowledges that for

cytosolic application of quinidine, no model of block fits the data with higher consistency than any of the other models (Tang *et al.*, 2010*b*).

1.3.3 Regulation of Slo3

1.3.3.1 Sloβ Subunits

Sloβ subunits are thought to physically interact through the S0 and S1/2 domains of the Slo1 α-subunit, which is within the region that mSlo1 and mSlo3 have the highest sequence identity (Schreiber *et al.*, 1998; Wu *et al.*, 2009). A study of the interactions between mSlo3 and Sloβ subunits found that all of the Sloβ subunits appear to be able to interact with mSlo3 (Yang *et al.*, 2009). Sloβ2 was found to functionally interact with mSlo3 and displayed trypsin-sensitive inactivation (Yang *et al.*, 2009). Of the four Sloβ subunits, only Sloβ4 has a gain of function effect on mSlo3 currents (Yang *et al.*, 2009). Sloβ4 co-expression with the mSlo3 α-subunit results in an eight-fold increase in the conductance recorded from macropatches and increased surface expression in oocytes. Expression of mSlo3 with Sloβ4 did not modify the voltage dependence, single channel conductance or the P_o of currents. This suggests that Sloβ4 only increases the surface expression level of the channels rather than the single channel electrophysiological properties. Sloβ4 was also found, using RT-PCR, to be expressed to a similar level as mSlo3 in testes and spermatozoa. Interestingly, Sloβ4 KO mice had no change in the reproductive capacity, as quantified by litter size (Yang *et al.*, 2009). This evidence suggests that there are other as yet unknown regulatory subunits that effect mSlo3 expression and channel function *in vivo*.

1.3.4 Physiological relevance of Slo3

1.3.4.1 IK_{Sper}

The alkaline activated I_{KSper} (K^+ channel of Sperm) current was first identified through patch clamp recordings from mouse CatSper1 KO mature spermatozoa (Navarro *et al.*, 2007). The properties of this current are similar to the mSlo3 channel mediated current, including the shape of the I/V curve, the potentiation of the current over a similar pH range (pH 6- pH 8) and weak voltage sensitivity. However, I_{KSper} is activated by a lower voltage range than mSlo3 and displays distinct inward current which is absent from mSlo3 recordings. I_{KSper} is the dominant hyperpolarizing conductance within the physiological range, and thus is believed to dictate the resting membrane potential of the spermatozoan. I_{KSper} current was found to be inhibited by the general motility and volume regulatory K^+ channel (TASK2 and

Kv1.5) inhibitors; quinine (1.4.2), clofilium (1.4.3) and mibefradil (1.4.4) (Navarro *et al.*, 2007). The original study was unable to confirm if mSlo3 channel is the I_{KSper} current mediator in mouse CatSper1 KO mature spermatozoa as the only commercially available anti-mSlo3 antibody is raised in mouse (NeuromAB) (Navarro *et al.*, 2007). In the original study the I_{KSper} current was found not to be modulated by the presence of membrane permeant cAMP analogs (Navarro *et al.*, 2007). This characteristic of I_{KSper} seems to contradict the subsequent reported mSlo3 characteristics (Martínez-López *et al.*, 2009). This subsequent study also found that the spermatocyte currents isolated after inhibition of the endogenous K_{ATP} and ENaC channels, were activated by high $[pH]_i$ and 8Br-cAMP. This discrepancy was explained to be due to the $[pH]_i$ used in the experiments, the original study used a $[pH]_i$ of 7, under which condition 8BR-cAMP is unable to activate the isolated spermatocyte currents. Activation with 8BR-cAMP was only seen when the $[pH]_i$ was 7.4 or higher (Martínez-López *et al.*, 2009). Like mSlo3, the alkalinisation activated sperm K^+ current is increased by the presence of DiC_8-PIP_2. This increase was on average 3.2 fold and reversible by application of epidermal growth factor (EGF), which in turn activates EGF receptors and hydrolyses the endogenous PIP_2 (Tang *et al.*, 2010*a*).

Recently two studies describe the generation of mSlo3 KO mice and the isolation of spermatozoa. As expected in both of these studies KO spermatozoa lacked or had a reduced alkalinisation activated K^+ current (Santi *et al.*, 2010; Zeng *et al.*, 2011). The discrepancy is due to the voltages used in the current recording protocols. In the initial study where no alkalinisation activated K^+ current was observed in the KO spermatozoa voltage steps were limited to the -80 mV to +60 mV range (Santi *et al.*, 2010). The second study used a voltage ramp from -100 mV to +100 mV to record currents from their KO spermatozoa and thus observed a second alkalinisation activated K^+ current, which they termed K_{res}, which is activated by potentials greater than +60 mV (Zeng *et al.*, 2011). The second study also found that they could distinguish K_{res} currents due to the reversibility of clofilium block (Zeng *et al.*, 2011). Both studies found that mSlo3 KO spermatozoa were unable to undergo the alkalinisation-activated hyperpolarisation required for capactiation (discussed in 1.3.4.2) and in fact depolarised under these conditions. The studies concluded that mSlo3 KO spermatozoa have reduced progressive motility (Santi *et al.*, 2010; Zeng *et al.*, 2011). The second study, interestingly, also found that mSlo3 KO spermatozoa were unable to maintain normal volume regulation under osmotic stress (Zeng *et al.*, 2011). Due to these characteristics of mSlo3 KO spermatozoa, both studies found that even with normal mating indictors (vaginal plugs) male mSlo3 KO mice were infertile and unable to produce offspring (Santi *et al.*, 2010; Zeng *et al.*, 2011). Neither of these studies has addressed the discrepancies observed between I_{KSper} and heterologously expressed mSlo3 in ooctytes. In

particular, that although the pH range (pH 6- pH 8) and weak voltage sensitivity of activation are similar in the two systems, both of these characteristics are shifted leftwards for I_{KSper} compared to mSlo3, suggesting that there is a yet unknown accessory or modulatory protein to mSlo3.

1.3.4.2 Capacitation and Acrosome Reaction

Capacitation is defined as the penultimate step in the maturation of spermatozoa in the female reproductive tract; this process was first reported in 1951 by two independent groups (Austin, 1951; Chang, 1951). During the process of capacitation, the spermatozoa acquire hyperactivated motility, chemotaxis and are readied for the acrosome reaction prior to fertilisation. Capacitation occurs after several hours in the female reproductive tract, in the fallopian tubes. From *in vitro* analysis capacitation requires the oviductal fluid to contain; albumin, bicarbonate and extracellular Ca^{2+} (Visconti *et al.*, 2002). The initiation of capacitation is currently unknown, but may be due to two effects of albumin on spermatozoa. Firstly removal of cholesterol from the membrane, modifying the membrane properties and secondly by directly stimulating the alkalinisation activated CatSper channels (Xia & Ren, 2009). In humans there is a third possible initiator of capacitation, progesterone, which has been shown to activate hCatSper but not mCatSper channels (Lishko *et al.*, 2011). The initial rise in $[Ca^{2+}]_i$ and $[HCO_3^-]_i$ activates soluble adenylyl cyclase (SACY), which in turn increases $[cAMP]_i$ levels and activation of PKA causing phosphorylation of a range of target proteins (Visconti *et al.*, 2002; Harrison & Gadella, 2005). The cAMP rise also causes a rise in pH_i by activation of HV1 channels in humans, and the Na^+-dependent Cl^-–HCO_3^- exchanger in mouse (Zeng *et al.*, 1996; Lishko *et al.*, 2010). The increase in intracellular pH is thought to activate I_{KSper} current and drives the membrane potential to negative potentials. This sequentially increases the driving force of Ca^{2+} entry via CatSper channels which are also activated by high pH_i (Kirichok *et al.*, 2006; Navarro *et al.*, 2007, 2008). The high pH_i and $[Ca^{2+}]_i$ levels cause the characteristic high amplitude, asymmetrical flagellar beating of hyperactivation by affecting the axoneme (Ho *et al.*, 2002).

Currently the chemoattractant for spermatozoa is unknown, it has been suggested that in humans the progesterone secreted by the cumulus cells can activate the hCatSper channels and cause chemotaxis by induced asymmetrical tail beating (Lishko *et al.*, 2011). However, other chemoattractants have been suggested and the importance of chemotaxis in mammalian systems is contentious (reviewed in (Eisenbach & Giojalas, 2006)). Once the capacitated spermatozoa reach the egg, hyperactivation of the spermatozoan flagella is essential to allow the spermatozoan to penetrate the protective outer layers of the egg

(Suarez, 2008). The protective outer layers of the egg consist of; the outermost layer, the cumulus oophorus, and the inner zona pellucida layer (Suarez, 2008). Hyperactivation of the spermatozoan flagella is enough to drive the spermatozoan through the cumulus oophorus; however, the zona pellucida matrix is too dense. To penetrate the zona pellucida the spermatozoan must undergo the acrosome reaction caused by exocytic fusion of the acrosomal vesicle with the spermatozoan's plasma membrane; this process allows fusion of the spermatocyte with the egg (Clark *et al.*, 1993; Dean, 2007).

1.3.4.3 K^+ channels in spermatozoan volume regulation

The finding that mSlo3 KO spermatozoa were unable to maintain normal volume regulation under osmotic stress suggests that mSlo3 channels play a role in the volume regulation of the spermatocyte (Zeng *et al.*, 2011). Spermatozoa undergo regulatory volume decrease (RVD) when they move from the vas deferens (≈350 mOsm) to the vaginal tract (≈280 mOsm). Defects in RVD result in angulations and coiling of the spermatozoan flagella, which is associated with infertility in domestic animals and mice. mSlo3 channels have been previously discounted for a role in RVD due to reported TEA sensitivity, leading to Kv1.5 and TASK2 channels being the primary channels theorised to mediate volume regulation and motility (Yeung & Cooper, 2001; Barfield *et al.*, 2005*a*, 2005*b*). However, their study used up to 10 mM TEA without seeing significant effects, which is below the mSlo3 IC_{50} of 49 mM at +60 mV (Barfield *et al.*, 2005*b*). The K^+ current that regulates volume and motility is also sensitive to as little as 200 μM quinine when applied for 5 minutes (Yeung & Cooper, 2001; Barfield *et al.*, 2005*b*). The volume regulatory K^+ current has also been shown to be to be sensitive to clofilium (10 μM) when applied for 75 minutes. The volume regulatory K^+ current is also sensitive to 4-AP, a K^+ channel inhibitor shown to have effects on spermatozoan volume regulation (Barfield *et al.*, 2005*a*). However, this compound was found to enhance rather than inhibit I_{KSper}, possibly in consequence of indirect alkalinisation of cells (Navarro *et al.*, 2007).

1.4 I_{KSper} K^+ current inhibitors

1.4.1 Barium

Barium ions (Ba^{2+}) are one of the earliest reported non-specific blockers of K^+ channels, Ba^{2+} block of a K^+ conductance was first observed in grasshopper and lobster mucle fibres, where Ba^{2+} application resulted in an "all or none" firing activity (Werman & Grundfest, 1961; Werman *et al.*, 1961). Further studies have since shown that Ba^{2+} blockade is non specific for K^+ channels as the binding site is within the highly conserved K^+ selectivity filter present in all K^+ channels (1.1.2.1). Ba^{2+} is able to enter the selectivity filter as it has a crystal radius of 1.34 Å which is almost undistinguishable from the K^+ crystal radius of 1.33 Å (Armstrong & Taylor, 1980). Early studies of the Ba^{2+} block of K^+ channels in squid giant axons and Slo1 channels in reconstituted bilayers led to a permeation pathway model with four distinct sites for K^+ binding, with Ba^{2+} able to occupy one of the sites with a slowed off rate (Figure 1.4.A) (Armstrong & Taylor, 1980; Neyton & Miller, 1988). Their model suggested that Ba^{2+} is able to access and cross the K^+ selective pore region. However in the presence of K^+ on both sides of the membrane, the high affinities of the "lock in" sites at either end of the filter are occupied by K^+. This means that the Ba^{2+} ion becomes "locked" within the pore, stopping K^+ ions from transversing. In high extracellular [K^+] (50 mM) there is a second extracellular site termed the "enhancement site", this is only occupied at high $[K^+]_e$ as it is very close to the Ba^{2+} binding site. Thus when the enhancement site is filled both ions will be subject to strong ionic repulsion "enhancing" the dissociation of Ba^{2+} to the internal solution. This finding also suggests that in the conducting K^+ channel (as crystallised later by Y. Zhou *et al.* (2001)) occupancy of all the sites in the pore results in mutual destabilisation of the ions in the pore, this allows an increased rate of escape of the pore and thus rapid conduction. This model also explains the voltage dependence of Ba^{2+} blockade whereby Ba^{2+} inhibition is relieved by membrane depolarisations. As, under physiological conditions, depolarisation of the membrane will unblock the external "lock-in" site and allow the Ba^{2+} to follow the electrogenic driving force and exit through the extracellular side of the pore (Neyton & Miller, 1988). This permeation pathway model was confirmed by the solving of the crystal structure of the KcsA pore bound with Ba^{2+} (Figure 1.4.B) (Jiang & MacKinnon, 2000).

A

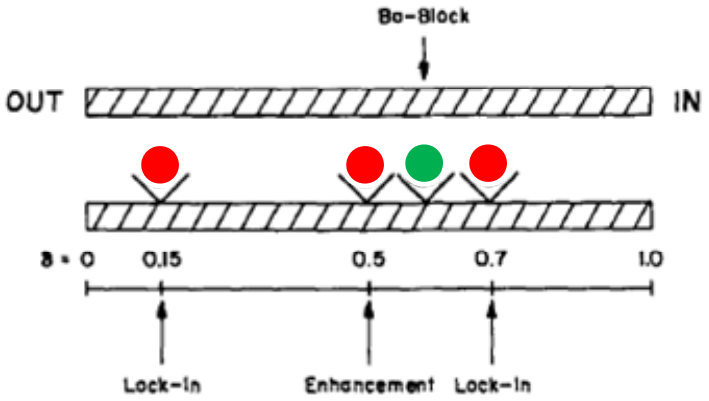

B

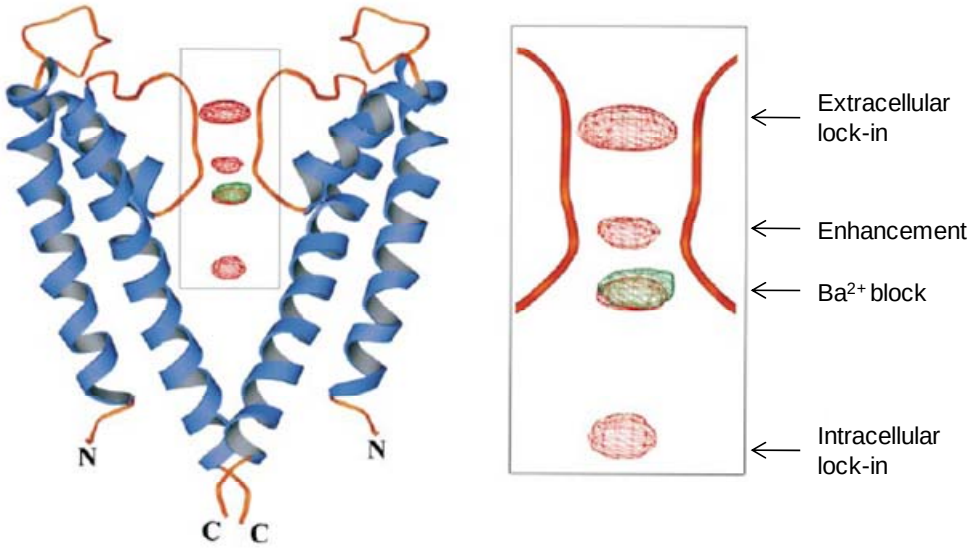

Figure 1.4 Localisation of the Ba^{2+} binding site within the K^+ selective filter. The original model of Ba^{2+} block of the K^+ pore (A), suggested by Neyton & Miller (1988), showing the location of the four K^+ binding sites and their respective distances through the membrane. This model also shows the suggested Ba^{2+} binding site (green) within the pore as well as the extracellular and intracellular lock in sites and enhancement site occupied with K^+ (red), which is only occupied at high $[K^+]_e$. The crystal structure (B) of the KcsA pore bound with Ba^{2+} and Rubidium (red), acting as a K^+ substitute, confirmed the original model. Modified from Neyton & Miller (1988) (A) and Y. Jiang & R. MacKinnon (2000) (B).

1.4.2 Quinine and Quinidine

Quinine (Figure 1.5.A) and quinidine (Figure 1.5.B) are steroisomers of the same chemical formulae, with similar inhibitory properties at K^+ channels. It has been suggested by previous studies that voltage dependent inhibition of K^+ channels by these compounds occurs due to the protonated form of the drug binding to the intracellular side of the channel (Zhang *et al.*, 1998; Sănchez-Chapula *et al.*, 2003; Tang *et al.*, 2010*b*). The reported differences in affinity such as for the human *ether-a-go-go*-related gene (hERG) K^+ channel that is more strongly inhibited by quinidine than quinine, may be partly due to the differing pKa values of these two compounds (Sănchez-Chapula *et al.*, 2003). As at pH ≈ 7.5, roughly physiological pH, 92.6% of quinidine (pKa, 8.6) is protonated in comparison to 90% of quinine (pKa, 8.5).

The S6 domain of the K^+ channel has been shown to be a major determinant of the characteristics of quinidine and quinine inhibition. Study of mutations in the S6 domain of the HERG K^+ channel have been shown to affect the characteristics of inhibition by quinidine and quinine. In HERG channels block is thought to be due to the aromatic groups of the quinoline π- stacking between the Y652 and F656 residues (Sănchez-Chapula *et al.*, 2003). S6 domain mutations in the rKv1.4 K^+ channel have also been shown to affect the characteristics of quinidine inhibition. Mutation of T529 in the S6 domain to a more hydrophobic residue results in slowing of the rate of deactivation and a negative shift in the voltage dependence of activation of currents. This effect is theorised to be due to the residue at 529, during the open state, faces away from the lumen and faces the other TM α-helices. Thus increasing the hydrophobicity of the residue at 529 stabilises this condition. These mutations in rKv1.4 channels also result in increased quinidine potency, due to quinidine binding by intercalation of the hydrophobic moiety of the compound into the protein interior during the open state (Zhang *et al.*, 1998). The importance of the S6 domain in quinidine potency has also been observed in Kv4.2 channels. In Kv4.2 channels it has been shown that the voltage dependence of quinidine inhibition can be disrupted by minor mutations in the S6 domain. (Caballero *et al.*, 2003).

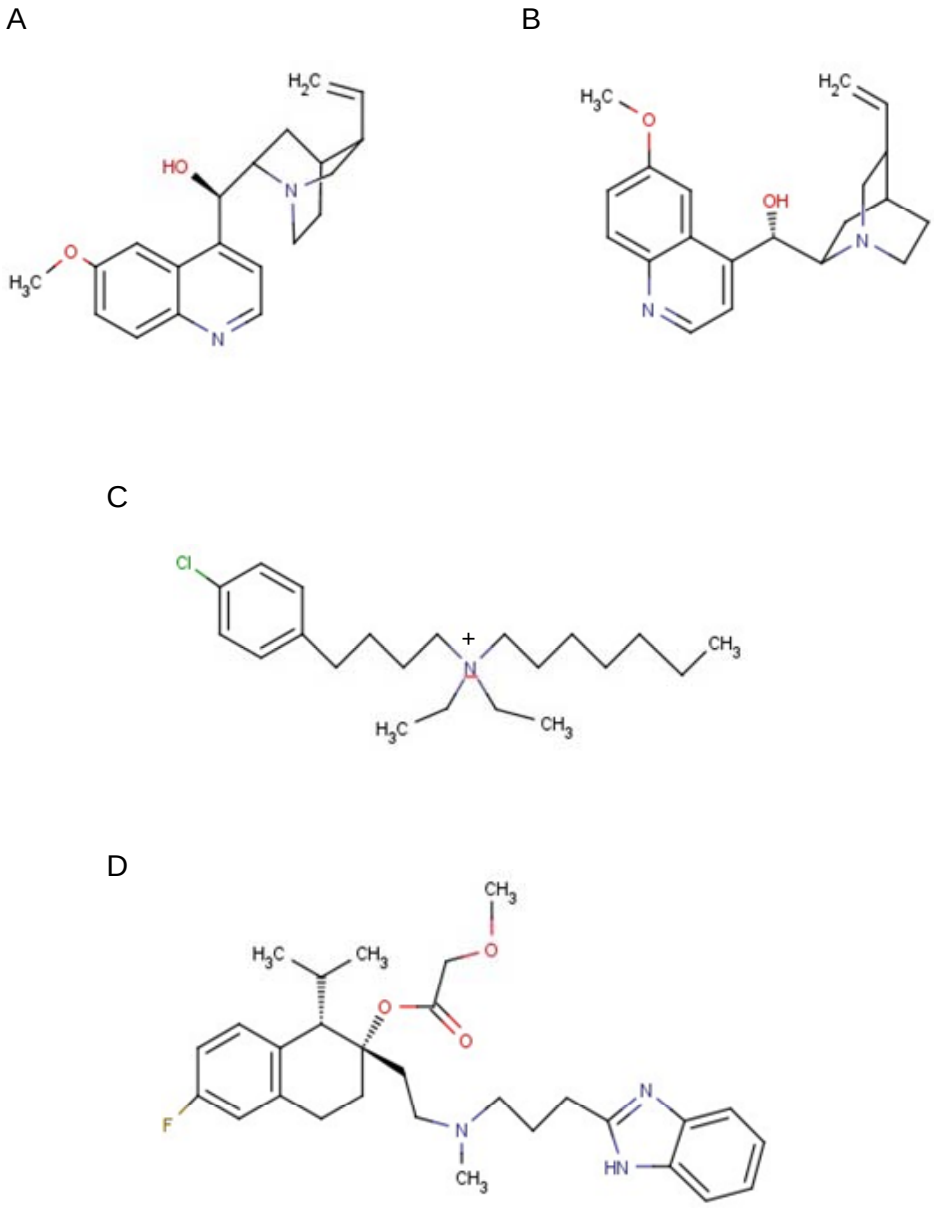

Figure 1.5 Structures of the non-specific K^+ channel inhibitors. Chemical structures of the non- specific K^+ channel inhibitors; quinine (A), quinidine (B), clofilium (C) and mibefradil (D). Chemical structures were drawn using MarvinSketch and coloured with the standard CPK colours (Chemaxon, 2011).

1.4.3 Clofilium

Clofilium (Figure 1.5.C) is a quaternary ammonium compound, which was first described as an antifibrillatory agent that selectively prolonged the cardiac action potential duration and the effective refractory period in canine Purkinje fibers (Steinberg & Molloy, 1979). It is currently thought that clofilium causes open channel block of K^+ channels in a use dependent manner via an "activation trap" mechanism by binding from the intracellular side of the K^+ channel and interacting with the selectivity filter (Steidl & Yool, 2001; Gessner & Heinemann, 2003). However, it has been shown that differing K^+ channels have slightly differing properties with regards to clofilium inhibition. Clofilium has a ≈ 100 fold lower potency for Kv1.5 channels over HERG and hEAG channels, also the onset and recovery of block is faster at Kv1.5 than at HERG/hEAG channels (Steidl & Yool, 2001; Gessner & Heinemann, 2003). This suggests that whilst the binding site for clofilium is conserved, the affinity of the binding site differs from channel to channel possibly due to interactions with the hydrophobic walls of the intracellular entry pathway.

1.4.4 Mibefradil

Mibefradil, originally called Ro 40-5967, (Figure 1.5.D) was originally developed by Roche as a Ca^{2+} channel inhibitor for treatment of hypertension (Osterrieder & Holck, 1989). However, less than ten years after the initial report mibefradil was withdrawn due to the potential for serious drug interactions. Since mibefradil was withdrawn from the market it has been shown to affect a range of voltage gated K^+ channels. K_{ATP} currents from adrenal cells were the first found to be inhibited by mibefradil, at a concentration lower than that required for T-type Ca^{2+} channels. Inhibition of this current is thought to arise through stabilisation of the closed state of the channel in a voltage independent manner (Gomora *et al.*, 1999). However, block of hKv1.5 channels expressed in CHO cells, was found to be voltage dependent and the study suggested that mibefradil blocks the open state of the channel in a use dependent manner (Perchenet & Clément-Chomienne, 2000). Interestingly, intermediate conductance calcium-activated channel ($IK_{Ca}1$) channel currents were affected biphasically by mibefradil application; currents were voltage dependently inhibited by concentrations higher than 5 μM but showed increased current amplitudes if mibefradil concentrations were less than 2 μM. It was suggested that this may be due to low concentrations of mibefradil increasing the sensitivity of the $IK_{Ca}1$ channel for Ca^{2+} (Yoo *et al.*, 2008). These differing effects of mibefradil suggest that whilst mibefradil is able to block a range of K^+ channels the binding site and mechanism of action may not be conserved.

1.5 Slo2.χ channels

1.5.1 Introduction to Slo2.χ channels

The Slo2.χ sub-family of channels were first identified in *Caenorhabditis elegans* from sequence homology with Slo1 and Slo3 channels. Expression of the encoded *C.elegans* Slo2 (cSlo2) protein displayed a channel with synergistic activation by Ca^{2+} and Cl^- with weak voltage dependence, due to the lack of positive charges in the S4 domain, and a single-channel conductance of 110 pS in symmetrical K^+ (Yuan *et al.*, 2000). Soon after the identification of cSlo2, mammalian orthologues were identified in both mouse (mSlo2) and rat (rSlo2), originally called Slack - Sequence like a Ca^{2+} activated K^+ channel. These channels differed from the cSlo2 in that rather than synergistic activation by Ca^{2+} and Cl^- they were instead activated by Na^+ and Cl^- with a unitary conductance of 165 pS, and irreversibly inhibited by Ca^{2+} (Joiner *et al.*, 1998; Yuan *et al.*, 2003). The rSlo2.2 channel had been previously identified as a member of the Slo family of channels when originally cloned, but activation of the channel by Na^+ or Cl^- had not been recognized.

1.5.2 Slo2.χ α-subunit variants

1.5.2.1 Slo2.2b

The rSlo2.2b α-subunit is the archetype of the Slo2.χ family, as this was the initially cloned subunit originally called Slack - Sequence like a Ca^{2+} activated K^+ channel (Joiner *et al.*, 1998). Slo2.2b α-subunits are the "classical" Slo2.2 channels, which have a long N-terminal domain that has little sequence identity to any of the other Slo2.χ family α-subunits. Hydrophilicity plots of the rSlo2.2 indicate that unlike mSlo1, the rSlo2.2 structure has only six TM domains, S1 through S6 (Figure 1.2.D). The lack of an S0 domain means that these α-subunits are unable to interact with Sloβ subunits. Sequence analysis of rSlo2.2 found that this α-subunit also lacks a positively charged S4 domain, believed to act as a component of the voltage sensor in voltage sensitive K^+ channels (1.1.2.2) (Joiner *et al.*, 1998). Surprisingly, it appears that rSlo2.2 mediated currents have weak voltage dependence of activation and outward rectification when expressed in Chinese hamster ovary (CHO) cells (Joiner *et al.*, 1998; Yuan *et al.*, 2000, 2003). Synergistic activation of the rSlo2.2 subunit by chloride is thought to occur through the "chloride bowl", a region of positively charged amino acids in a homologous position to the negatively charged residues in the rSlo1 "Calcium Bowl" (Yuan *et al.*, 2000, 2003). The synergistic activation by sodium of the rSlo2.2 subunit is thought to occur partly through a motif that is similar to those found in

Na^+ sensitive Kir subunits ($Kir_{3.2}$ and $Kir_{3.4}$). The Na^+ sensing domain consists of the region between D818 and H823 in the RCK2 domain of the rSlo2.2 α-subunit. Mutations of these residues in the Na^+ sensing domain reduced but did not abolish Na^+ sensitivity and reduced the ability of Cl^- to activate the channel (Zhang *et al.*, 2010). Slo2.2b channels activate in a biphasic manner, with an instantaneous component followed by a slow time dependent component that takes several hundred milliseconds to reach a level of steady state current (Brown *et al.*, 2008). At the single channel level rSlo2.2b currents have large openings with a single sub-conductance state (Joiner *et al.*, 1998; Bhattacharjee *et al.*, 2003; Brown *et al.*, 2008). rSlo2.2b α-subunits are unique within the Slo2.χ family as these subunits have been shown to form heteromeric channels with other members of the Slo channel family. rSlo2.2b α-subunits have been observed to be able to form functional tetramers with the hSlo1 subunit with distinctive pharmacology and an intermediate conductance (Joiner *et al.*, 1998). In oocytes, rSlo2.2b α-subunits have also been shown to form intermediate conductance channels with rSlo2.1 subunits (Chen *et al.*, 2009).

1.5.2.2 Slo2.2a

The presence of Slo2.2 splice variants was first indicated by the discrepancy between the expression profiles from *in-situ* hybridisation (ISH) and immunohistochemical (IHC) results (1.5.4.1) (Bhattacharjee *et al.*, 2002, 2005). From PCR analysis exon 1a was found approximately 14 kb upstream of the exon previously described to form the amino terminus (exon 1b). Exon 1a encodes a novel N-terminus regulated by a differing promoter, the α-subunit with this sequence was termed, Slo2.2a. A second variant of both rSlo2.2a and rSlo2.2b was also found that was missing exon 2 from the sequence (Slo2.2ax and Slo2.2bx). Compared to the rSlo2.2b α-subunit the rSlo2.2a α-subunits have a shorter N-terminal domain which has a high level of sequence identity (78.1%) to the Slo2.1 N-terminal sequence. The rest of the α-subunit sequence is identical between the two variants. rSlo2.2a channels have distinct electrophysiological characteristics from rSlo2.2b currents. rSlo2.2a whole cell currents activate rapidly in response to a voltage step, in a manner similar to rSlo2.1 channels. However, introduction of the rSlo2.2b N-terminal sequence to Slo2.1α-subunit failed to slow the rate of activation, suggesting that potentially there is N-C terminus communication that mediates this property. At the single channel level rSlo2.2a channels have multiple sub-conductance states whereas rSlo2.2b channels have one main sub-conductance state. rSlo2.2a single channel recordings have a mean open time six-fold shorter than rSlo2.2b due to shorter openings to the fully open state (Brown *et al.*, 2008). The rSlo2.2a and rSlo2.2b α-subunit also differ in their ability to form heteromeric channels with the rSlo2.1 subunit (Chen *et al.*, 2009).

1.5.2.3 Slo2.2m

The last of the Slo2.2 isoforms, Slo2.2m, was discovered at the same time as the Slo2.2a isoform. rSlo2.2m has a unique 1.2 kb 5' sequence directly upstream of exon 3, this is a third unique N-terminal sequence as the S1 domain encoding begins at exon 4. As with rSlo2.2a the rest of the subunit sequence is identical to rSlo2.2b. The electrophysiological properties and the expression profile of rSlo2.2m channels have not been defined (Brown *et al.*, 2008).

1.5.2.4 Slo2.1

The last distinct Slo channel sub family member is rSlo2.1, this sister channel was named Slick - Sequence like an intermediate conductance K^+ channel. The rSlo2.1 α-subunit was discovered as a protein with 74% identity to the rSlo2.2 α-subunit sequence. Like rSlo2.2, the S0 domain and charges in the S4 domain are absent from the rSlo2.1 sequence. The Slo2.1 currents are activated by Na^+/Cl^- but the channel is inhibited by intracellular ATP. As the rSlo2.1 sequence has an ATP binding site motif (GXXXXGKT) subsequent to the RCK2 domain. The sensitivity to the endogenous activators was shown to differ with rSlo2.1 being less sensitive to Na^+ and more sensitive to Cl^- in comparison with rSlo2.2. The rSlo2.1 currents show weak voltage dependence of activation, however, whole cell recordings displayed a faster activation rate compared to rSlo2.2b currents. rSlo2.1 currents were first described as being a functional hybrid between K_{Na} and ATP-sensitive (K_{ATP}) K^+ channels (Bhattacharjee *et al.*, 2003). As discussed later (1.5.4.2) Slo2.1 α-subunits are differentially controlled by endogenous modulators compared to rSlo2.2 subunits (Santi *et al.*, 2006). As mentioned earlier (1.5.2.1) rSlo2.1 α-subunits can form heteromeric channels with the rSlo2.2b, but not the rSlo2.2a, α-subunit. These heteromeric channels have been shown to form intermediate conductance channels in oocytes. From results of co-immunopreciptation techniques performed on rat brain tissue it appears that these heteromeric Slo2.1/Slo2.2b channels are able to be formed *in vivo* (Chen *et al.*, 2009).

1.5.3 Pharmacology of Slo2.χ channels

The class I and IV anti-arrhythmic drugs, quinidine and bepridil (respectively), were originally shown to inhibit K_{Na} currents in cardiac tissue (Mori *et al.*, 1998). Further investigation of the affects of these compounds has determined their full profile against rSlo2.2b channels. Quinidine inhibition of rSlo2.2b appears to be voltage independent. In rSlo2.2b transfected human embryonic kidney (HEK) cells quinidine has an IC_{50} of 89.6 μM. Examination of channel kinetics indicated that quinidine produced a marked and reversible decrease in channel activity. This was due to a decrease in the mean open time of the channel. Bepridil inhibition of rSlo2.2b appears similar to quinidine in that it is also voltage independent and reversible. In transfected HEK cells bepridil was shown to be more potent with an estimated IC_{50} of 1.0 μM. Examination of channel kinetics displayed that bepridil also decreased the mean open time of the channel. These results signify that quinidine and bepridil inhibition has a direct effect on rSlo2.2b, rather than an effect on intracellular Na^+ levels (Yang *et al.*, 2006). rSlo2.2b channels, like some of the voltage gated K^+ channels, have also been shown to be inhibited by forskolin in a cAMP independent manner (Nuwer *et al.*, 2009).

Currently only one non-endogenous activator of rSlo2.2b has been observed; bithionol (1.6), a bis-phenol anti-parasitic compound. Activation by bithionol (EC_{50} = 0.77 μM) showed an interesting characteristic, the weak voltage dependence of the Slo2.2 currents was modified. In the presence of bithionol the activation voltage is shifted to more negative potentials, allowing more channels to be open for a given voltage (Yang *et al.*, 2006). *In vivo* bithionol has also been shown to increase the speed of decay of AMPA induced excitatory postsynaptic current in lamprey spinal neurons by enhancement of a K_{NA} current, resulting in a decreased synaptic response (Nanou *et al.*, 2008). Application of bithionol to MNTB neurons has been shown to enhance the accuracy of timing of action potentials during high frequency firing of the neuron and thus increasing the fidelity of the information encoded (Yang *et al.*, 2007). These studies were either performed solely on rSlo2.2b channels or in native cells, without examination of the possible effects on either rSlo2.2a or rSlo2.1 channels, thus it is unknown if the pharmacology described is distinctive. hSlo2.1 channels have been shown to be activated by niflumic acid (NFA) with an EC_{50} of 2.08 ± 0.04 mM. Whilst the molecular basis of NFA activation of K^+ channels is unknown, the rapidity of activation of hSlo2.1 from extracellular application suggests that the binding site is readily accessible from the extracellular solution (Dai *et al.*, 2010). As with previous pharmacological studies this activator was not tested on any of the other Slo2.χ subunits.

1.5.4 Physiological Relevance of Slo2.χ

1.5.4.1 Expression profile of Slo2.χ channels

It has been difficult to determine separate physiological functions for Slo2.1 and Slo2.2 with regards to mediating the K_{Na} current. This is partially due to the overlap between endogenous activators and the tissue expression pattern of rSlo2.1 and rSlo2.2. K_{Na} currents have been shown to be present in cardiomyocytes (Kameyama *et al.*, 1984; Choisy *et al.*, 2004) and a range of neurons (Dryer, 1994; Bischoff *et al.*, 1998; Yang *et al.*, 2007; Gao *et al.*, 2008). In the rat brain, the expression profile of Slo2.1 and Slo2.2 α-subunits, have been further explored utilizing *in-situ* hybridization (ISH) and immunohistochemical (IHC) methods (Bhattacharjee *et al.*, 2002, 2005). These methods showed wide-spread and overlapping expression of the Slo2.χ channels throughout the brain (Table 1). IHC staining of the Slo2.2 channel showed relatively high protein levels in the olfactory bulb, midbrain and brainstem. IHC staining conflicted with the ISH results in regions such as the piriform cortex, ventral cochlear nucleus, CA3 of the hippocampus, and cerebellar nuclei (Bhattacharjee *et al.*, 2002). However, this discrepancy was due to the epitope chosen for the original anti-Slo2.2 antibody, the first 15 amino acids of the N-terminus. This region of the protein is now known to be a site of variation due to splice variants (1.5.2.1) (Brown *et al.*, 2008).

Brain region	Slo2.1		Slo2.2	
	In situ hybridization	Immunocytochemisty	*In situ* hybridization	Immunocytochemisty
Olfactory bulb	++++	++++	N/A	++
Cerebral cortex	+++	+++	++	+
Frontal cortex	++	++	++	++
Piriform cortex	+++	+++	++	-
Hypothalamus	++	+++	N/A	N/A
Hippocampus				
CA1	++++	++++	-	-
CA2	++++	+++	-	-
CA3	++++	+++	++++	+
Dentate gyrus	++++	+++	+	+
Habenula	++++	++	++	+
Thalamus	++	++	++	+++
Substantia nigra	++	+++	+++	+++
Red nucleus	+++	+++	+++	++++
Oculomotor nucleus	+++	+++	+++	++++
Trapezoid nucleus	+++	+++	++++	++++
Cerebellar nuclei	+++	+++	+++	+/-
Motor trigeminal	++	++	+++	+++
Facial nucleus	+++	+++	N/A	+++
Ventral cochlear nucleus	++	+++	+++	+/-

Table 1.1: Slo2.χ expression patterns in the rat brain. The number of (+) indicates the relative level of expression, (-) indicates no expression and N/A indicates region was not interrogated. Modified from (Bhattacharjee *et al.*, 2002, 2005).

1.5.4.2 Physiological modulators of Slo2.χ channels

Neurons, *in vivo*, do not express Slo2.χ channels in isolation. Slo2.χ channels have been shown to be targets of modulation by Gαq-protein coupled receptors (GqPCR). Slo2.1 has been shown to be inhibited in cardiac myocytes by activation of α_{1A} adrenoceptors. This modulation was shown to be a PLC independent pathway, as the addition of PLC inhibitors failed to change the effect of phenylephrine on these cells (Choisy *et al.*, 2004). Similar inhibition has also been shown in rat striatal cholinergic neurons, with activation of mGluR1/5 providing the inhibitory stimulus. Inhibition of Slo2.1 was not the main target for modulation in these cells, except under heavy firing conditions (when Na^+ was sufficient) or during ischaemia (Berg *et al.*, 2007). Interestingly it was shown by Santi *et al.*, (2006) that whilst Slo2.1 is inhibited by GqPCR activation, Slo2.2 mediated currents were enhanced. This inverse modulation was dependent on protein kinase C (PKC) activation. Application of 60 nM phorbol 12-myristate 13-acetate (PMA), a PKC activator, caused a reduction of approximately 90% in the Slo2.1 mediated currents. 160 nM PMA was found to increase Slo2.2 mediated currents by approximately five fold. Further investigation of PKC regulation demonstrated that Slo2.1 had an IC_{50} of 20 nM, whereas Slo2.2 had an EC_{50} of 50 nM for PMA. This differential regulation was found to be dependent on the C-terminal tails, as Slo2.1 has several unique PKC phosphorylation sites. The physiological significance of this contrary effect of PKC activation by GqPCRs on Slo2.χ has yet to be determined (Santi *et al.*, 2006).

Unlike PKC, protein kinase A (PKA) does not directly modulate Slo2.2 currents; as neither application of 8Br-cAMP nor PKA catalytic subunit had effects on the electrophysiological characteristics of the heterologously expressed rSlo2.2 channels (Nuwer *et al.*, 2009). However, it has been shown that PKA activation in dorsal root ganglion (DRG) neurons causes a reduction in the K_{Na} component of the K^+ current. This reduction in K_{Na} component has been shown to be, at least in part, to internalisation of Slo2.2 subunits in a PKA dependent manner (Nuwer *et al.*, 2010). The rSlo2.2b channel has been determined to be activated by the Fragile X mental retardation protein (FMRP) in a reversible manner. FRMP increases the number of channels openings, but reduce the openings to subconductance states. The interaction of FRMP is thought to be through the C-terminal domain of rSlo2.2b between amino acids 804-1237. These findings suggest that some of the neuronal abnormalities observed in Fragile X syndrome may be due to the effects on K_{Na} currents resulting in altered firing patterns (Brown *et al.*, 2010).

Slo2.2 has been shown to be activated directly by 17β-estradiol (E2). It was shown that 10 μM E2 increased the P_o of Slo2.2 from 0.035 to 0.32. This effect was theorized to be possibly due to enhanced phosphorylation, concurrent with GqPCR activation of the channel. Whilst 10 μM exceeds the observed plasma concentration, localized tissue concentrations may surpass global concentrations (Zhang *et al.*, 2005). The effect of high levels of E2 suggests Slo2.χ may contribute neuroprotection in response to estradiol during ischemic conditions (reviewed in (Amantea *et al.*, 2005)). Slo2.2 has also been shown to be modulated by other factors that are characteristic of ischaemia and hypoxia, namely pH and intracellular CO_2. Reduction of pH was observed to reduce the number of openings (NP_o) in a dose-dependent manner. This inhibition was partially reversible on return to pH 7.3, and was attenuated by high intracellular Na^+. An increase in intracellular CO_2 was also shown to have a similar inhibitory affect, although this is probably due to a concurrent drop in pH. Thus under ischemic/hypoxic conditions Slo2.2 activity is modulated by conflicting factors, increased Na^+ and decreased pH (Ruffin *et al.*, 2008).

1.5.4.3 Known physiological functions of Slo2.χ channels in neurons

Slo2.χ channels appear to have a variety of physiological functions depending on cell type and differing $[Na]_i$ levels in subcellular localisations. Three major functional roles of Slo2.χ channels in neurons have been reported, in the depolarizing after-potential, spike frequency timing and establishment of the RMP. There was initially disagreement in the literature as to involvement of K_{Na} currents in mediating the depolarizing after-potential. This was due to initial studies finding the EC_{50}'s for Na^+ of ≈40 mM (rSlo2.2) and ≈80 mM (rSlo2.1), both of which are greater than the reported resting $[Na^+]_i$ in neurons (4-15 mM). However, further studies have found that in the presence of NAD^+ the EC_{50} is shifted to ≈20 mM $[Na^+]_i$, near the physiological range (Tamsett *et al.*, 2009). Secondly Slo2.χ channels are assumed to co-localise with Na^+ channels (Dryer, 1994), and have been shown to co-localise with AMPA receptors (Nanou *et al.*, 2008), thus localised $[Na^+]_i$ may be higher than in the whole cell. This co-localisation is probably due to both Slo2 and GluR1 subunits containing PDZ binding domains. PDZ binding domains allow these channels to bind to the scaffolding protein postsynaptic density-95 (PSD-95), which have three PDZ domains, and scaffolds proteins at excitatory postsynaptic membranes (Hayashi *et al.*, 2000; Uchino *et al.*, 2003). In rat medium-diameter (25-35 μm) DRG neurons and CA1 pyramidal cells, Slo2.χ channels have been shown to be able to mediate the depolarizing after-potential of single action potentials (Gao *et al.*, 2008). In cells isolated from the olfactory bulb and striatum, it has been shown that Slo2.2 channels mediate a large delayed outward current. This current was found to be controlled by a TTX sensitive persistent inward Na^+ current (Budelli *et al.*,

2009). It has been shown that in Kv1.3 KO mice, the K_{Na} current is up-regulated in olfactory neurons; this is thought to be a compensatory mechanism to allow some control of spike timing (Lu *et al.*, 2010).

Interestingly whereas in rat it appears both Slo2.1 and Slo2.2 contribute to spinal cord K_{Na}, it has been shown in lamprey spinal cord to be mediated solely by Slo2.2. In lamprey spinal cord neurons, the role is slightly different; Slo2.2 mediates part of the slow afterhyperpolarisation (sAHP). The contribution of this channel is increased under high frequency firing of the neuron. This is theorised to be a safety mechanism to ensure frequency regulation (Wallén *et al.*, 2007). This physiological function has also been determined for Slo2.χ in the medial nucleus of the trapezoid body (MNTB) in the auditory brainstem. In the MNTB increasing K_{Na} augments the accuracy of timing of action potentials at high frequency firing of the neuron. This in turn increases the fidelity of the information encoded (Yang *et al.*, 2007). Bischoff *et al.*, (1998) concluded that the K_{Na} current, mediated by Slo2.χ channels, contribute to the establishment of RMP in physiological conditions and have a secondary role of stabilizing the neuron under pathophysiolgical conditions such as hypoxia. This conclusion may have been due to the cell type observed in the study, rat small-diameter (20-25 μm) DRG neurons. Small DRG neurons have an action potential frequency of 0.5-2 Hz, under physiological conditions, approximately 15-fold too low to cause a high localised Na^+ concentration to activate K_{Na} currents. Secondly small DRG neurons lack the anatomical architecture to facilitate Na^+ accumulation such as the node of Ranvier or an axon hillock with a high density of Na^+ channels (Bischoff *et al.*, 1998). It has been suggested that K_{Na} have a role in the mediation of inflammatory pain by DRG neurons. PKA activation has shown to be critical to mediation of inflammatory pain (Malmberg *et al.*, 1997). Thus the PKA dependent internalization of Slo2.2 is thought to play a part in causing the hyper-excitability characteristic of nociceptive firing (Nuwer *et al.*, 2010).

1.6 Bithionol

Bithionol is a bis-phenol anti-parasitic compound, originally used in antibacterial soaps (Hopper & Wood, 1958). At the molecular level bithionol has been shown to inhibit the glutamate dehydrogenase enzyme (GDH). GDH, with NAD^+ or $NADP^+$ as a cofactor, catalyzes the deamination of L-glutamate to 2-oxogluterate which is then fed into the Krebs cycle. Bithionol molecules bind as a pair to the GDH protein in the cleft between the neighbouring subunit dimers of the hexamer preventing the expansion and contraction of the enzymatic cleft and thus stopping the reaction (Li *et al.*, 2009). The only K^+ channel shown to be affected by bithionol application is the K_{Na} current mediating channel, rSlo2.2b (1.4.2) (Yang *et al.*, 2006).

1.7 Primary aims of the Thesis

This thesis has three main aims; firstly in Chapter III to investigate if mSlo3 currents in oocytes share pharmacological properties with the I_{KSper} current in spermatocytes described by Navarro *et al.* (2007). We hypothesise that mSlo3 channels may underlie a component of I_{KSper}, due to similar electrophysiological properties and range of pH sensitivity. I_{KSper} is a critical component of the capacitation reaction (1.3.4.2), causing hyperpolarisation of the membrane in turn increasing the driving force of Ca^{2+} entry via CatSper channels. Recent Slo3 KO mice studies were found to have a reduced I_{KSper} current in spermatozoa, resulting in infertile spermatozoa (Santi *et al.*, 2010; Zeng *et al.*, 2011). However, KO models often result in down-regulation of unintended targets or up-regulation of compensatory mechanisms. Confirmation of the effects of the I_{KSper} inhibitors on mSlo3 channel will strengthen the case that the mSlo3 channel mediates part of the I_{KSper} current. A recent chimaera of mSlo3/Slo1 (MC13) has been shown to share some of the I_{KSper} pharmacological profile but this has not been tested on the WT mSlo3 channel (Tang *et al.*, 2010*b*). Due to the overlap in pharmacology, sensitivity of mSlo3 channels to the I_{KSper} inhibitors will also suggest that mSlo3 currents are a component of the K^+ current involved in motility and volume regulation.

The second aim of this thesis, described in Chapter IV, is to determine if a range of expressed sequence tags (EST's) encode a novel isoform of the mSlo3 α-subunit. A range of EST's have been identified in a range of tissues, particularly neuronal tissue, which correspond to the mSlo3 sequence. This is potentially an exciting find as previous studies have shown mSlo3 α-subunit expression is limited to the testis and spermatozoa, which is

contrasted by the ubiquitous expression of the related mSlo1 α-subunit (Schreiber *et al.*, 1998).

The third aim of the thesis is to characterise hSlo2.2a currents with respect to their sensitivity to intracellular NaCl and I/V relationships, from heterologous expression in HEK cells (Chapter V). The majority of studies of the Slo2 sub-family have been performed using the rat homologues of these channels. However no study has examined the human Slo2.2a and Slo2.1 of these channels. The human homologues have the more K^+ selective GYG selectivity filter sequence in the pore domain rather than the GFG sequence found in rat. This chapter also aims to determine if bithionol, which is known to activate rSlo2.2b channels, also activates the hSlo2.2 and hSlo2.1 channels. The specificity of bithionol activation will be tested by application to the endogenous Kv K^+ channels of HEK cells and the pancreatic type K_{ATP} channels of 832/13 INS cells. Lastly, the thesis aims to examine the effects of bithionol activation of endogenous K_{Na} currents from *ex vivo* rat DRG cells.

Chapter II: Methods

2.1 General molecular biology

The methods that are described in this section were used for the construction and subcloning of constructs. Further details of the general molecular biology methods can be found in Molecular Cloning: A Laboratory Manual (3rd Edition) (Sambrook & Russell, 2000).

2.1.1 Materials

A) Chemicals and reagents

All chemicals were purchased from Sigma Chemical Company and VWR (BDH) unless stated otherwise. Bacterial growth media were purchased from BD Biosciences (Difco) and Oxoid. Distilled water was used for preparation of growth media. Sterile nuclease free water (Sigma) was used for DNA/RNA application solutions. Oligonucleotide primers were purchased from Invitrogen. *Pfu* Turbo DNA polymerase was purchased from Stratagene; Phusion DNA polymerase was from Finnzymes; all other DNA modifying enzymes were purchased from New England Biolabs.

B) Plasmids (source/donor)

For cRNA production:

pBF-KCNMA3: a 6.3 kb plasmid, which contains a sequence that confers ampicillin resistance in *E. coli*. A cDNA encoding the full length α-subunit of mSlo3 was cloned downstream of the SP6 promoter (Lippiat).

pBF-KCNMA1: 6.5 kb plasmid, containing an gene that confers ampicillin resistance in *E. coli*. A cDNA encoding a the full length α-subunit of hSlo1 was cloned downstream of the SP6 promoter (Lippiat).

pYX-Asc-CV562866: 2.4 kb plasmid, containing an gene that confers ampicillin resistance in *E. coli*. A cDNA encoding the CV562866 fragment was cloned downstream of the T7 promoter (Genbank).

For mammalian expression:

pcDNA6-hSlo2.2-EGFP: 9.5 kb plasmid, which contains a gene that confers ampicillin resistance in *E. coli.* The cDNA encodes the full length α-subunit of hSlo2.2a, which is tagged at the C-terminus with GFP to allow verification of transfection efficiency and subcellular localisation (Lippiat).

pcDNA6-hSlo2.1: 9.4 kb plasmid, which contains a gene that confers ampicillin resistance in *E. coli.* The cDNA encodes the full length α-subunit of hSlo2.1 (Lippiat).

pEGFP: 4.7 kb plasmid, which contains a gene that confers kanmycin resistance in *E. coli.* The cDNA encodes EGFP to allow verification of transfection efficiency (Lippiat).

pcDNA6-hSlo2.1-RFP: 9.4 kb plasmid, which contains a gene that confers ampicillin resistance in *E. coli.* The cDNA encodes the full length α-subunit of hSlo2.1, tagged at the C-terminus with RFP to allow verification of transfection efficiency and subcellular localisation (Newson/Lippiat).

C) Bacterial growth media

SOB Medium: 2 % (w/v) bactotryptone, 0.5 % (w/v) yeast extract, 10 mM NaCl, 2.5 mM KCl, adjusted to pH 7.0 with NaOH. The after cooling the medium was supplemented with sterile 10 mM $MgCl_2$

LB: Lysogeny broth 1X (Sigma)

LB agar: Lysogeny broth agar 1X (Sigma)

(All media was autoclaved)

D) Antibiotics and media supplements

Ampicillin (1000x): 100 mg/ml ampicillin salt in H_2O.

Kanamycin (1000x): 30 mg/ml kanamycin sulphate in H_2O.

(All aqueous solutions were filter sterilised using a 0.22 μm filter)

E) Solutions required for preparation of DNA

TE buffer (100x): 1 M Tris.Cl (tris(hydroxymethyl)aminomethane hydrochloride), pH 8.0, 0.1 M EDTA (ethylenediaminetetraacetic acid)

TAE (50x): 2 M Tris.Cl pH 8.5, 50 mM EDTA, 1.2 % acetic acid

EtBr: 10 mg/ml ethidium bromide in H_2O.

F) Solutions for PCR

dNTPs: 2 mM dATP, 2 mM dCTP, 2 mM dGTP, 2 mM dTTP, in sterile H_2O.

***Pfu* buffer (10x):** 100 mM KCl, 100 mM $(NH_4)_2SO_4$, 200 mM Tris.Cl pH 8.8, 20 mM $MgSO_4$, 1 % Triton X-100, 1 mg/ml nuclease-free bovine serum albumin (Stratagene)

2.1.2 Site-directed mutagenesis

Site-directed mutagenesis is a non-exponential PCR based method that is a useful tool for introduction/reversion of point mutations, and deletion or insertion of small nucleotide sequences (up to approximately 20 nucleotides). The primers were designed for the Stratagene Quikchange site-directed mutagenesis kit. Complementary forward and reverse primers were designed to contain the desired sequence and flanking sequence; with Tm values of ~75 ºC. The primers were diluted to 2 pmole/µl and added to a PCR reaction mixture containing 1x *Pfu* buffer, 0.2 mM dNTPs, 5 % glycerol, 50 ng template plasmid DNA, 1 U *Pfu* Turbo DNA polymerase, in H_2O, to a final reaction volume of 50 µl. The PCR protocol required an initial denaturing step at 95 ºC for 30 seconds, followed by repeating cycles (x 16) of 95 ºC for 30 s, 55 ºC for 1 min, 68 ºC for ~1 min per 500 bp, with a final extension step of 68 ºC for 7 min. The reaction mixture was then incubated with 20 U of *Dpn*I endonuclease for 1 hr at 37 ºC to specifically remove the methylated template plasmid DNA, prior to transformation of the PCR product into cells. The presence of the mutation was determined by transforming sequences into *E.coli* (2.1.8) and DNA sequencing of plasmid DNA isolated from the transformants (2.1.9).

2.1.3 Rapid Amplification of cDNA Ends (RACE)

RACE PCR is a technique that allows cloning of full length RNA transcripts, converted to cDNA, found within a cell from short sequences, such as expressed sequence tags (EST). Primers were designed using NCBI primer blast design software (www.ncbi.nlm.nih.gov) utilising the mSlo3 WT related EST sequence identified in a cDNA library from mouse head, GenBank Acc: CV562866, (2.1.1b). All 50 µl PCR reactions had the following composition (µl) ; H_2O 35.5, Buffer HF 10, dNTP 1, cDNA template 1, forward primer 1, reverse primer 1, Phusion polymerase (Finnzymes) 0.5. Marathon RACE PCR was performed using mouse brain Marathon-ready™ cDNA (Clontech) to isolate the potential neuronal isoform. Marathon-ready™ cDNA is double stranded cDNA made from mRNA isolated from male/female mice brains, aged 8-12 weeks. The cDNA is supplied ligated to the marathon adaptor at both the 5' and 3' end. First round PCR was performed under conditions described in Table 2.1, with CVstart/CVend run against Adaptor Primer (AP) 1.

The APs are targeted to the adapter ligated to all the ds-cDNA sequences in the sample. The products of these reactions were used as template for second round (nested) PCR, the EST specific internal CVF*/CVR* against AP2, targeted to the inner adapter. Second round products were then cleaned (2.1.6) and then ligated (2.1.4) for amplification.

	First Round PCR			Second Round PCR		
Phase	Temperature (^{O}C)	Time (s)	Number of cycles	Temperature (^{O}C)	Time (s)	Number of cycles
Initial Denaturation	98	30	1	98	30	1
Denaturation	98	7	35	98	7	35
Annealing	68	20		62±6	20	
Extension	72	45		72	30	
Final Extension	72	300	1	72	300	1

Table 2.1: Marathon RACE PCR Conditions

2.1.4 Blunt End Ligation of DNA

The ligation of DNA requires a specific enzyme, DNA ligase, which is capable of covalently joining DNA ends by catalysis of ATP dependent formation of phosphodiester bonds between the 3' hydroxyl and 5'phosphate termini. The StrataClone Blunt PCR Cloning Kit (Stratagene) for ligation of RACE PCR products (2.1.3) into plasmids to allow transformation and sequencing (2.1.8-10) was used. Products were ligated into the kit plasmid, pSC-B-amp/kan, as specified by the manufacturer. The kit vector mix contains two blunt ended DNA strands; these have toperisomerase I charged arms, either side of the insert site. After the 5 minute ligation reaction the DNA-enzyme intermediate can be transformed into the supplied competent cells (2.1.8). The intermediate is then circularised by the Cre-recombinase enzyme in the supplied competent cells, which recognises the *lox-P* site at the opposing end of the vector.

2.1.5 Endonuclease digestion of DNA

Restriction-endonuclease enzymes bind specific DNA sequence motifs and catalyse hydrolysis of a specific phosphodiester bond resulting in fragmentation of DNA molecules. Enzymatic digest of samples was used for restriction analysis of plasmid DNA. Digestion of DNA was typically accomplished by ≈10 U of endonuclease per reaction and in the presence of the recommended buffer, diluted to the required concentration with H_2O. Reactions were incubated at the optimal temperature (normally 37 ^oC) for 1 to 16 hrs, depending on DNA concentration and enzyme activity.

2.1.6 Purification of DNA fragments from reaction mixtures

The purification of DNA from reaction mixtures such as PCR or restriction-endonuclease digests that contain unwanted DNA, enzymes and chemical contaminants is necessary in preparation for subsequent cloning steps. Extraction of DNA from a heterogeneous mixture of different sized fragments required size separation by agarose gel electrophoresis. Homogeneous mixtures, where only one DNA fragment was present, were purified directly from the reaction mixture. Purification was performed using a QIAEX II Gel Extraction Kit (Qiagen) following the kit instructions.

The reaction mixture was separated by agarose gel electrophoresis, using either 1 % or 2% agarose gels. Electrophoresis was conducted in fresh 1x TAE buffer to prevent contamination, at 60 V for 90 min (dependent on fragment size and agarose percentage). The DNA band of interest was excised using a cleaned/fresh scalpel, from the gel under low-level UV transillumination. Approximately 600 µl QX1 buffer, 3 volumes to 1 volume of gel, was added to the gel section containing the DNA band of interest. The reaction mixture was supplemented with 20 µl QIAEX II, which was resuspended by vortexing before addition. This mixture was then incubated at 50 ^oC for 10 mins, with agitation by vortexing every two minutes. Once the agarose was solubilised, the sample was centrifuged, and the supernatant removed. The pellet was then washed first with QX1 then twice with buffer PE. The pellet was then air-dried by centrifugation at 2000 rpm for ≈12 minutes. DNA was then eluted from the QIAEX II glass milk pellet, by resuspension in 20 µl RNA-free water; this mixture was then incubated for 5 minutes and centrifuged. The supernatant was then pipetted into a fresh microcentifuge tube and stored at -20 ^oC for later use.

2.1.7 Agarose gel electrophoresis

Agarose gel electrophoresis was used to differentiate DNA samples by molecular weight. DNA was detected by staining with ethidium bromide (EtBr) and visualised under UV light. Usually, agarose gels consisted of 1 or 2 % agarose in 1x TAE buffer, supplemented with 0.5 µg/ml EtBr. The gel was placed in a horizontal electrophoresis tank and submerged in 1x TAE buffer. The DNA sample was mixed with either 5x/6x loading buffer and loaded into a well on the gel. Into a parallel well DNA ladder, Hyperladder^{TM} I (Bioline), was loaded for size and concentration estimation of fragments in the sample DNA. The electrophorisis protocols typically consisted: 90 V for 30 min for standard 1 % gels; and 60-70 V for 1-1.5 hrs for 2% gels.

2.1.8 Transformation of competent *E. coli*

Competent *E. coli* (20-50 µl of cell suspension) were gently mixed with the DNA to be transformed (typically 2-5 µl). Following incubation for 30 min on ice, the cell mixture was heat-shocked at 42 ºC for 45 s and returned to ice. The cell mixture was diluted in LB-broth (500 µl) and for kanamycin selective samples, incubated at 37 ºC in a shaking incubator (200 rpm.) for 1 hour. A portion of the diluted cell mixture (75-100 µl) was spread on a LB agar plate supplemented with a selective antibiotic and incubated overnight at 37 ºC.

2.1.9 Purification of plasmid DNA from *E. coli*

Plasmid DNA was purified from *E. coli* using the alkali-lysis method with a MiniPrep Spin Kit (Qiagen). This involved lysis of the cells with NaOH/SDS, precipitation of SDS coated cell components including chromosomal DNA. This renders the super-coiled plasmid DNA soluble. The super-coiled DNA is then immobilised, de-salted by alcohol precipitation and eluted in sterile water. Colonies picked from LB Agar plates were used to inoculate 2-5 ml of LB broth (supplemented with the selective antibiotic corresponding to plasmid) and incubated for 9 hours/overnight at 37 ºC in a shaking incubator (200 rpm). Cells were harvested in 1.5 ml microcentrifuge tubes and the MiniPrep Spin Kit (Qiagen) instructions were followed.

2.1.10 DNA sequencing

Automated dye-terminated DNA sequencing services were provided by either FBS sequencing services or GATC (GATC Biotech AG). Sequencing primers were either supplied as part of the sequencing service or custom designed (Tm 60-65 ºC). The sequencing window was typically +20 nucleotides downstream of the primer site, up to +500-600 nucleotides, prior to degeneration of the sequencing reaction.

2.2 General protein methods

2.2.1 Materials and reagents

Chemicals and solutions as used in previous sections, unless stated otherwise.

2.2.2 Preparation of Protein Samples

A) Solutions

Homogenisation Buffer: 50 mM Tris-HCl pH 8.0, 100 mM KCl, 1 mM EDTA

Lysis Buffer: 50 mM Tris-HCl pH 8.0, 100 mM KCl, 1 mM EDTA, 1% Triton X-100

Sample Buffer: 0.5 M Tris, 2% Glycerol, 4% 10% SDS, 0.05% Bromophenol blue, 1% H_2O

B) Homogenisation

Homogenisation buffer was aliquoted to 10 mls and supplemented with protease inhibitors (Roche). Tissue samples were retrieved from adult rats *post mortem* (all procedures were carried out in accordance with current UK Home Office requirements), samples were frozen at the point of retrieval with liquid nitrogen. Samples were then placed on ice, following which they were diced using a clean scalpel blade. After dicing, samples were placed in 5 mls of homogenisation buffer and mechanically homogenised using a glass homogeniser. Samples were centrifuged to remove cell debris for 13000 rpm at 4 ^{O}C for 15 mins.

C) Separation of Membrane Fractions

After centrifugation the cell lysate was recovered into an ultracentrifuge tube; tubes were then balanced. Ultracentrifugation was performed using a Beckman TLA120.2 rotor and ultracentrifuged at 55 krpm at 4 ^{O}C for 1 hour. Ultracentrifuged supernatant was isolated and stored. The membrane pellet was resuspended in lysis buffer and transferred to a clean microcentrifuge tube for storage. Before running on gels (2.2.4) samples were diluted with 2x sample buffer supplemented with 2% β-mercaptoethanol

2.2.3 The BCA assay

A) Solutions

Reagent mix: 1 volume of 4% (w/v) $CuSO_4$, 50 volumes of Bicinchoninic acid (BCA) solution

BSA standards: 0.2, 0.4, 0.6, 0.8 or 1.0 mg/ml bovine serum albumin (BSA) made up in identical buffer as relevant protein sample

B) The assay

The reduction of Cu^{2+} by peptide bonds in an alkaline environment results in the generation of Cu^{1+} ions. Cu^{1+} ions are chelated by BCA in a 1:2 ratio; this reaction results in production of a purple coloured product. Protein concentration of the sample was measured by mixing a 10 µl with 200 µl of reagent mix in a flat bottomed 96-well plate. The plate was incubated for 30 mins at 37 ^{O}C, and then absorbance at λ 570 nm was measured on an automated plate-reader. Protein concentration was determined from the OD_{570nm} using a BSA protein standard concentration curve.

2.2.4 SDS-PAGE

A) Solutions

Resolving Gel: 3 mls 30% Acrylamide/bisacrylamide, 2.5 mls 1.5M Tris.Cl pH8.8, 0.1 mls 10% SDS, 0.1 mls 20% Ammonium persulphate (APS), 0.005 mls Tetramethylethylenediamine (TEMED), 4 mls H_2O

Stacking Gel: 0.85 mls 30% Acrylamide/bisacrylamide, 0.625 mls 1.5 M Tris.Cl pH6.8, 0.05 mls 10% SDS, 0.05 mls 20% Ammonium persulphate (APS), 0.005 mls TEMED, 3.4 mls H_2O

B) Production of Polyacrylamide gels

10% resolving gels were formulated as described above. TEMED component was added lastly before pouring the gel. After pouring, the exposed gel surface was covered with butanol to avoid oxygen inhibition of acrylamide crosslinking. After ~30mins the butanol layer was poured off and stacking gel made up as described in 2.2.4.A and added to the gel, and a lane comb inserted to form the wells. After ~30 minutes either the lane comb was removed and the gel used immediately, or the gel was stored at 4 ^{O}C overnight in a moist environment.

C) Electrophoresis

Proteins were separated by electrophoresis in 25 mM Tris, 192 mM glycine, 0.1 % (w/v) SDS, pH~ 8.3 (running buffer). Protein size was estimated using the PageRuler^{TM} plus prestained protein ladder that covers the kDa 11-250 molecular weight (Mw) range. Electrophoresis was carried out in a Bio-Rad Protean III tank, which were assembled according to manufactures instructions. The electrophoresis control box (Bio-Rad PowerPac) was programmed for 180 mV, for 50 min, until the dye front nearly reached the bottom of the gel.

2.2.5 Western blotting

A) Solutions and antibodies

Transfer Buffer: 25 mM Tris, 192 mM glycine, 20 % (v/v) MeOH, 0.1 % (w/v) SDS

PBS-T: PBS pH 8.0, 20 % Tween-20

Blocking buffer: PBS-T, 5 % low-fat skimmed milk powder

Antibody incubation buffer: PBS-T, 0.5 % low-fat skimmed milk powder

Rat anti-Slo3 high-affinity primary antibody (Neuro-Mab): 1:1000 dilution

Goat anti-mouse HRP-conjugated secondary antibody (Bio-Rad): 1:50000 dilution

B) Western transfer of proteins onto nitrocellulose membrane

After SDS-PAGE, gels to be western blotted were incubated in ice cold transfer buffer for approximately 5 min. The gel was then placed in good contact with a pre-soaked Hybond^{TM} nitrocellulose membrane (GE healthcare), sandwiched between blotting paper and thin card (soaked in transfer buffer), and placed in the semi-dry transfer apparatus (Bio-Rad). A current of 0.3-0.6 mA was applied for an hour to transfer the proteins from the gel onto the nitrocellulose membrane.

C) Immunoblotting of nitrocellulose membrane

Post transfer, the nitrocellulose membrane was first washed three times with PBS-T for an hour to remove any residual methanol. After washing, the membrane was incubated in blocking buffer for an hour with agitation at room temperature. The membrane was washed in PBS-T for an hour. The membrane was then incubated in the Slo3 antibody incubation buffer with gentle agitation overnight at 4 °C. The primary antibody was discarded and the membrane was washed three times in PBS-T for a total of an hour, and incubated in HRP-conjugated secondary antibody, at room temperature for an hour with agitation. Finally, the membrane was washed three times for a total of an hour, prior to chemiluminescence.

D) Visualisation of immunoblotted protein bands by enhanced chemiluminescence (ECL)

The membranes were transferred from PBS-T to a glass plate and excess PBS-T wiped away. The surface of the membrane was evenly covered with 0.6 ml SuperSignal West Femto Chemiluminescence (Thermo). These substrates consist of two components: luminol and peroxide buffer. The components were mixed in equal volumes (0.3 ml of each), and the membrane incubated in the solution for approximately 1 min in the dark at RT. The membrane was then drained of excess fluid, excess SuperSignal wiped away, and wrapped in cling film. Under dark room conditions, the membrane was exposed to Biomax XAR film (Kodak) for between 10 s and 10 min. The film was then developed, fixed (Kodak), rinsed in water, and allowed to dry.

2.3 Heterologous expression in *X. laevis* oocytes

2.3.1 Materials and reagents

As in previous sections, except for the following:

A) General solutions

Anaesthetic: 0.2 % (w/v) Tricaine mesylate (MS222), pH 7.5 by addition of Tris Base powder

OR-Mg: NaCl 82 mM, KCl 2 mM, $MgCl_2$ 20 mM, HEPES 5 mM, pH 7.5

ND-96: NaCl 96 mM, KCl 2 mM, $MgCl_2$ 1 mM, HEPES 5 mM, $CaCl_2$ 1.8 mM, pH 7.5, 50 μg/ml G418

Barths (modified): NaCl 84 mM, KCl 1 mM, $NaHCO_3$ 2.4 mM, $MgSO_4$ 0.82 mM, $CaCl_2$ 0.41 mM, $Ca(NO_3)_2$ 0.33 mM, HEPES 5 mM, pH 7.4. Supplemented with 100 IU/ml penicillin/streptomycin, 2 mM pyruvate and 50 mg/ml genatmycin

F304Y Barths (modified): NaCl 84 mM, KCl 23 mM, $NaHCO_3$ 2.4 mM, $MgCl_2$ 0.82 mM, $CaCl_2$ 0.41 mM, $Ca(NO_3)_2$ 0.33 mM , HEPES 5 mM and pH 7.4. Supplemented with 100 IU/ml penicillin/streptomycin, 2 mM pyruvate and 50 mg/ml genatmycin

Ringer's solution: NaCl 115 mM, KCl 2.5 mM, $CaCl_2$ 1.8 mM, HEPES 10 mM, pH 7.2

High K^+ solution: NaCl 17.5 mM, KCl 100 mM, $CaCl_2$ 1.8 mM, HEPES 10 mM, pH 7.2

B) Inhibitor Stock Solutions

Quinine: 500 mM in DMSO

Clofilium: 9.8 mM in Ringer's Solution (10mg in 2ml)

Mibefradil: 8.79 mM in Ringer's Solution (5mg in 1ml)

Quinidine: 250 mM in DMSO

Barium: 1 M in Ringer's or High K^+ Solution

2.3.2 Synthesis of cRNA

The *in vitro* synthesis of complimentary-RNA (cRNA) was required for cRNA microinjection into *X. laevis* oocytes, in order to enable expression of channel constructs (as described in section 2.3.3). The plasmid pBF, containing channel constructs downstream of a SP6 promoter was linearised by *Mlu*I endonuclease. The linearised plasmid DNA was purified directly from the reaction mixture (as described in section 2.1.6). The purified DNA (1 μg) was used as a template for SP6 RNA polymerase directed cRNA production, which was supplied as an RNase free kit, mMessage machine synthesis kit (Ambion) (utilising a 2

hr incubation for maximal yield). The cRNA was analysed for homogenicity by agarose gel electrophoresis and quantified by UV spectrometry at $A_{260\,nm}$ (A 1.0 = 40 μg/ml RNA).

2.3.3 X. laevis oocyte preparation and microinjection

Female *X. laevis* frogs were anaesthetised and handled in accordance with Home-Office schedule 1 guidelines by registered personnel. The level of anaesthesia was tested by reaction of the withdrawal involuntary response. The frogs were killed by spinal bisection and pithing, and the ovarian lobes were removed from the torso by a midline incision. The ovarian lobes were used on the day of sacrifice or stored in OR-Mg buffer at 4 °C for up-to 3-4 days. The ovarian lobes were transferred to fresh OR-Mg buffer. The lobes were initially physically disrupted into small clumps. The follicular membranes of the *X. laevis* oocytes were removed by transfer to OR-Mg containing 1 mg/ml collagenase type 1A (Sigma-Aldrich, UK) for 45 min at RT, with gentle mixing. The defolliculated *X. laevis* oocytes were washed four times in OR-Mg buffer, and then incubated for a second time in the presence of 1 mg/ml collagenase for 30 min at RT. Collagenased *X. laevis* oocytes were washed thoroughly in 1x OR-Mg (5-6 washes), before being washed twice and stored in ND-96 at 18 °C. *X. laevis* oocytes in the late stages of mitosis (stages V and VI) were visually selected and transferred to a separate dish for later microinjection. The selected *X. laevis* oocytes were approximately 1 mm in diameter, which had clearly defined vegetal (light side) and animal poles (dark side). The *X. laevis* oocytes were typically injected either on the day or the day after preparation.

Baked glass capillaries were pulled to make injection pipettes using an automatic pipette puller. The tips were pulled using a two stage program designed to give a fine tip and long shank, then trimmed to the correct diameter using a pair of forceps. Pre-prepared samples of cRNA were injected into each *X. laevis* oocyte using a Pneumatic PicoPump pressure injection system (World Precision Instruments; following the manufacturer's instructions). The injection volume was set to ≈50 nl by adjusting either the diameter of the pipette tip or by altering the length of the pneumatic pulse. The loaded injection pipette was aligned with a *X. laevis* oocyte by micromanipulation; the injection pipette was jabbed in to the vegetal pole near the border with the animal side, followed by a pneumatic pulse, and withdrawal of the pipette tip from with in the *X. laevis* oocyte. The injected *X. laevis* oocytes were incubated individually in a 96-well plate containing 1x Barth's solution at 18 ^{O}C, for 1-3 days, prior to experimentation to allow for expression. mSlo3-F304Y injected oocytes were stored in F304Y Barth's solution, designed using the Goldman-Hodgkin-Katz voltage

(GHK) equation (Hille, 2001) to set the resting membrane potential (RMP) to ≈ -30 mV (3.2.2).

2.3.4 Electrophysiology – Two electrode voltage clamp

A) Current recordings

The *X. laevis* oocyte currents were recorded at room temperature (≈ 25 ± 20 ^{O}C) in Ringer's solution perfused at a rate of 2 ml/min. The microelectrodes were made from thin-walled borosilicate glass (GC100F-15, Harvard apparatus LTD) using a PMP-100D electrode puller (Microdata Instrument, Inc.) filled with 3 M KCl, connected to the headstage by silver wires electroplated with chloride. The resistance of the voltage electrode was between 1 and 5 MΩ, and the resistance of the current electrode was between 0.3 and 2.5 MΩ. A silver/silver chloride pellet electrode was used as the bath reference.

After insertion of the microelectrodes, the *X. laevis* oocyte was left for up to 5 min to allow the membrane to reseal around the electrodes. Membrane potential was controlled using a GeneClamp 500 amplifier (Axon), monitored by a TekTronix 2205 Oscilliscope, digitised using a NI USB-6211 (National Instruments) and recorded using WinWCP (V 4.0.5). Recordings were filtered at 5 kHz and sampled at 4 kHz. Typically for I/V protocols, *X. laevis* oocytes were voltage-clamped at a holding potential of -80 mV, and the voltage was stepped up in +10 mV increments (with a 3 s interpulse period), up to 140 mV for 400 ms. During inhibition protocols oocytes were held voltage-clamped at a potential of -80 mV, then stepped for 200 ms to +100 mV. After a 1s interval during which the oocyte was clamped at -80 mV, a voltage ramp from -80 mV to +100 mV over 1.5 s duration was applied. The interpulse period for the inhibition protocols was 1 s. Sample traces for the I/V and inhibitor protocols are provided in the relevant figure legends. Inhibitors were applied until steady state inhibition of the +100 mV recording pulse occurred.

B) Analysis of Electrophysiological Recordings

Raw data were analysed using Clampfit 9.2 (Molecular Devices) and then compiled using Excel 2003 (Microsoft Ltd) and OriginPro 7.5 (Originlab) software packages. I/V curves and RMP values were collated and averaged (±S.E.M) before plotting. Activation time constants (τ) were fitted in WinWCP software with equation 1.

Equation 1: $$y(x) = A.\left(1 - EXP\left(-\frac{x}{\tau_{act}}\right)\right)^{P}$$

Where *A* is the peak current amplitude and τ_{act} is the activation time constant. Individual I/V relationships were converted to conductance-voltage (G/V) relationships. G/V plots were plotted over the -50 to +140 mV range to minimise intrinsic error due to erroneous points around the reversal potential, created by the conversion from current to conductance. Plots were fitted with unconstrained Boltzmann function (equation 2) to determine the predicted maximal conductance (G_{max}).

Equation 2: $$G = \frac{G_{max} - G_0}{1 + e^{\frac{\left(V - V_{\frac{1}{2}}\right)}{k}}} + G_0$$

Where G_0 is the initial conductance, $V_{1/2}$ is the half-activation voltage and k is a measure of the voltage dependence. Conductance values were normalised to the predicted G_{max}, and plotted fitting with a Boltzmann function asymptoted to G_{max} of 1 to gain individual measurements of the $V_{1/2}$ and k values (slope). Average G/V plots were generated from the average (± SEM) of the individual data and plotted.

Percentage current remaining ($I_{\%}$) of current was calculated by normalisation of inhibition induced current (I) to vehicle (either 0.5% DMSO or Ringer's) induced current (*I*[B]0):

Equation 3: $$I_{\%} = \left(\frac{I}{I[B]_0}\right) * 100$$

Inhibition curves were fitted individually to the normalised data for each oocyte with maxima asymptoted to 100% with equation 4.

Equation 4: $$I = \frac{I[\mathrm{B}]_0}{\left(1 + \left(\frac{[\mathrm{B}]}{IC_{50}}\right)^{\mathrm{H}}\right)}$$

Where H is the Hill coefficient, [B] is inhibitor concentration and *I*[B]0 is the current in the absence of inhibitor. IC_{50} values were collated and averaged (±S.E) to determine final IC_{50} values for each construct. The voltage dependence of quinine, quinidine and barium block of mSlo3 currents were determined by calculating values of zδ, the fraction of the electric field that the blocker experiences and the valency of the blocker, from the estimates of IC_{50} values obtained at +20, +40, +60, +80 and +100 mV ($K_{0.5}$(V))according to the Woodhull equation (Woodhull, 1973) for individual oocytes. The apparent δ and $K_{0.5}(0)$, the apparent affinity at 0 mV, for each oocyte were calculated according to the transformed Woodhull (equation 5).

Equation 5: $$lnK_{0.5}(V) = lnK_{0.5}(0) + \left(\frac{\delta zVF}{RT}\right)$$

Where V is membrane potential, R is the gas constant, T is absolute temperature and F is Faraday's constant. Data were then collated and analysed to give average apparent δ and $K_{0.5}(0)$ values. All data are presented as mean ± SEM and all results are $n \geq 3$. Statistical tests and significance were performed using GraphPad Prism 4 (GraphPad Software Inc) as described in section 2.5.

2.4 Heterologous expression in HEK293 cells

2.4.1 Materials and reagents

As in previous sections, except for the following:

A) Tissue culture solutions

HEK293 media: Dulbecco's Modified Eagle Medium - GlutaMAX™-I (GIBCO ®), 10% Fetal bovine Serum, 50 units Penicillin and 5µg/ml Streptomycin

DPBS: Dulbecco's Phosphate-Buffered Saline (GIBCO ®)

Opti-MEM: Opti-MEM® I Reduced Serum Media (GIBCO ®)

Serum free media (SFM): Dulbecco's Modified Eagle Medium - GlutaMAX™-I (GIBCO ®), 50 units/ml Penicillin and 5µg/ml Streptomycin

Trypsin: Trypsin, 0.05% with EDTA 4Na (GIBCO ®)

B) Electrophysiological solutions

Extracellular Solution: NaCl 140 mM, KCl 5 mM, $CaCl_2$ 1 mM, Glucose 29 mM, HEPES 25 mM, pH 7.4, ≈330 mOsm

Intracellular solution (0 mM Na^+): KCl 130 mM, EGTA 5 mM, HEPES 10 mM, pH 7.4, ≈294 mOsm

Low Cl^- Intracellular solution (0 mM Na^+ 1 mM Cl^-): KCl 1 mM, K-gluconate 129 mM EGTA 5 mM, HEPES 10 mM, pH 7.4, ≈294 mOsm

B) Activator stock solutions

Bithionol: 10 mM in DMSO

Bithionol Sulfoxide: 10 mM in DMSO

2.4.2 Transfection of HEK293 Cells

In vitro synthesis of plasmids was required before plasmid transfection into HEK293 cells (as described in section 2.1.9). The transfection mixture was produced with the composition (per 35 mm well of a six well plate): 100 µL pre warmed (37°C) SFM or Optimem, 3 µL Fugene® 6 (Roche), 1-1.5 µg of cDNA. The mixture was incubated for 20-30 mins at RT before being added to ~50% confluent cells. Cells were incubated for 24-48 hrs and then replated into a 35 mm dish at lower density for electrophysiological study 3-24 hours later.

2.4.3 Electrophysiology - Whole cell patch clamp

A) Setup

The microelectrode pipettes were made from thin-walled filimented borosilicate glass (GC150TF-15, Harvard Apparatus Ltd) using a PP-830 (Narishige) electrode puller. Pipettes were fire-polished after pulling with a MF830 (Narishige) micro-forge. HEK293 medium in 35mm dishes was gently exchanged with approximately 2 mls of extracellular solution, 5 mins prior to patching. The 35 mm dish was then placed on a modified stage of a Nikon TE2000 Microscope (Nikon), and connected to the ground (silver/silver chloride pellet) electrode with an agar bridge. Agar bridges were produced, before patching, by dissolving 0.5% agar in extracellular solution and using this solution to fill reshaped thin walled glass. Transfected cells were identified by fluorescence; pipettes were first backfilled with intracellular solution (making sure of the absence of air bubbles). For variable $[Na^+]_i$ experiments intracellular (and low Cl^- intracellular) solutions were modified with the addition of NaCl (or Na-gluconate) to the required concentration before the pipette was filled. Once filled the pipette was mounted on the EPC10 headstage (HEKA) ensuring good contact between the intracellular solution and the silver chloride wire. Slight positive pressure was applied to the pipette before the pipette was manoeuvred so that it was in contact with the extracellular solution. The resistance of the voltage electrode was between 1 and 3.5 MΩ, pipettes with higher resistance were discarded. The pipette voltage offset was zeroed; taking into account the Liquid Junction Potential (LJP) of the solutions calculated using Clampex 9.2 (Molecular Devices). The pipette was then manoeuvred so that it was gently touching the membrane of the cell. Suction was applied until a seal of ~ 100 MΩ formed and then the suction was released, until a GΩ seal was formed. The pipette was then voltage clamped at -80 mV, and the fast capacitance (C-fast) of the pipette was cancelled. Gentle suction was then applied to break through the membrane, ceasing on the appearance of slow capacitance (C-Slow) spikes. C-slow was then cancelled, however if the series resistance of the breakthrough was more than twice the pipette resistance, more suction was applied until this situation had occurred. Exceptions occurred when using low Cl^- intracellular solution, when thrice the pipette resistance was deemed usable.

B) Current Recording

Pipette potential was controlled using the Patchmaster software through an EPC10 amplifier (HEKA). After membrane breakthrough (2.4.3A) the HEK293 cell was clamped at -80 mV, and a voltage ramp was applied. From a -70 mV holding voltage, command voltage was stepped down to -100 mV for 100 ms then ramped to +100 mV over 500 ms before stepping back to -70 mV. The interpulse period for the ramp protocol was 5 s and the sample rate was

1 kHz. Throughout the recording the reversal potential and conductance was monitored through the online analysis function of the Patchmaster software. Typically for I/V protocols, cells were voltage-clamped at a holding potential of -80 mV and the voltage was stepped up in +10 mV increments (with a 3 s interpulse period), up to 100 mV for 200 ms. The sample rate for the I/V protocol was 10 kHz. Sample traces for I/V and ramp protocols are provided in the relevant figure legends.

For dose response and single dose protocols a voltage ramp (as previously described) was applied for ~250 s to allow not only the intracellular solution to dialyse the cell but also to allow currents to stabilise. Then compounds were applied by perfusion until the conductance reached a steady state of at least 10 sweeps of the ramp protocol. For single dosage applications perfusion of vehicle (extracellular solution) was executed until currents reached steady state. For dose response experiments wash steps of vehicle (extracellular solution) were performed after 1, 10, 30 µM dosages to ensure that there was an accurate baseline and that observed current was not due to leak currents between the pipette and cell.

C) Analysis of Electrophysiological Recordings

Raw data were analysed using the online analysis function of the Patchmaster software and then compiled using Excel 2003 (Microsoft Ltd) and OriginPro 7.5 (Originlab) software packages. Conductance and current were first internally normalised to the calculated capacitance of each cell. Values were collated and averaged (±SEM) before plotting. To generate dose response curves for pharmacologically active compounds, which resulted in a change in conductance, firstly steady state conductance density was averaged. Once averaged the conductance density for each concentration, $G[A]_{\chi}$, was normalised to the average vehicle conductance density, $G[A]_0$, using equation 6.

Equation 6: $$G_{norm} = \left(G[A]_{\chi} \,/\, G[A]_0\right) * 100$$

Activation curves were fitted individually to the normalised data for each cell with a logistic dose response curve:

Equation 7: $$y = G'[A]_0 + \left(\frac{G'[A]_{\chi} - G'[A]_0}{1+10^{(\log(EC_{50}-\chi)H}}\right)$$

Where H is the Hill coefficient, $G'[A]_{\chi}$ is the maximal conductance density in the presence of the activator and $G'[A]_0$ is the average conductance density in the absence of activator. EC_{50} values were collated and averaged (±SEM) to determine final EC_{50} values for each compound. All data are presented as mean ± SEM and all results are $n \geq 3$. Statistical tests and significance were performed using GraphPad Prism 4 (GraphPad Software Inc) as described in section 2.5.

2.5 General bioinformatics and statistical analysis methods

2.5.1 Bioinformatics

The RCK domains of the Mouse Slo1 (NP_034740) protein as described by (Yusifov *et al.*, 2008) were aligned with the homologous regions in mSlo3 WT (NP_032458) using ClustalW2 (EBI). The DomPred Protein Domain Prediction Server (Marsden *et al.*, 2002) was used to predict the secondary protein structure of the RCK homologous regions of mSlo3 WT (NP_032458). The online modelling server, SWISS MODEL, was used in the first approach mode for homology modelling and alignment of protein sequences (Peitsch, 1995; Arnold *et al.*, 2006; Kiefer *et al.*, 2009). The first approach mode requires sequence homology throughout the protein of interest and the template sequence. Therefore, deletion of non-homologous regions in the protein of interest was required for complete homology modelling and alignment. The model building process is carried out in three stages:

1) Sequence identity check (>25 % threshold)
2) Generation of models with ProModII
3) Energy minimisation of models with Grosmos96

2.5.2 Statistical analysis

Data are expressed as mean ± standard error of the mean (SEM). Parametric data were tested for significance using Student's t-test (Student, 1908) with Welch's correction for unequal variance when comparing two groups or when multiple comparisons were required analysis of variance (ANOVA) tests were performed with the correct post-hoc tests. For non-parametric data a Kruskal–Wallis one-way analysis of variance test was performed. Post-hoc tests were performed in order to observe internal significance between the multiple groups compared. Bonferroni post-hoc tests were preferred for internal comparison between all groups. Nonparametric analysis required Dunn's multiple comparison post hoc tests to compare the groups. Significance was determined as a p value of less than 0.05.

Chapter III: Pharmacology of mSlo3

3.1 Chapter 3 Introduction

3.1.1 Characteristics of the mSlo3 channel

The large-conductance Ca^{2+}-activated K^+ channels (Slo1, BK_{Ca}) are highly characterised for their gating by voltage and intracellular Ca^{2+} (Butler *et al.*, 1993). Slo1 is distinctive due to the large unitary conductance but also has distinctive "regulator of K^+ conductance" (RCK) domain architecture in the large C-terminus tail that provides most of the physiological modulatory sites. The closest relative mSlo3 was identified via an expressed sequence tag (EST) with homology to the C-terminal region of mSlo1 and PCR analysis of a variety of tissues (Schreiber *et al.*, 1998). The *Slo3*-encoded channel was found to be expressed solely in spermatozoa and testis (Schreiber *et al.*, 1998). The mSlo1 and mSlo3 channels have highest homology in the core domain which contains the six TM domains and RCK1. The mSlo1 S0 through to S8 shares 56% identity to the mSlo3, S0 through to S8 regions. The S9 and S10 regions are more divergent and there is only 39% identity between mSlo3 and mSlo1. The mSlo3 channel was found to be modulated by internal pH and voltage whereas mSlo1 also displays voltage dependent activation but it is modulated by Ca^{2+} rather than intracellular alkalisation (Schreiber *et al.*, 1998). When expressed in *Xenopus* oocytes mSlo3 displayed a lower unitary conductance of 106 pS in 160 mM symmetrical K^+ (Schreiber *et al.*, 1998). The pharmacology of mSlo3 differs in comparision to Slo1; mSlo3 is largely insensitive to extracellular tetraethylammonium (TEA) with an IC_{50} of 49 mM in comparison to block of Slo1 which has an IC_{50} of 0.14 mM (Schreiber *et al.*, 1998). This difference in TEA sensitivity is due to the lack of a tyrosine (Y294), when mutated in Slo1 results in mSlo3 levels of inhibition (Tang *et al.*, 2010*b*). mSlo3 channels are also insensitive to the scorpion toxins, iberiotoxin and charybdotoxin, the "classical" Slo1 inhibitors (Tang *et al.*, 2010*b*). The channel properties of mSlo3 have been difficult to discern due to two reasons. Firstly successful expression in mammalian cells has proved elusive for unknown reasons. Secondly to attain detectable expression in *Xenopus* oocytes a level of 40 ng of cRNA is required for injection; oocytes also have to be kept for three to fourteen days in order to observe significant currents. This is an exceptionally high amount of RNA in comparison to Slo1, which requires 20-fold less cRNA and an incubation time of only 1-3 days to attain significant channel expression. The original study also noted that the mSlo3 channel had a short mean open time and a low open probability (P_o) at physiological voltages (Schreiber *et al.*, 1998).

mSlo3 is activated in alkaline buffers in the range of pH 7.0 - pH 9. pH 9 is not a defined physiological limit to channel activation, as at a pH higher than 9 patch stability cannot be maintained. Analysis of the effects of pH on P_o of the channel suggested that multiple protonation sites exist on the mSlo3 C-terminus domain (Zhang *et al.*, 2006*a*). Interestingly, analysis of the activation and deactivation time courses of macroscopic currents exposed fast and slow exponential components. Their work suggested that there are two distinct inter-converting channel populations. Increasing pH was found to affect the amplitude of activation; whilst the time course of activation remained constant. This finding suggested a shift between populations was dependent on the level of protonation of the mSlo3 channel (Zhang *et al.*, 2006*a*). This theory is reliant on the distinct populations each having a discrete steady state P_o, however this was not observed in analysis of single channel traces (Zhang *et al.*, 2006*b*). One curious aspect of the fast component of channel deactivation is the minimal dependence on pH. However single channel traces exhibited a rapid opening and closing that prevented simple definition of a unitary current level. Thus it was concluded that there is insufficient evidence to determine the effects of pH on the gating steps controlling mSlo3 activation time course (Zhang *et al.*, 2006*b*).

3.1.2 Physiological relevance of mSlo3

The function of the mSlo3 channel in native tissues, testis and spermatozoa, has yet to be fully elucidated. Using mouse CatSper1 KO mature spermatozoa the I_{KSper} current was identified, the properties of which are similar to the mSlo3 channel mediated current, including the shape of the I/V curve, the potentiation of the current over a similar pH range (pH 6 - pH 8) and weak voltage sensitivity. The original study was unable to confirm if mSlo3 channel is the I_{KSper} current mediator in mouse CatSper1 KO mature spermatozoa due to the only commercially available anti-mSlo3 antibody having been raised in mouse (NeuromAB) (Navarro *et al.*, 2007). I_{KSper} is the dominant hyperpolarising conductance within the physiological range, and thus is believed to dictate the resting membrane potential of the spermatozoan. During the process of capacitation, the spermatozoa acquire chemotatic behaviour, hyperactivated motility and are readied for the acrosome reaction prior to fertilisation. The spermatozoan cytoplasm undergoes alkalinisation in the female reproductive tract due to activation of HV1 channels in humans, and the Na^+-dependent Cl^-–HCO_3^- exchanger in mouse (Zeng *et al.*, 1996; Lishko *et al.*, 2010). The increase in intracellular pH is thought to activate I_{KSper} and drive the membrane potential to negative potentials. This sequentially increases the driving force of Ca^{2+} entry via the alkalinisation activated CatSper channels, in turn increasing level of hyperactivated motility (Kirichok *et*

al., 2006; Navarro *et al.*, 2007, 2008). I_{KSper} current is sensitive to the general motility and volume regulatory K^+ channel (TASK2 and Kv1.5) inhibitors; quinine, clofilium and mibefradil (Navarro *et al.*, 2007). Quinine and clofilium have been shown to exert their effects on spermatozoan volume regulation and motility by inhibiting a TEA-insensitive K^+ current (Yeung & Cooper, 2001; Barfield *et al.*, 2005*a*, 2005*b*). A recent study showed a chimaeric mSlo3 (MC13), with residues 1-181 substituted with Slo1 was blocked by the stereoisomer of quinine, quinidine. Quinidine block was proposed to be due to the protonated form binding to the intracellular side of the MC13 channel with a higher affinity for the closed state (Tang *et al.*, 2010*b*).

3.1.3 Chapter Aims

3.1.3.1 Can we modify the channel properties to increase channel activity?

There is difficulty in getting detectable mSlo3 currents from injected *Xenopus* oocytes due to the low intrinsic Po of mSlo3. Thus to increase the activity of the channel we tested an S6 domain (F304Y) mutation. This mutation is homologous to the F380Y mutation in the S6 domain of hSlo1, which stabilises the open state of the channel by reducing the closing rate and shifting the voltage dependence of the opening rate (Lippiat *et al.*, 2000). Therefore if the F304Y mutation has similar effects we should be able to get more consistent detectable currents allowing for easier measurement of channel properties.

3.1.3.2 What effect does our mutation have on intracellular pore blockers?

We aim to test the effect of our mutation on the relative potency of quinine, a compound that has been used extensively to test volume regulation and mobility in spermatozoa. Defined properties for the potency of inhibition may allow easier identification of mSlo3 currents as a component of I_{KSper} current. We aim to also test the optical isomer quinidine, a compound that has been suggested to bind to the intracellular side of the channel in the close state. Thus we hypothesise quinidine inhibition will be reduced in the F304Y injected oocytes as this mutation should reduce the amount of channels in the closed state.

3.1.3.3 What effect does our mutation have on extracellular pore blockers?

Ba^{2+} ions inhibit K^+ currents, in a voltage dependent manner, by blocking the selectivity filter in the K^+ channel. Ba^{2+} inhibition can be relieved by increased concentration of K^+ ions resulting in increased competition for occupancy of the selectivity filter (Armstrong & Taylor, 1980; Neyton & Miller, 1988; Jiang & MacKinnon, 2000). We theorise that our F304Y mutation should not affect the potency of Ba^{2+} inhibition. As the mutation should only increase the open probability of the mSlo3 channel, thus the selectivity filter should be unaffected.

3.1.3.4 Do mSlo3 currents share pharmacological properties with I_{KSper}?

We hypothesise that mSlo3 channels may underlie a component of I_{KSper}, due to similar electrophysiological properties and range of pH sensitivity. We aim to trial the pharmacological profile described for the I_{KSper} current on mSlo3 expressed in *Xenopus* oocytes (Navarro *et al.*, 2007). Confirmation of the effects of these inhibitors will strengthen the case that the mSlo3 channel mediates at least part of the I_{KSper} current. Also, because of the overlap in pharmacological properties, sensitivity of mSlo3 channels to the inhibitor range will also suggest that mSlo3 currents are a component of the K^+ current involved in motility and volume regulation.

3.2 Chapter 3 Results

3.2.1 Effects of mutation of F304 on electrophysiological properties

Currents from oocytes were measured using two-electrode voltage clamp during a 100 ms voltage step of -100 to +140 mV in 10 mV increments, from a -80 mV holding potential. mSlo3-injected ooctyes (Figure 3.1) displayed currents similar to those previously described by Schreiber *et al*. (1998), a voltage dependent delayed rectifier current with no inactivation, properties that are distinct from the endogenous current (Figure 3.1). The sample traces of the mSlo3 (Figure 3.1.A), F304Y (Figure 3.1.B) and endogenous channels (Figure 3.1.C) show that this pulse is of sufficient duration for currents to reach steady state activation. The average plots of I/V relationship show the distinction of the experimental currents from the contaminating endogenous currents, which display activation above +100 mV. F304Y currents (Figure 3.1.B) show similar properties to mSlo3 currents, a voltage dependent delayed rectifier current with no inactivation, but display activation from lower voltage potentials. Analysis of the F304Y current traces display significantly ($P<0.05$, Student's t-test) faster activation kinetics τ_{+100mV} (3.31 ± 0.07 ms, n=26) compared to mSlo3 τ_{+100mV} (5.69 ± 0.09 ms, n=29). Traces were sampled to generate average current-voltage (I/V) relationships (± SEM) (Figure 3.1.D).

The average I/V curves show a leftward shift of ≈40 mV in voltage activation caused by the mutant F304Y, in comparison with the mSlo3 currents. Thus individual I/V relationships were converted to conductance-voltage (G/V) relationships, averaged (± SEM) and plotted as described in 2.3.4.B. Whilst in the plots of the average G/V relationships, shown in Figure 3.2, F304Y currents display a leftward shift in the voltage activation in comparison to mSlo3 currents. However, the Boltzmann function fits of the individual G/V data sets found that the average F304Y $V_{1/2}$ (30.83 ± 38.17 mV, n=26) was not significantly ($P>0.05$, Student's t-test) shifted from the mSlo3 $V_{1/2}$ (55.79 ± 63.33 mV, n=29). The voltage dependence, as quantified by the slope, of the conductance relationship, was not significantly ($P>0.05$, Student's t-test) changed by the F304Y mutation (50.57 ± 10.78 mV, n=26) compared to mSlo3 (67.49 ± 24.90 mV, n=29).

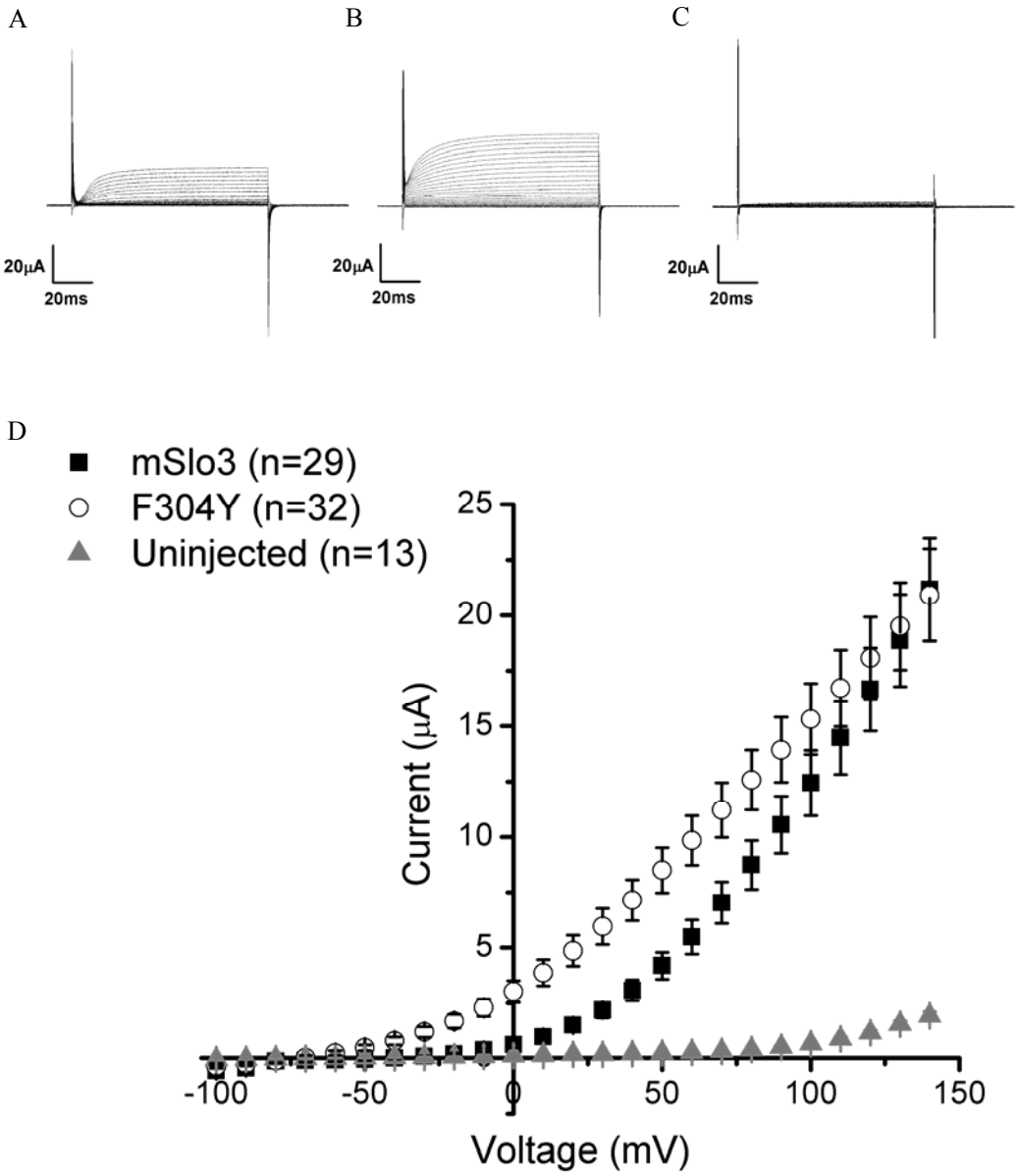

Figure 3.1 Electrophysiological properties of oocytes expressing wildtype and mutant mSlo3 channels. Sample traces of (A) mSlo3, (B) F304Y and (C) uninjected oocytes are shown in response to the voltage step protocol, -100 mV to 100 mV in 10 mV intervals. Traces were complied to generate I/V curves (D), which show the leftward shift in voltage activation caused by the mutant F304Y. Also shown is the distinction of the experimental currents from the control endogenous uninjected currents.

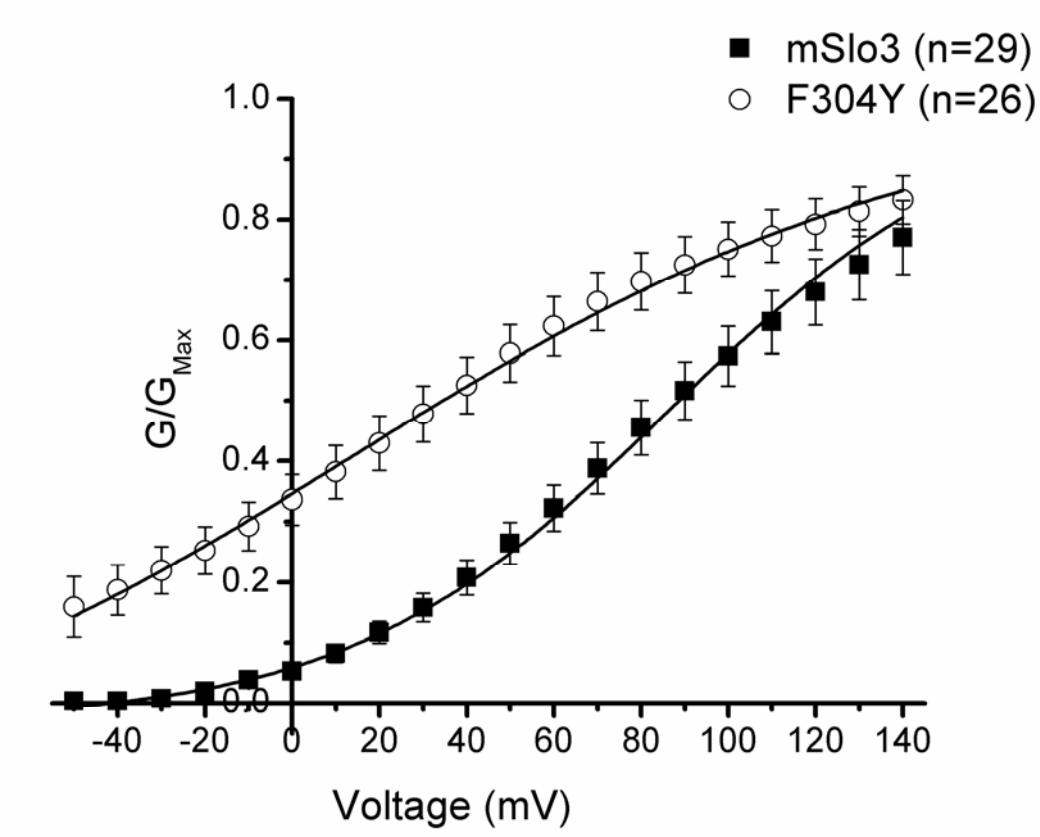

Figure 3.2 Effects on the conductance-voltage relationship due to F304Y mutation. Individual I/V relationships were converted to conductance-voltage relationships before collating and plotting. Plots were fitted with Boltzmann function asymptoted to maxima of 1. The average F304Y $V_{1/2}$ (30.83 ± 38.17 mV) was found to be not significantly (P>0.05, T-test) shifted from the mSlo3 $V_{1/2}$ (55.79 ± 63.33 mV). The voltage dependence (as quantified by the slope) of the conductance relationship, was also not significantly (P>0.05, T-test) changed by the F304Y mutation (50.57 ± 10.78 mV) compared to mSlo3 (67.49 ± 24.90 mV).

3.2.2 Effects of F304Y on oocyte resting membrane potential

mSlo3 currents are not a major determinant of RMP, unlike I_{KSper} (Navarro *et al.*, 2007), as no significant difference between mSlo3 RMP (-38.4 ± 2.68 mV, n=32) and uninjected RMP (-24.1 ± 3.23 mV, n=12) (Figure 3.3) was observed. However, oocytes have endogenous channels that contribute to RMP, as can be seen in Figure 3.1C and D. If the significance threshold was relaxed to P<0.1 the mSlo3 RMP was found to be significantly lower than the uninjected RMP. The F304Y mutant channels, that are open across a wider voltage range (Figure 3.1D), were a major determinant of RMP (-68 ± 4.93 mV, n=26) and displayed a significant difference (P<0.05, Kruskal–Wallis, Dunn's post hoc test) in comparison with mSlo3 and uninjected RMP.

The effects of F304Y expression on oocyte RMP's were so pronounced, storage in modified Barth's solution (2.3.1.A), appeared to be ootoxic. Surviving oocytes had a more negative RMP, near E_K, of ≈-79 mV in comparison to an uninjected oocyte (≈-30 mV). Modified Barth's solution (2.3.1.A) was adapted using the Goldman-Hodgkin-Katz voltage (GHK) equation (Hille, 2001) (equation 8) to adjust the RMP to ≈-30 mV to compensate for the hyperpolarised RMP of F304Y injected oocytes.

Equation 8:
$$V_m = \frac{RT}{F} \ln \left(\frac{P_{Na^+}[Na^+]_{out} + P_{K^+}[K^+]_{out} + P_{Cl^-}[Cl^-]_{in}}{P_{Na^+}[Na^+]_{in} + P_{K^+}[K^+]_{in} + P_{Cl^-}[Cl^-]_{out}} \right)$$

Where V_m is membrane potential, R is the gas constant, T is absolute temperature, F is Faraday's constant, P_{ion} is the permeability coefficient of the ion across the membrane and $[ion]_\chi$ is the concentration of the ion where χ is the orientation of the membrane. Intracellular ion concentrations and ion permeability of collagenased *Xenopus* oocytes were measured in an earlier study (Costa *et al.*, 1989). Using the values for our standard modified Barth's solution gave a calculated V_m of -27.83 mV for uninjected oocytes. Rearranging the equation we calculated P_{K^+} for our F304Y injected oocytes, twelve-fold higher than for uninjected oocytes. Using these calculated values (P_{K^+}, $P_{Na^+}$and P_{Cl^-}), the extracellular KCl concentration was varied until a calculated V_m of -36 mV was achieved. This composition of extracellular solution was termed F304Y Barth's solution; F304Y injected oocytes were stored in this solution during the 1-3 day incubation. This method increased oocyte viability with a survival rate of ≈ 90%.

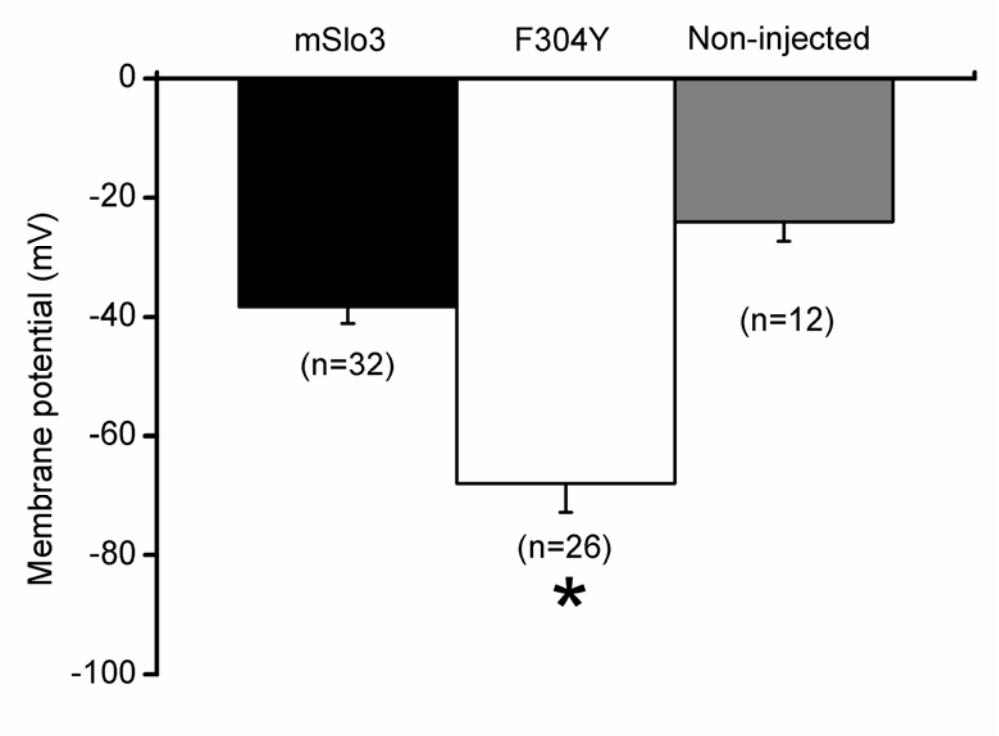

Figure 3.3 Effects of wild-type and mutant mSlo3 channels expression on the membrane potential of oocytes. The RMP of oocytes was recorded before voltage clamp was applied, then collated and averaged. Analysis of the RMP showed a significant difference in F304Y injected oocytes ($P<0.05$, Kruskal–Wallis, Dunn's post hoc test). However the RMP of mSlo3 injected oocytes was not significantly different in comparison to uninjected oocyte's RMP.

3.2.3 Quinine sensitivity of mSlo3 currents

Inhibition curves were generated by application of increasing concentrations of quinine ranging from 0.5 μM to 1 mM and recording current amplitude in response to a +100 mV pulse from -80 mV, as can be seen in the sample traces (Figure 3.4.A and 3.4.B). Inhibition curves were normalised to vehicle control (0.5% DMSO), plotted as Figure 3.4.C and fitted using a logistic dose response curve with maxima asymptoted to 100%. Block of the F304Y mutant channel (IC_{50} = 15.9 ± 3.31 μM, n=16) was significantly more sensitive ($P<0.05$, one-way ANOVA; Bonferroni post hoc test) in comparison to mSlo3 channels (IC_{50} = 169.4 ± 40.1 μM, n=12). The F304Y mutation alters the Hill slope value, (0.69 ± 0.02) compared to mSlo3 (1.00 ± 0.21), however this affect is not significant ($P>0.05$, Student's t-test). The inhibition curve for currents in uninjected oocytes shows that the inhibition observed in the injected oocytes is not due to inhibition of endogenous channels. This is firstly due to the low level of current at this voltage (Figure 3.1.D) and the currents in uninjected oocytes have an increased quinine IC_{50} = 253.7 ± 69.3 μM (n=4) (Figure 3.4.C).

The voltage dependence of quinine block of mSlo3 and F304Y currents were determined from calculated individual oocyte IC_{50} values obtained at +20,+40, +60, +80 and +100 mV from currents evoked by a -80 to +100 mV voltage ramp. IC_{50} values were then averaged (± SEM) and plotted against the respective voltage (Figure 3.5). Straight line fits were fitted to individual data sets and used to calculate values of zδ, the product of the fraction of the electric field that the blocker experiences (δ) and the valence of the blocker (z) and the potency of block at 0 mV (K_{0mV}) according to the transformed Woodhull equation (Woodhull, 1973) (2.3.4.B). Quinine inhibition of mSlo3 was calculated to have a zδ = -0.12 ± 0.07 (n=12) with the F304Y mutation significantly ($P<0.05$, Two-way ANOVA; Bonferroni post hoc test) increasing this value (zδ = -0.49 ± 0.06, n=12). The negative value for zδ suggests that quinine block is incompatible with the classical Woodhull model of a positively charged molecule binding from the extracellular side to a site within the membrane. However, a negative value for zδ for a positively charged molecule suggests that the molecule is binding from the intracellular side of the channel. These findings also suggest that the binding site of quinine to the F304Y channel is four-fold deeper in the electric field than in the mSlo3 channel. The F304Y mutation (K_{0mV} = 48.78 ± 11.91 μM, n=12) also significantly ($P<0.05$, Two-way ANOVA; Bonferroni post hoc test) increases the sensitivity of the channel at 0 mV to quinine in comparison to mSlo3 channels (214.45 ± 45.03 μM, n=12).

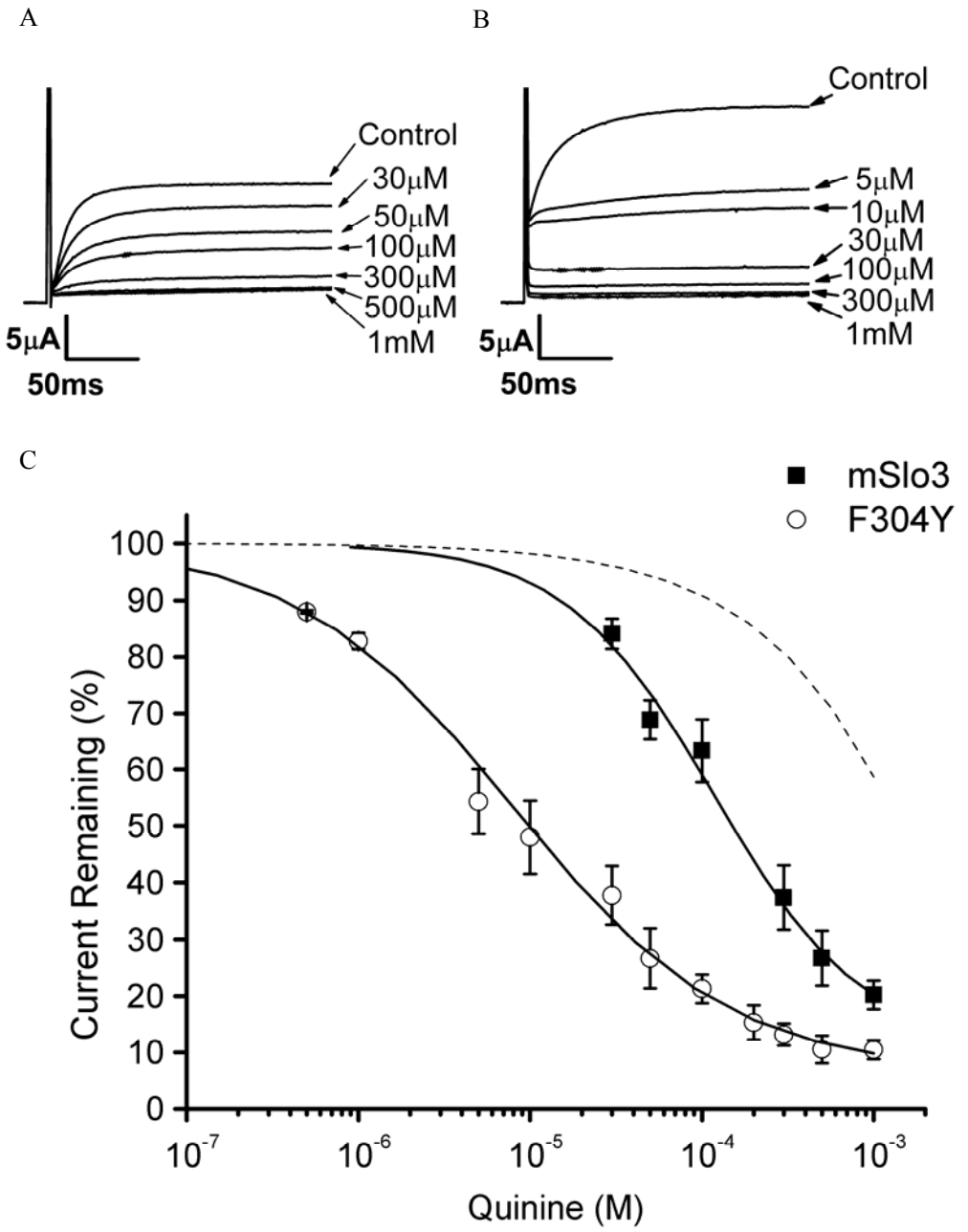

Figure 3.4 Concentration response of quinine inhibition on mSlo3 and F304Y. Sample traces of (A) mSlo3 and (B) F304Y are shown in response to a +100mV pulse with sample range of increasing quinine concentrations. The difference in sensitivity of mSlo3, F304Y and uninjected currents in response to quinine block is shown in C. Inhibition curves were fitted with a dose response curves with maxima asymptoted to 100% current. Block the of F304Y mutant (IC_{50}=15.94 ± 3.31 μM, n=16) was significantly more sensitive (P<0.05, one-way ANOVA; ; Bonferroni post hoc test) in comparison to mSlo3 (IC_{50}=169.35 ± 40.08 μM, n=12). It appears that the F304Y mutation affects the Hill slope, (0.69 ± 0.02) compared to mSlo3 (1.00 ± 0.21), however this effect is not significant (P>0.05, T-test).

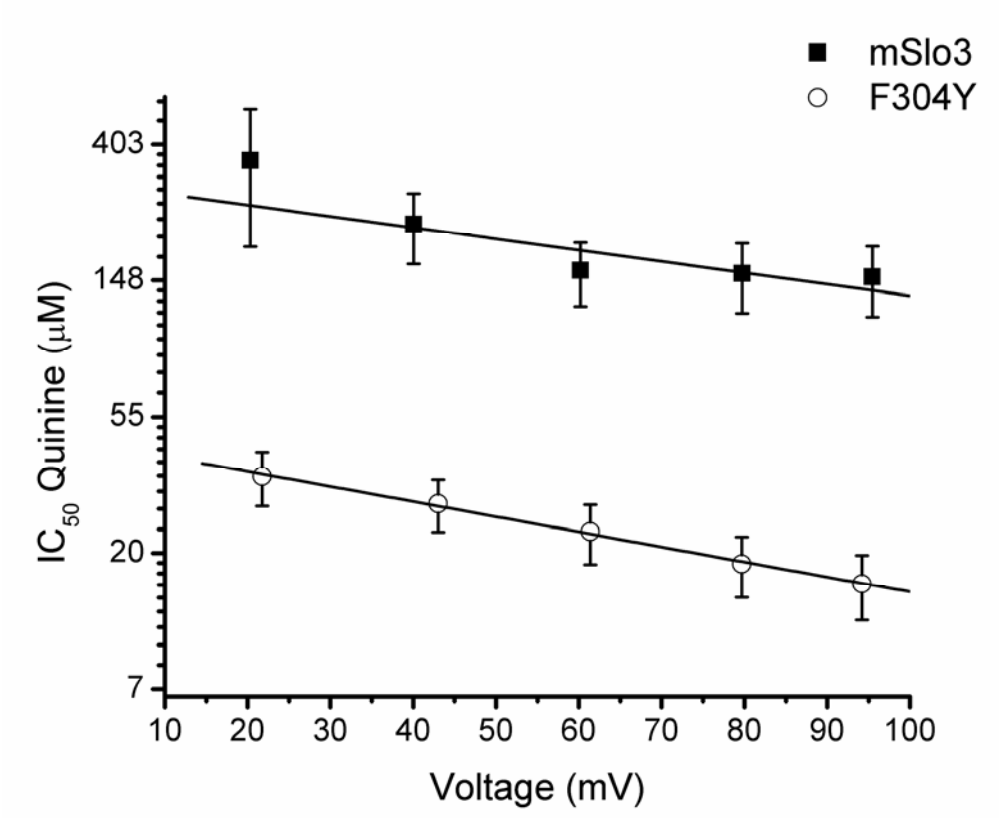

Figure 3.5 Voltage dependence of quinine inhibition. The voltage dependence of quinine block of mSlo3 and F304Y currents were determined by estimates of IC_{50} values obtained from ramp traces at +20, +40, +60, +80 and +100 mV and plotted to the transformed Woodhull equation. Straight line fits of individual oocytes were used to calculate values of zδ, and the potency of block at 0 mV (K_{0mV}). Quinine inhibition of mSlo3 was calculated to have a zδ = -0.12 ± 0.07 (n=12) with the F304Y mutation significantly ($P<0.05$, Two-way ANOVA; Bonferroni post hoc test) increasing this value (zδ = -0.49 ± 0.06, n=12). The F304Y mutation (K_{0mV} = 48.78 ± 11.91 μM, n=12) also significantly ($P<0.05$, Two-way ANOVA; Bonferroni post hoc test) increased the sensitivity of the channel at 0 mV to quinine in comparison to mSlo3 channels (K_{0mV} = 214.45 ± 45.03 μM, n=12)

3.2.4 Quinidine sensitivity of mSlo3 currents

Currents were recorded during application of increasing concentrations of quinidine ranging from 0.1 μM to 400 μM in response to +100 mV pulse from -80 mV, as can be seen in the sample traces (Figure 3.6.A and 3.6.B). Data were normalised to the maximal current response and plotted and fitted using a logistic dose response curve with maxima asymptoted to 100% (Figure 3.6.C). Quinidine block the of F304Y channels (IC_{50} = 2.42 ± 0.60 μM, n=9) was significantly more sensitive (P<0.05, Student's t-test) in comparison to mSlo3 channels (IC_{50} = 19.89 ± 1.42 μM, n=7). It appears that the F304Y mutation significantly (P<0.05, Student's t-test) effects the Hill slope value, (0.76 ± 0.06) compared to mSlo3 (1.15 ± 0.15). The current traces (Figure 3.6.B) show characteristics mimicking inactivation of the channel, in particular the 1 μM quinidine concentration trace. The inhibition curve for currents in uninjected oocytes (Figure 3.6.C) shows that the inhibition observed in the injected oocytes is not due to inhibition of endogenous channels.

The voltage dependence of quinidine block of mSlo3 and F304Y currents were determined by estimates of individual oocyte IC_{50} values obtained at +20,+40, +60, +80 and +100 mV from currents evoked by a -80 to +100 mV voltage ramp and the average (±SEM) plotted in Figure 3.7. Straight line fits were fitted to individual data sets and used to calculate values of zδ, and K_{0mV} according to the transformed Woodhull equation (Woodhull, 1973) (2.3.4.B). Quinidine inhibition of mSlo3 was calculated to have a zδ = -0.12 ± 0.15, (n=7) with the F304Y mutation significantly (P<0.05, Two-way ANOVA; Bonferroni post hoc test) increasing this value (zδ = -0.46 ± 0.05, n=7). These findings suggest that, like quinine, the binding site of quinidine in the F304Y channel is four-fold deeper within the electric field than in the mSlo3 channel. The negative value for zδ suggests that quinidine block, like quinine block, is caused by a positively charged molecule binding from the intracellular side of the channel. Interestingly when comparing quinine and quinidine block, it appears that for neither mSlo3 channels nor F304Y channels there is no significant difference (P>0.05, Two-way ANOVA; Bonferroni post hoc test) in the zδ values dependent on drug. The F304Y mutation (K_{0mV} = 6.23 ± 1.27 μM, n=7) also significantly (P<0.05, Two-way ANOVA; Bonferroni post hoc test) increases the sensitivity of the channel at 0 mV to quinidine in comparison to mSlo3 channels (19.98 ± 4.17 μM, n=7).

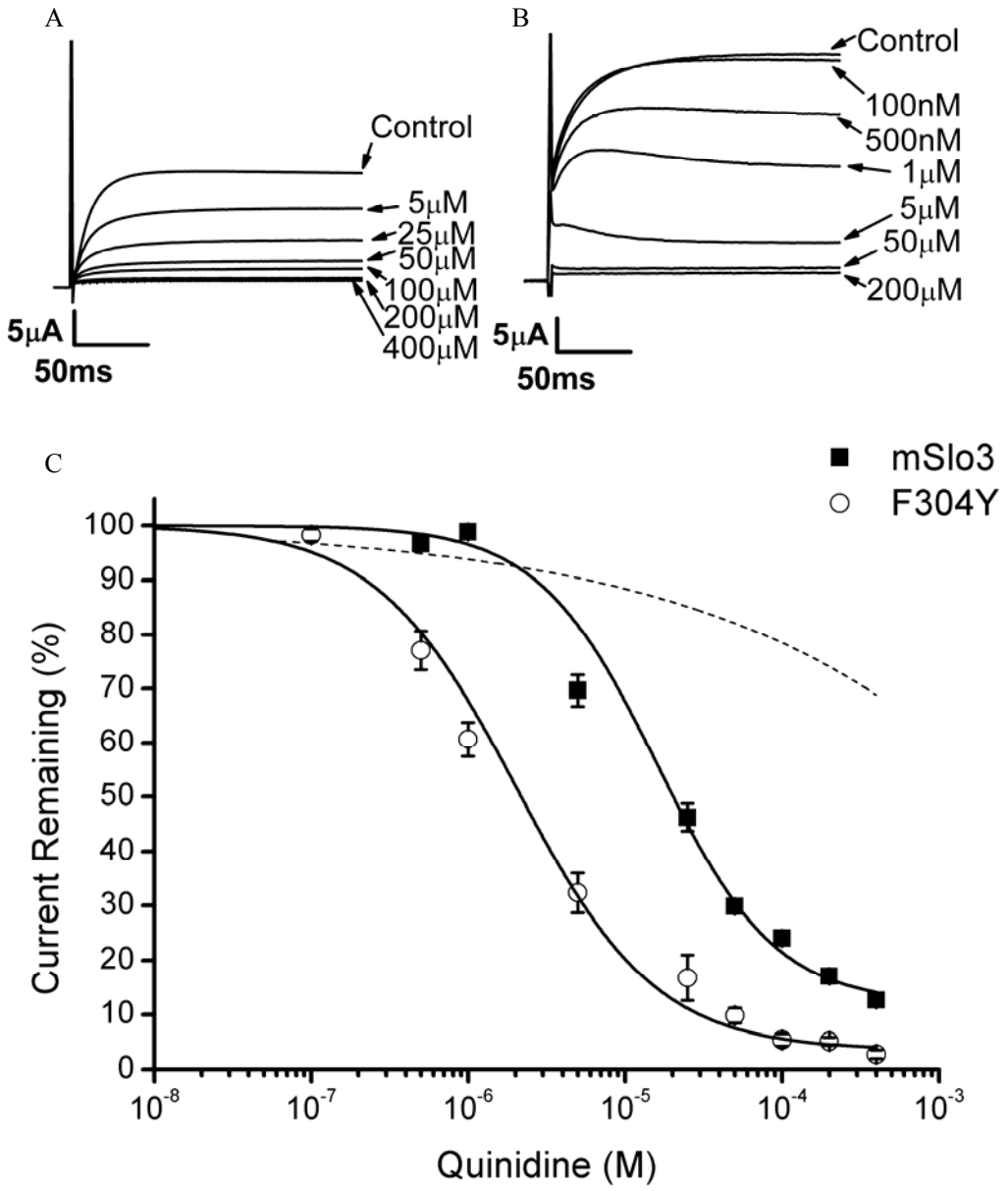

Figure 3.6 Concentration response of quinidine inhibition on mSlo3 and F304Y. Sample traces of (A) mSlo3 and (B) F304Y are shown in response to a +100mV pulse with sample range of increasing quinidine concentrations. The difference in sensitivity of mSlo3, F304Y and uninjected currents in response to quinidine block is shown in C. Inhibition curves were fitted with a dose response curves with maxima asymptoted to 100% current. Block the of F304Y mutant (IC_{50}=2.42 ± 0.60 μM, n=9) was significantly more sensitive (P<0.05, T-test) in comparison to mSlo3 (IC_{50}=19.89 ± 1.42 μM, n=7). Interestingly the F304Y mutation also significantly affects (P<0.05, T-test) the Hill slope for quinidine inhibition, (0.76 ± 0.06) in comparison to mSlo3 (1.15 ± 0.15).

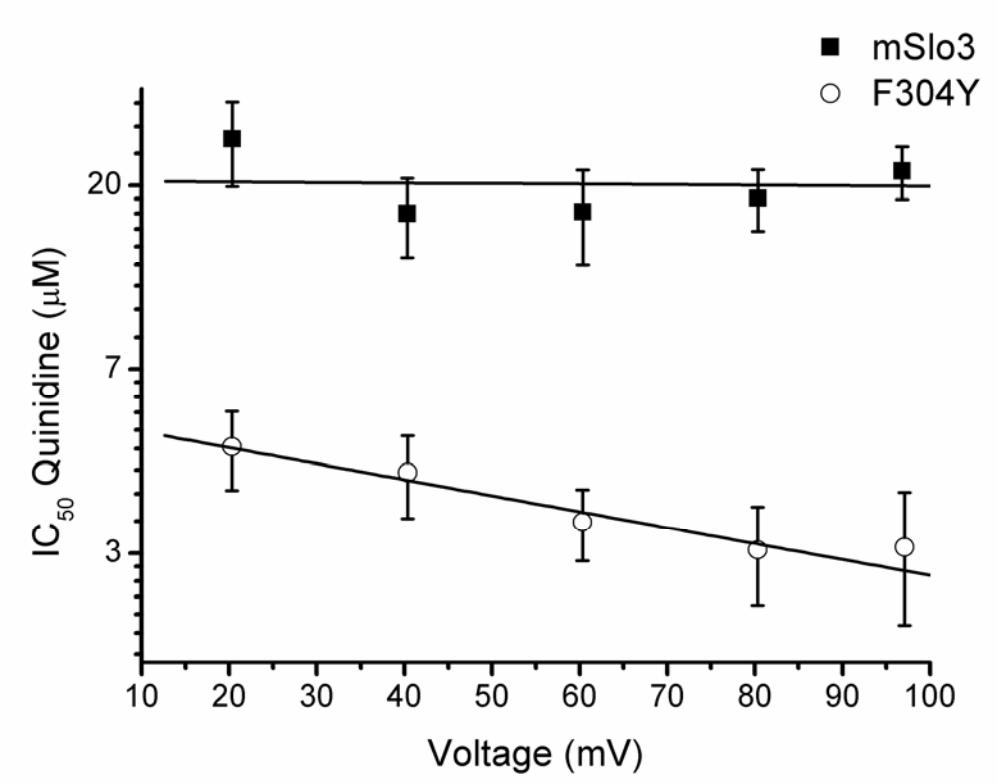

Figure 3.7 Voltage dependence of quinidine inhibition. The voltage dependence of quinidine block of mSlo3 and F304Y currents were determined by estimates of IC_{50} values obtained from ramp traces at +20, +40, +60, +80 and +100 mV and plotted according to the transformed Woodhull equation. Straight line fits of individual oocytes were used to calculate values of zδ, and K_{0mV}. Quinidine inhibition of mSlo3 was calculated to have a zδ = -0.12 ± 0.15, (n=7) and K_{0mV} = 19.98 ± 4.17 μM. F304Y channels gave significantly different calculated values ($P<0.05$, Two-way ANOVA; Bonferroni post hoc test), zδ = -0.46 ± 0.05, (n=7) and K_{0mV} = 6.23 ± 1.27 μM.

3.2.5 Ba^{2+} sensitivity of mSlo3 currents

Inhibition curves were generated by application of increasing concentrations of Ba^{2+} ranging from 20 μM to 10 mM and recording current amplitude in response to a +100 mV pulse from -80 mV, as can be seen in the sample traces (Figure 3.8.A and 3.8.B). Inhibition curves were normalised to the maximal current response and plotted as Figure 3.8.C and fitted using a logistic dose response curve with maxima asymptoted to 100%. Block the of F304Y mutant (IC_{50} = 524.55 ± 96.99 μM, n=5) was not significantly more sensitive (P>0.05, Student's t-test) in comparison to wild type mSlo3 (IC_{50} = 646.28 ± 100.27 μM, n=6). The F304Y mutation does not effect (P>0.05, Student's t-test) the Hill slope values, (1.05 ± 0.12) compared to mSlo3 (0.883 ± 0.11). Approximately twenty percent of current in both the F304Y and mSlo3 recordings remain at the highest Ba^{2+} concentration. This can be largely attributed to the endogenous currents in uninjected oocytes, which were unaffected by addition of 10mM Ba^{2+}. Ba^{2+} inhibition was observed in the sample traces, Figure 3.8.A and 3.8.B, to visibly slow the rate of activation. Individual currents were fitted with activation curves (Figure 3.9.A and 3.9.B) to gain τ_{+100mV} values, τ_{+100mV} was found to increase for both F304Y and mSlo3 currents in a linear concentration dependent fashion (Figure 3.9.C). Interestingly, the Ba^{2+} dependence of τ_{+100mV} of the F304Y mutant currents (0.28 ± 0.05 ms/μM, n=5) was significantly slowed (P<0.05, Student's t-test) in comparison to mSlo3 currents (0.09 ± 0.01 ms/μM, n=6).

The voltage dependence of Ba^{2+} block of mSlo3 and F304Y currents were determined by estimates of individual oocyte IC_{50} values obtained at +20,+40, +60, +80 and +100 mV from currents evoked by a -80 to +100 mV voltage ramp and the average (±SEM) plotted in Figure 3.10. Straight line fits were fitted to individual data sets and used to calculate values of zδ, and K_{0mV} according to the transformed Woodhull equation (Woodhull, 1973) (2.3.4.B). Ba^{2+} inhibition of mSlo3 was calculated to have a δ = 0.66 ± 0.46, (n=5) with the F304Y mutation not significantly (P>0.05, Student's t-test) changing this value (δ = 0.12 ± 0.05, n=5). However if one of the mSlo3 fits is excluded as it has an unfeasible calculated δ of ≈ 2, the δ value changes to 0.20 ± 0.09 (n=4), suggesting that in both mSlo3 and F304Y block by Ba^{2+} is quite shallow in the electric field. The positive value for δ suggests Ba^{2+} inhibition is caused by the positively charged ion entering the channel from the extracellular side. Ba^{2+} inhibition of mSlo3 was calculated to have K_{0mV} = 293.57 ± 74.48 μM (n=5). Inhibition of F304Y gave a significantly different (P<0.05, Student's t-test) calculated K_{0mV} = 521.08 ± 39.00 μM (n=5). Exclusion of the same data set for mSlo3 as before, shifts the K_{0mV} value to 339.80 ± 75.38 μM, and removes the significance difference in K_{0mV} (P>0.05, Student's t-test).

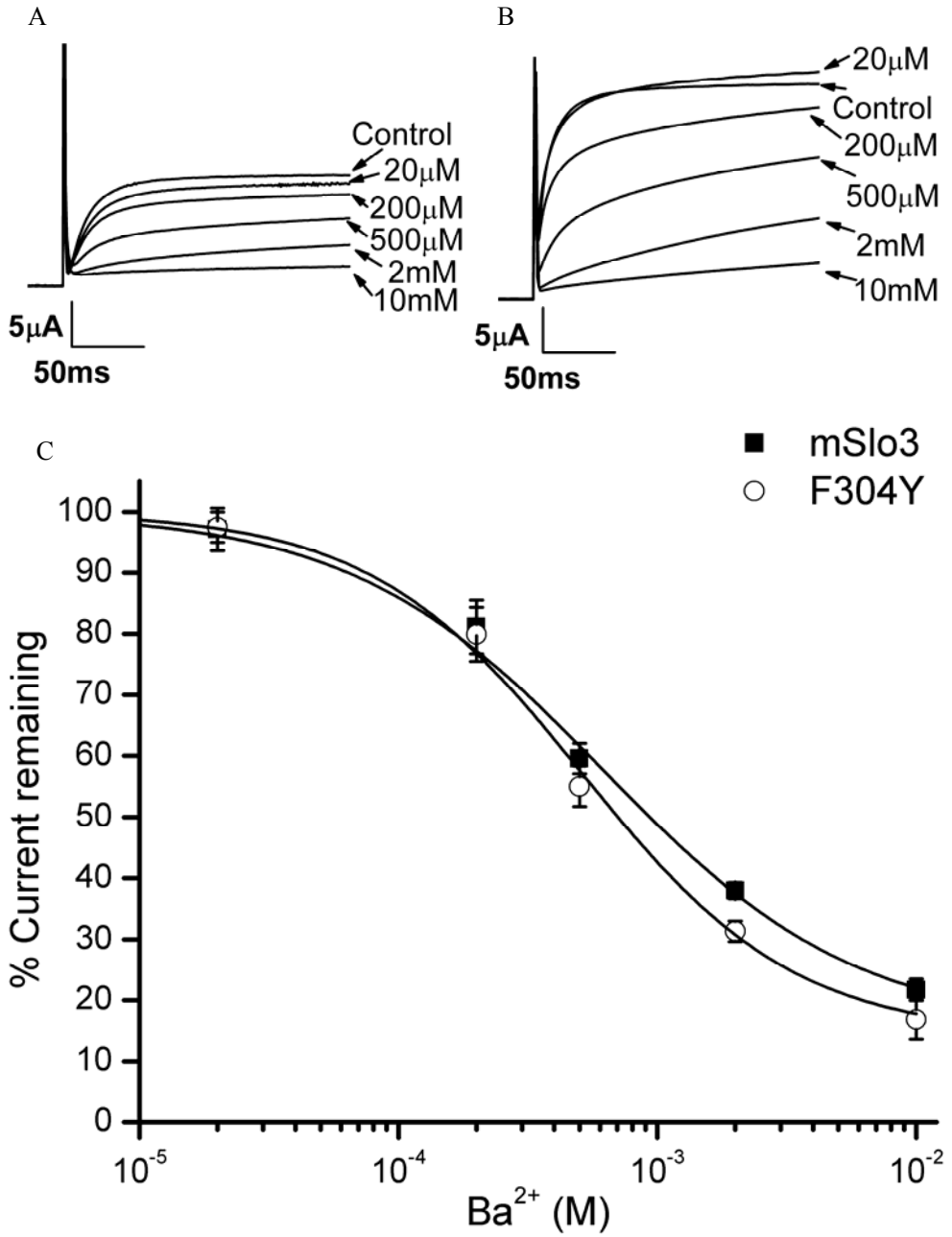

Figure 3.8 Concentration response of Ba^{2+} inhibition on mSlo3 and F304Y. Sample traces of (A) mSlo3 and (B) F304Y are shown in response to a +100mV pulse with sample range of increasing Ba^{2+} concentrations. The difference in sensitivity of mSlo3 and F304Y currents in response to Ba^{2+} block is shown in C. Inhibition curves were fitted with a dose response curves with maxima asymptoted to 100% current. Block the of F304Y mutant (IC_{50}=524.55 ± 96.99 μM, n=5) was not significantly more sensitive (P>0.05, T-test) in comparison to mSlo3 (IC_{50}=646.28 ± 100.27 μM, n=6).The F304Y mutation also does not significantly affect (P>0.05, T-test) the Hill slope, (1.05 ± 0.12) compared to mSlo3 (0.88 ± 0.11).

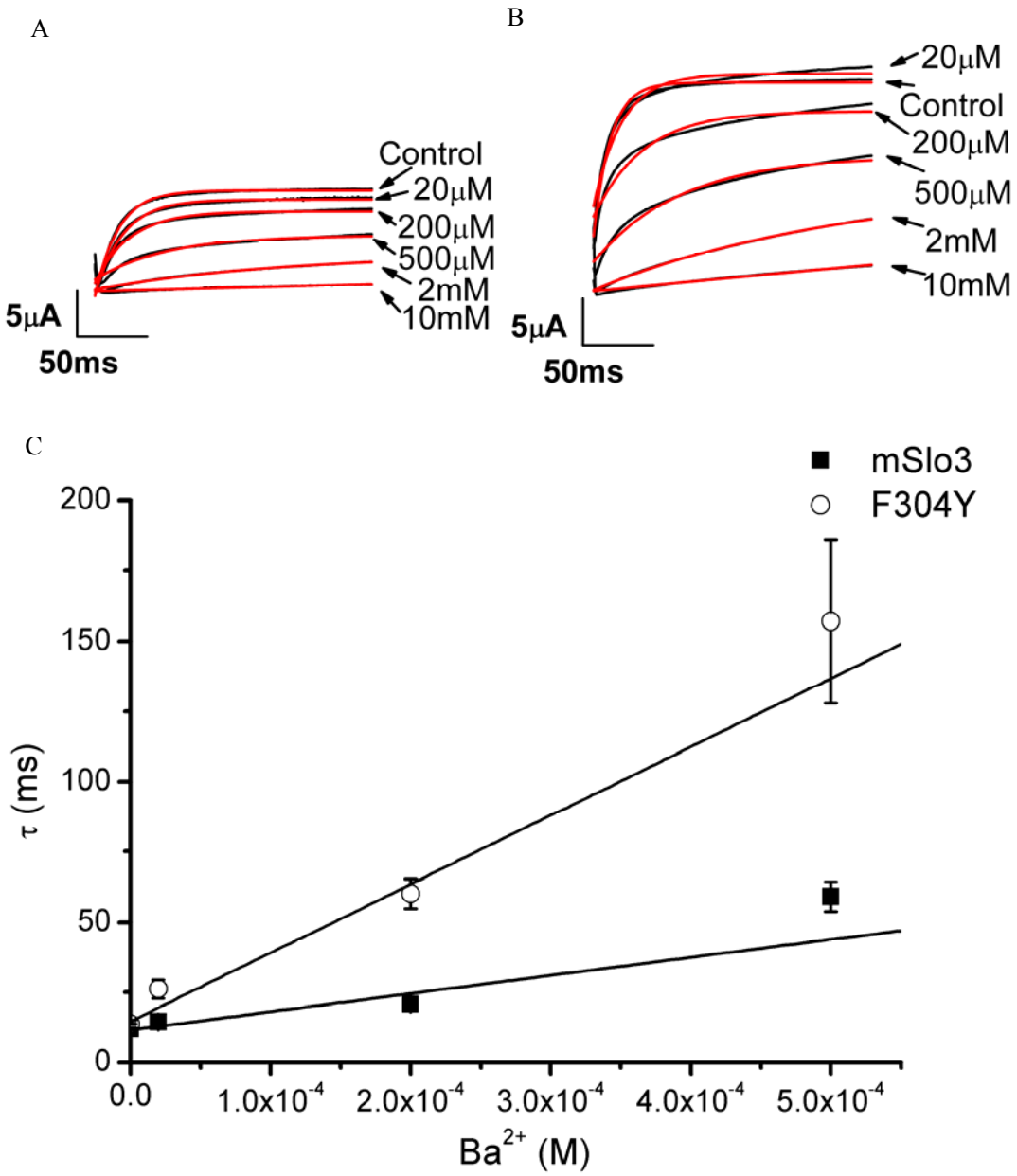

Figure 3.9 Ba^{2+} dependent slowing of τ. Individual oocyte currents for mSlo3 (A) and F304Y (B) were fitted with activation curves (red line) to gain τ_{+100mV} values, before plotting against the respective Ba^{2+} concentration (C). τ_{+100mV} was found to increase for both F304Y and mSlo3 currents in a linear concentration dependent fashion. The concentration dependence of τ_{+100mV} of the F304Y mutant currents (0.28 ± 0.05 ms/μM, n=5) was significantly slowed ($P<0.05$, T-test) in comparison to mSlo3 currents (0.09 ± 0.01 ms/μM, n=6).

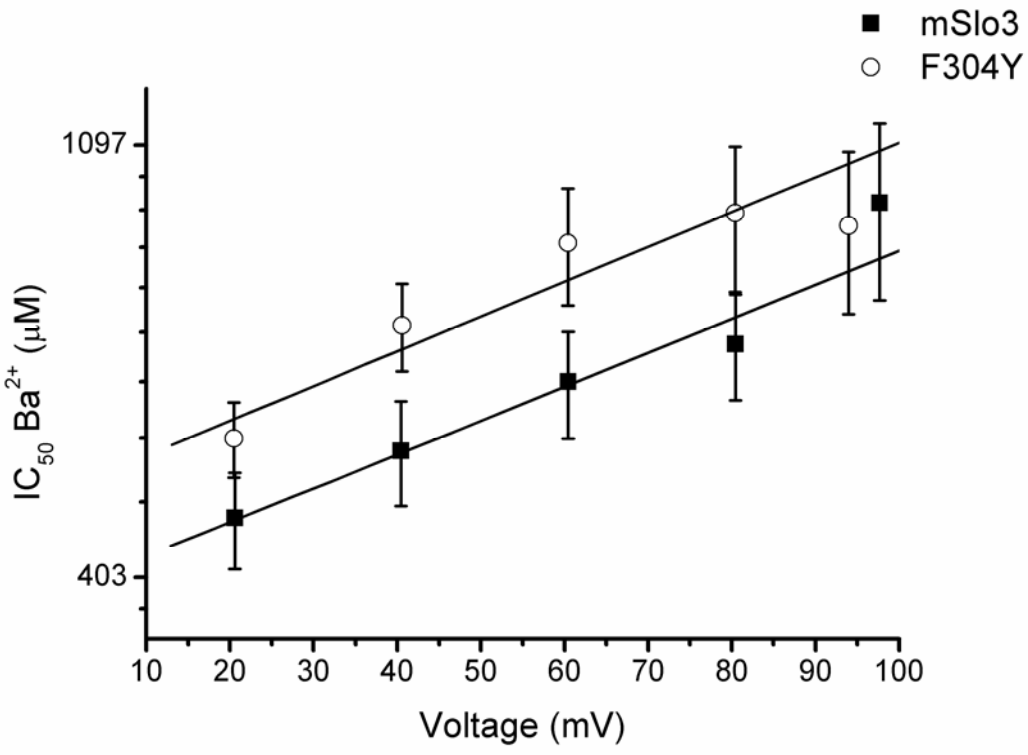

Figure 3.10 Voltage dependence of Ba^{2+} inhibition. The voltage dependence of Ba^{2+} block of mSlo3 and F304Y currents were determined by estimates of IC_{50} values obtained from ramp traces at +20, +40, +60, +80 and +100 mV and plotted to the transformed Woodhull equation. Straight line fits were used to calculate values of δ, the fraction of the electric field that the blocking ion experiences and the potency of block at 0 mV (K_{0mV}). Ba^{2+} inhibition of mSlo3 was calculated to have K_{0mV} = 293.57 ± 74.48 μM (n=5), however inhibition of F304Y gave a significantly different ($P<0.05$, T-test) calculated K_{0mV} = 521.08 ± 39.00 μM (n=5). δ was found not to be significant ($P>0.05$, T-test) between mSlo3 (0.66 ± 0.46) and F304Y (0.12 ± 0.05)

3.2.6 Pharmacological profile of mSlo3

The profile of the pharmacology of the mSlo3 channel was determined by application of inhibitors, dissolved either directly into either DMSO or Ringers to generate stock solutions, and then diluted to the required concentrations in standard Ringers solution. Inhibitors were then applied until steady state inhibition of a +100 mV recording pulse occurred, then washed with Ringers solution to relieve the inhibition as can be seen in Figure 3.11.A. Inhibition levels were measured and averaged and compared to the I_{KSper} values calculated by (Navarro *et al.*, 2007). Inhibition by 500 μM quinine (73.3 ± 4.87 %, n=11) was found to be not largely different from the reported I_{KSper} data (88 %, n=9). Mibefradil 5 μM (18 ± 3.27%, n=4) and clofilium 50 μM (59 ± 9.5 %, n=4) were sizeably different from the reported I_{KSper} data, 69 % (n=4) and 92 % (n=6) inhibition, respectively. As a control 20 mM TEA was applied and resulted in inhibition of 20.2 ± 0.74 % (n=6). 2 mM Ba^{2+} was also applied, the same concentration used by Navarro *et al* (2007), inhibited 70.04 ± 3.73 % (n=3) of the current in normal K^+ levels. When High K^+ solution (2.3.1) was perfused with 2mM Ba^{2+} inhibition was significantly ($P>0.05$, Student's t-test) reduced to 10.65 ± 2.32 % (n=3). This is consistent with the findings of Navarro *et al* (2007) who found I_{KSper} currents were Ba^{2+} insensitive in equipotent K^+ (160 mM), but were sensitive to Ba^{2+} when Na^+ was the dominant extracellular ion. As can be seen in the sample traces (Figure 3.11.A) the quinine (500 μM), clofilium (50 μM) and TEA (20 mM) inhibition is reversible. Ba^{2+} was partially reversible at 2.5 mM extracellular K^+ and completely reversible at 100 mM extracellular K^+. Interestingly the mibefradil (5 μM) sample trace (Figure 3.11.A), indicates that relief of inhibition results in an increased current, as shown by the light grey trace.

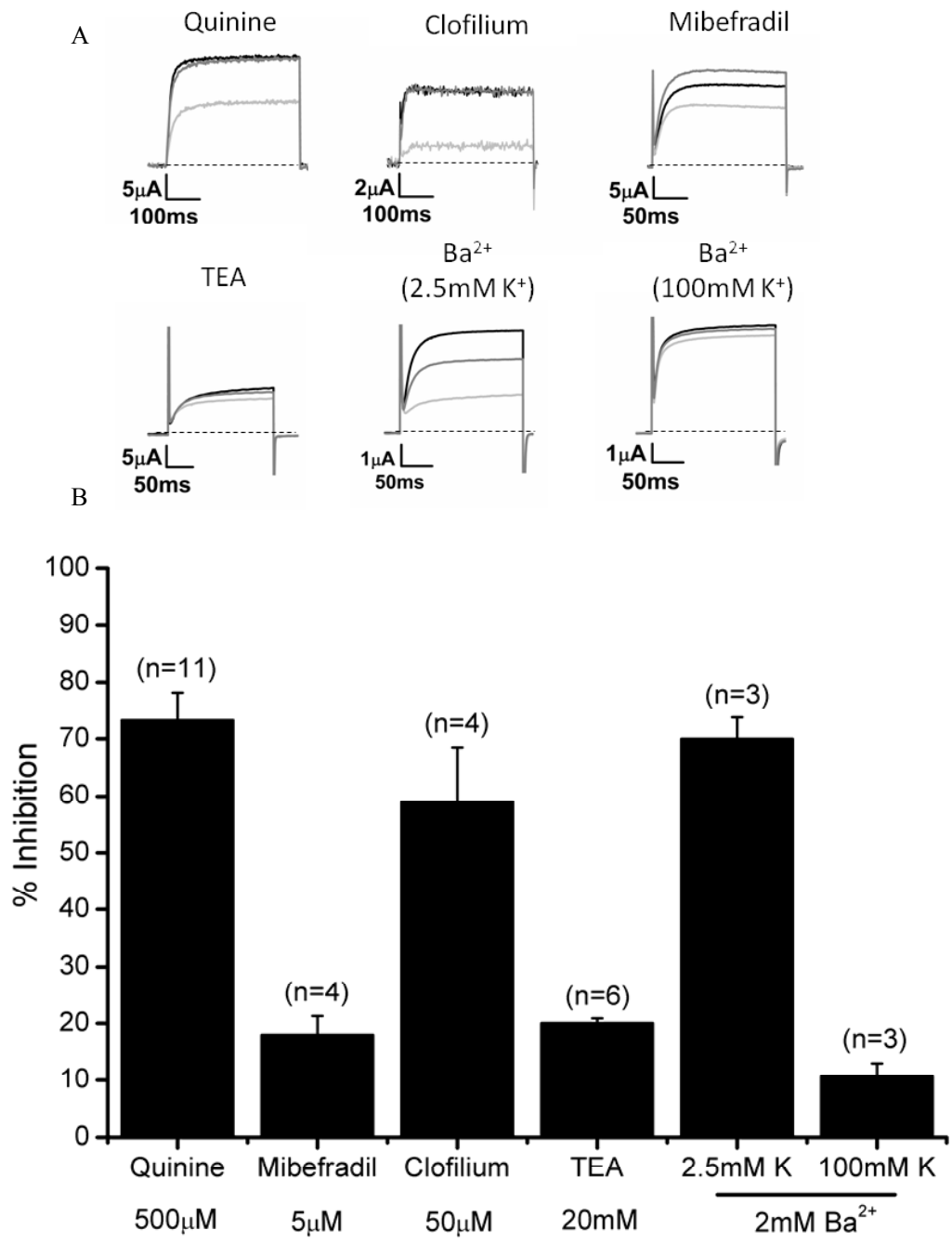

Figure 3.11 Pharmacological profile of mSlo3. The profile of the pharmacology of the mSlo3 channel was determined by application of inhibitors until steady state inhibition (light gray trace) of the -80 to +100 mV recording pulse occurred, then washed with Ringers to relieve the inhibition (dark gray trace). The mibefradil sample trace appears to indicate that relief of inhibition increases the current. The bar chart (B) shows the comparison of the average inhibition of the current in response to a range of compounds.

3.3 Chapter 3 Discussion

3.3.1 Electrophysiological effects of the F304Y mutation

The current understanding of the function and structure of the mSlo3 channel is limited; predominately due to the lack of recordable expression in mammalian cell lines. Functional mSlo3 expression has only been detected by injection of cRNA into oocytes. Although oocytes need to be injected with a near maximal level of ≈50 nl of the mSlo3 cRNA (≈1 μg/μl) to gain currents that are distinct from endogenous channels. In comparison hSlo1 cRNA can be diluted 20-400 fold and distinct recordable currents attained. mSlo3 current recordings in poorly expressing oocytes are contaminated by the endogenous currents at positive potentials (> +100 mV). Previous studies in hSlo1 revealed mutation of phenylalanine in position 380 in the S6 domain to tyrosine (F380Y) stabilises the open state of the channel by reducing the closing rate and shifting the voltage dependence of the opening rate (Lippiat *et al.*, 2000). The mSlo3 channel has a homologous phenylalanine in position 304. Thus we introduced the homologous mutation F304Y to attempt to solve the difficulties with channel activation and reduce the requirement for high cRNA levels by stabilising the open state of the channel.

Thus the F304Y mutation in mSlo3 should cause a leftward shift in the voltage dependence of the current and increase the conductance allowing a lower cRNA level to be injected. Our results show this mutation in mSlo3 causes a leftward shift in the current-voltage relationship and an increase in the $\tau_{+100\ mV}$. However the $V_{1/2}$ and voltage dependence values for F304Y calculated from the G/V curves showed no significant difference from the mSlo3 values. This lack of difference in the G-V relationship may be due to the fact that neither channel reaches a quantifiable plateau of G_{Max} at +140 mV. Thus, calculated G_{Max} values with intrinsic error, had to be utilised to normalise the data. To achieve a measurable G_{Max} value for the channels would require voltages greater than +140 mV. This would introduce two new problems, a larger proportion of contaminating endogenous current and increasing problems with voltage drop and capacitance. This requirement for a non-physiological range of positive voltages to reach G_{Max} is consistent with previous studies of mSlo3 when the currents failed to reach a measurable G_{Max} plateau in macroscopic patches pulled from oocytes at voltages up to +300 mV (Zhang *et al.*, 2006*a*; Tang *et al.*, 2010*b*).

The effects of the F304Y mutation on the voltage range of activation were very clear from the assessment of the change in oocyte RMP. F304Y expressing oocytes required a modified

Barth's solution that shifted the E_K value to ≈-36 mV, as calculated by the GHK equation, for successful incubation. This demonstrates that the major determinant of the RMP of the F304Y injected oocytes is a K^+ current, with a 12 fold higher P_{K^+}. Our analysis of the RMPs found that unlike I_{KSper}, mSlo3 expression does not significantly affect the RMP of expressing oocytes. However this is likely to be dependent on the ≈-44 mV shift in RMP due to F304Y expression which statistically masks the ≈-14 mV difference between the mSlo3 induced RMP and uninjected RMP. However, if the significance value is relaxed to $P<0.1$ the mSlo3 RMP was found to be significantly lower than in uninjected oocytes. Therefore our findings show that effect of the F304Y mutation on mSlo3 is parallel to the effects of the F380Y mutation on hSlo1 (Lippiat *et al.*, 2000). This suggests that like hSlo1 this residue may have a critical function in the gating mechanism. Mutation from a nonpolar to polar amino acid potentially alters the sensitivity to a range of activators. Our current study does not encompass changes in the sensitivity of pH or pharmacological activators of mSlo3. This is predominantly because mSlo3 has no known agonists and past attempts to acidify/alkalise the intracellular oocyte solution using varied extracellular solutions in the absence of the chloride current blocker DIDS was observed to have opposing effects on endogenous currents (Schreiber *et al.*, 1998). Supplementing our solutions with 1 mM DIDS would inhibit the endogenous currents; however the amounts required for our pharmacology studies would be prohibitively expensive.

3.3.2 Method of Inhibition by Quinine and Quinidine of mSlo3

Quinine and, the stereoisomer quinidine, are non specific K^+ channel inhibitors, for which the full mechanism of block has not been defined. Quinine block of rSlo1 has been shown to display the characteristics of open-channel block, primarily inducing "flickery" block and reducing current amplitude (Franciolini *et al.*, 2001). Quinidine inhibition of mSlo1 shows a weak voltage dependence of block and can be fitted with an open channel block scheme (Tang *et al.*, 2010*b*). This theory of the mechanism of quinine and quinidine inhibition offers an explanation as to why F304Y channels are more sensitive compared to mSlo3, as these channels are open across more of the voltage range, thus have a higher Po resulting in an increased apparent affinity. Observations of the inhibition trace (Figure 3.6.B) in particular the 1 μM concentration trace, displays characteristics mimicking inactivation of the channel. However, fitting a voltage dependent activation and inactivation equation to the data gave poor fits and inconsistent values. This is most probably due to a combination of high variability in the levels of starting current and problems with control of the voltage clamp of ooctyes over-expressing F304Y with currents greater than 30 nA at +100 mV. This theory, however, appears to be contrary to a previous study's findings using an mSlo1/mSlo3

chimaera (MC13), which has the residues 1-181 substituted with Slo1, had a higher affinity for the closed state. However this study admits that for cytosolic application of quinidine, no model of block fits the data any better than the other (Tang *et al.*, 2010*b*). These findings support our suggestion that the F304Y mutation appears to have similar effects to the F380Y mutation in hSlo1 and stabilises the open state of the channel.

3.3.3 Site of Inhibition by Quinine and Quinidine of mSlo3

Quinidine inhibition is thought to result from binding of the protonated form to the intracellular side of the channel. This has been proposed by earlier studies that found that application of cytosolic quinidine on Slo1 channels and the MC13 chimaera was ≈ 5 fold more potent than extracellular application. Their study also found that variance of the pH, which in turn varies the percentage of protonated quinidine, proportionally varied the block of mSlo1 channels (Tang *et al.*, 2010*b*). Our studies fit with these previous findings as negative values for zδ suggest that quinine and quinidine block is incompatible with the classical Woodhull model of a positively charged molecule binding from the extracellular side to a site within the membrane. However, negative values for zδ for a positively charged molecule suggest that the molecule is binding from the intracellular side of the channel. Comparison of quinine and quinidine block, shows for both F304Y and mSlo3 channels there is no significant difference ($P>0.05$, Two-way ANOVA; Bonferroni post hoc test) of the zδ values dependent on isomer applied. This suggests that quinine and quinidine bind to the same site within the channel but with different affinities. However, the differing pKa values of quinine and quinidine, due to the differing spatial orientation, may also contribute to the differing IC_{50} values observed.

Previous studies have suggested that block occurs due to the protonated form of the drug binding the channel (Zhang *et al.*, 1998; Sănchez-Chapula *et al.*, 2003; Tang *et al.*, 2010*b*). At the resting oocyte pH ≈ 7.5, 92.6% of quinidine (pKa, 8.6) is protonated in comparison to 90% of quinine (pKa, 8.5) (Schreiber *et al.*, 1998). Therefore the rightwards shift in IC_{50}, may be partly due to the higher intracellular levels of a protonated compound. Full protonation of both compounds would occur at pH ≈ 6.5, below the required pH range for activation of the mSlo3 (Zhang *et al.*, 2006*a*). Our finding that quinidine is more potent than quinine in inhibiting the mSlo3 channel agree with the observation that the Human *ether-a-go-go*-related gene (HERG) K^+ channel is also more strongly inhibited by quinidine than quinine (Sănchez-Chapula *et al.*, 2003). This is to be anticipated as the compounds have distinct three-dimensional orientations, therefore it is to be expected that the binding properties may be different at the same site.

Secondly the S6 domain of the K^+ channel has been shown to be a major determinant of the characterisitics of quinidine inhibition. Study of mutations in the S6 domain of the HERG K^+ channel have been shown to affect the characteristics of inhibition by quinidine and quinine (Sănchez-Chapula *et al.*, 2003). Also S6 domain mutations in the rKv1.4 K^+ channel affect the characteristics of inhibition by quinidine (Zhang *et al.*, 1998). Although not significant, the shift in the Hill slope for F304Y channels compared to mSlo3, suggests that the explanation for the apparent increased open channel block may not be as simple as an increased P_o. There is a second explanation for the increase in the apparent affinities of the F304Y channels to these compounds. It has been shown that the equivalent residue to F304 in the HERG K^+ channel, Y652 in the S6 domain, affects the characteristics of inhibition by quinine and quinidine. Interestingly comparing our F304Y K_{0mV} values to the WT HERG IC_{50} recorded at 0 mV found no difference for either quinine or quinidine. However mutation of Y652 to F (Y652F) in HERG channels, the inverse of our mutation in mSlo3, does not affect the potency of block but decreases the voltage dependence of inhibition by these compounds (Sănchez-Chapula *et al.*, 2003) this is in contrast to our mSlo3 K_{0mV} values which show a ≈ 4 fold reduction in potency compared to F304Y channels. Interestingly, chloroquine inhibition, (a related quinoline with two protonation sites) of HERG channels shows a ten fold reduction in potency at 0 mV dependent on the mutation of Y652F (Sánchez-Chapula *et al.*, 2002). We see a similar change in our finding that F304Y currents were ≈ 10- fold more potently inhibited by quinine or quinidine compared to mSlo3 at +100 mV. In HERG channels block is thought to be due to the aromatic groups of the quinoline π-stacking between the Y652 and F656 residues (Sănchez-Chapula *et al.*, 2003). The mSlo3 channel, however, has an isoleucine (I308) in the homologous position to F656 and thus π-stacking to this residue is not possible.

Dependence on the F304 position in mSlo3 is probably increased for binding of quinine or quinidine. In rKv1.4 channels mutation of T529, equivalent to L303 in mSlo3, to a more hydrophobic residue results in slowing of deactivation and a negative shift in the voltage dependence of activation (Zhang *et al.*, 1998). This effect is theorised to be due to the residue at 529, during the open state, faces away from the lumen and face the other TM α-helices, thus increasing the hydrophobicity of the residue at 529 stabilises this condition (Zhang *et al.*, 1998). These mutations in rKv1.4 channels also result in increased quinidine potency, which is proposed to be due to quinidine binding by intercalation of the hydrophobic moiety of the compound into the protein interior during the open state (Zhang *et al.*, 1998). Mutation of the T529 residue to T529Y, however, abolished rKv1.4 current expression, this was proposed to be due to tyrosine being too bulky to intercalate into the

protein interior (Zhang *et al.*, 1998). This is in contrast with our F304Y mutation; however our mutation is 1 residue further down the α-helix. Thus it is likely that this residue is already partly intercalated with the other TM α-helices and requires less energy to fully intercalate and stabilise the open state. These findings explain why we observed significant increases in F304Y zδ values for both quinine and quinidine, compared to mSlo3. zδ values, a measure of the fraction of the electric field that the blocker experiences, are also a measure of the voltage dependence of block. Thus the observed IC_{50} shift dependent on the F304Y mutation is probably due to a combination of the mutation revealing/increasing the binding site and increasing the P_o. Although the quinine/quinidine binding site is a conserved architectural feature of voltage gated K^+ channels, the potency of inhibition is dependent on the surrounding residues. Thus these compounds may be difficult to use in channel identification as cells rarely express a single type of K^+ channel. This theory has been supported by a study performed on mSlo3 knock out (KO) spermatozoa where quinidine IC_{50} values were not significantly different for K^+ currents in the WT and KO spermatozoan (Zeng *et al.*, 2011).

3.3.4 Ba^{2+} Inhibition

Ba^{2+} is a voltage-dependent pore blocker of K^+ channels, with well-known binding site mechanisms (Armstrong & Taylor, 1980; Neyton & Miller, 1988; Jiang & MacKinnon, 2000). Extracellular Ba^{2+} binds to the pore without channel activation but is relieved by depolarisation (Armstrong & Taylor, 1980; Neyton & Miller, 1988). This can be seen in our finding that the τ_{+100mV} values are increased in a linear concentration dependent relationship. This characteristic of Ba^{2+} block also explains why we see no significant difference in the IC_{50} values between F304Y and mSlo3 channels. Therefore the F304Y mutation effects are due to effects on gating mechanism rather than the selectivity of the channel pore. We used straight line fits plotted to individual oocyte values using the transformed Woodhull equation to calculate values of δ, and K_{0mV} for Ba^{2+} for both the F304Y and WT mSlo3 channel (Woodhull, 1973) (2.3.4.B). Ba^{2+} inhibition of mSlo3 was calculated to have a $\delta = 0.66 \pm 0.46$, (n=5) with the F304Y mutation not significantly ($P>0.05$, Student's t-test) changing this value ($\delta = 0.12 \pm 0.05$, n=5). However if we excluded one of the mSlo3 fits, which has a calculated $\delta \approx 2$, which is impossible as $\delta > 1$ for an extracellular positive ion would mean the Ba^{2+} ion would bind further through the pore than the intracellular side of the electric field. Rejecting this value, the δ value for Ba^{2+} ion in mSlo3 channels changes to a more realistic 0.20 ± 0.09 (n=4). These findings suggest that in both mSlo3 and F304Y channel block by extracellular Ba^{2+} is quite shallow in the electric field. Our finding that Ba^{2+} block is shallow is inconsistent with previous studies and the model of Ba^{2+} block in the

KcsA crystal structure which found the Ba^{2+} site is between the enhancement site ($\delta = 0.5$) and internal lock-in site ($\delta = 0.7$) (Armstrong & Taylor, 1980; Neyton & Miller, 1988; Jiang & MacKinnon, 2000). However our finding of $\delta \approx 0.16$ for Ba^{2+} suggests that Ba^{2+} is binding to the external lock-in site ($\delta = 0.15$) in the pore. This is probably due to our experimental technique of using a ramp protocol rather than discrete voltage steps as Ba^{2+} blockade of K^+ channels is reduced by depolarisation (Armstrong & Taylor, 1980). This is exemplified if we compare the IC_{50} values at +100 mV pulse from -80 mV to the +100 mV IC_{50} from the ramp traces there is a significant ($P<0.05$, paired-Student's t-test) increase of nearly double the IC_{50} value that is independent of the F304Y mutation. Thus it is possible that in our ramp experiments the Ba^{2+} ion cannot reach the "classical" binding site due to the constant flow of ions through the pore and thus is only able to block the pore through binding to the external lock-in site.

3.3.5 Pharmacological Profiling of mSlo3 currents

In this study we attempt to elucidate the function of mSlo3 by defining the pharmacological profile and comparing with the described profile of the I_{KSper} current. The pharmacological profile of our mSlo3 channels does not align perfectly with the reported profile of I_{KSper}, the pH dependent current observed in spermatozoa (Navarro *et al.*, 2007), though all compounds caused some degree of inhibition. Clofilium, a quaternary ammonium compound, was the most divergent from the observed I_{KSper} inhibition as it not only showed a reduction in the level of inhibition but also a reversibility of the inhibition that was not observed with the I_{KSper} current. This difference in binding properties may be due to the mechanism of clofilum block. It has been suggested that clofilium may cause channel block via an "activation trap" mechanism (Steidl & Yool, 2001). This has been suggested by the findings that Kv1.5 channel recovery from block was slower at hyperpolarised potentials, however increased extracellular $[K^+]$ accelerated recovery (Steidl & Yool, 2001). This may explain why I_{KSper} displayed an irreversible inhibition, as the membrane potential was only depolarised to -20 mV (Navarro *et al.*, 2007), whereas in our protocol the membrane potential was depolarised to +100 mV with each pulse, thus hastening the relief of inhibition. Clofilium has also been used to distinguish between K^+ currents in spermatozoa, with apparent I_{KSper} specificity (Zeng *et al.*, 2011). Although currents were pulsed to +200 mV, most of the current at +100 mV remained inhibited (Zeng *et al.*, 2011). This difference is probably due to the timescale of application as we found that reversal of clofilium inhibition took 10 minutes or more whereas their study only washed for ≈ 3 minutes. The increase of the current during wash post mibefradil inhibition (5 μM) may be due to low mibefradil concentrations still present in the solutions. $IK_{Ca}1$ channel currents were decreased by concentrations of mibefradil

higher than 5 μM but showed increased current amplitudes with mibefradil concentrations ≤2 μM (Yoo *et al.*, 2008). The variation in IC_{50} values of mibefradil and clofilium may well be due to the difference in expression system as I_{KSper} was recorded from intact Catsper KO spermatozoan, whereas, our system utilised expression in *Xenopus* oocytes. This system potentially lacks accessory proteins that may interact or modulate channel function; these may affect the P_o and thus cause the observed differences in the apparent affinities. In addition I_{KSper} is a current; thus it may be dependent on more than one type of channel. Lastly with use of patch clamp intracellular conditions can be controlled, whereas TEVC lacks this facility. Using cut open oocyte or macropatch techniques to record would allow control of these conditions.

3.3.6 A potential role for mSlo3 channels in spermatozoa volume regulation.

The pharmacological profile we have described also suggests additional roles for mSlo3 channels in spermatozoa in volume regulation and motility. mSlo3 channels have been previously discounted for these roles due to reported TEA sensitivity (IC_{50} of 49 mM at +60 mV), leading to Kv1.5 and TASK2 channels being the channels theorised to mediate volume regulation and motility (Yeung & Cooper, 2001; Barfield *et al.*, 2005*a*, 2005*b*). However their study only used up to 10 mM TEA without seeing significant effects (Barfield *et al.*, 2005*b*). Our study shows that even at concentrations of 20 mM TEA is only able to inhibit 20% of the current, therefore the exclusion of the mSlo3 channel as a potential component of volume regulation seems premature. The K^+ current that regulates volume and motility is sensitive to as little as 200 μM quinine when applied for 5 minutes (Yeung & Cooper, 2001; Barfield *et al.*, 2005*b*). Although this concentration is double the IC_{50} for the mSlo3 channel, the timescale of inhibition is similar to our findings. This study also shows that the mSlo3 channels are sensitive to clofilium (50 μM); however clofilium application takes ≈10 minutes to reach steady state (personal observation). The volume regulatory K^+ current has also been shown to be to be sensitive to clofilium (10 μM) when applied for 75 minutes but not 5 minutes; this timescale correlates with our observations. The regulatory K^+ current is also sensitive to 4-AP, a K^+ channel inhibitor shown to have effects on spermatozoan volume regulation (Barfield *et al.*, 2005*a*). However, this compound was found to enhance rather than inhibit I_{KSper}, possibly in consequence of indirect alkalinisation of cells (Navarro *et al.*, 2007), thus this compound was excluded from our study. Whilst our study cannot define mSlo3 as the sole channel mediating volume regulation and motility in the spermatozoan, we suggest that it has been prematurely discounted as a component of this K^+ current. This theory is supported by recent studies on mSlo3 KO spermatozoa from transgenic mice that have shown reduced mobility, the second of the studies also showed

that mSlo3 KO spermatozoa were unable to maintain normal volume regulation under osmotic stress (Santi *et al.*, 2010; Zeng *et al.*, 2011).

3.3.7 Challenges for the future

Challenges for the future will be to examine: (a) if the effects of the F304Y mutation are concurrent for the other I_{KSper} inhibitors; (b) utilising macro-patches of oocyte membranes the effects of the F304Y mutation can be investigated further; (c) the pharmacological characteristics of the compounds using oocyte macro-patches; (d) screening for a specific reversible pharmacological antagonist using a high throughput oocyte recording system; (e) if there are any accessory proteins that modify expression levels (partly addressed in Chapter 4) with a view to gaining expression in mammalian systems.

3.3.8 Chapter Summary

This data reveals that the mutation of the conserved phenylalanine in the S6 domain (Slo3-F304/Slo1- F380) to tyrosine has conserved effects on Slo channel properties, namely a negative shift in voltage dependence of activation and increase the channel conductance. This mutation is in the conserved quinoline binding site and thus affects the potency of these compounds; however, extracellular pore blockers like Ba^{2+} are unaffected. Lastly the pharmacological properties we have found of mSlo3 match fairly well with the reported I_{KSper} profile and suggest a role in volume regulation of spermatozoa.

Chapter IV: Self Regulation of mSlo3

4.1 Chapter 4 Introduction

4.1.1 Structural features of the Sloα family

The Slo channel family is a family of ligand gated K^+ channels that are homologous to Kv channels. These channels consist of six TM domains (like the voltage gated K^+ (Kv) channels). Slo and Kv subunits share an archetypal topology consisting of six TM helices (S1-S6), these subunits are arranged as a tetramer to form a single ion conducting pore (Hille, 2001). However, unlike the Kv channel family, Slo1 and Slo3 channels possess an additional N-terminal helix (S0), creating an extracellular N-termini. More importantly, the Slo channel family possess large C-terminal cytoplamic domains. This domain is composed of a tandem arrangement of non-identical regulators of K^+ conductance (RCK) domains, and it is these domains that confer ligand gating properties upon channel activation. Structural studies show that the RCK domain forms an octomeric gating ring in close proximity to the TM ion conduction pore, and potentially forming a cytoplasmic ion conduction pathway for ions moving through the channel (Yuan *et al.*, 2010; Wu *et al.*, 2010). The RCK domains are thought to undergo ligand dependent conformational change that alters the kinetics of the transition between the open/closed states of the channel activation gate. The Slo family of channels are exemplified by the Slo1 (also referred to as BK_{Ca} or MaxiK in the literature) have been extensively investigated due to the wide expression profile and high unitary conductance (260 pS) in symmetrical K^+ (160 mM) (Butler *et al.*, 1993). Previous studies have demonstrated that the Slo1 channel is gated by voltage (via the voltage sensor) and Ca^{2+} via the cytoplasmic RCK domains. RCK1 contains three residues (D362, D367 and M513) that are critical for high-affinity Ca^{2+} sensitivity. RCK2, however, has a "calcium bowl" formed from five consecutive negatively charged aspartates (D894–D898) (Yusifov *et al.*, 2008).

The mouse Slo3 (mSlo3) channel was first detected via an expressed sequence tag (EST), from the mouse promyelocytic WEHI-3 lymphocyte cell line, with homology to the C-terminal "tail" of mSlo1. The cDNA's from WEHI-3 were found to be either truncated or improperly spliced, suggesting that the full length channel was not expressed in this cell line. Using PCR analysis of a variety of tissues, the *KCNU1* gene encoded channel (mSlo3) was found to be expressed solely in spermatozoa and testis. However, the study did admit that

the techniques used could not exclude restricted expression within tissues or low expression levels (Schreiber *et al.*, 1998). Topology modeling from hydrophilicity profiling of the mSlo3 sequence indicated that like mSlo1 there are 11 hydrophobic domains, S0 through S10. The mSlo1 and mSlo3 sequences have highest similarity in the core domain containing the six TM domains and RCK1. The mSlo1 core, S0 through to S8, shares 56% sequence identity to the mSlo3 core region. The orthologs mSlo1 and dSlo1 share 62% identity through this core region. The S9 and S10 regions are more divergent and have only 39% identity between mSlo3 and mSlo1. The Slo3 channel, when expressed in *Xenopus* oocytes, was found to be modulated by internal pH, with channel activation at low $[H^+]$, and voltage rather than by Ca^{2+} and voltage like the Slo1 channel and the channel had a lower unitary conductance (106 pS) in symmetrical K^+ (160 mM) (Schreiber *et al.*, 1998).

Interestingly, despite the complexity of the RCK domain structure and ligand interaction properties, this domain is conserved in prokaryotic K+ channels. These channels are exemplified by the MthK Ca^{2+}-gated K^+ channel from the bacteria *Methanobacterium thermoautotrophicum*. However, rather than a tandem RCK domain, these channels possess only a single RCK subunit (RCK1) that is tethered to the TM domains. These channels compensate for this loss by expression of an identical, separate RCK subunit (RCK2). The soluble RCK2 domain is encoded within the MthK gene itself, due to the presence of an internal start codon (M107) and assembles with RCK1 to form the octameric gating ring (Jiang *et al.*, 2002*b*). The binding of Ca^{2+} to the RCK domains alters the conformation of the gating ring, thereby opening the gate (Li *et al.*, 2007). This hypothesis has been proved correct by the two crystal structures of the isolated RCK domains which show a tetramer with each subunit containing two RCK domains. In these structures RCK1 acts like the inner RCK domain and RCK2 contributing the role of the soluble MthK RCK domain (Yuan *et al.*, 2010; Wu *et al.*, 2010). The MthK octomer, however, differs in the response to decreased pH in comparison with the Slo1 octamer. Below a pH of 7.5, MthK becomes insensitive to Ca^{2+} activation, because the RCK octamer tends to disassemble as it is structurally unstable at this pH. Alkaline pH (>7.5) increases the open probability (Po) for a given $[Ca^{2+}]$ and can activate the channel in the absence of Ca^{2+} (Lingle, 2007). This activation in response to pH (>7.5) is similar to the Slo3 channel characteristics (Schreiber *et al.*, 1998). However, Slo1 is activated by low intracellular pH due to D367, one of the three residues that forms the RCK1 Ca^{2+} binding site, interaction with H365 and H394 (Yusifov *et al.*, 2008; Hou *et al.*, 2008). Interestingly mutation of both these histidine residues affected the Ca^{2+} sensitivity, suggesting that they also contribute to the RCK1 Ca^{2+} binding site (Hou *et al.*, 2008).

4.1.2 Regulation of mSlo3 channel expression by accessory subunits

Slo1 channels *in vivo* are not only formed solely from Slo1 α-subunits; there are four known Sloβ subunits, which have a range of effects on the functional properties of the channel. Sloβ have a conserved structure, consisting of two TM helices linked by a large extracellular loop. Sloβ subunits are thought to physically interact through the S0 and S1/2 domains of the Slo1 α-subunit, which is the region that mSlo1 and mSlo3 have the highest homology (Wu *et al.*, 2009).

A previous study of the interactions between mSlo3 and Sloβ subunits found that all of the Sloβ subunits appear to be able to interact with mSlo3. Sloβ2 was found to functionally interact with mSlo3 and displayed trypsin-sensitive inactivation (Yang *et al.*, 2009). However of the four Sloβ subunits, only Sloβ4 has a gain of function effect on mSlo3 currents. Sloβ4 injection with mSlo3 α-subunit results in an eight-fold increase in the conductance recorded from macropatches and increased surface expression. Expression of mSlo3 with Sloβ4 did not modify the voltage dependence, single channel conductance or the P_o of currents. This suggests that Sloβ4 only affects expression level of the channels rather than the electrophysiological properties. Interestingly, for such an increase in expression, Sloβ4 KO mice had no change in the reproductive capacity, as quantified by litter size (Yang *et al.*, 2009). This evidence suggests that there are other regulatory subunits that effect mSlo3 expression *in vivo*.

4.1.3 Chapter aims

4.1.3.1 To determine if neuronal EST's encode an isoform of mSlo3

Expression of mSlo3 α-subunit is restricted to the testis and spermatozoa, unlike the mSlo1 α-subunit (Schreiber *et al.*, 1998). However a range of expressed sequence tags (EST's) have been identified in a range of tissues, particularly neuronal tissue, that correspond to the mSlo3 sequence. We aim to use RACE PCR (2.1.3) to examine if these EST's encode a novel splice variant of the α-subunit of mSlo3. If the RACE PCR of the EST's finds a sequence with an ORF, the amino acid sequence will be determined and compared to the known mSlo3 sequence. Secondly if the variant contains the mSlo3 epitope recognised by the NeuroMab mouse anti-mSlo3 antibody we will be able to probe an assortment of tissue homogenates to see if this unique isoform is expressed outside the restricted profile for mSlo3.

4.1.3.2 What architectural features of mSlo3 are also present in the isoform

The C-terminal domain of the α-subunit of mSlo3 is believed to contain two RCK domains, homologous to the mSlo1α structure. Thus as most of the EST sequences appear to be analogous to large parts of the mSlo3 C-terminal domain, we aim to align the sequences with the previously reported RCK sequences (Yusifov *et al.*, 2008) and determine the secondary structure to establish if any of the architectural features of mSlo1 are preserved in the mSlo3/isoform sequence.

4.1.3.3 What effect does the isoform have on Sloα-subunit expression

Alpha subunits of the mSlo1 channel have been previously shown to hetromultimerise with other α-subunits (Joiner *et al.*, 1998). However, mSlo1/Slo3 hetromultimeric currents have been impossible to distinguish from mSlo1 currents primarily due to the difficulty in mslo3 expression and the size of the mSlo1 currents. Thus we aim to co-inject our isoform in oocytes to see if we can observe any effects on mSlo1 and mSlo3 mediated currents. Secondly we aim to see if the isoform has any effect on the previously reported increase of mSlo3 currents dependent on the co-injection of the hSloβ4 (Yang *et al.*, 2009).

4.2 Chapter 4 Results

4.2.1 Sequence alignment of EST's

Mouse EST's with homology to the mSlo3 cDNA sequence were identified using the UniGene database (Pubmed). Of most interest were the EST's that were expressed outside the testis/spermatozoa, in a variety of neuronal tissues. Three were expressed in the adult male hippocampus (AK083174, BB428821 and BB653287), one from the subfornical organ and postrema (BQ175543), one in the upper head (CV562866) and one from the lateral wall of lateral ventricle (CX213584). EST's were aligned to the mSlo3 cDNA sequence using ClustalW2 in figure 4.1. EST sequences that were homologous to the mSlo3 sequence were highlighted in grey to emphasise the high level of homology, bar a few SNP's. The EST sequences were divergent from the mSlo3 sequence at the 5' end; however there was internal consistency between the four EST sequences over this region.

4.2.2 Probing for neuronal isoforms of mSlo3

RACE PCR is a technique that allows cloning of full length RNA transcripts found within a cell from short sequences such as EST's. Primers were designed using NCBI primer blast design software (Rozen & Skaletsky, 2000) utilising the mSlo3 WT related EST CV562866 (*CV*) as a template, this EST was chosen as it had a divergent 5' and an unknown 3' sequence. Marathon RACE PCR was performed using mouse brain Marathon-ready™ cDNA (Clontech) to isolate any potential neuronal isoforms. First round PCR was performed under conditions described in 2.1.3, with CVstart/CVend run against Adaptor Primer (AP) 1. The result of the first round of Marathon RACE PCR, of the two *CV* specific primers against the outer adaptor primer (AP1) can be seen in figure 4.2.A. When visualised on ethidium bromide agarose gels the first round PCR products displayed smears with faint bands at 1000-1500 bp. The products of these reactions were used as a template for second round PCR, the EST specific internal CVF*/CVR* against AP2, targeted to the inner adapter. Products were visualised, figure 4.2.B, forward EST internal primers produced high molecular weight bands of ≈1.5 kb. The reverse EST internal primer reactions produced only low molecular weight bands, between 200-600 bp. Second round products were then cleaned and then blunt end ligated, 2.1.4 before sequencing.

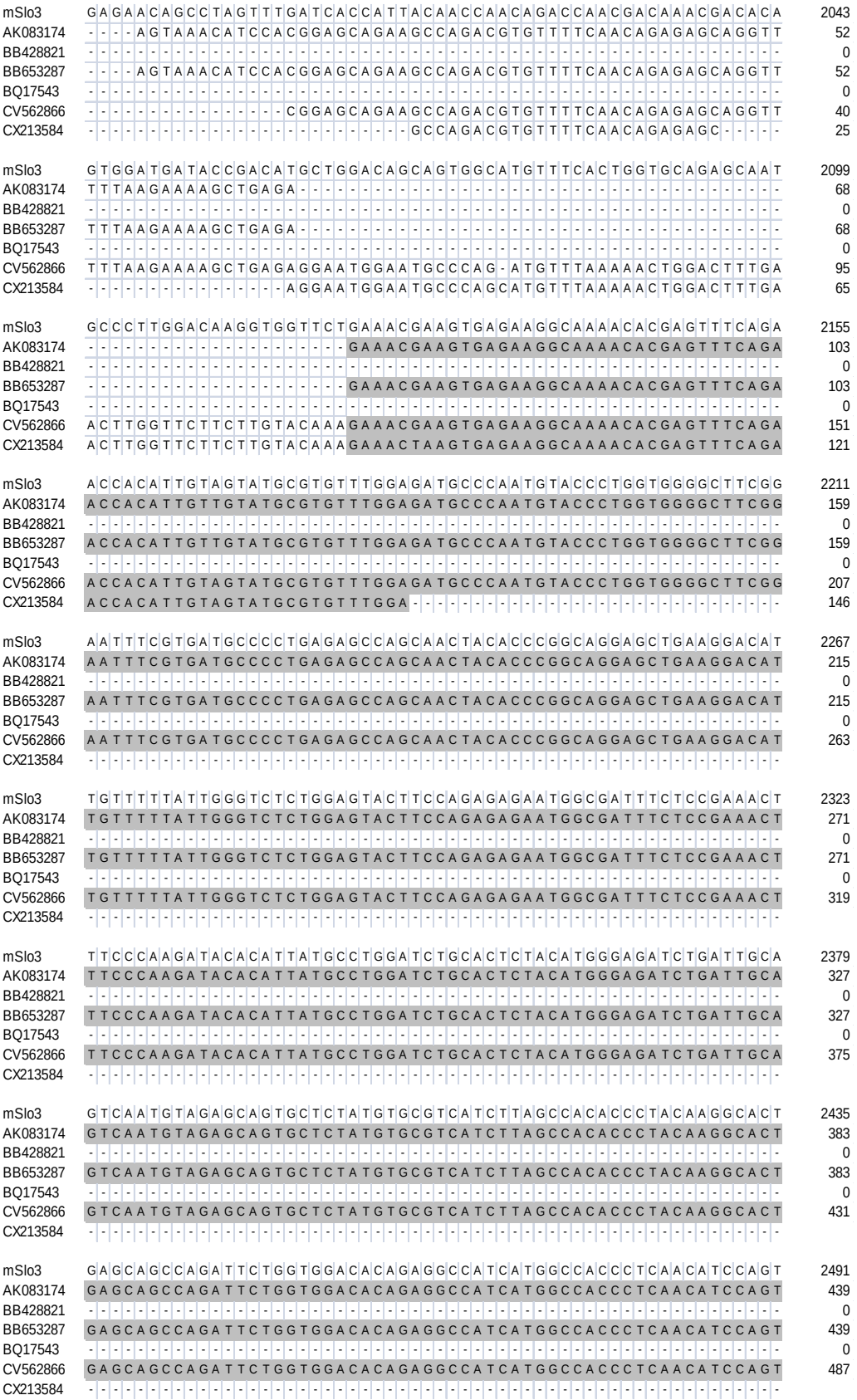
mSlo3 GAGAACAGCCTAGTTTGATCACCATTACAACCAACAGACCAACGACAAACGACACA 2043
AK083174 ----AGTAAACATCCACGGAGCAGAAGCCAGACGTGTTTTCAACAGAGAGCAGGTT 52
BB428821 -- 0
BB653287 ----AGTAAACATCCACGGAGCAGAAGCCAGACGTGTTTTCAACAGAGAGCAGGTT 52
BQ17543 -- 0
CV562866 ----------CGGAGCAGAAGCCAGACGTGTTTTCAACAGAGAGCAGGTT 40
CX213584 ----------GCCAGACGTGTTTTCAACAGAGAGC---- 25
mSlo3 GTGGATGATACCGACATGCTGGACAGCAGTGGCATGTTTCACTGGTGCAGAGCAAT 2099
AK083174 TTTAAGAAAAAGCTGAGA---------- 68
BB428821 ---------- 0
BB653287 TTTAAGAAAAAGCTGAGA---------- 68
BQ17543 ---------- 0
CV562866 TTTAAGAAAAAGCTGAGAGGAATGGAATGCCCAG-ATGTTTAAAAACTGGACTTTGA 95
CX213584 ----------AGGAATGGAATGCCCAGCATGTTTAAAAACTGGACTTTGA 65
mSlo3 GCCCTTGGACAAGGTGGTTCTGAAACGAAGTGAGAAGGCAAAACACGAGTTTCAGA 2155
AK083174 ----------GAAACGAAGTGAGAAGGCAAAACACGAGTTTCAGA 103
BB428821 ---------- 0
BB653287 ----------GAAACGAAGTGAGAAGGCAAAACACGAGTTTCAGA 103
BQ17543 ---------- 0
CV562866 ACTTGGTTCTTCTTGTACAAAGAAACGAAGTGAGAAGGCAAAACACGAGTTTCAGA 151
CX213584 ACTTGGTTCTTCTTGTACAAAGAAACTAAGTGAGAAGGCAAAACACGAGTTTCAGA 121
mSlo3 ACCACATTGTAGTATGCGTGTTTGGAGATGCCCAATGTACCCTGGTGGGGCTTCGG 2211
AK083174 ACCACATTGTTGTATGCGTGTTTGGAGATGCCCAATGTACCCTGGTGGGGCTTCGG 159
BB428821 ---------- 0
BB653287 ACCACATTGTTGTATGCGTGTTTGGAGATGCCCAATGTACCCTGGTGGGGCTTCGG 159
BQ17543 ---------- 0
CV562866 ACCACATTGTAGTATGCGTGTTTGGAGATGCCCAATGTACCCTGGTGGGGCTTCGG 207
CX213584 ACCACATTGTAGTATGCGTGTTTGGA---------- 146
mSlo3 AATTTCGTGATGCCCCTGAGAGCCAGCAACTACACCCGGCAGGAGCTGAAGGACAT 2267
AK083174 AATTTCGTGATGCCCCTGAGAGCCAGCAACTACACCCGGCAGGAGCTGAAGGACAT 215
BB428821 ---------- 0
BB653287 AATTTCGTGATGCCCCTGAGAGCCAGCAACTACACCCGGCAGGAGCTGAAGGACAT 215
BQ17543 ---------- 0
CV562866 AATTTCGTGATGCCCCTGAGAGCCAGCAACTACACCCGGCAGGAGCTGAAGGACAT 263
CX213584 ----------
mSlo3 TGTTTTTATTGGGTCTCTGGAGTACTTCCAGAGAGAATGGCGATTTCTCCGAAACT 2323
AK083174 TGTTTTTATTGGGTCTCTGGAGTACTTCCAGAGAGAATGGCGATTTCTCCGAAACT 271
BB428821 ---------- 0
BB653287 TGTTTTTATTGGGTCTCTGGAGTACTTCCAGAGAGAATGGCGATTTCTCCGAAACT 271
BQ17543 ---------- 0
CV562866 TGTTTTTATTGGGTCTCTGGAGTACTTCCAGAGAGAATGGCGATTTCTCCGAAACT 319
CX213584 ----------
mSlo3 TTCCCAAGATACACATTATGCCTGGATCTGCACTCTACATGGGAGATCTGATTGCA 2379
AK083174 TTCCCAAGATACACATTATGCCTGGATCTGCACTCTACATGGGAGATCTGATTGCA 327
BB428821 ---------- 0
BB653287 TTCCCAAGATACACATTATGCCTGGATCTGCACTCTACATGGGAGATCTGATTGCA 327
BQ17543 ---------- 0
CV562866 TTCCCAAGATACACATTATGCCTGGATCTGCACTCTACATGGGAGATCTGATTGCA 375
CX213584 ----------
mSlo3 GTCAATGTAGAGCAGTGCTCTATGTGCGTCATCTTAGCCACACCCTACAAGGCACT 2435
AK083174 GTCAATGTAGAGCAGTGCTCTATGTGCGTCATCTTAGCCACACCCTACAAGGCACT 383
BB428821 ---------- 0
BB653287 GTCAATGTAGAGCAGTGCTCTATGTGCGTCATCTTAGCCACACCCTACAAGGCACT 383
BQ17543 ---------- 0
CV562866 GTCAATGTAGAGCAGTGCTCTATGTGCGTCATCTTAGCCACACCCTACAAGGCACT 431
CX213584 ----------
mSlo3 GAGCAGCCAGATTCTGGTGGACACAGAGGCCATCATGGCCACCCTCAACATCCAGT 2491
AK083174 GAGCAGCCAGATTCTGGTGGACACAGAGGCCATCATGGCCACCCTCAACATCCAGT 439
BB428821 ---------- 0
BB653287 GAGCAGCCAGATTCTGGTGGACACAGAGGCCATCATGGCCACCCTCAACATCCAGT 439
BQ17543 ---------- 0
CV562866 GAGCAGCCAGATTCTGGTGGACACAGAGGCCATCATGGCCACCCTCAACATCCAGT 487
CX213584 ----------

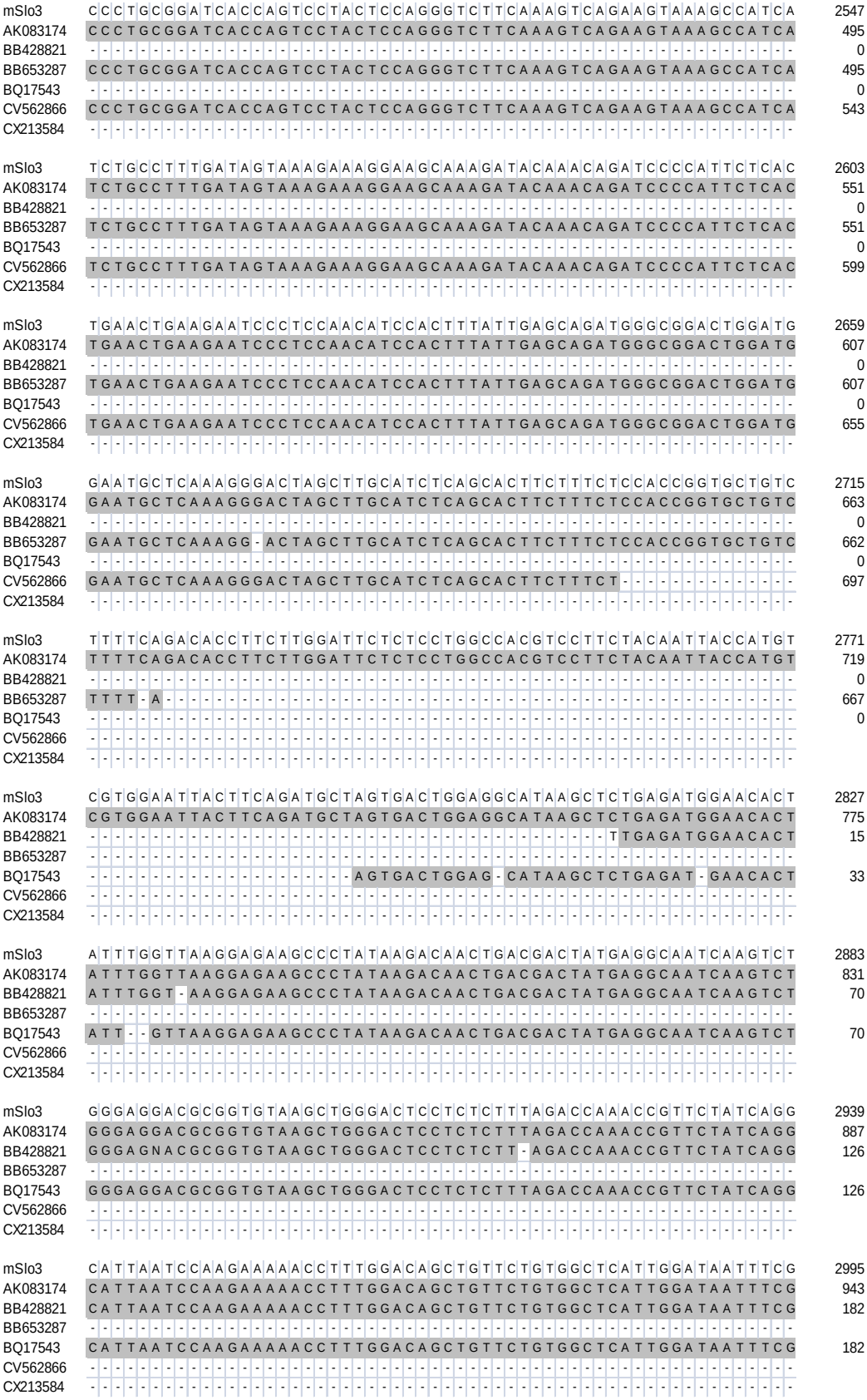
mSlo3 CCCTGCGGATCACCAGTCCTACTCCAGGGTCTTCAAAGTCAGAAGTAAAGCCATCA 2547
AK083174 CCCTGCGGATCACCAGTCCTACTCCAGGGTCTTCAAAGTCAGAAGTAAAGCCATCA 495
BB428821 0
BB653287 CCCTGCGGATCACCAGTCCTACTCCAGGGTCTTCAAAGTCAGAAGTAAAGCCATCA 495
BQ17543 0
CV562866 CCCTGCGGATCACCAGTCCTACTCCAGGGTCTTCAAAGTCAGAAGTAAAGCCATCA 543
CX213584
mSlo3 TCTGCCTTTGATAGTAAAGAAAGGAAGCAAAGATACAAACAGATCCCCATTCTCAC 2603
AK083174 TCTGCCTTTGATAGTAAAGAAAGGAAGCAAAGATACAAACAGATCCCCATTCTCAC 551
BB428821 0
BB653287 TCTGCCTTTGATAGTAAAGAAAGGAAGCAAAGATACAAACAGATCCCCATTCTCAC 551
BQ17543 0
CV562866 TCTGCCTTTGATAGTAAAGAAAGGAAGCAAAGATACAAACAGATCCCCATTCTCAC 599
CX213584
mSlo3 TGAACTGAAGAATCCCTCCAACATCCACTTTATTGAGCAGATGGGCGGACTGGATG 2659
AK083174 TGAACTGAAGAATCCCTCCAACATCCACTTTATTGAGCAGATGGGCGGACTGGATG 607
BB428821 0
BB653287 TGAACTGAAGAATCCCTCCAACATCCACTTTATTGAGCAGATGGGCGGACTGGATG 607
BQ17543 0
CV562866 TGAACTGAAGAATCCCTCCAACATCCACTTTATTGAGCAGATGGGCGGACTGGATG 655
CX213584
mSlo3 GAATGCTCAAAGGGACTAGCTTGCATCTCAGCACTTCTTTCTCCACCGGTGCTGTC 2715
AK083174 GAATGCTCAAAGGGACTAGCTTGCATCTCAGCACTTCTTTCTCCACCGGTGCTGTC 663
BB428821 0
BB653287 GAATGCTCAAAGG-ACTAGCTTGCATCTCAGCACTTCTTTCTCCACCGGTGCTGTC 662
BQ17543 0
CV562866 GAATGCTCAAAGGGACTAGCTTGCATCTCAGCACTTCTTTCT 697
CX213584
mSlo3 TTTTCAGACACCTTCTTGGATTCTCTCCTGGCCACGTCCTTCTACAATTACCATGT 2771
AK083174 TTTTCAGACACCTTCTTGGATTCTCTCCTGGCCACGTCCTTCTACAATTACCATGT 719
BB428821 0
BB653287 TTTT-A 667
BQ17543 0
CV562866
CX213584
mSlo3 CGTGGAATTACTTCAGATGCTAGTGACTGGAGGCATAAGCTCTGAGATGGAACACT 2827
AK083174 CGTGGAATTACTTCAGATGCTAGTGACTGGAGGCATAAGCTCTGAGATGGAACACT 775
BB428821 TTGAGATGGAACACT 15
BB653287
BQ17543 AGTGACTGGAG-CATAAGCTCTGAGAT-GAACACT 33
CV562866
CX213584
mSlo3 ATTTGGTTAAGGAGAAGCCCTATAAGACAACTGACGACTATGAGGCAATCAAGTCT 2883
AK083174 ATTTGGTTAAGGAGAAGCCCTATAAGACAACTGACGACTATGAGGCAATCAAGTCT 831
BB428821 ATTTGGT-AAGGAGAAGCCCTATAAGACAACTGACGACTATGAGGCAATCAAGTCT 70
BB653287
BQ17543 ATT--GTTAAGGAGAAGCCCTATAAGACAACTGACGACTATGAGGCAATCAAGTCT 70
CV562866
CX213584
mSlo3 GGGAGGACGCGGTGTAAGCTGGGACTCCTCTCTTTAGACCAAACCGTTCTATCAGG 2939
AK083174 GGGAGGACGCGGTGTAAGCTGGGACTCCTCTCTTTAGACCAAACCGTTCTATCAGG 887
BB428821 GGGAGNACGCGGTGTAAGCTGGGACTCCTCTCTT-AGACCAAACCGTTCTATCAGG 126
BB653287
BQ17543 GGGAGGACGCGGTGTAAGCTGGGACTCCTCTCTTTAGACCAAACCGTTCTATCAGG 126
CV562866
CX213584
mSlo3 CATTAATCCAAGAAAAACCTTTGGACAGCTGTTCTGTGGCTCATTGGATAATTTCG 2995
AK083174 CATTAATCCAAGAAAAACCTTTGGACAGCTGTTCTGTGGCTCATTGGATAATTTCG 943
BB428821 CATTAATCCAAGAAAAACCTTTGGACAGCTGTTCTGTGGCTCATTGGATAATTTCG 182
BB653287
BQ17543 CATTAATCCAAGAAAAACCTTTGGACAGCTGTTCTGTGGCTCATTGGATAATTTCG 182
CV562866
CX213584

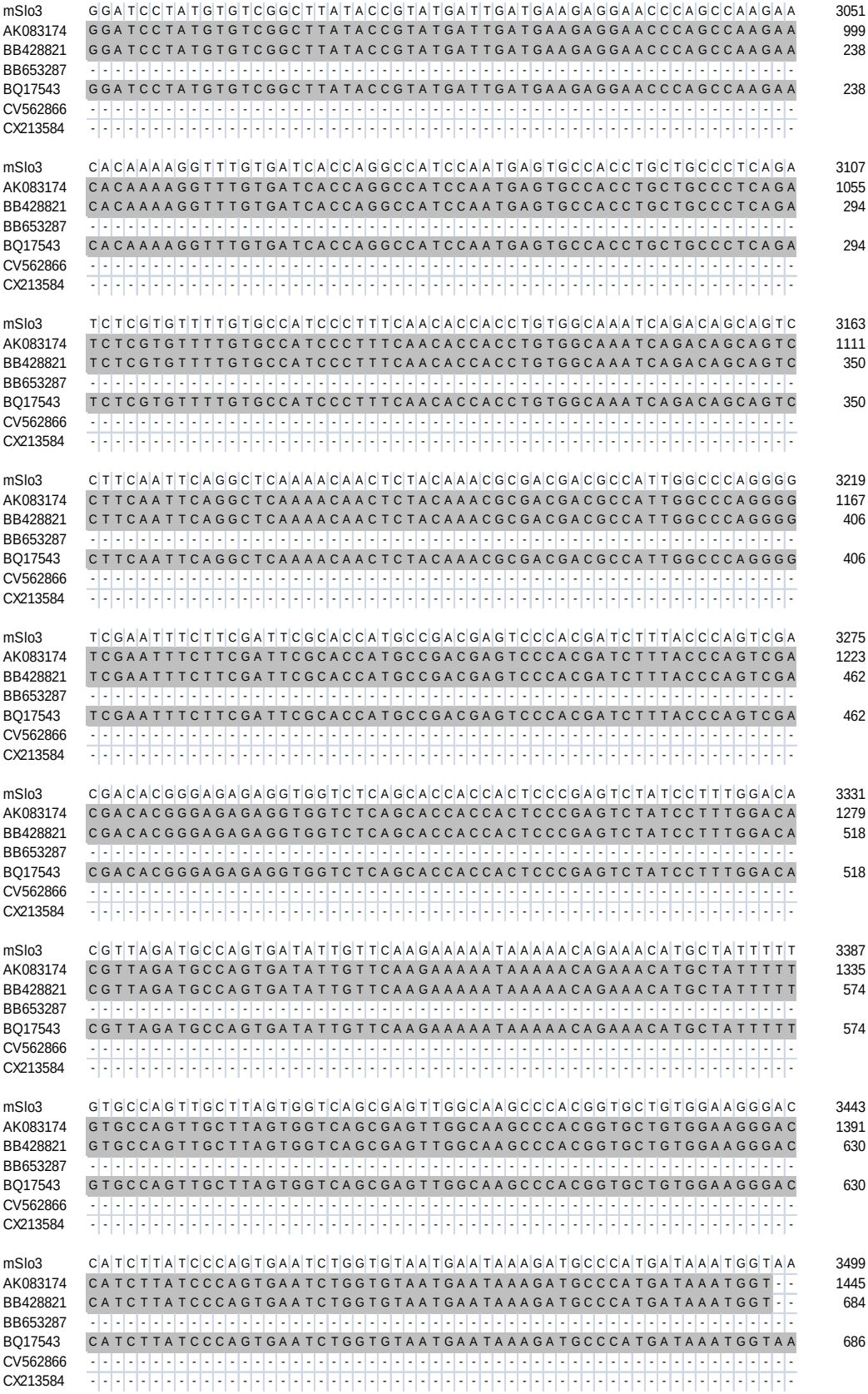
mSlo3 GGATCCTATGTGTCGGCTTATACCGTATGATTGATGAAGAGGAACCCAGCCAAGAA 3051
AK083174 GGATCCTATGTGTCGGCTTATACCGTATGATTGATGAAGAGGAACCCAGCCAAGAA 999
BB428821 GGATCCTATGTGTCGGCTTATACCGTATGATTGATGAAGAGGAACCCAGCCAAGAA 238
BB653287
BQ17543 GGATCCTATGTGTCGGCTTATACCGTATGATTGATGAAGAGGAACCCAGCCAAGAA 238
CV562866
CX213584
mSlo3 CACAAAAGGTTTGTGATCACCAGGCCATCCAATGAGTGCCACCTGCTGCCCTCAGA 3107
AK083174 CACAAAAGGTTTGTGATCACCAGGCCATCCAATGAGTGCCACCTGCTGCCCTCAGA 1055
BB428821 CACAAAAGGTTTGTGATCACCAGGCCATCCAATGAGTGCCACCTGCTGCCCTCAGA 294
BB653287
BQ17543 CACAAAAGGTTTGTGATCACCAGGCCATCCAATGAGTGCCACCTGCTGCCCTCAGA 294
CV562866
CX213584
mSlo3 TCTCGTGTTTTGTGCCATCCCTTTCAACACCACCTGTGGCAAATCAGACAGCAGTC 3163
AK083174 TCTCGTGTTTTGTGCCATCCCTTTCAACACCACCTGTGGCAAATCAGACAGCAGTC 1111
BB428821 TCTCGTGTTTTGTGCCATCCCTTTCAACACCACCTGTGGCAAATCAGACAGCAGTC 350
BB653287
BQ17543 TCTCGTGTTTTGTGCCATCCCTTTCAACACCACCTGTGGCAAATCAGACAGCAGTC 350
CV562866
CX213584
mSlo3 CTTCAATTCAGGCTCAAAACAACTCTACAAACGCGACGACGCCATTGGCCCAGGGG 3219
AK083174 CTTCAATTCAGGCTCAAAACAACTCTACAAACGCGACGACGCCATTGGCCCAGGGG 1167
BB428821 CTTCAATTCAGGCTCAAAACAACTCTACAAACGCGACGACGCCATTGGCCCAGGGG 406
BB653287
BQ17543 CTTCAATTCAGGCTCAAAACAACTCTACAAACGCGACGACGCCATTGGCCCAGGGG 406
CV562866
CX213584
mSlo3 TCGAATTTCTTCGATTCGCACCATGCCGACGAGTCCCACGATCTTTACCCAGTCGA 3275
AK083174 TCGAATTTCTTCGATTCGCACCATGCCGACGAGTCCCACGATCTTTACCCAGTCGA 1223
BB428821 TCGAATTTCTTCGATTCGCACCATGCCGACGAGTCCCACGATCTTTACCCAGTCGA 462
BB653287
BQ17543 TCGAATTTCTTCGATTCGCACCATGCCGACGAGTCCCACGATCTTTACCCAGTCGA 462
CV562866
CX213584
mSlo3 CGACACGGGAGAGAGGTGGTCTCAGCACCACCACTCCCGAGTCTATCCTTTGGACA 3331
AK083174 CGACACGGGAGAGAGGTGGTCTCAGCACCACCACTCCCGAGTCTATCCTTTGGACA 1279
BB428821 CGACACGGGAGAGAGGTGGTCTCAGCACCACCACTCCCGAGTCTATCCTTTGGACA 518
BB653287
BQ17543 CGACACGGGAGAGAGGTGGTCTCAGCACCACCACTCCCGAGTCTATCCTTTGGACA 518
CV562866
CX213584
mSlo3 CGTTAGATGCCAGTGATATTGTTCAAGAAAAATAAAAACAGAAACATGCTATTTTT 3387
AK083174 CGTTAGATGCCAGTGATATTGTTCAAGAAAAATAAAAACAGAAACATGCTATTTTT 1335
BB428821 CGTTAGATGCCAGTGATATTGTTCAAGAAAAATAAAAACAGAAACATGCTATTTTT 574
BB653287
BQ17543 CGTTAGATGCCAGTGATATTGTTCAAGAAAAATAAAAACAGAAACATGCTATTTTT 574
CV562866
CX213584
mSlo3 GTGCCAGTTGCTTAGTGGTCAGCGAGTTGGCAAGCCCACGGTGCTGTGGAAGGGAC 3443
AK083174 GTGCCAGTTGCTTAGTGGTCAGCGAGTTGGCAAGCCCACGGTGCTGTGGAAGGGAC 1391
BB428821 GTGCCAGTTGCTTAGTGGTCAGCGAGTTGGCAAGCCCACGGTGCTGTGGAAGGGAC 630
BB653287
BQ17543 GTGCCAGTTGCTTAGTGGTCAGCGAGTTGGCAAGCCCACGGTGCTGTGGAAGGGAC 630
CV562866
CX213584
mSlo3 CATCTTATCCCAGTGAATCTGGTGTAATGAATAAAGATGCCCATGATAAATGGTAA 3499
AK083174 CATCTTATCCCAGTGAATCTGGTGTAATGAATAAAGATGCCCATGATAAATGGT-- 1445
BB428821 CATCTTATCCCAGTGAATCTGGTGTAATGAATAAAGATGCCCATGATAAATGGT-- 684
BB653287
BQ17543 CATCTTATCCCAGTGAATCTGGTGTAATGAATAAAGATGCCCATGATAAATGGTAA 686
CV562866
CX213584

Figure 4.1 Alignment of EST's with mSlo3. Non-spermatozoa EST's were aligned to the mSlo3 cDNA sequence using ClustalW2. Conserved nucleotides of the EST sequences to the mSlo3 sequence are highlighted in grey. A high level of sequence identity was observed except around the 5' end of the EST sequences where there was internal consistency but divergence from the mSlo3 sequence.

A

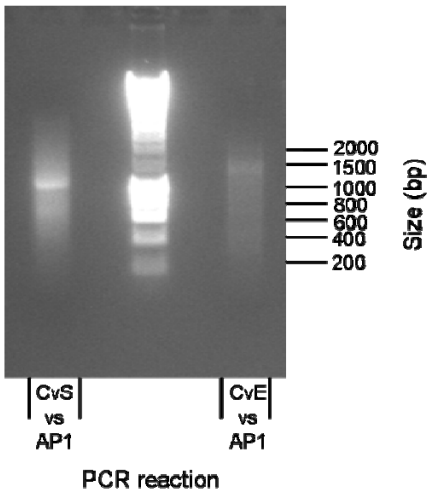

B

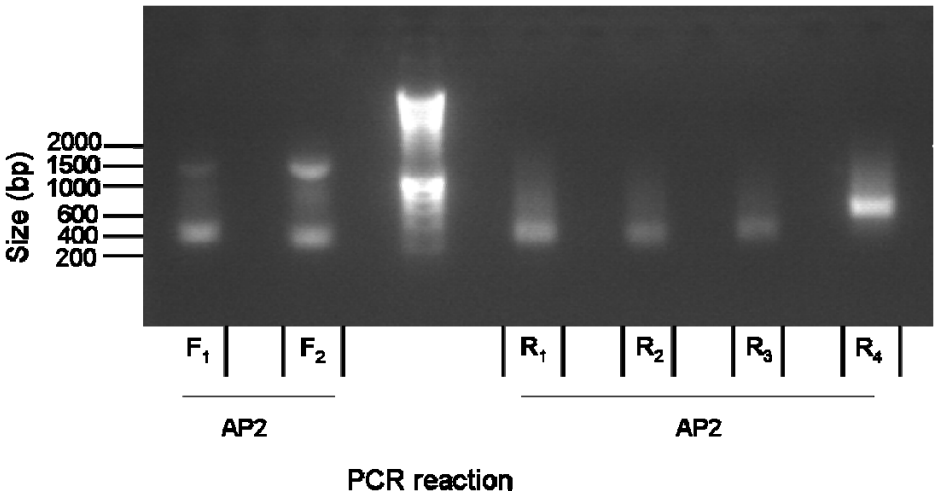

Figure 4.2 Visualisation of Marathon RACE PCR products. PCR products were separated on ethidium bromide agarose gels. The result of the first round of Marathon RACE PCR, of the two *CV* specific primers against the outer adaptor primer (AP1) can be seen in (A). The products displayed smears which show faint bands at 1000-1500 bp. The second round of Marathon RACE PCR (B) using the EST specific internal primers against the inner AP2 primer. As can be seen in (B) forward EST internal primers gave high molecular weight bands of ≈1.5 kb. The reverse EST internal primer reactions produced only low molecular weight bands, between 200-600 bp.

4.2.3 Expression of CV562866

cDNA sequences from the Marathon RACE PCR reactions were sequenced and a full length *CV562866* sequence constructed. This sequence was translated and found to contain an ORF starting at nucleotide 217 (Met740). The product of the ORF was aligned with the mSlo3 protein sequence using SWISS MODEL, figure 4.3 (Peitsch, 1995; Arnold *et al.*, 2006; Kiefer *et al.*, 2009). Alignment of the ORF protein (CV) with the mSlo3 sequence demonstrated a hundred percent sequence identity to the C-terminus of the mSlo3 sequence. As the CV sequence contains the epitope sequence recognised by the NeuroMab Anti-Slo3 antibody, we were able to investigate if ESTs are expressed at the protein level. Western blotting (4.4.A) was performed using CV562866 and full length mSlo3 (α3) expressed in HEK293 cells as control. Tissues were retrieved from adult Wistar rats, homogenised and then lysed and centrifuged to isolate the membrane fraction. Proteins from the tissue samples, membrane and supernatant, were separated on a 10% SDS gel (2.2.5) and later transferred to a nitrocellulose membrane. The membrane was probed with 1:1000 mouse anti-mSlo3 antibodies and visualised with 1:1000 anti-mouse-HRP secondary antibody. Transient transfection of HEK293 cells with pYX-Asc-CV562866 showed a band at between 36-55 kDa which was not present in the mSlo3 or control HEK cells and was consistent with the predicted molecular weight (Mw) of 47 kDa for CV. CV was also detected in blood, cytoplasmic fractions of liver and kidney and both the membrane and supernatant fractions from testis. Interestingly a high molecular weight band, of ≈100 kDa, was also observed in these tissues, the Mw of which is approximate to the lower band found in the mSlo3 control transfected cells. Localisation within the brain was defined using immunohistochemical techniques, brain slices were probed with 1:1000 anti-mSlo3 antibodies and visualised with Alexa 555. However when looking at the sample section, 4.4.B, a 60x image from the sub dentate gyrus region, shows widespread non-specific binding.

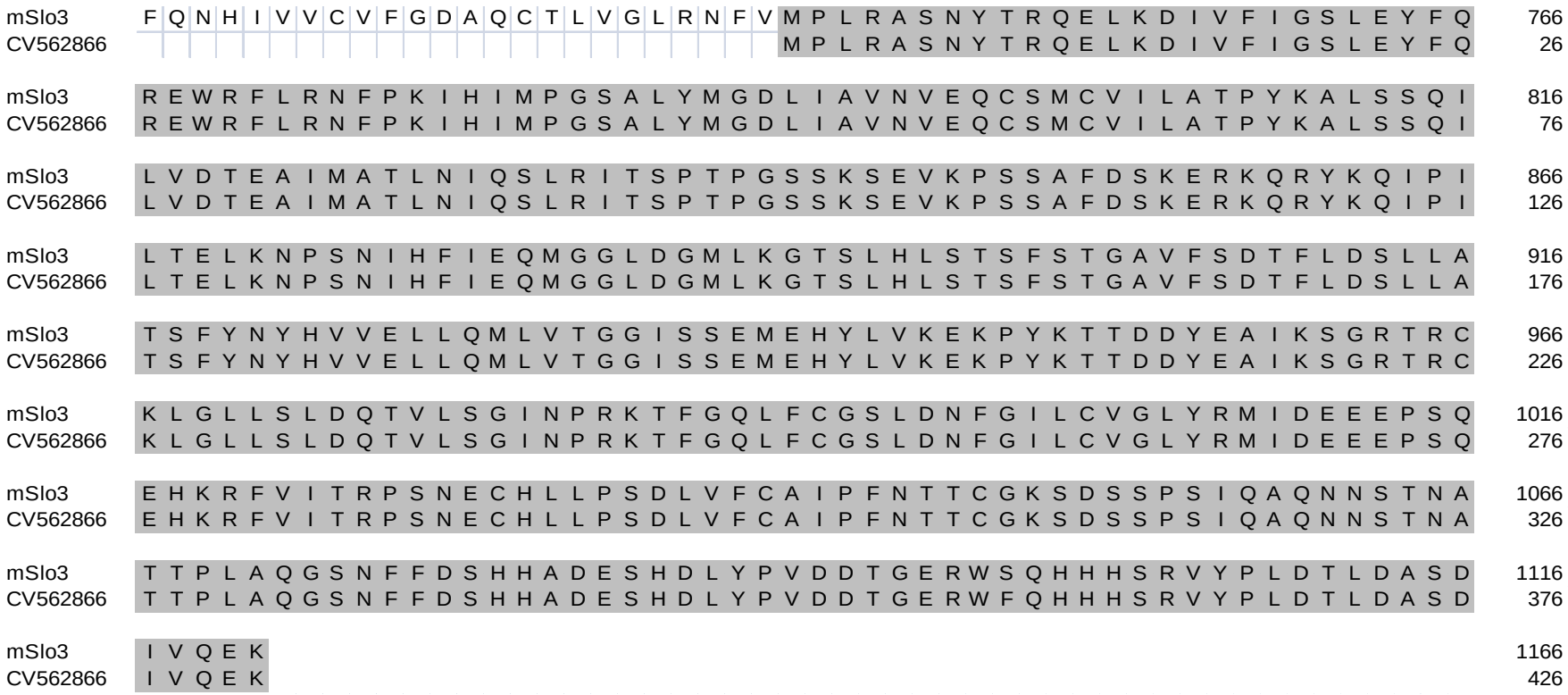

Figure 4.3 Alignment of CV562866 ORF with mSlo3 sequence. CV562866, the EST used for primer design, when sequenced was found to have an ORF starting at nucleotide 217 (Met740). This ORF was translated and aligned with the mSlo3 protein sequence using SWISS MODEL (Peitsch, 1995; Arnold *et al.*, 2006; Kiefer *et al.*, 2009). The sequence was found to have a hundred percent sequence identity to the C-Terminus of mSlo3 sequence.

A

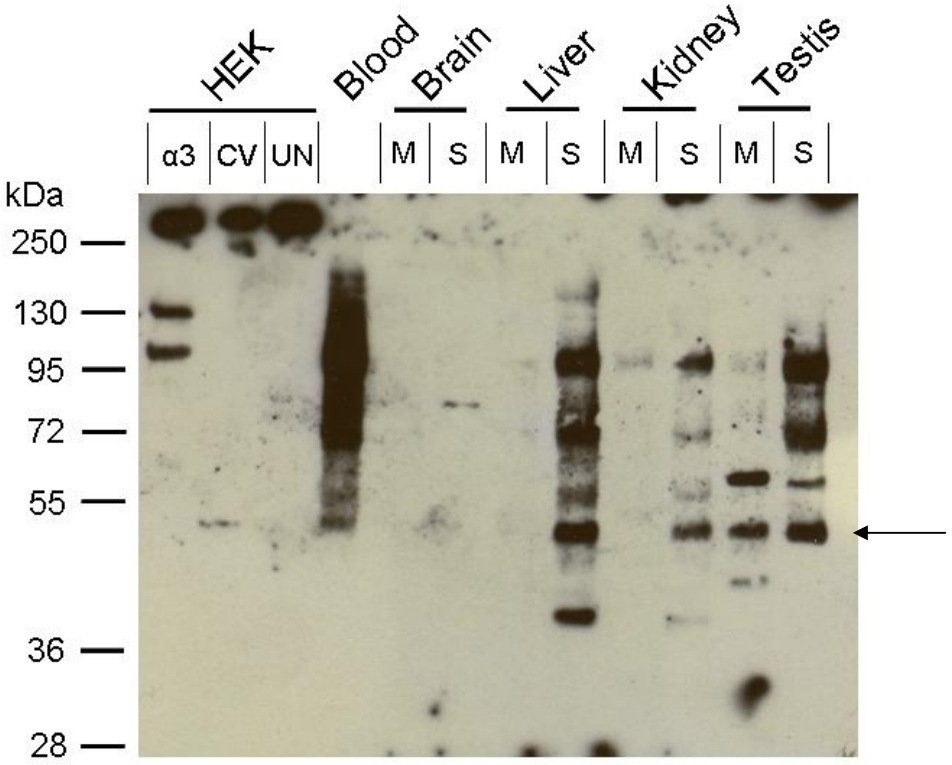

B

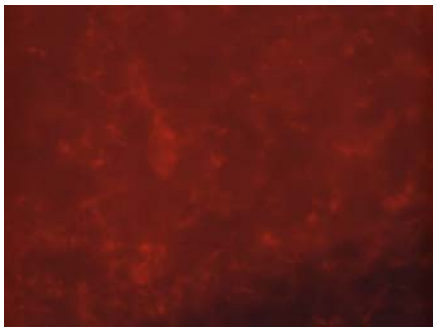

Figure 4.4 Physiological Expression of CV562866. As CV contains the epitope for the NeuroMab Anti-Slo3 antibody we were able to determine if ESTs are expressed at the protein level. Western blotting (A) was performed using CV and full length mSlo3 (α3) expressed in HEK293 cells as control. Tissues were retrieved from adult Wistar rats, homogenised and then lysed to isolate the membrane fraction. Membrane was probed with 1:1000 mouse anti-mSlo3 antibodies and visualised with 1:1000 anti-mouse-HRP secondary antibody. Tissue staining of brain tissue (B), showed widespread non-specfic binding when probed with 1:1000 anti-mSlo3 antibody and visualised with Alexa 555.

4.2.4 Structural prediction of Slo3 RCK domains

As the EST sequence contains the final 426 amino acids of the C-terminus of mSlo3, we determined if this region contains any RCK domains. Protein sequence alignment (Figure 4.5) of the previously described two RCK domains of mSlo1 (Yusifov *et al.*, 2008) and the homologus MthK RCK domain to the homologous regions of mSlo3 was performed. The RCK1 homologous region (4.5.A) showed a high sequence identity to the mSlo1 RCK1 and the MthK RCK domain. Whereas a lower sequence identity was observed when the homologous RCK2 region of mSlo3 was aligned to the mSlo1 RCK2 and the MthK RCK domain (4.5.B). Using the DomPred Protein Domain Prediction Server the secondary structures of the homologous regions to the mSlo1 RCK1 and RCK2 were determined. The homologous mSlo3 residues to the mSlo1 RCK βαβαβ Rossmann-fold structure (Lingle, 2007) were underlined and if corresponding to the structural elements annotated above the predicted structure (Figure 4.6). The secondary structures of the first RCK homologue of mSlo3 WT are shown with the known mSlo1 secondary structures annotated show a reasonably high level of parity (4.6.A). However, the second RCK domain subsequent to the αd helix, the region homologous to the "Calcium bowl" of mSlo1, the predicted secondary structure of the mSlo3 RCK2 differs from the homologous mSlo1 βαβαβ Rossmann-fold structure (4.6.B).

A

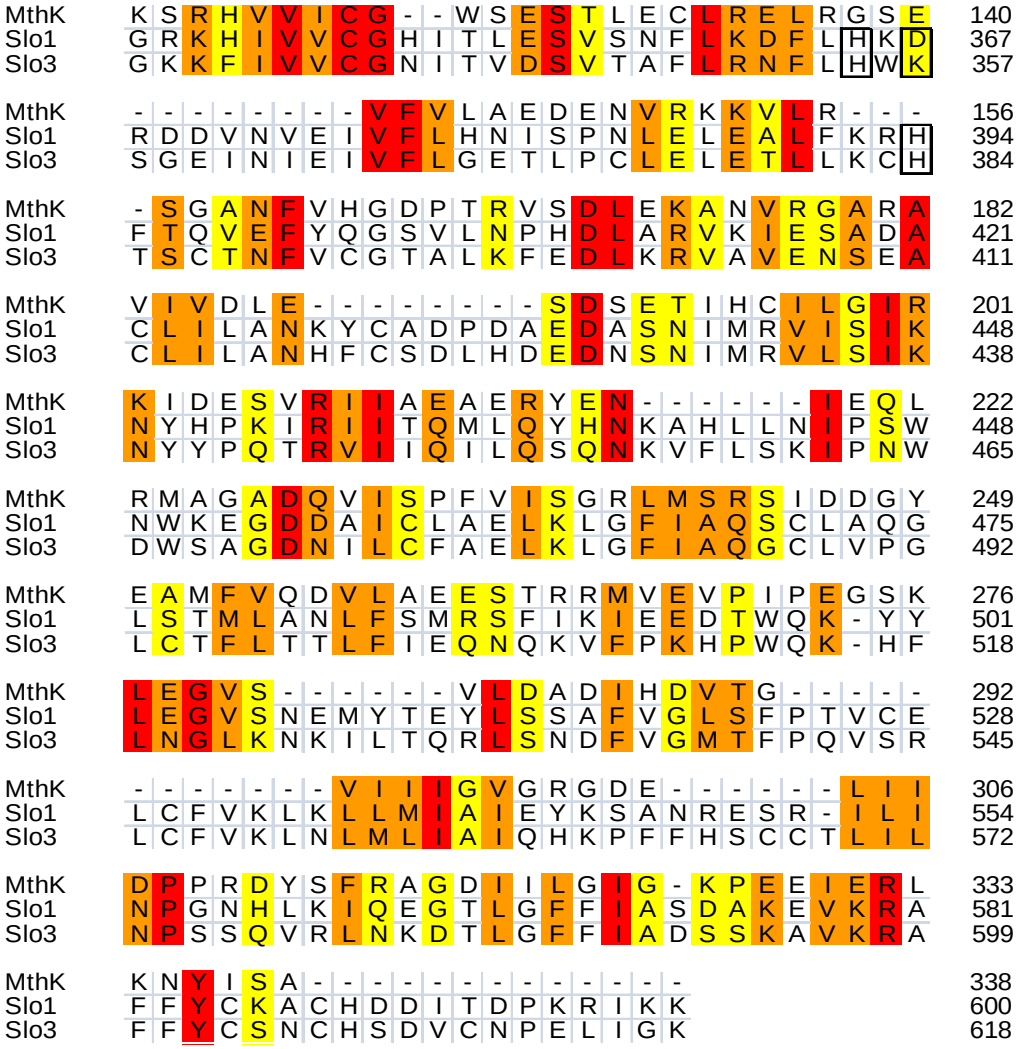
MthK K S R H V V I C G - - W S E S T L E C L R E L R G S E 140
Slo1 G R K H I V V C G H I T L E S V S N F L K D F L H K D 367
Slo3 G K K F I V V C G N I T V D S V T A F L R N F L H W K 357
MthK - - - - - - - - V F V L A E D E N V R K K V L R - - - 156
Slo1 R D D V N V E I V F L H N I S P N L E L E A L F K R H 394
Slo3 S G E I N I E I V F L G E T L P C L E L E T L L K C H 384
MthK - S G A N F V H G D P T R V S D L E K A N V R G A R A 182
Slo1 F T Q V E F Y Q G S V L N P H D L A R V K I E S A D A 421
Slo3 T S C T N F V C G T A L K F E D L K R V A V E N S E A 411
MthK V I V D L E - - - - - - - - - S D S E T I H C I L G I R 201
Slo1 C L I L A N K Y C A D P D A E D A S N I M R V I S I K 448
Slo3 C L I L A N H F C S D L H D E D N S N I M R V L S I K 438
MthK K I D E S V R I I A E A E R Y E N - - - - - - I E Q L 222
Slo1 N Y H P K I R I I T Q M L Q Y H N K A H L L N I P S W 448
Slo3 N Y Y P Q T R V I I Q I L Q S Q N K V F L S K I P N W 465
MthK R M A G A D Q V I S P F V I S G R L M S R S I D D G Y 249
Slo1 N W K E G D D A I C L A E L K L G F I A Q S C L A Q G 475
Slo3 D W S A G D N I L C F A E L K L G F I A Q G C L V P G 492
MthK E A M F V Q D V L A E E S T R R M V E V P I P E G S K 276
Slo1 L S T M L A N L F S M R S F I K I E E D T W Q K - Y Y 501
Slo3 L C T F L T T L F I E Q N Q K V F P K H P W Q K - H F 518
MthK L E G V S - - - - - - V L D A D I H D V T G - - - - - 292
Slo1 L E G V S N E M Y T E Y L S S A F V G L S F P T V C E 528
Slo3 L N G L K N K I L T Q R L S N D F V G M T F P Q V S R 545
MthK - - - - - - V I I I G V G R G D E - - - - - - L I I 306
Slo1 L C F V K L K L L M I A I E Y K S A N R E S R - I L I 554
Slo3 L C F V K L N L M L I A I Q H K P F F H S C C T L I L 572
MthK D P P R D Y S F R A G D I I L G I G - K P E E I E R L 333
Slo1 N P G N H L K I Q E G T L G F F I A S D A K E V K R A 581
Slo3 N P S S Q V R L N K D T L G F F I A D S S K A V K R A 599
MthK K N Y I S A - - - - - - - - - - - - - 338
Slo1 F F Y C K A C H D D I T D P K R I K K 600
Slo3 F F Y C S N C H S D V C N P E L I G K 618

B

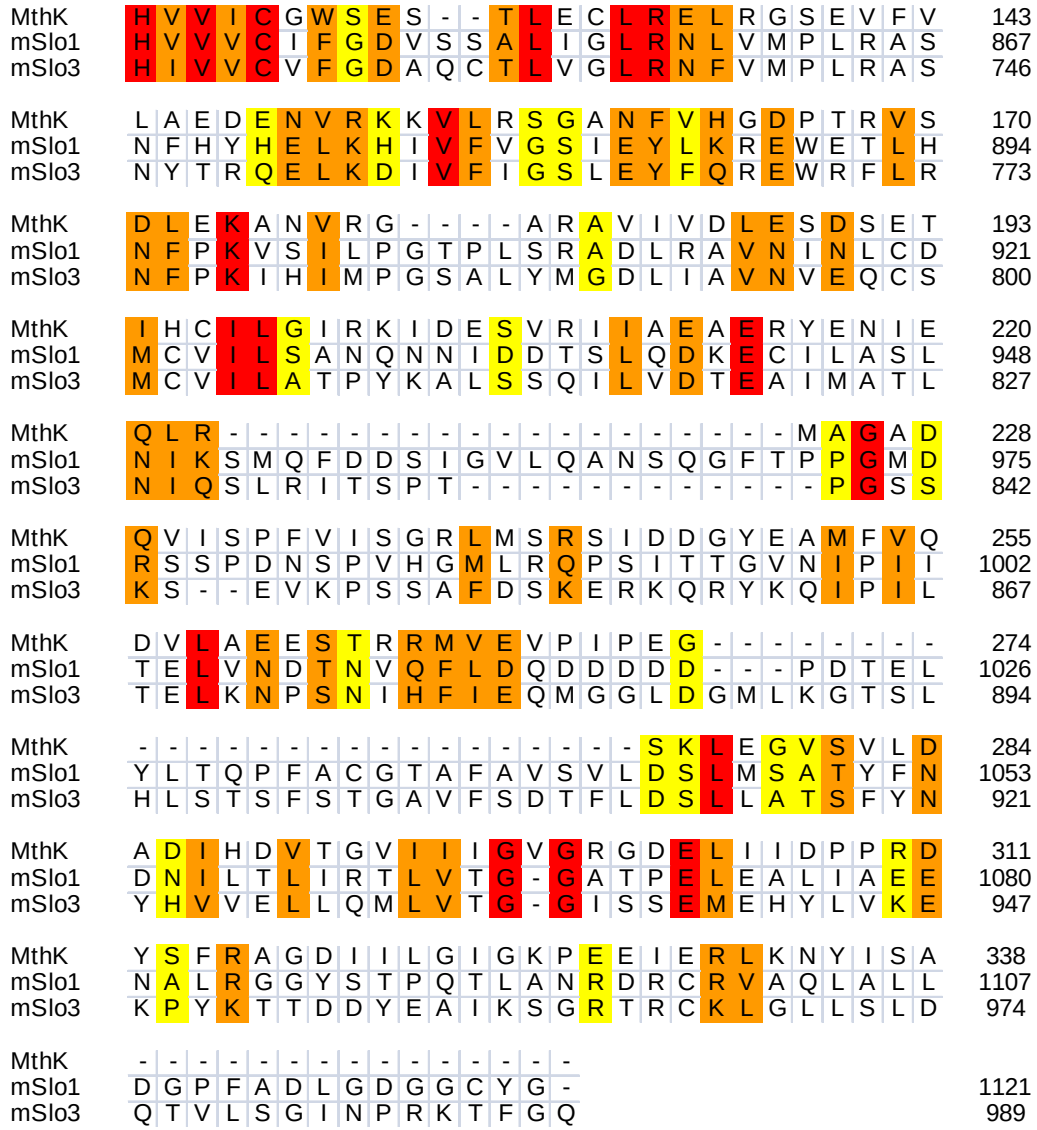

Figure 4.5 Alignments of RCK Domains. The RCK domains of mSlo1 and MthK were aligned with the homologous regions in the mSlo3 protein structure. Red highlighted residues are fully conserved residues; orange residues are residues of strongly similar properties (e.g. polarity) - scoring > 0.5 in the Gonnet PAM 250 matrix and yellow residues are conserved between residues of weakly similar properties - scoring < 0.5 in the Gonnet PAM 250 matrix. The RCK1 homologous region (A) showed a high sequence identity to the mSlo1 RCK1 and the MthK RCK domain. Whereas a low sequence identity is seen in the mSlo3 RCK2 homologous region (B) alignment to the mSlo1 RCK2 and the MthK RCK domain.

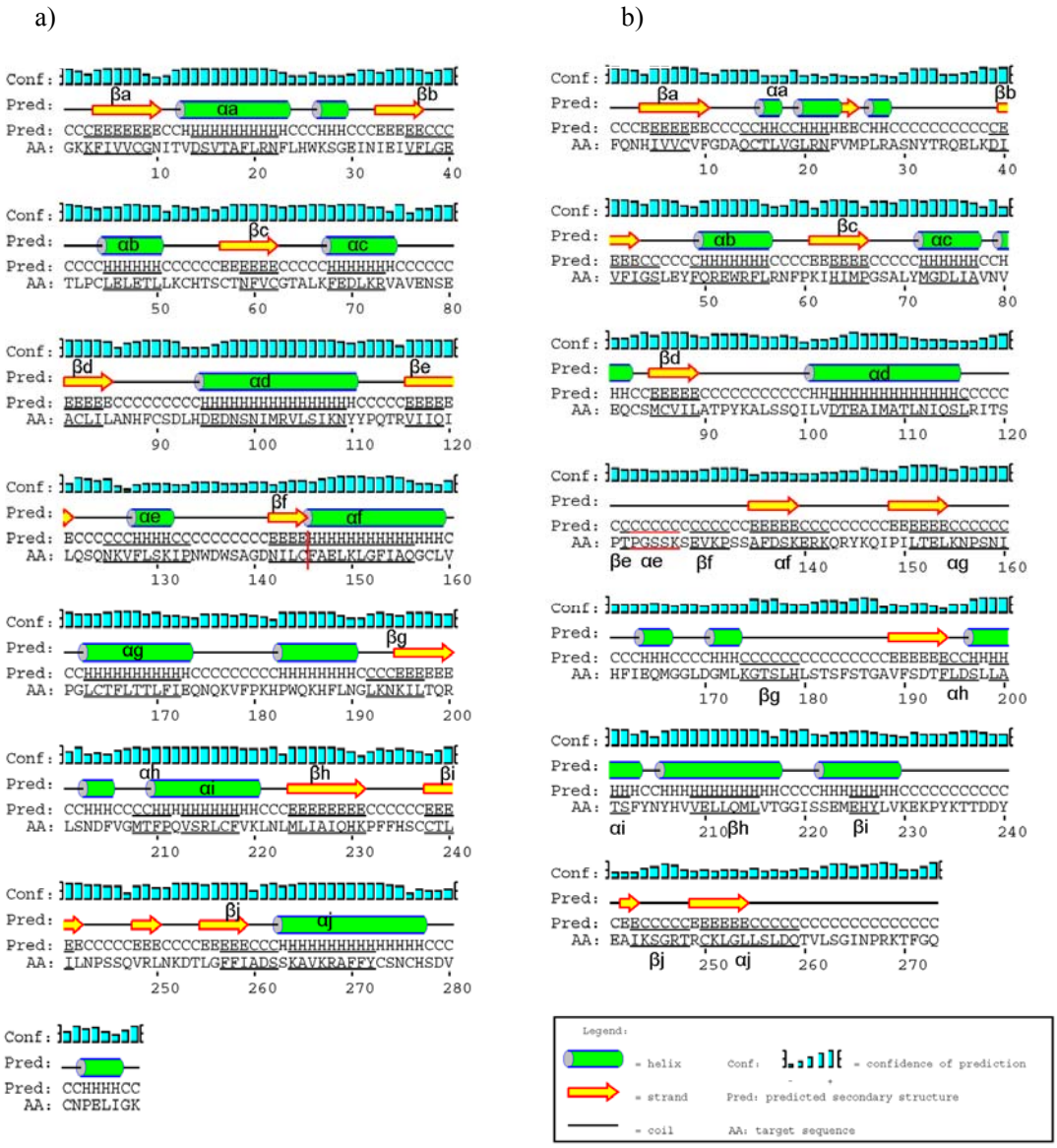

Figure 4.6 Predicted secondary structures of mslo3 RCK domains. Secondary protein structures were predicted using the DomPred Protein Domain Prediction Server. The homologous mSlo3 residues to the mSlo1 RCK βαβαβ Rossmann-fold structure was underlined and if corresponding to the structural elements annotated above the predicted structure. This can be seen to align fairly well in the RCK1 structure a) however the RCK2 structure b), subsequent to the αd helix, the predicted secondary structure of the mSlo3 RCK2 differs from the homologous mSlo1 βαβαβ Rossmann-fold structure.

4.2.5 Electrophysiological effects of CV562866 Expression on Sloα subunits

Oocytes were prepared and injected, as described in 2.3.3, with α-subunit mRNA diluted with either water or the respective accessory subunits (CV/hSloβ4) to ensure final concentrations were consistent within the experiments. Oocytes were then incubated for 2-3 days at 18 ^{O}C before being voltage clamped at a -80 mV holding potential (2.3.4). I/V relationships were determined by subjecting the oocyte to a 100 ms voltage step of -100 to +140 mV in 10 mV increments. Interestingly mSlo3/CV562866 expressing oocytes had significantly reduced currents evoked by depolarisations greater than +120 mV ($p<0.05$, Two-way ANOVA; Bonferroni post hoc test) (n=20) in comparison to the currents in mSlo3/H_2O injected oocytes (Figure 4.7). The current decrease caused by CV co-expression was on average 0.64 μA. In the absence of injected pore forming subunits the CV expressing oocyte currents were not significantly different from the endogenous currents ($P>0.05$, Two-way ANOVA; Bonferroni post hoc test). In contrast to mSlo3, the effect on mSlo1 mediated currents was opposite in the presence of CV, figure 4.8, with significantly increased currents evoked by depolarising pulses greater than +120 mV ($P<0.05$, Two-way ANOVA; Bonferroni post hoc test) (n=37). The average current increase dependent on CV co-expression with mSlo1 was 0.82 μA.

mSlo3 with Sloβ4 co-expression resulted in a significant ($P<0.05$, Two-way ANOVA; Bonferroni post hoc test) increase at voltages greater than +100 mV compared to mSlo3 currents (Figure 4.9). This is consistent with previous studies, however the size of the effect in our studies was less than the eight fold increase reported (Yang *et al.*, 2009). Interestingly, this increase in current was abolished by CV co-expression ($P>0.05$, Two-way ANOVA; Bonferroni post hoc test) when compared to mSlo3 injected oocyte currents. Consistent with our previous experiment expression of CV with just mSlo3 again significantly reduced mSlo3 currents evoked by depolarising greater than +120 mV ($P<0.05$, Two-way ANOVA; Bonferroni post hoc test) (n=20).

Activation constant (τ) at +100 mV to +140 mV depolarisation steps were analysed for all the experiments but no significant effects were found dependent on the CV co-expression ($P>0.05$, Two-way ANOVA; Bonferroni post hoc test). G-V relationships were not constructed for any of the combinations because as discussed earlier (3.3.1) the currents do not reach a defined G_{Max} plateau.

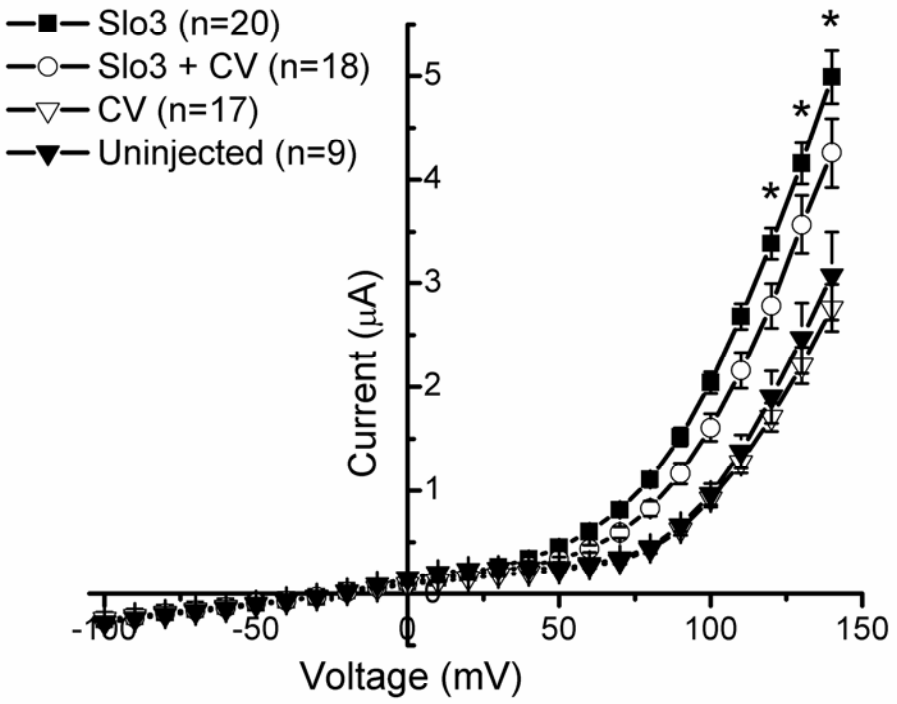

Figure 4.7 Effects of CV562866 expression on mSlo3 currents. Functional effects of the CV protein were studied by expressing mSlo3 channels in *Xenopus* oocytes and recording membrane currents using two-electrode voltage clamp. Depolarisations were stepped in 10 mV intervals from -100 mV to +140 mV. Surprisingly co-expression of CV significantly reduced mSlo3 mediated current evoked by depolarisations greater than +120 mV ($P<0.05$, Two-way ANOVA; Bonferroni post hoc test) (n=20). The average current decrease dependent on CV co-expression was 0.64 μA.

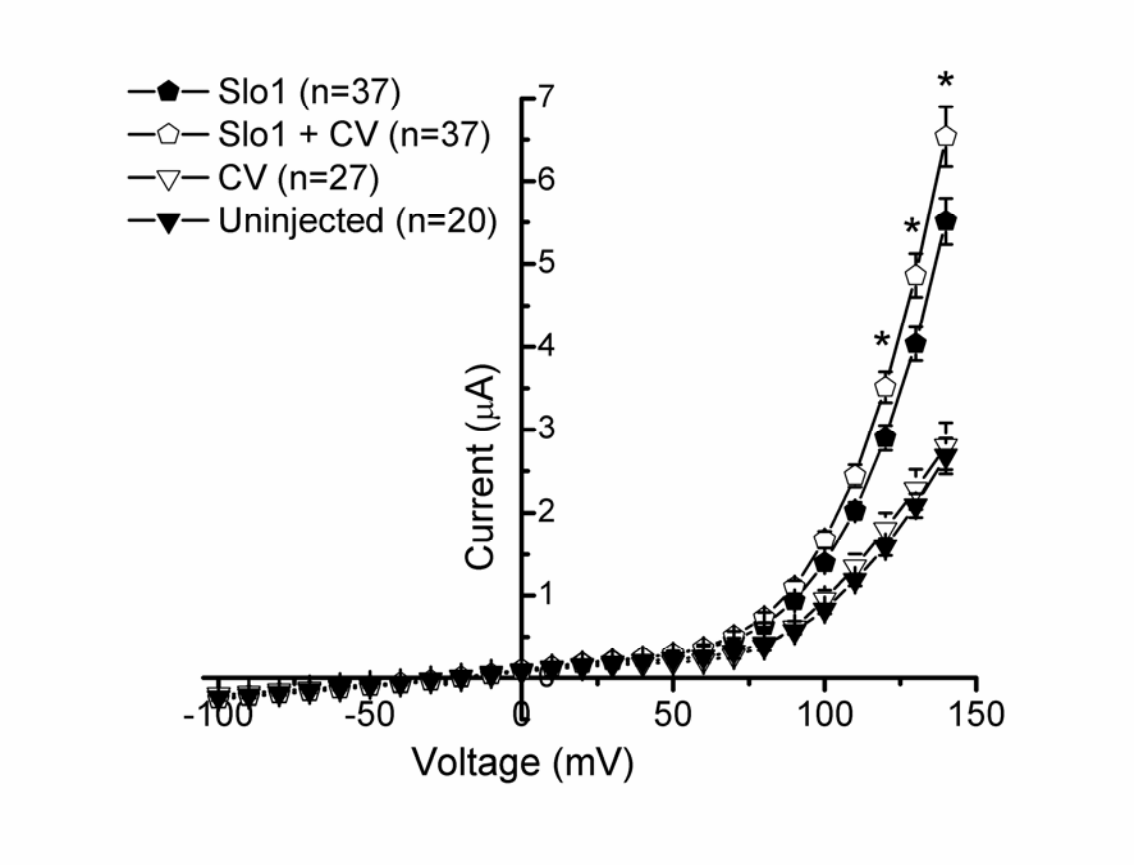

Figure 4.8 Effects of CV562866 expression on mSlo1 currents. Functional effects of the CV protein were studied by expressing mSlo1 channels in *Xenopus* oocytes and recording membrane currents using two-electrode voltage clamp. Depolarisations were stepped in 10 mV intervals from -100 mV to +140 mV. CV expression with Slo1 channels, significantly increased currents evoked by depolarising pulses greater than +120 mV ($P<0.05$, Two-way ANOVA; Bonferroni post hoc test) (n=37). The average current increase dependent on CV co-expression with mSlo1 was 0.82 μA.

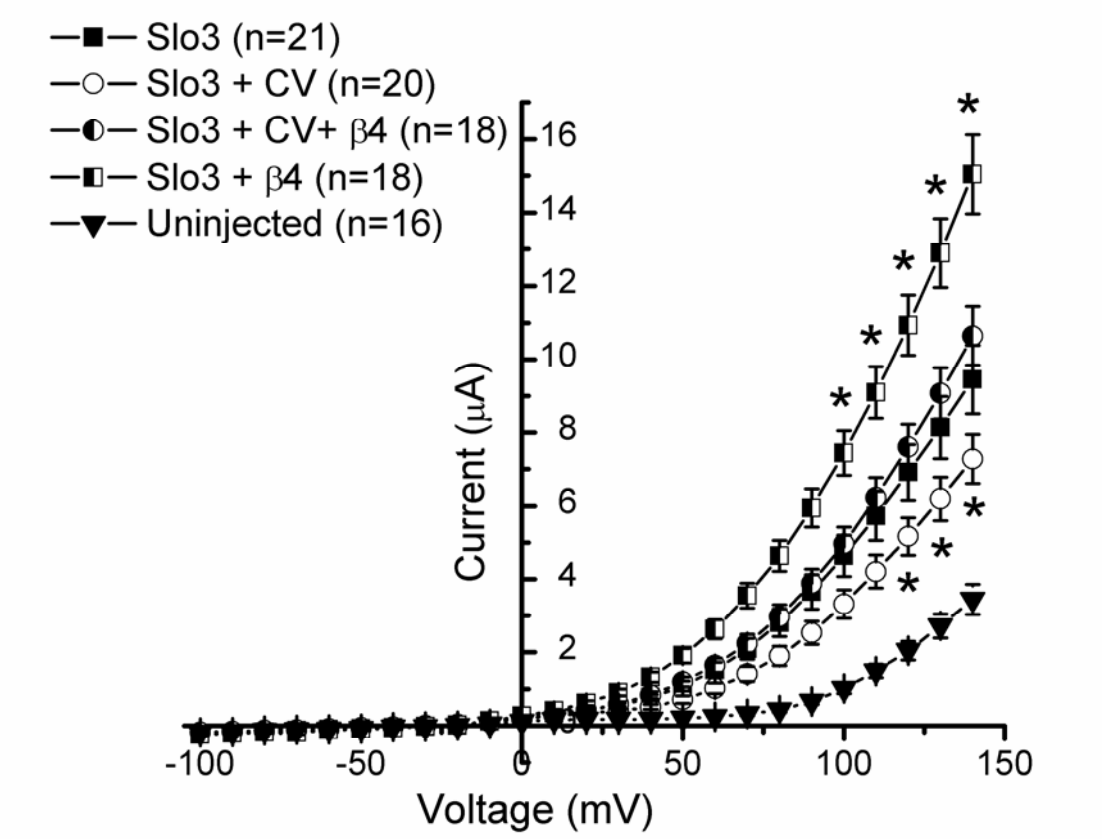

Figure 4.9 Effects of CV562866 expression on mSlo3/Sloβ4 currents. Functional effects of CV were studied by expressing mSlo3 channels in *Xenopus* oocytes and recording membrane currents using two-electrode voltage clamp. Depolarisations were stepped in 10 mV intervals from -100 mV to +140 mV. The significant increase in Slo3 currents by Sloβ4 co-assembly ($P<0.05$, Two-way ANOVA; Bonferroni post hoc test) were eliminated by CV co-expression (not significant) when compared to solitary Slo3 currents. Expression of CV with mSlo3 again significantly reduced mSlo3 currents evoked by depolarising greater than +120 mV ($P<0.05$, Two-way ANOVA; Bonferroni post hoc test) (n=20)

4.3 Chapter 4 Discussion

4.3.1 A novel isoform of mSlo3

Using the UniGene database we found several EST's, expressed outside the testis/spermatozoa, that have a high sequence identity to the mSlo3 cDNA sequence. Three of the EST's were isolated from adult male hippocampus (AK083174, BB428821 and BB653287), one from the subfornical organ and postrema (BQ175543), one from the upper head (CV562866) and one from the lateral wall of lateral ventricle (CX213584). We aligned EST's to the mSlo3 cDNA sequence using ClustalW2 (4.2.1) and EST sequences homologous to the mSlo3 sequence were highlighted in grey. All the EST's were found to be divergent from the mSlo3 sequence at the 5' end; however there was internal consistency between the four EST sequences over this region. This divergence at the 5' end of the sequence explains why Schreiber *et al*. (1998) only found expression restricted to testis, as their probes were designed to the full length, the S8-S9 domains and the S9-S10 domains. Whilst the EST's encode most of the S9-S10 domains, the first 72 bases are in the divergent region, thus RT-PCR probes would be unable to bind as the target sequence is absent.

It appears that all of the EST's are not a 3' fragment of degraded full length mSlo3 cDNA, but are splice variants in their own right. Using Marathon RACE PCR on mouse brain Marathon-ready^{TM} cDNA (Clontech) any potential neuronal isoforms were isolated. Interestingly, whilst the forward EST internal primers in the second round of PCR gave high molecular weight bands (≈1.5 kb), the reverse EST internal primer reactions produced only low molecular weight bands, between 200-600 bp. If the *CV* sequence encoded a full length α-subunit, it would be expected that the reverse EST internal primer Marathon RACE PCR should show a band of ≈3.5 kb, thus *CV* only encodes a short length sequence. This finding was reinforced when PCR of mouse brain cDNA library was performed using a pore region specific primer against a *CV* reverse primer, resulting in a blank gel. The full length *CV* sequence was constructed and aligned to the mouse genomic and transcript library sequence using the NCBI nucleotide blast software (Altschul *et al.*, 1990). The results of this alignment were the discovery of two new exons, 19a and 19b (named respective to the full length mSlo3), which align to sequence between exons 19 and 20 of the *KCNU1* gene. The full length *CV* sequence contains exons 20-26 of the full length mSlo3 sequence. This supports our Marathon RACE PCR findings that *CV* is a novel isoform rather than a degraded mRNA sequence of a longer form.

The full *CV* sequence was found to contain an ORF starting at nucleotide 217 with a hundred percent sequence identity to the C-terminus of the mSlo3 subunit, starting at M740. This region in mSlo3 is the most divergent from the mSlo1 sequence (39% homology); thus it was used as the epitope (amino acids 1052-1121) for the NeuroMab Anti-Slo3 antibody. As the CV sequence also encodes this region we were able to determine if CV was expressed as a protein or if it was an untranslated RNA. Western blots of transiently transfected CV562866-HEK293 cells showed a band at ≈ 55 kDa which was not present in the mSlo3 or control HEK cells. Whilst not a precise measure of Mw this was consistent with the predicted Mw of CV, 47 kDa, suggesting that it is expressed as a distinct protein. Using a range of tissues we found a diverse expression profile in supernatant fractions, consistent with our finding that the CV protein lacks TM domains. The finding that the blood sample contains a corresponding band may explain why highly vascularised tissues like the liver and kidney also contain a ≈ 55 kDa band. This finding also probably contributes to the widespread non-specific binding observed in fixed brain slices. Interestingly, in the Western blots a high molecular weight band of ≈100 kDa was observed in the tissues that also express CV. This band appears to be approximately the same weight as the lower band found in the mSlo3 control transfected cells. However, it is unlikely that this band is due to full length rSlo3 α-subunit as previous studies were unable to find expression outside of the testis (Schreiber *et al.*, 1998). This band is possibly due to the formation of CV dimers or non specific binding due to the high level of antibody required for visualisation. However, the band in the membrane fraction from testis is unlikely to be due to CV, as this protein lacks TM domains. This band may be due to degraded full length rSlo3, as this tissue is the only tissue that Slo3 has been shown to express in (Schreiber *et al.*, 1998).

4.3.2 Predicted structural features of the CV562866 protein

Expression of a soluble C-terminus is similar to the *MthK* gene that generates a "soluble" form of the tail region that contains the single RCK domain, which is required so the octameric gating ring can be formed (Jiang *et al.*, 2002*b*). Thus as the CV sequence contains the final 426 amino acids of the C-terminus of mSlo3, we determined if this region contains a RCK domain, which could act as in the MthK channel. Using alignment to the RCK domains of mSlo1 and MthK and prediction of the secondary protein structure of the homologous regions, we ascertained that in mSlo3 whilst RCK1 was intact RCK2 lacked the characteristic βαβαβ Rossmann-fold structure. This may mean that the octomeric RCK ring of mSlo3 does not form correctly; this may contribute to the requirement for higher concentration of mRNA in comparison with mSlo1 for recordable currents. For example,

when the internal start codon in MthK channels for the soluble RCK domain is mutated, M107I, the expression of the mutant MthK channel is drastically reduced in comparison with the wild type (Jiang *et al.*, 2002). The presence of an intact RCK1 domain also suggests a possible mechanism for pH sensitivity of mSlo3 channels. Three residues in RCK1 of Slo1, D367 and H365/H394, are vital for the activation of the channel by low pH (Hou *et al.*, 2008). The mSlo3 RCK1 has homologous histadines in the structure; however the homologous D367 is replaced with lysine. This shift from an acidic amino acid interacting to a basic amino acid interacting may characterise the shift from activation in the presence of H^+, to the inhibition. As in the current theory the interaction of the protonated histadines and D367 stabilises the RCK structure to preferentially open the channel gate (Hou *et al.*, 2008). Therefore with the inversion of side chain charge, protonated histadines may stabilise the RCK1 structure to preferentially close the mSlo3 channel gate.

4.3.3 Effects on α-subunit expression

To test if CV had analogous effect on mSlo expression to the MthK increased surface expression due to the soluble C-terminus, we used co-injection experiments to establish any effects of CV expression on mSlo α-subunits. Interestingly currents from CV co-injected with mSlo3 oocytes were decreased at depolarisations greater than +120 mV in comparison to the mSlo3/H_2O injected oocyte currents. This is possibly due to a range of potential effects of CV expression; saturation of forward trafficking motifs, saturation of protein synthesis mechanisms or disruption of formation of the channel tetramer by interactions with the C-terminus of the α-subunit. All of these effects would result in reduced trafficking to the oocyte membrane and reduced current. In contrast the effect on mSlo1 mediated currents was opposite in the presence of CV, with significantly increased currents evoked by depolarising pulses greater than +120 mV. This may be due to CV increasing surface expression of mSlo1 by saturating retention proteins and thus enhancing forward trafficking. Previous studies have shown that the surface expression of Slo1 channels can be regulated by the extreme C-terminus sequence (Kim *et al.*, 2007). In Slo1 the presence of VEDEC rather than QEERL at the extreme C-terminus, requires the addition of growth factors to cause surface expression. The same study observed that, addition of a soluble protein of the final 42 amino acids was also able to increase surface expression, implicating that this region binds to proteins that cause retention of the VEDEC channels in intracellular stores. It is possible that the extreme end of mSlo3/CV protein sequence, DIVQEK, is also an intracellular retention signal. The theory that CV affects mSlo3 surface expression rather than causing changes in kinetics was supported by our findings that expression of CV abolished the current increase due to Sloβ4 co-expression with mSlo3. Previous studies have

shown that Sloβ4 increases the surface expression of mSlo3 (Yang *et al.*, 2009). However, the increase in current we observed due to Sloβ4/mSlo3 was less than the eight-fold increase previously reported by C.-T. Yang *et al* (2009). This is possibly due to the difference of technique used; we used TEVC whereas they used macro-patches pulled from ooctyes. Thus it is possible that Sloβ4 not only causes an increase in surface expression but may also cause mSlo3 channel clustering. Measurement of the activation constants of the currents found no significant effect dependent on CV expression supporting the theory that the effects are due to changes in expression or trafficking rather than channel kinetics. As expected in the absence of injected α-subunits, CV injection had no effects on endogenous currents.

4.3.4 Challenges for the future

Challenges for the future will be to examine: (a) if the effects of the CV562866 protein on Slo1 expression is an artefact of the oocyte expression system by repetition in stable cell lines; (b) utilising macro-patches of oocyte membranes and patch cramming to see if the CV562866 protein causes increased recycling; (c) if CV562866 can be used to pull down other proteins that may be able to interact with mSlo3 and modify expression; (d) if it is possible to design a more specific antibody to mSlo3 (possibly using S8-S9 as an epitope) to allow more selective probing of tissues.

4.3.5 Chapter Summary

This data reveals a novel splice variant of the mSlo3 channel, CV562866, which lacks TM domains and has a wider apparent expression profile. This variant appears to be expressed as a protein *in vivo*, and contains most of the nominal RCK2 domain. Our investigation into the structure, however, suggests that the RCK2 domain of the splice variant and full length channel lacks the correct secondary architecture. CV562866 appears to affect the expression of both mSlo3 and mSlo1 channels, but has opposing effects.

Chapter V:

Characterisation and Pharmacology of hSlo2 channels

5.1 Chapter 5 Introduction

5.1.1 Characteristics of the Slo2 Subfamily

The Slo2.χ subfamily of channels was first identified in *Caenorhabditis elegans* from sequence homology with Slo1 and Slo3 channels. Expression of the encoded protein displayed a channel with synergistic activation by Ca^{2+} and Cl^- with weak voltage dependence, due to the lack of positive charges in the S4 domain and a single-channel conductance of 110 pS in symmetrical K^+ (Yuan *et al.*, 2000). Soon after the identification of *C.elegans* Slo2, mammalian orthologues were identified in both mouse (mSlo2) and rat (rSlo2), originally called Slack - Sequence like a Ca^{2+} activated K^+ channel. These channels differed from the *C.elegans* Slo2 in that rather than synergistic activation by Ca^{2+} and Cl^- they were instead activated by Na^+ and Cl^- with a unitary conductance of 165 pS (Yuan *et al.*, 2003). The rSlo2.2 channel had been previously identified as a member of the Slo family of channels when originally cloned, but activation of the channel by Na^+ or Cl^- had not been recognised (Yuan *et al.*, 2003). Another homologue was also discovered, rSlo2.1, this sister channel was named Slick - Sequence like an intermediate conductance K channel, due to its resemblance to Slo2.2. The Slo2.1 channel was first described as being a functional hybrid between K_{Na} and ATP-sensitive (K_{ATP}) K^+ channels, as it is activated by Na^+/Cl^- but the channel is also inhibited by intracellular ATP. The sensitivity to these endogenous activators was shown to differ with Slo2.1 being less sensitive to Na^+ and more sensitive to Cl^- in comparison with Slo2.2 (Bhattacharjee *et al.*, 2003).

It has been difficult to determine separate physiological functions for Slo2.1 and Slo2.2 with regards to mediating the K_{Na} current. This is partially due to the overlap between endogenous activators and the expression patterns of rSlo2.1 and rSlo2.2. In the rat brain, expression profiles have been explored utilising in-situ hybridisation (ISH) and immunohistochemical (IHC) methods (Bhattacharjee *et al.*, 2002, 2005). These methods showed wide-spread and overlapping expression of the Slo2.χ channels throughout the brain. IHC staining of the Slo2.2 channel showed relatively high protein levels in the olfactory bulb, midbrain and brainstem. IHC staining, however, conflicted with the ISH results in regions such as the piriform cortex, ventral cochlear nucleus, CA3 of the hippocampus, and cerebellar nuclei (Bhattacharjee *et al.*, 2002). However, this discrepancy was due to the

epitope chosen for the original anti-Slo2.2 antibody, the first 15 amino acids of the N-terminus. This region of the protein is now known to be a site of variation due to splice variants (Brown *et al.*, 2008). Their study found three major variants; Slo2.2a, Slo2.2b and Slo2.2m. Slo2.2b channels are the "classical" Slo2.2 channels, which have a long N-terminal domain. Slo2.2a channels, however, have a shorter N-terminal domain which has a high level of sequence identity (78.1%) to the Slo2.1 N-terminal sequence. Slo2.2a channels have distinct electrophysiological characteristics from Slo2.2b currents. Slo2.2a whole cell currents activate rapidly in response to a voltage step, in a manner akin to Slo2.1 channels. Slo2.2b channels activate in a biphasic manner, with an instantaneous component that is followed by a slow time dependent component that takes several hundred milliseconds to reach a level of steady state current. At the single channel level Slo2.2a channels have multiple sub-conductance states whereas Slo2.2b channels had one main sub-conductance state. Slo2.2b channels also had a mean open time six times longer than Slo2.2a, in part due to longer openings to the fully open state (Brown *et al.*, 2008). Slo2.2a and Slo2.2b also differ in their ability to form heteromeric channels with the Slo2.1 subunit. rSlo2.2b subunits, in oocytes, have been shown to form intermediate conductance channels with rSlo2.1 subunits, whereas rSlo2.2a subunit are unable to form channels with these properties. Using co-immunopreciptation techniques on rat brain tissue it appears that these heteromeric channels are formed *in vivo* (Chen *et al.*, 2009).

5.1.2 Physiological Relevance of Slo2.χ channels in neuronal tissues

Slo2.χ channels appear to have a variety of physiological functions depending on cell type and differing $[Na]_i$ levels in subcellular localisations. Three major functional roles of Slo2.χ channels in neurons have been reported, in the depolarising after-potential, spike frequency timing and establishment of the RMP. There was initially disagreement in the literature as to involvement of K_{Na} currents in mediating the depolarising after-potential. This was due to initial studies finding the EC_{50}'s for Na^+ of ≈40 mM (rSlo2.2) and ≈80 mM (rSlo2.1), both of which are greater than the reported resting $[Na^+]_i$ in neurons (4-15 mM). However, further studies have found that in the presence of NAD^+ the EC_{50} is shifted to ≈20 mM $[Na^+]_i$, near the physiological range (Tamsett *et al.*, 2009). Secondly Slo2.χ channels are assumed to co-localise with Na^+ channels (Dryer, 1994), and have been shown to co-localise with AMPA receptors (Nanou *et al.*, 2008), thus localised $[Na^+]_i$ may be higher than in the whole cell. In rat medium-diameter (25-35μm) DRG neurons and CA1 pyramidal cells, Slo2.χ have been shown to be able to mediate the depolarising after-potential of single action potentials (Gao *et al.*, 2008). Interestingly whereas in rat it appears both Slo2.1 and Slo2.2 contribute to spinal cord K_{Na}, it has been shown in lamprey spinal cord to be mediated solely by Slo2.2. In

lamprey spinal cord neurons, the role is slightly different; Slo2.2 mediates part of the slow afterhyperpolarisation (sAHP). The contribution of this channel is increased under high frequency firing of the neuron. This is theorised to be a safety mechanism to ensure frequency regulation (Wallén *et al.*, 2007). This physiological function has also been determined for Slo2.χ in the medial nucleus of the trapezoid body (MNTB) in the auditory brainstem. In the MNTB increasing K_{Na} augments the accuracy of timing of action potentials at high frequency firing of the neuron. This in turn increases the fidelity of the information encoded (Yang *et al.*, 2007). Bischoff *et al.*, (1998) concluded that the K_{Na} current, mediated by Slo2.χ channels, contribute to the establishment of RMP in physiological conditions and have a secondary role of stabilising the neuron under pathophysiolgical conditions such as hypoxia. This conclusion may have been due to the cell type observed in the study, rat small-diameter (20-25 μm) DRG neurons. Small DRG neurons have an action potential frequency of 0.5-2 Hz, under physiological conditions, approximately 15-fold too low to cause a high localised Na^+ concentration to activate K_{Na} currents. Secondly small DRG neurons lack the anatomical architecture to facilitate Na^+ accumulation such as the node of Ranvier or an axon hillock with a high density of Na^+ channels (Bischoff *et al.*, 1998). It has been suggested that K_{Na} have a role in the mediation of inflammatory pain by DRG neurons. PKA activation has shown to be critical to mediation of inflammatory pain (Malmberg *et al.*, 1997). Thus the PKA dependent internalisation of Slo2.2 is thought to play a part in causing the hyper-excitability characteristic of nociceptive firing (Nuwer *et al.*, 2010).

5.1.3 Pharmacology of Slo2.χ channels

Class I and IV anti-arrhythmic drugs, quinidine and bepridil (respectively), were originally shown to inhibit K_{Na} currents in cardiac tissue (Mori *et al.*, 1998). Further investigation of the affects of these compounds has determined their full profile against rSlo2.2b channels. Quinidine inhibition of rSlo2.2b appears to be voltage independent. In transfected human embryonic kidney (HEK) cells quinidine has an IC_{50} of 89.6 μM. Examination of channel kinetics indicated that quinidine produced a marked and reversible decrease in channel activity. This was due to a decrease in the mean open time of the channel. Bepridil inhibition of rSlo2.2b appears similar to quinidine in that it is also voltage independent and reversible. In transfected HEK cells bepridil was shown to more potent with an estimated IC_{50} of 1.0 μM. Examination of channel kinetics displayed that bepridil also decreased the mean open time of the channel. These results signify that quinidine and bepridil inhibition has a direct effect on rSlo2.2b, rather than an effect on intracellular Na^+ levels (Yang *et al.*, 2006). Currently only one non-endogenous activator has been observed; bithionol, a bis-phenol anti-parasitic compound. Activation by bithionol (EC_{50} = 0.77 μM) showed an interesting

characteristic, the weak voltage dependence of the Slo2.2 currents was modified. In the presence of bithionol the activation voltage is shifted to more negative potentials, allowing more channels to be open for a given voltage (Yang *et al.*, 2006). Bithionol has also been shown to increase the speed of decay of AMPA induced excitatory postsynaptic current in lamprey spinal neurons by enhancement of a K_{Na} current, resulting in a decreased synaptic response (Nanou *et al.*, 2008). These studies were either performed solely on rSlo2.2b channels or in native cells, without recourse to examination of the possible effects on either rSlo2.2a or rSlo2.1 channels, thus it is unknown if the pharmacology described is distinctive.

5.1.4 Chapter Aims

5.1.4.1 Characterisation of hSlo2.2a currents

The majority of studies of the Slo2 subfamily have been performed using the initial isoform rSlo2.2b, with few studies performed on the rSlo2.1 and rSlo2.2a. However no study has examined the human homologues of these channels, which have the more selective GYG selectivity filter in the pore domain. We aim to study the hSlo2.2a isoform, in transfected HEK cells using whole cell patch clamp, in order to characterise the currents and the minimum sensitivity to intracellular NaCl concentrations.

5.1.4.2 Are hSlo2.2a channels activated by bithionol?

The bisphenol anthelmintic compound, bithionol has been shown previously to activate rSlo2.2b channels in transiently transfected HEK cells (Yang *et al.*, 2006). We aim to test if the hSlo2.2a channels are sensitive to this compound. If hSlo2.2a channels are activated we aim to test if bithionol activation is affected by the intracellular $[Na^+]$ and $[Cl^-]$. Secondly we aim to test the potency of bithionol and the related bithionol sulfoxide at hSlo2.2a channels is similar to the previously reported potency of bithionol on rSlo2.2b channels. Lastly using homology modelling to the hSlo1 channel structure, we aim to model the bithionol binding site of the hSlo2.2a channel.

5.1.4.3 Are the effects of bithionol channel specific?

K^+ channels are rarely expressed in physiological cells in isolation, normally a wide variety of K^+ channels are expressed with overlapping sensitivities and functions. Thus we aimed to test the potency of bithionol on the endogenous HEK Kv channels as a control to our previous experiments. Also we aimed to test bithionol on the other K_{Na} subunit hSlo2.1, to see if bithionol could be used to distinguish this subtype from hSlo2.2 channels. Lastly we also aim to test bithionol on K_{ATP} currents recorded from 832/13 INS cells.

5.1.4.4 Can bithionol activate Slo2.χ in DRG neurons?

Bithionol has been shown to be an activator of heterologously expressed rSlo2.2b channels and *ex vivo* lamprey K_{Na} currents. Thus we aim to test the physiological effects of bithionol application on currents from *ex vivo* rat DRG cells. We aim to do this by whole cell patch clamp isolated rat DRG cells with 5 mM $[Na^+]_i$ and subjected to -100 to 0 mV voltage ramps. Secondly we aim to test the effects of bithionol application on the RMP of rat DRG cells using a current clamp protocol.

5.2 Chapter 5 Results

5.2.1 Characteristics of hSlo2.2a Currents

hSlo2.2a-EGFP transiently transfected HEK MSR cells were whole cell patch clamped at -80 mV for recording. Cells were clamped at -80 mV and then subjected to -100 to +100 mV voltage ramps over a 500 s period, at a frequency of 0.25 Hz, to allow currents to run up. Currents were measured during a 200 ms voltage step of -100 to +100 mV in 10 mV increments, from a -80 mV holding potential (Figure 5.1). The sample traces in the absence (Figure 5.1.A) and presence of 20 mM $[NaCl]_i$ (Figure 5.1.B), shown in response to a voltage step protocol from -100 to 20 mV, demonstrate that this pulse is of sufficient duration for currents to reach steady state activation. In the absence of $[NaCl]_i$ (Figure 5.1.A), currents appear to be similar to endogenous Kv currents recorded from HEK cells. The presence of 20 mM $[NaCl]_i$ (Figure 5.1.B), appears to have an increased instantaneous current, increased peak current and a small inward current. Cell currents were normalised to individual cell capacitance before compiling to generate the $(I/C_{cell})/V$ plots (Figure 5.1.C). These plots showed a significant ($P<0.05$, Student's t-test) increase in hSlo2.2a current density in the presence (n=8) of 20 mM $[NaCl]_i$ between -40 and +20 mV compared to absence (n=7). Interestingly, the hSlo2.2a currents in the presence of 20 mM $[NaCl]_i$ have differing characteristics compared to rSlo2.2a current recorded in CHO cells (Brown *et al.*, 2008). hSlo2.2a currents, unlike rSlo2.2a, display a linear current-voltage relationship with no rectification. Their study also observed that rSlo2.2a currents reverse at -50 mV, whereas our study the hSlo2.2a currents reverse at ≈ -75 mV in the presence of 20 mM $[NaCl]_i$. The only similar characteristic between hSlo2.2a and rSlo2.2a is rapid channel activation.

Conductance and reversal voltage recordings were also made over the 500 s that hSlo2.2a transiently transfected HEK MSR cells were subjected to -100 to +100 mV voltage ramps at a frequency of 0.25 Hz. Conductance and reversal potential measurements were recorded in the presence and absence of 20 mM $[NaCl]_i$ following breakthrough and over the 500 s of voltage ramps. Individual cell conductance recordings (n=6) were normalised to cell capacitance before collating and plotting. Interestingly although there is a clear increase in the conductance density (Figure 5.2.A) due to the presence of 20 mM $[NaCl]_i$ this was not found to be significantly different ($P>0.05$, Student's t-test) compared to in the absence of 20 mM $[NaCl]_i$ after 500s. If the significance threshold was relaxed to $P<0.1$, there is a significant increase due to the presence of 20 mM $[NaCl]_i$. However, measurement of the

reversal potential (Figure 5.2.B) found a significant ($P<0.05$, Student's t-test) negative shift in the presence of 20 mM $[NaCl]_i$ compared to recordings in the absence of 20 mM $[NaCl]_i$.

5.2.2 Cooperativity of Na^+ and Bithionol Activation

hSlo2.2a currents were recorded from transfected HEK MSR cells by whole cell patch clamp using a -100 to 100 mV voltage ramp with differing intracellular $[Na^+]$ and $[Cl^-]$. Cells were left to equilibrate until the conductance reached a plateau, then 10 μM of bithionol (Figure 5.3.H) was applied until plateau for ten sweeps was attained, following which cells were washed with extracelluar solution. Average curves were plotted (± SEM) for each condition. $[Na^+]_i$ was varied by addition of NaCl to the intracelullar solution and the effects of bithionol application on conductance density measured; 0 mM (Figure 5.3.A), 5 mM (Figure 5.3.C), 10 mM (Figure 5.3.E) and 20 mM (Figure 5.3.F). Conductance density measurements from the currents in figure 5.3 were collated and averaged. Application of 10 μM bithionol, in all conditions, was found to significantly ($P<0.05$, Two-way ANOVA; Bonferroni post hoc test) increase the conductance density of hSlo2.2a transfected cells. The increase in conductance density due to bithionol application was reversible with washing with the exception of 20 mM $[Na^+]$ (Figure 5.3.F).

To determine if the increase in current density with bithionol was sodium or chloride cooperative, low $[Cl^-]_i$ solutions, 1 mM $[Cl^-]_i$, were made by substituting Cl^- with gluconate. Current densities were measured as before, in low $[Cl^-]_i$ solutions, with 0 mM $[Na^+]_i$ (Figure 5.3.B) and 5 mM $[Na^+]_i$ (Figure 5.3.D). Comparison of conductance density (Figure 5.4) showed no significant difference in the conductance densities of the low $[Cl^-]_i$ solutions ($P>0.05$, Two-way ANOVA; Bonferroni post hoc test) compared to high $[Cl^-]_i$ solutions. As a control 10 μM bithionol was also tested on untransfected HEK cells with 20 mM $[Na^+]_i$ (Figure 5.3.G). Bithionol application was found to have no significant ($P>0.05$, Two-way ANOVA; Bonferroni post hoc test) effect on the recorded conductance density in untransfected HEK cells.

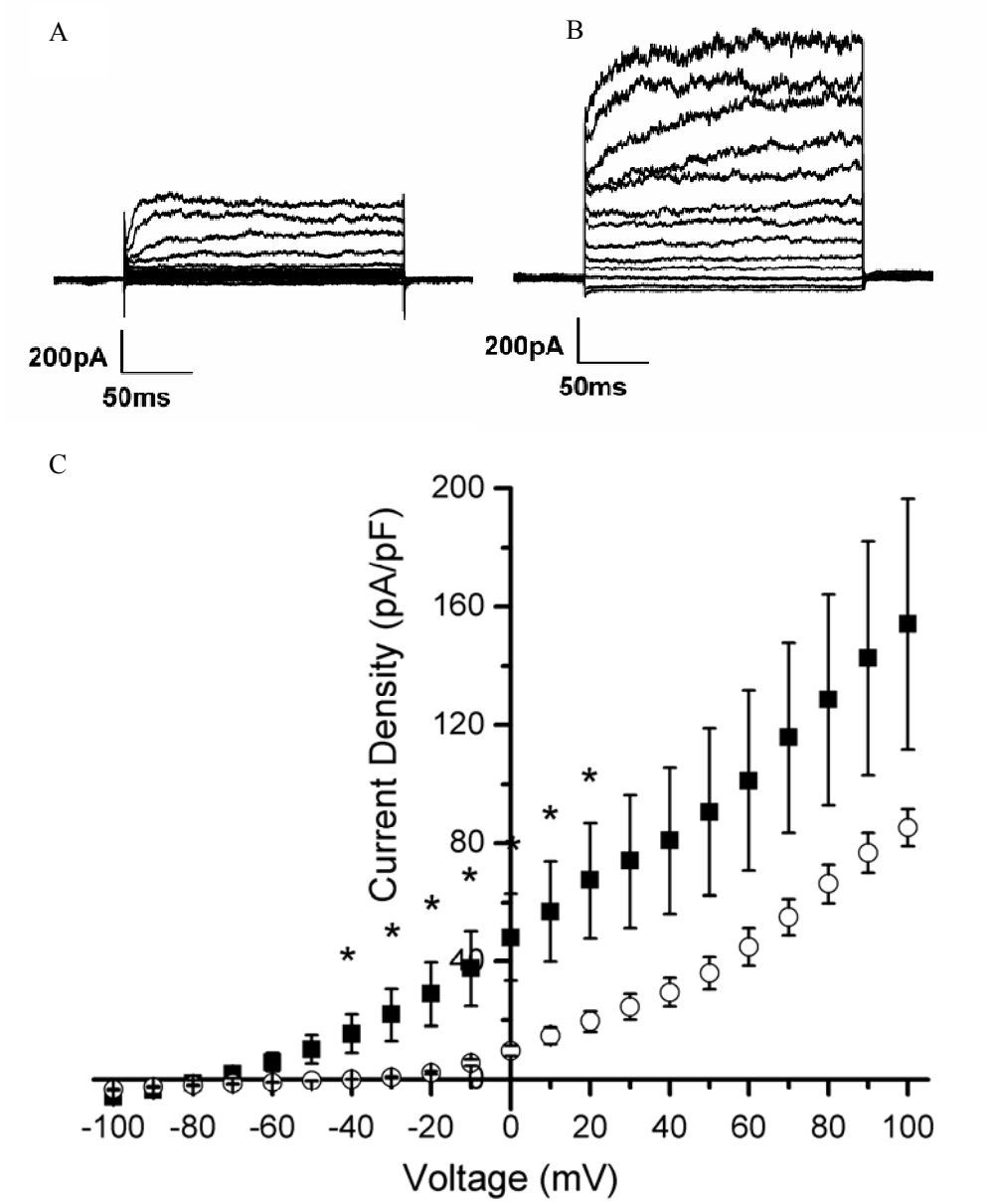

Figure 5.1 Whole cell patch clamp recordings from HEK MSR cells transiently transfected with hSlo2.2a-EGFP. Cells were clamped at -80 mV and then subjected to -100 to 100 mV voltage ramps over a 500 s period, and then a voltage step protocol was applied. Sample traces with (a) 0 mM and (b) 20 mM $[Na^+]_i$ are shown in response to a voltage step protocol from -100 to +20 mV. Traces were compiled to generate the $(I/C_{cell})/V$ plots (c), over a -100mv to +100 mV range, which showed a significant (* = $P<0.05$, T-test) increase in current density between the presence (filled squares) (n=8) and absence (open circles) (n=7) of intracellular 20 mM NaCl between -40 and +20 mV.

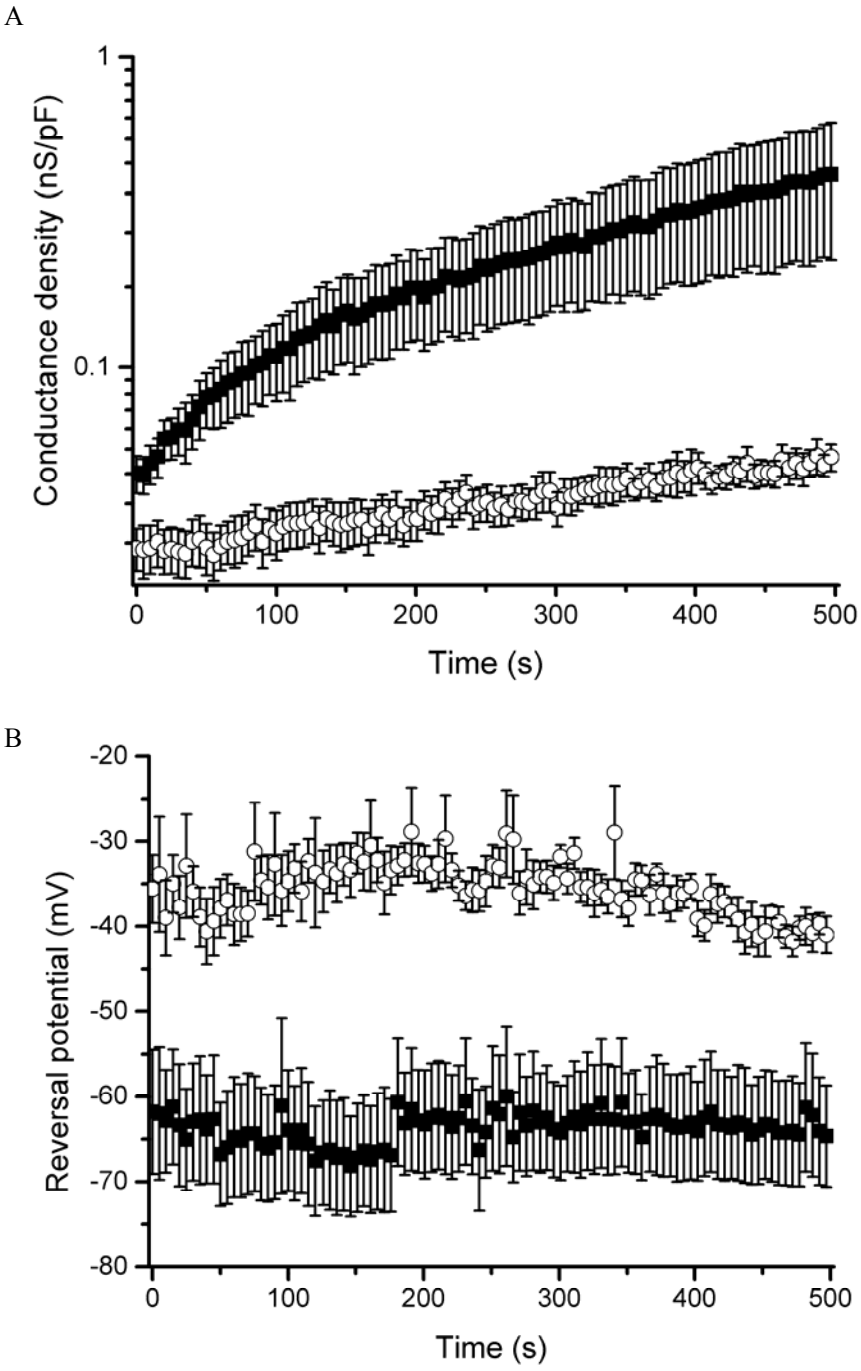

Figure 5.2 Electrophysiological characteristics of HEK MSR cells transiently transfected with hSlo2.2a-EGFP. Cells were clamped at -80 mV and then subjected to -100 to 100 mV voltage ramps over a 500 s period. Conductance density (A) and reversal potential (B) measurements were recorded in the presence (filled squares) and absence (open circles) of 20 mM $[NaCl]_i$ following breakthrough and over the 500s of voltage ramps. Conductance density was found to be not significantly different ($P>0.05$, T-test) between the presence and absence of 20 mM $[NaCl]_i$. However, the reversal potential was found have a significant ($P<0.05$, T-test) negative shift in the presence of 20 mM $[NaCl]_i$.

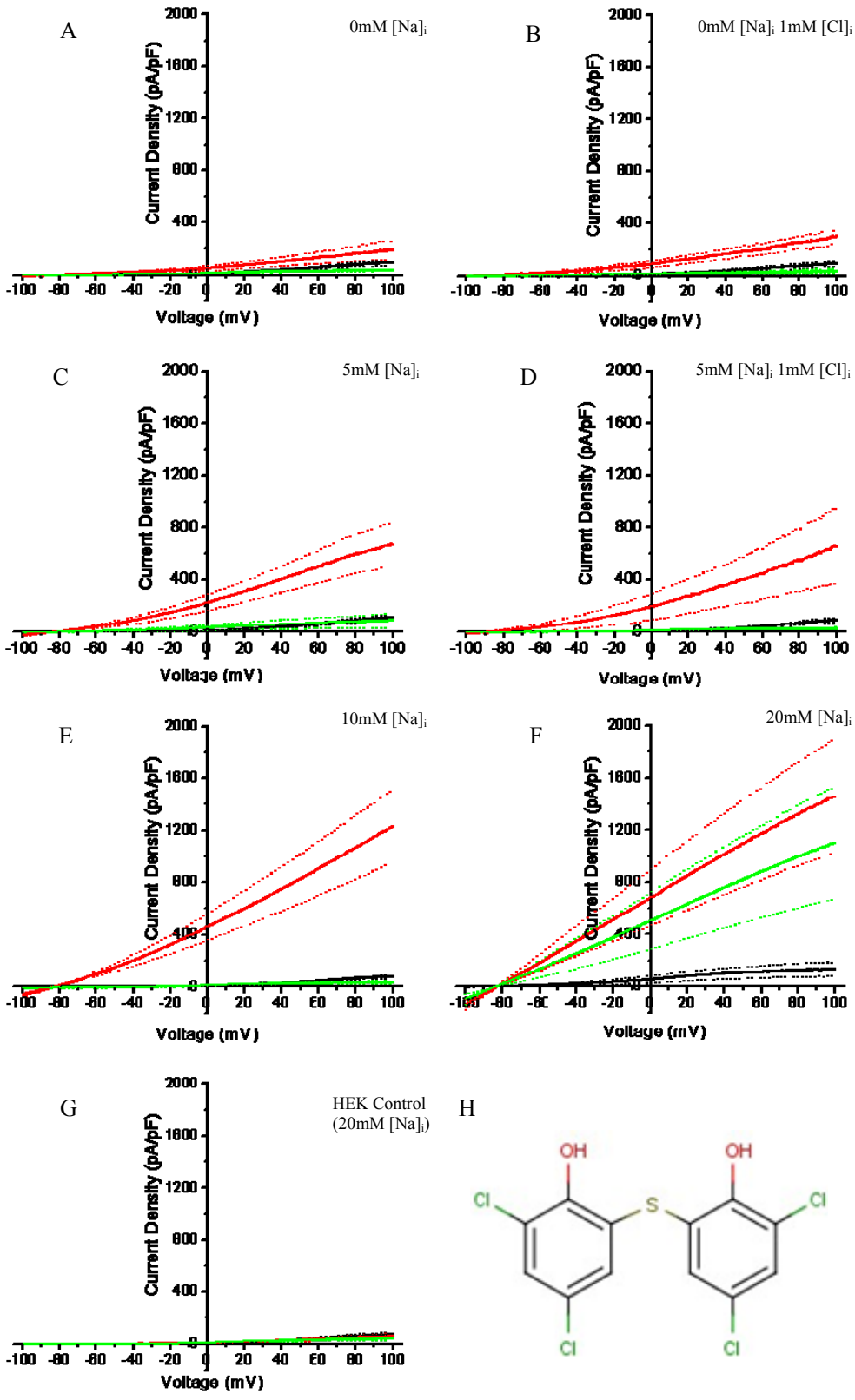
A
0mM [Na]i
B
0mM [Na]i 1mM [Cl]i
C
5mM [Na]i
D
5mM [Na]i 1mM [Cl]i
E
10mM [Na]i
F
20mM [Na]i
G
HEK Control
(20mM [Na]i)
H
Current Density (pA/pF)
Voltage (mV)
OH
Cl
S

Figure 5.3 Cooperativity between $[Na^+]_i$ and Bithionol activation of hSlo2.2a-EGFP. hSlo2.2a currents were recorded from transfected HEK MSR cells by whole cell patch clamp using a -100 to 100 mV voltage ramp with differing $[Na^+]_i$ and $[Cl^-]_i$. Cells were left to equilibrate until the conductance plateaued (black trace). 10 μM of bithionol (H) was applied until the conductance reached a plateau (red trace) and then washed (green trace). Average curves were plotted (± SEM (dotted trace)) for each condition. $[Na^+]_i$ was varied by addition of NaCl to the intracelullar solution; (A) 0 mM, (C) 5 mM, (E)10 mM and (F) 20 mM. To determine if the increase in current density with bithionol was sodium or chloride cooperative, low $[Cl^-]_i$ solutions, 1 mM $[Cl^-]_i$, were made by substituting Cl^- with gluconate. Current densities were measured as before in (B) 0 mM $[Na^+]_i$ (D) 5 mM $[Na^+]_i$ conditions. The lack of bithionol effect on untransfected HEK cells with 20 mM $[Na^+]_i$ is shown in (G).

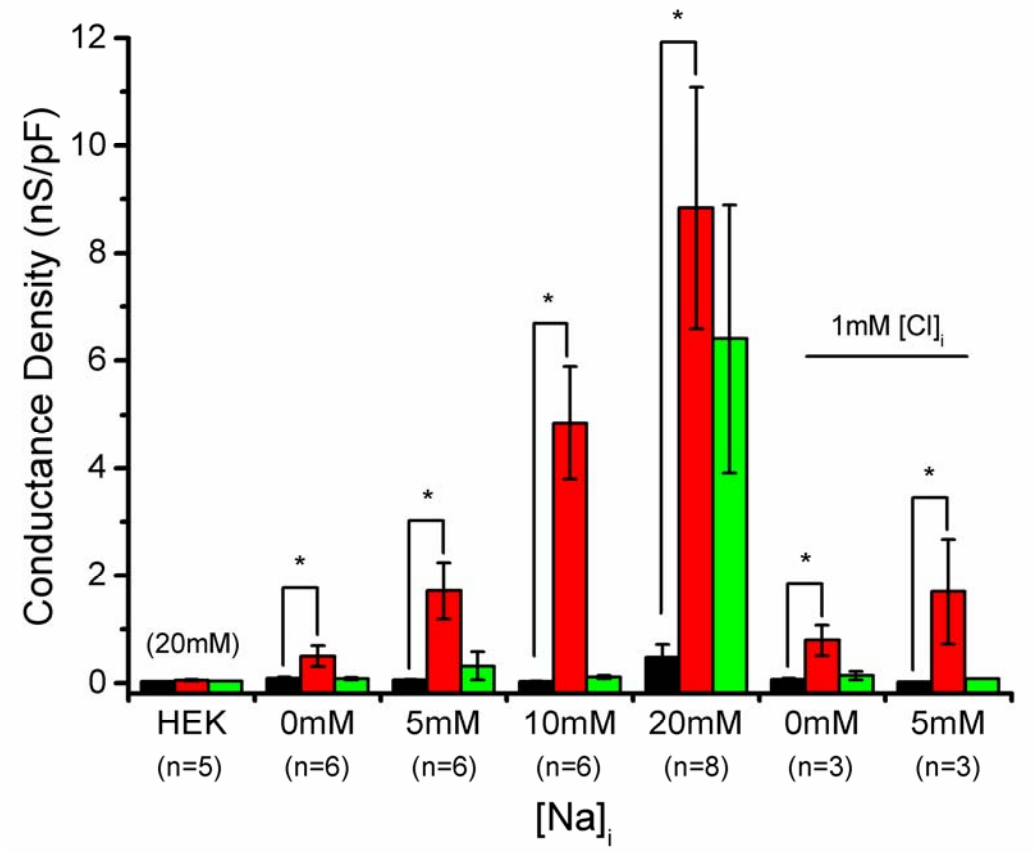

Figure 5.4 Summary of the cooperativity between $[Na^+]_i$ and Bithionol activation of hSlo2.2a-EGFP. Conductance density measurements from the currents in figure 5.3 were collated and averaged. Application of 10 μM bithionol (red trace) was found to significantly ($P<0.05$, Two-way ANOVA; Bonferroni post hoc test) increase the conductance density of hSlo2.2a transfected cells, in all conditions. Comparison of conductance density showed no significant difference in the conductance densities of the low $[Cl^-]_i$ solutions ($P>0.05$, Two-way ANOVA; Bonferroni post hoc test) compared to high $[Cl^-]_i$ solutions.

5.2.3 Bithionol sensitivity of hSlo2.2a currents

HEK MSR cells expressing hSlo2.2a were whole cell patch clamped with 0 mM $[Na]_i$ and subjected to a -100 to 100 mV ramp. Activation curves were generated by application of increasing concentrations of bithionol from 10 nM to 30 μM and recording the conductance. Data were first normalised to cell capacitance and then normalised to zero bithionol (averaged from before application and wash steps after 1, 10, 30 μM) before collating and plotting (Figure 5.5). Individual EC_{50} values were collated to give an average EC_{50} of 1.29 ± 0.12 μM (n=5) and an average hill slope of 8.22 ± 3.89.

5.2.4 Modelling the Bithionol binding site

The RCK Domains of hSlo2.2a were modelled by Dr Jon Lippiat on the reported hSlo1 RCK1 and RCK2 tetramer (Figure 5.6) (Yuan *et al.*, 2010). Using the bithionol binding site described for glutamate dehydrogenase (Li *et al.*, 2009) the structure was scanned to determine regions of homologous positively charged amino acids. Candidate amino acids were highlighted, including the proposed "Cl^- bowl" (Yuan *et al.*, 2000), that may contribute to bithionol binding and activation of the hSlo2.2a channel.

5.2.5 Bithionol Sulfoxide sensitivity of hSlo2.2a currents

hSlo2.2a-EGFP transfected HEK cells were whole cell patch clamped with 5 mM $[Na]_i$ subjected to a -100 to +100 mV voltage ramp at a frequency of 0.25 Hz. As can be seen in the sample recording of conductance density (Figure 5.7.A) cell conductance was allowed to plateau, then 10μM bithionol was applied to confirm channel activity, cells were then washed with extracelluar solution. After washing 10 μM bithionol sulfoxide was applied until plateau and then washed for a final time. Data were collated and summarised (n=3) (Figure 5.7.B) showing a significant increase ($P<0.05$, One-way ANOVA; Bonferroni post hoc test) dependent on 10 μM bithionol and a non significant ($P>0.05$, One-way ANOVA; Bonferroni post hoc test) effect due to 10 μM bithionol sulfoxide compared to the control and wash steps.

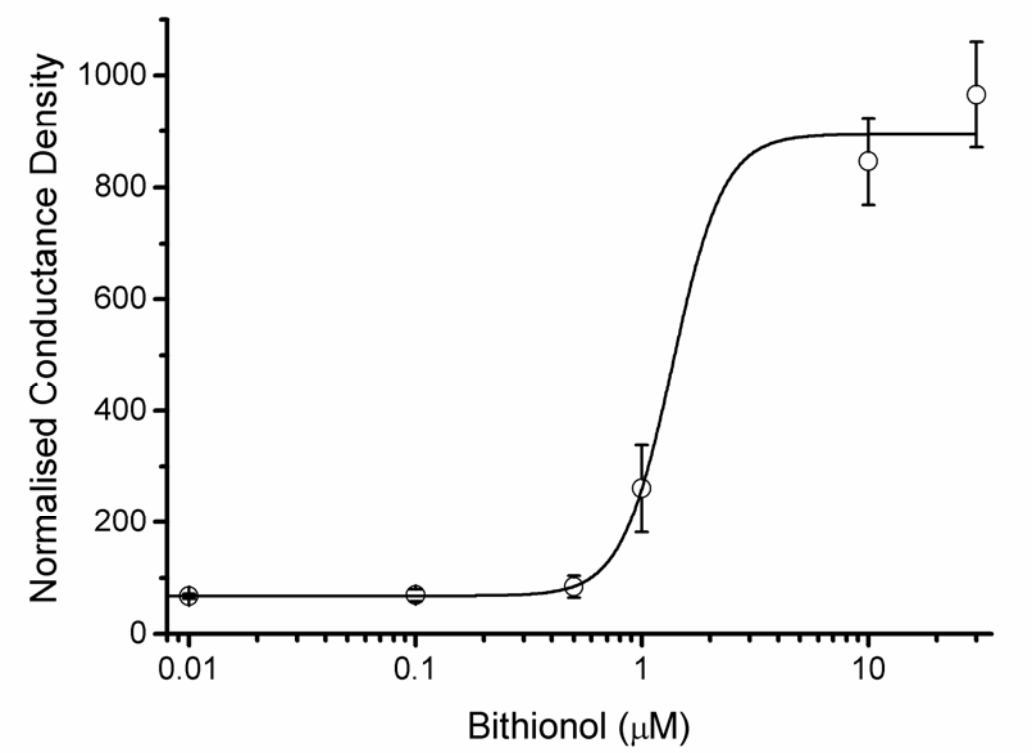

Figure 5.5 Concentration Response of Activation of hSlo2.2a-EGFP by Bithionol. HEK MSR cells expressing hSlo2.2a were whole cell patch clamped with 0 mM $[Na]_i$ and subjected to a -100 to 100 mV ramp. Drug concentrations were applied until the conductance reached a plateau. Data were then normalised to zero bithionol (averaged from before application and wash steps after 1, 10, 30 μM). Individual EC_{50} values were collated to give an average EC_{50} of 1.29 ± 0.12 μM (n=5).

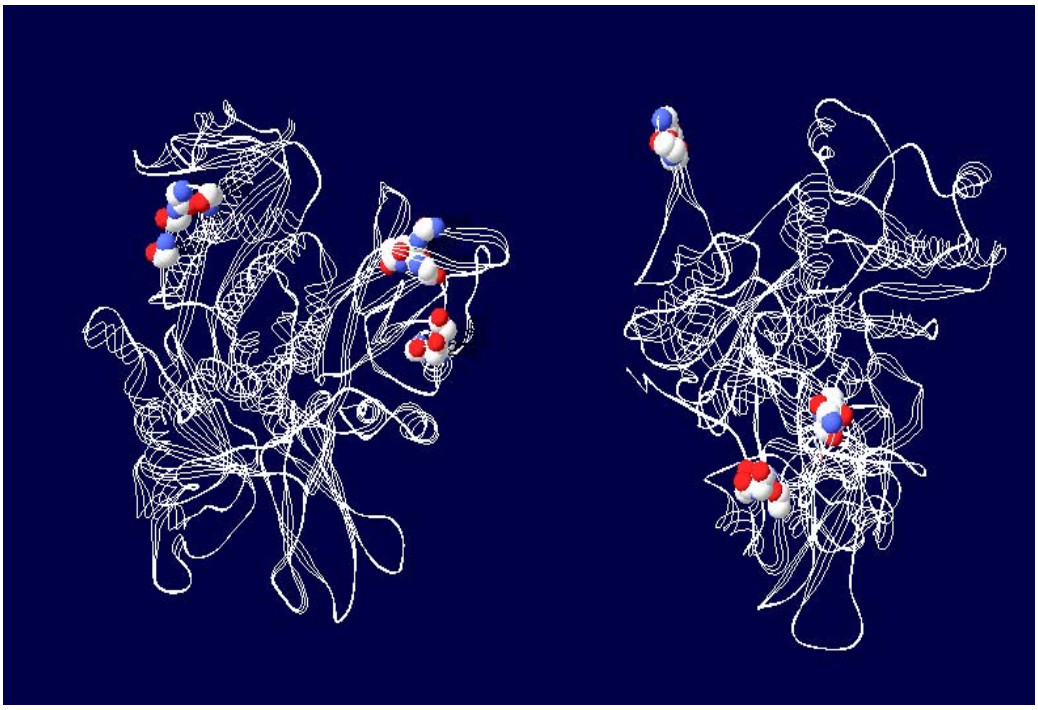

Figure 5.6 Homology model of the Bithionol binding site in hSlo2.2a channels. Homology modelling of the hSlo2.2a RCK domains based on the published human Slo1 crystal structure (Yuan *et al.*, 2010). Highlighted residues are areas of positively charged amino acids, including the proposed "Cl^- bowl" (Yuan *et al.*, 2000), that may contribute to bithionol binding and activation of the channel.

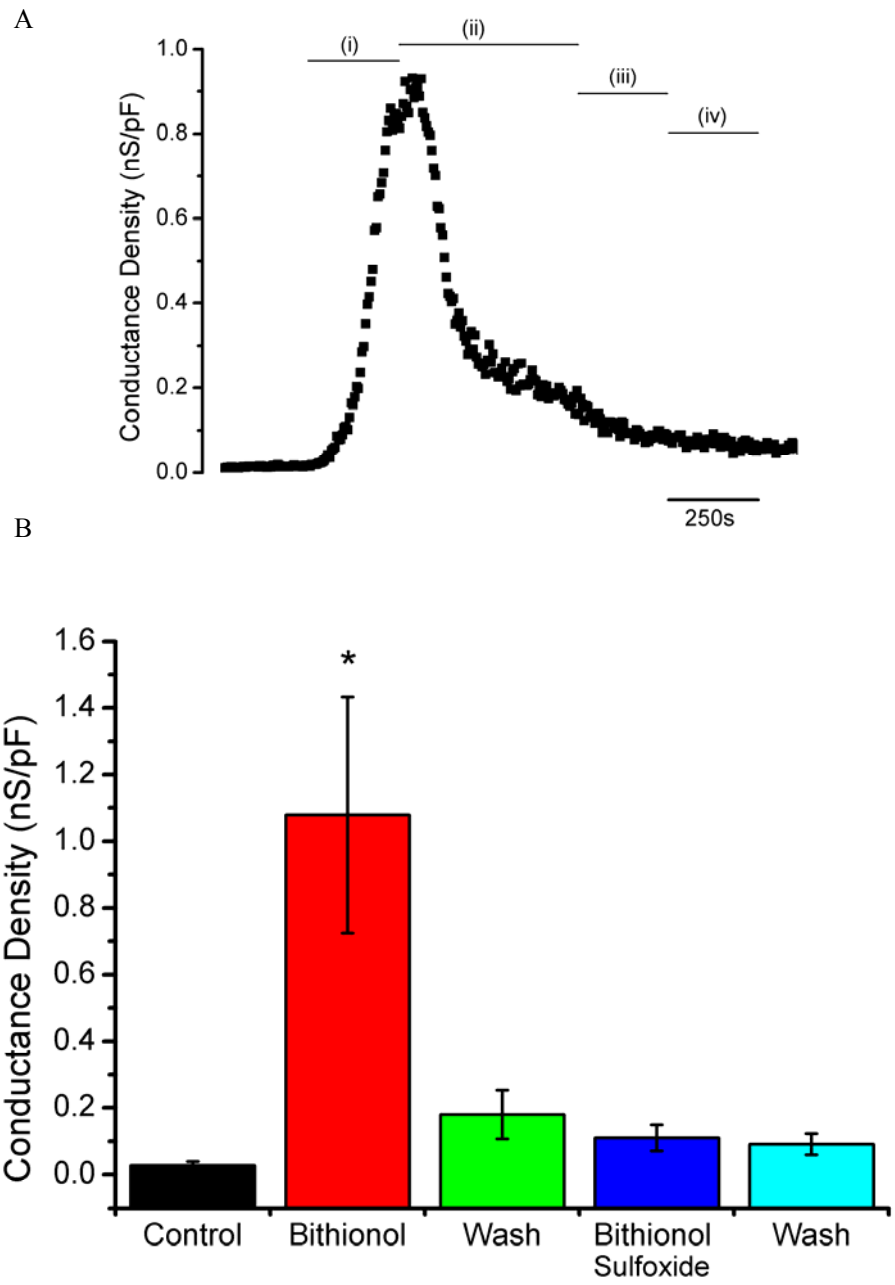

Figure 5.7 Effects of Bithionol Sulfoxide on hSlo2.2a channels. hSlo2.2a-EGFP transfected HEK cells were subjected to a -100 to +100 mV voltage ramp with 5 mM $[Na]_i$. As can be seen in the sample data (A) cell conductance was allowed to plateau, then 10 µM bithionol was applied (i), cells were then washed (ii), then 10µM bithionol sulfoxide was applied (iii) and a final wash was applied (iv). Data were collated and summarised (B) showing a significant increase ($P<0.05$, One-way ANOVA; Bonferroni post hoc test) dependent on 10 µM bithionol and a non significant ($P>0.05$, One-way ANOVA; Bonferroni post hoc test) increase due to 10 µM bithionol sulfoxide (n=3) compared to the control and wash steps.

5.2.6 hSlo2.1 activation by Bithionol

HEK MSR cells were cotransfected with hSlo2.1 and EGFP, and subjected to a -100 to +100 mV voltage ramp with 5 mM $[Na]_i$. Cells were left to equilibrate until the conductance reached a plateau, then 10 μM of bithionol was applied until plateau for ten sweeps was attained, following which cells were washed with extracelluar solution. Conductance measurements were normalised to cell capacitance collating and averaging (Figure 5.8). Application of 10 μM bithionol was found to increase the conductance density compared to control. However, the observed increase in the conductance density of hSlo2.1 transfected cells was not significantly ($P>0.05$, Student's t-test) different from the effects on endogenous currents from untransfected HEK cells.

5.2.7 Effects of Bithionol on K_{ATP}

832/13 INS cells, which are a rat pancreatic β-cell-derived line that express K_{ATP} channels, were whole cell patch clamped and subjected to a -100 to +100 mV voltage ramp with 5 mM $[Na]_i$. As can be seen in the sample data (Figure 5.9.A), measurements of conductance were allowed to run up until plateau, then 10 μM bithionol was applied until a plateau, cells were then washed with extracellular solution. Changes in the conductance density of individual cells were collated and average (±SEM) data were plotted (Figure 5.9.B). 10 μM bithionol was found to cause a significant reduction in conductance density ($P<0.5$, One-way ANOVA; Bonferroni post hoc test) (n=5). The effect of bithionol application was found to be irreversible within the timeframe.

5.2.8 Physiological effects of Bithionol

To see the physiological effects of bithionol application, isolated rat DRG cells were whole cell patch clamped with 5 mM $[Na^+]_i$ and subjected to -100 to 0 mV voltage ramps. DRGs were left to equilibrate until the conductance plateaued, then 10 μM of bithionol was applied until the conductance reached a plateau and then washed with extracellular solution, as can be seen in the sample trace (Figure 5.10.A). Conductance measurements were normalised to cell capacitance and then normalised to the control period (before application) and collated before plotting (Figure 5.10.B). 10 μM bithionol was found to significantly ($P<0.05$, One-way ANOVA; Bonferroni post hoc test) increase the conductance density by 2.24 ± 0.54 fold (n=7) compared to pre-application. The effect of bithionol application was found to be irreversible within the timeframe of the experiment. Assessment of the effects of bithionol found that no significant difference was observed ($P>0.05$, Two-way ANOVA; Bonferroni

post hoc test), if data were divided into small (<25 pF) and large (>25 pF) DRG cells. As we observed a change in the reversal potential of rat DRG cells therefore we investigated if bithionol affected the RMP of the cell. Isolated rat DRG cells were whole cell patch clamped in the current clamp configuration with 5 mM $[Na^+]_i$ and subjected a constant 0 pA current. As can be seen in the sample trace (Figure 5.11.B) DRGs were left to equilibrate until the RMP plateaued then 10 μM of bithionol was applied until RMP reached a plateau and then washed with extracellular solution. Changes in the RMP of individual cells were plotted before collating and averaged (±SEM) data were plotted (Figure 5.11.B). 10 μM bithionol was found to cause an average significant hyperpolarisation ($P<0.05$, One-way ANOVA; Bonferroni post hoc test) of ≈10 mV (n=4). The effect of bithionol application was found to be irreversible within the timeframe of the experiment.

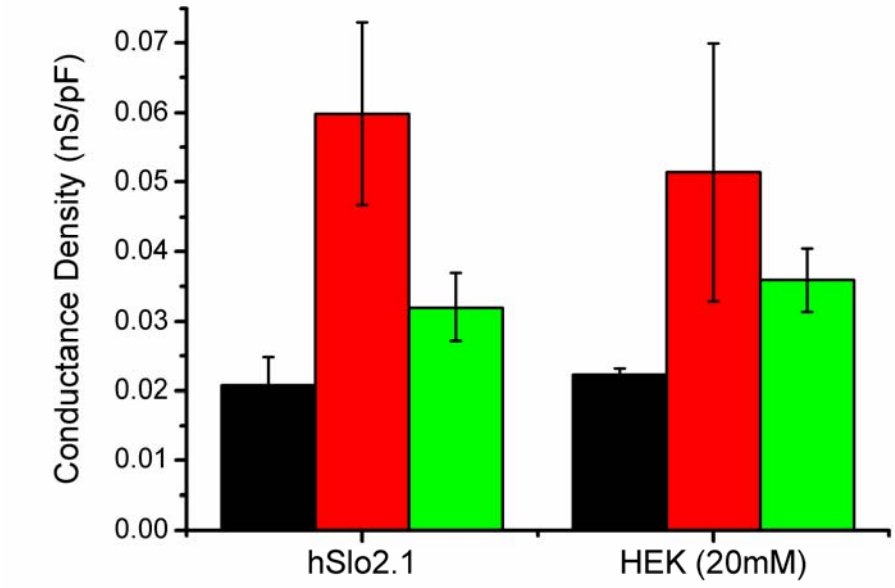

Figure 5.8 Bithionol activation of hSlo2.1. Conductance density measurements from the currents were collated and averaged. Application of 10 μM bithionol (red bar) was found to not significantly ($P>0.05$, T-test) increase the conductance density of hSlo2.1 transfected cells compared to HEK endogenous currents with 20 mM $[Na^+]_i$.

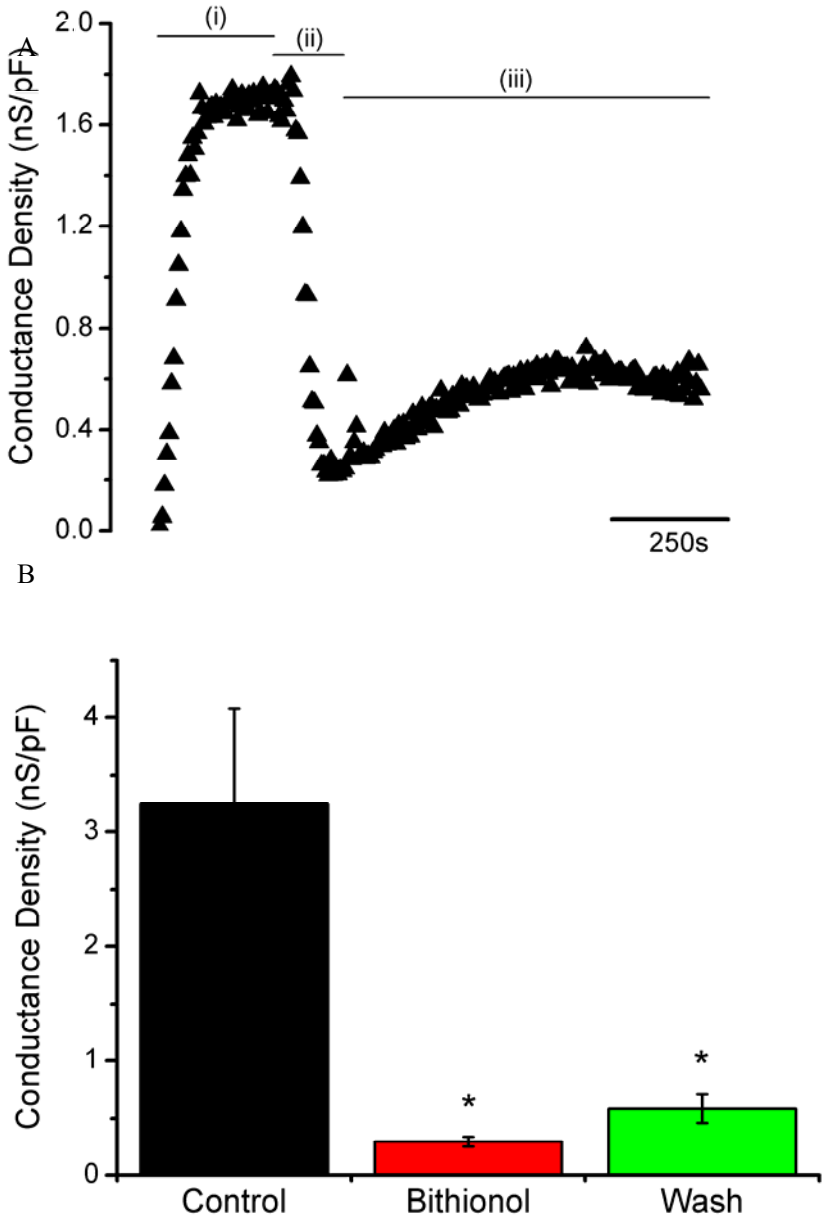

Figure 5.9 Bithionol Effect on K_{ATP} Currents. 832/13 INS cells were subjected to a -100 to +100 mV voltage ramp with 5 mM $[Na]_i$. As can be seen in the sample curve (A), currents were allowed to run up and plateau (i), then 10 μM bithionol was applied (ii) until plateau, cells were then washed (iii). Changes in the conductance density were collated and average (±SEM) data were plotted (filled triangles) (B). 10 μM bithionol was found to cause a significant reduction in conductance density ($P<0.5$, One-way ANOVA; Bonferroni post hoc test) compared to control (n=5). The effect of bithionol application was found to be irreversible within the timeframe.

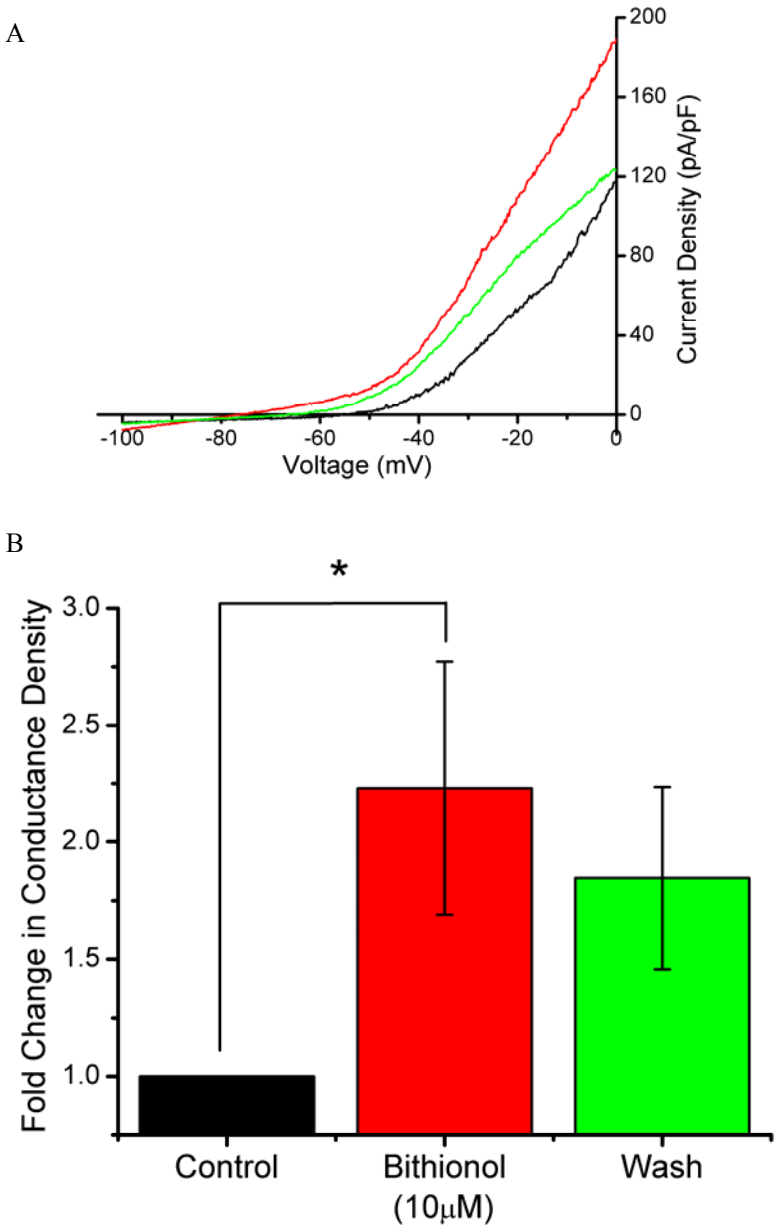

Figure 5.10 Bithionol Effects on rat DRG currents. Rat DRG cells were whole cell patch clamped with 5 mM $[Na^+]_i$ and subjected to -100 to 0 mV voltage ramps. DRGs were left to equilibrate until the conductance plateaued (black trace). 10 μM of bithionol was applied until the conductance reached a plateau (red trace) and then washed (green trace), as can be seen in the sample traces (A). Conductance densities were normalised to the control period (before application) and collated before plotting (B). 10 μM bithionol was found to significantly ($P<0.05$, One-way ANOVA; Bonferroni post hoc test) increase the conductance density by 2.24 ± 0.54 fold (n=7) compared to pre-application. The effect of bithionol application was found to be irreversible within the timeframe.

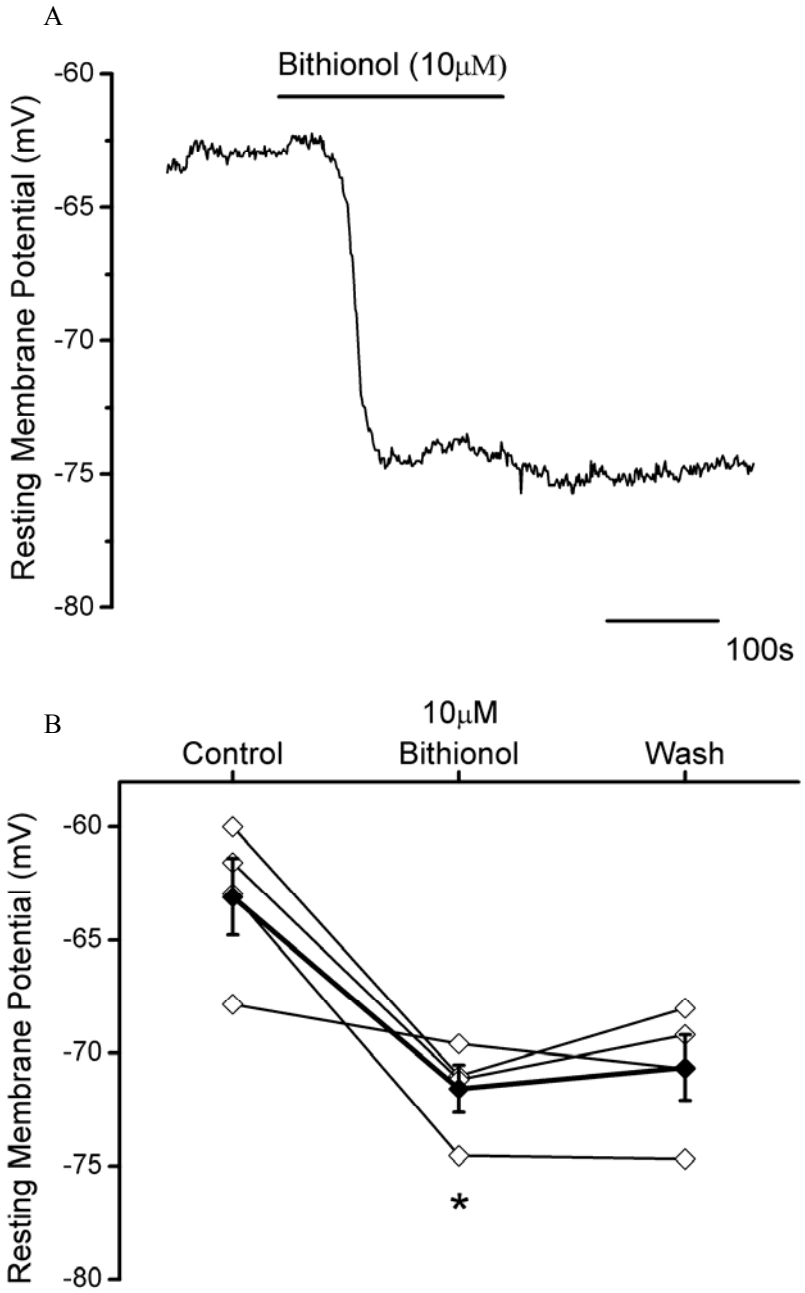

Figure 5.11 Effect of Bithionol on the resting membrane potential of DRGs. Rat DRG cells were whole cell patch clamped with 5 mM $[Na^+]_i$ and subjected a constant 0 pA current. DRGs were left to equilibrate until the RMP plateaued. 10 μM of bithionol was applied until RMP reached a plateau and then washed, as can be seen in the sample trace (A). Changes in the RMP of individual cells (open diamonds) were plotted before collating and averaged data were plotted (filled diamonds) (B). 10 μM bithionol was found to cause an average significant hyperpolarisation ($P<0.05$, One-way ANOVA; Bonferroni post hoc test) of ≈10 mV (n=4). The effect of bithionol application was found to be irreversible within the timeframe.

5.3 Chapter 5 Discussion

5.3.1 Characteristics of hSlo2.2a currents in HEK cells

hSlo2.2a-EGFP currents in transiently transfected HEK MSR cells were recorded by whole cell patch clamp. Interestingly, the hSlo2.2a currents in the presence of 20 mM $[NaCl]_i$ have differing characteristics compared to rSlo2.2a current recorded in CHO cells (Brown *et al.*, 2008). The only similar characteristic we observed between hSlo2.2a and rSlo2.2a currents was rapid channel activation. This characteristic appears to be a function of the Slo2.2a N-terminus, which has high sequence identity to the Slo2.1 N-terminus (Brown *et al.*, 2008). hSlo2.2a currents, unlike rSlo2.2a, display a linear current-voltage relationship with no rectification. If a p/4 leak subtraction protocol was used on the voltage step protocols used to create the $(I/C_{cell})/V$ plots, currents became outwardly rectifying and thus similar to currents previously reported from rSlo2.2a channels. However previous studies are unclear if a p/4 leak subtraction, or any other leak subtraction protocol, was used in their recording protocols (Brown *et al.*, 2008). Their study also observed that rSlo2.2a currents reverse at -50 mV, whereas using the same solution composition in our study, hSlo2.2a currents reverse at ≈ -75 mV in the presence of 20 mM $[NaCl]_i$. This is possibly due to the heterologous expression system used, HEK cells have endogenously expressed Kv channels (Jiang *et al.*, 2002*a*) which are absent from the CHO cell line. Due to these endogenous contaminating K^+ currents, we needed to supplement our intracellular solution with 20 mM $[NaCl]_i$ in order to observe distinct currents. Whereas in CHO cells it is assumed that under their conditions there is adequate $[Na^+]_i$ in the CHO cell, entering through a presumed Na^+ leak channel or other pathways (Joiner *et al.*, 1998; Bhattacharjee *et al.*, 2003; Brown *et al.*, 2008). Thus it is probable that our $[Na^+]_i$ was higher, resulting in a relative increase in the number of open hSlo2.2a channels, which drive the reversal potential closer to the calculated E_K of -83 mV. Alternatively, the difference in reversal potential may be due to the difference in selectivity filter sequence, as rSlo2.2a has the less K^+ selective GFG pore sequence, thus there may be some contaminating Na^+ flux.

Our study also differs from previous studies as voltage step recordings were made once conductance densities has reached a plateau, due to our observation that hSlo2.2 currents "run up" after breakthrough. In comparison, the previous study recorded I/V relationships apparently shortly after breakthrough to the cell (Brown *et al.*, 2008). Interestingly although we recorded a clear (≈ 8 fold) increase in the conductance density (Figure 5.2.A) due to the presence of 20mM $[NaCl]_i$ the increase was found to be not significantly different ($P>0.5$,

Student's t-test) between the presence and absence of 20mM $[NaCl]_i$. If the significance threshold was relaxed to $P<0.1$, there is a significant increase due to the presence of 20 mM $[NaCl]_i$. This is probably due to the high variance in the recorded hSlo2.2a conductance density in the presence of 20 mM $[NaCl]_i$, resultant from the unpredictability of channel expression level in transient transfections. Interestingly whilst the conductance density "ran up" after breakthrough the reversal potentials were fairly stable over the 500 s time period this suggesting that perfusion of the cell with intracellular solution was rapid, and a small increase in the conductance density due to hSlo2.2a activation results in a significant ($P<0.5$, Student's t-test) negative shift (≈-25 mV) in the reversal potential of currents.

5.3.2 Bithionol Activation of hSlo2.2a

To test the sensitivity of hSlo2.2a currents to bithionol activation we recorded from transfected HEK MSR cells by whole cell patch clamp using a range of differing intracellular $[Na^+]$ and $[Cl^-]$. 10 μM bithionol application, in all intracelluar conditions, increased the conductance density of hSlo2.2a transfected cells. $[Na^+]_i$ was varied by addition of NaCl to the intracellular solution and bithionol application was observed to increase conductance density in a cooperative manner. Due to the previously observed sodium and chloride dependence of this family of channels (Joiner *et al.*, 1998; Yuan *et al.*, 2000; Bhattacharjee *et al.*, 2003; Brown *et al.*, 2008) we decided to determine if the increase in current density with bithionol was sodium or chloride cooperative. As a consequence low $[Cl^-]_i$ solutions, with 1 mM $[Cl^-]_i$, were made by substituting Cl^- with gluconate. The conductance density measurements using the low $[Cl^-]_i$ showed no significant difference ($P>0.05$, Two-way ANOVA; Bonferroni post hoc test) when compared to measurements in high $[Cl^-]_i$ solutions. This finding suggests that bithionol activation of hSlo2.2a channels is cooperative with $[Na^+]_i$ rather than $[Cl^-]_i$. The increases in conductance density due to bithionol application was reversible in all conditions with washing, except the 20 mM $[Na^+]_i$ condition. This irreversibility is possibly due to one of two explanations. Firstly that the co-operative activation may slow down the off rates for bithionol above a critical $[Na^+]_i$. Alternatively, this data suggests that at high $[Na^+]_i$ the channels are "locked" open and thus are unable to close even after the agonist is removed. As a control, 10 μM bithionol was also tested on untransfected HEK cells with 20 mM $[Na^+]_i$ and no significant ($P>0.05$, Two-way ANOVA; Bonferroni post hoc test) increase in the recorded conductance density was observed. Thus the increases we see due to bithionol application in the conductance density must be due to the hSlo2.2a channels rather than endogenous Kv channels. A concentration response relationship for bithionol activation of hSlo2.2a in 0 mM $[Na]_i$ was constructed with an average EC_{50} of 1.29 ± 0.12 μM (n=5). However, we are unable to determine if this

value is significantly different from the previously reported EC_{50} for rSlo2.2b channels (0.77 μM) (Yang *et al.*, 2006). This is predominantly due to the previous study utilising only four concentrations and high variability around the highest concentration leading to poor curve fitting. Thus we are unable to state if it is possible to use bithionol potency as an indicator for determining the identity of the Slo2.2 channels underlying K_{Na} currents *in vivo*. Our plot of the concentration response relationship is not perfect however, as there is a high SEM value for the calculated average hill slope (8.22 ± 3.89). This is probably because of our lack of values in the 1-10 μM range which reduces the accuracy of the fit, this range would be filled in with further experimentation.

Dr Jon Lippiat modelled the RCK Domains of hSlo2.2a on the reported hSlo1 RCK1 and RCK2 tetramer (Yuan *et al.*, 2010). The structure was scanned to determine regions of positively charged amino acids homologous to the bithionol binding site described for glutamate dehydrogenase (Li *et al.*, 2009). The model suggested that the bithionol binding site is formed by a dimer of RCK domains, with each α-subunit contributing one pair of RCK 1 and RCK2 domains. This implies that in the conducting tetrametic channel there are four potential binding sites between the monomers of the octomeric RCK complex. From the concentration response curve the average hill slope was calculated to be 8.22 ± 3.89. This suggests that like bithionol binding to glutamate dehydrogenase (Li *et al.*, 2009), two molecules of bithionol have to bind to each binding site and all sites have to be occupied to result in channel activation. This requirement for all sites to be occupied may, however, be due to our experimental design for generating the concentration response relationship. As concentration response relationships were performed in the absence of $[Na]_i$ to eliminate any co-operativity of activation observed in earlier experiments. Thus it may be that in the presence of $[Na]_i$ the number of sites needed to be occupied by bithionol for channel activation is reduced. Interestingly, included in the candidate amino acids was the proposed "Cl^- bowl" region (Yuan *et al.*, 2000). The suggestion that the Cl^- binding site in the hSlo2.2a structure also forms part of the bithionol binding site is concurrent with our findings that there is no significant ($P>0.05$, Two-way ANOVA; Bonferroni post hoc test) difference in the conductance densities of the low $[Cl^-]_i$ solutions compared to high $[Cl^-]_i$ solutions in the presence of 10 μM bithionol. It also appears that the bithionol binding site in hSlo2.2a channels may have a high specificity. Our experiments with bithionol sulfoxide, (which has a double bonded oxygen of the middle sulphur), found it was unable to activate hSlo2.2 currents. To ensure that this lack of activation was not due to low/non expressing HEK cells or a requirement for the presence of $[Na]_i$, cells were patched with 5 mM $[Na]_i$ and responses to 10 μM bithionol were elicited before 10 μM bithionol sulfoxide was applied. The lack of activity of bithionol sulfoxide is not due to a difference in membrane

permability of the compounds, as when the Log P permeability coefficient was calculated using the MarvinSketch calculator (Chemaxon, 2011), both compounds gave a highly positive value of ≈ 5.95, suggesting that both of the compounds are highly membrane permeable. The lack of activity of bithionol sulfoxide is probably due to the large negative charge that is introduced by the sulfoxide group. This negative charge would prevent the back to back orientation of the two molecules required to bind to the binding site to activate the hSlo2.2a channel.

5.3.3 Effects of Bithionol on other K^+ channels

From our experiments it appears that bithionol has specificity for hSlo2.2 channels over hSlo2.1. As whilst application of 10 μM bithionol increased the conductance density compared to the control condition, this increase was not significantly ($P>0.05$, Student's t-test) different from the increase observed of endogenous Kv currents from untransfected HEK cells. Bithionol activation, however, is probably not hSlo2.2 specific as the hSlo2.1 transfections were performed with an untagged plasmid of hSlo2.1. Thus it is possible that the EGFP fluorescence used to identify transfected cells was due solely to EGFP expression rather than co-expression of hSlo2.1 with EGFP. This theory is supported by our attempts to transfect a RFP tagged hSlo2.1 (hSlo2.1-RFP) into HEK cells, in all cases fluorescence was only observed in rounded non-adherent cells. This suggests that hSlo2.1 expression may be toxic, possibly due to constitutive activity.

We utilised 832/13 INS cells, that express K_{ATP} channels, composed of Kir6.2 and SUR1, which are K^+ channels that are inhibited by [ATP] at Kir6.2 but activated by MgATP and MgADP at SUR1 (Seino, 2003). These cells were used as a model to observe neuronal K_{ATP} currents, which are mediated by channels that are composed of the same subunits (Liss & Roeper, 2001). These cells were whole cell patch clamped with 5 mM $[Na]_i$ and subjected to a -100 to +100 mV voltage ramp. As can be seen from our data these conditions evoked an initial run up of current as the cell was perfused with the intracellular solution which lacks ATP, activating the K_{ATP} channels. We found that application of 10 μM bithionol was found to cause significant reduction in the conductance density which was irreversible within the timeframe. However, this inhibition may not be due to direct action of bithionol on either of the subunits that form the K_{ATP} channel. The inhibition could be due to bithionol inhibiting glutamate dehydrogenase stopping the TCA cycle and thus the production of ATP (Li *et al.*, 2009), in the total absence of ATP, K_{ATP} currents run down. This run down is probably due to the depletion of $PIP_{2,}$ in the membrane and depletion of the MgATP stimulus at SUR1. This also may explain why currents were irreversible in the time frame, as [ATP] would

reach the level required to reset cell homeostasis to allow K_{ATP} channels to leave the inactive state.

5.3.4 Physiological effects of Bithionol

In our study we tested the effects of bithionol application in an *ex vivo* system, isolated rat DRG cells, DRG's have been previously reported to express endogenous K_{Na} currents (Bischoff *et al.*, 1998; Gao *et al.*, 2008). DRG's were whole cell patch clamped with 5 mM $[Na^+]_i$ and subjected to -100 to 0 mV voltage ramps, ramps to higher voltages were not used due to action potential firing which would change the $[Na^+]_i$. Application of 10 μM bithionol was found to increase the conductance density by 2.24 ± 0.54 fold compared to pre-application. We found that the effects of bithionol application were found to be irreversible within the timeframe of the experiment. This irreversibility may be due to the fact that neurons have a resting $[Na^+]_i$ of 4-15 mM, thus the irreversibility may be due to the channels becoming "locked open" in a similar manner as suggested by our heterologously expressed hSlo2.2a experiments with 20 mM $[Na^+]_i$ (5.3.2). There may also be additional factors in DRG cells as these will also contain any accessory proteins or physiological modulators that may increase the sensitivity of Slo2.χ channels. The finding that the effects of bithionol are not DRG type specific suggests that all DRG's contain K_{Na} channels, however, the composition of these channels could not be determined. We also observed a change in the reversal potential of rat DRG cells thus we decided to investigate if bithionol activation of K_{Na} channels affects the RMP of the cell. We found that on average application of 10 μM of bithionol, hyperpolarised the RMP towards E_K by ≈10 mV, implicating the activation of a K^+ current. This finding suggests that, as previously reported (Bischoff *et al.*, 1998), K_{Na} channels have a role in mediating the RMP of DRG cells. The irreversibility of the effect of bithionol application is probably due to the lack of depolarising channels active at ≈-70 mV that would be able to reset the RMP.

5.3.5 Challenges for the future

Challenges for the future will be to examine: (a) if mutations of the amino acids suggested by our model effect the potency of bithionol activation of hSlo2.2a; (b) the specificity of the bithionol binding site in hSlo2.2a by testing the channel with the compounds Hexachlorophene (Pestanal), 2-Hydroxy-2'3'5'Tricholobenzophenone and Carbonylcyanide 3-Cholro-Phenyl Hydrazone; (c) If application of a generalised K^+ blocker, quinidine, to media allows for survival of hSlo2.1-RFP transfected cells to allow recordings; (d) if it is possible to clone the hSlo2.2b channel and observe if this has mediating effects on hSlo2.1 expression through heterometric channel formation; (e) if application of bithionol can modify the spike timing frequency of *ex vivo* DRG neurons; (f) if application on bithionol *in vivo* to a neuropathic pain model has analgesic effects.

5.3.6 Chapter Summary

This data reveals that, unlike the previously reported rSlo2.2a channel, hSlo2.2a channels mediate a non rectifying K^+ current. The bis-phenol anthelmintic compound, bithionol was found to activate this channel through binding to the large C-terminal domain near the Cl^- binding site. Bithionol had converse effects on K_{ATP} mediated current, probably due to interrupting the upstream pathway, whereas it had no effect on the range of endogenous Kv channels expressed by HEK cells. Determination of the selectivity of bithionol application on the Slo2.χ family of channels was not possible due to toxicity of hSlo2.1 expression. Our data suggests that *in vivo* in neurons these channels act as background K^+ conductance which is activated under a variety of conditions to stabilise the resting membrane potential of the cell.

Chapter VI: General Discussion

6.1 Slo3

This study provides evidence that supports the findings from experiments with mSlo3 KO mice (Santi *et al.*, 2010; Zeng *et al.*, 2011), in showing that the Slo3 channel mediates at least a component of the I_{KSper} current. The I_{KSper} current plays a vital role in the capacitation of spermatozoa, a critical step priming the spermatozoa for fertilisation (Navarro *et al.*, 2007). We suggest that there are two major applications for research into Slo3 channels, firstly pharmacological inhibition to reduce the viability of fertilisation as a male "pill". This treatment should have a low risk of side effects due to the limited expression profile of Slo3. However, whilst this appears an attractive pathway for Slo3 research issues surrounding compliance may limit interest from pharmacological companies. The second application of Slo3 research is in treatment of some conditions that result in infertility. As has been shown by the mSlo3 KO mice models the absence of this channel results in the loss of the alkalinisation-activated hyperpolarisation required for capacitation and reduced motility of the spermatozoa resulting in infertility. Reduced expression of the CatSper channel forming CatSper1 subunit, another channel critical to the process of capacitation, can be correlated to sub-fertility in humans due to reduced spermatozoa motility. However, not all of the patients observed in this study showed this correlation (Nikpoor *et al.*, 2004), therefore, suggesting there may be other pathways through which the same physiological effect can occur.

Thus it is not unconceivable that some conditions underling reduced motility in humans may be due to a reduced Slo3 current. Further genetic screening for variations in the Slo3 gene (KCNU1) in infertile humans and an analysis of expression/properties is required to determine if this theory is correct. Pharmacological activators of Slo3 would be unlikely to be of use in treating conditions arising due to reduced mSlo3 expression. As the current understanding of capacitation (1.3.4.2) suggests that, unlike the CatSper channels, Slo3 channels are unable to initiate the cascade that initiates capacitation. However, infertility conditions arising from reduced mSlo3 function could be treated *in vitro* by pharmacological activators. *In vivo* treatment would be complicated due to difficulty in targeting/delivery of the activator, as capacitation occurs in the fallopian tube.

Conversely, infertility can also result from premature capacitation of the spermatozoa as the hyperactivation of the spermatozoan flagella cannot be sustained. Thus infertility conditions caused by this molecular mechanism could be treated with Slo3 inhibitors either *in vivo* or in

the process of *in vitro* fertilisation. Inhibition of the Slo3 channel would result in a reduced I_{KSper} current, thus reducing the Ca^{2+} influx through the CatSper channels and in turn reducing the hyperactivation of the spermatozoan flagella. Our study also suggests a potential non-pharmacological method of modulating the I_{KSper} current by over-expression of the CV562866 protein, as we found that expression of this protein reduced total mSlo3 currents. However, directed transfection of this sequence may be difficult and undirected transfection may have unwanted side effects due to effects on Slo1 expression in surrounding tissues.

The recent mSlo3 KO mice models (Santi *et al.*, 2010; Zeng *et al.*, 2011) have somewhat overshadowed our aim to pharmacologically profile mSlo3 currents to determine if properties are shared with the I_{KSper} current from spermatozoa, as these studies are able to directly show that mSlo3 is a major component of the I_{KSper} current. However, KO models often result in down-regulation of unintended targets or up-regulation of compensatory mechanisms. This is exemplified in smooth muscle in the bladder where undirected KO of the Slo1 α-subunit results in up-regulation of a range of compensatory proteins, which are absent when the Slo1 α-subunit is KO specifically in smooth muscle (Sprossmann *et al.*, 2009). Our pharmacological profile for mSlo3, in combination with the KO models, suggests that the mSlo3 channel is potentially a component of the K^+ current which mediates volume regulation and motility of the spermatozoan. mSlo3 channels were previously discounted for these roles due to the reported TEA sensitivity of the mSlo3 channel. This led to Kv1.5 and TASK2 channels being theorised as the channels that mediate volume regulation and motility. However, the TEA concentrations used in the early studies were well below the mSlo3 sensitivity as shown by our and previous studies. Whilst the pharmacology we have described is not specific for the mSlo3 channel, it provides a basis for determining a more specific pharmacology in future studies. Unfortunately, our study is unable to define pharmacologically if mSlo3 is the sole channel mediating volume regulation and motility in the spermatozoan, due to the non specificity of the inhibitors. mSlo3 channels are a good pharmacological target, due to their highly limited expression profile to spermatozoa.

The findings in Chapter IV show that whilst EST's of Slo3 are expressed outside the testis, these EST's encode a short soluble protein that lacks TM domains (CV562866) rather than a splice variant containing a pore forming domain. Thus any pharmacology involving the TM domains, including the pore, of Slo3 should not affect the CV562866 protein and its opposing affects on the expression of both mSlo3 and mSlo1 channels. However, pharmacologically targeting to the pore domain may also affect Slo1 channels, as this region has the highest sequence identity between these two channels. The limited expression of the

full length mSlo3 α-subunit bodes well for pharmacological modulation as many side-effects of drugs are due to expression of the drug target outside of the intended tissue of action.

The findings of Chapter IV suggest that the current presumption that the mSlo3 α-subunit contains two RCK domains like the mSlo1 α-subunit may be incorrect. As our investigation into the secondary structure, suggests that the RCK2 domain of the CV562866 splice variant and full length channel lacks the correct βαβαβ Rossmann motif for a RCK domain. This observation suggests that earlier theories that the RCK2 domain is the major site for modulation by endogenous modulators may be incorrect as these theories are based on the Slo1 structure. However, our findings may be incorrect as they are based solely on a predicted secondary structure and not on an actual crystal structure. The crystal structure of mSlo3 may take a long time to solve as it is probable that there will be difficulty in expression in heterologous systems. Secondly due to the limited background research and general interest of the scientific community of mSlo3, it is likely that crystallisation of this channel will be of low priority in crystallography groups.

Our study also shows that whilst the RCK domains differ between mSlo1 and mSlo3 channels, we have uncovered a conserved Slo channel gating mechanism. Mutation of the conserved phenylalanine in the S6 domain (mSlo3- F304/hSlo1- F380) to tyrosine has similar effects on Slo channel properties, namely a negative shift in voltage dependence of activation and increased channel activity. This may be due to increased hydrophobicity of the residue, which in the open state faces away from the lumen and face the other TM α-helices (Zhang *et al.*, 1998). Thus increasing the hydrophobicity of the residue at 304 in mSlo3 or 380 in mSlo1 stabilises the open state. Interestingly a recent study, has shown that M379 in hSlo1, if replaced with histidine, stabilises the open state when protonated suggesting that this residue faces the lumen of the pore during the active state (Chen & Aldrich, 2011). These findings suggest that the S6 domain undergoes an anti-clockwise rotation, relative to the amino acid sequence, during activation of the channel. However, use of these mutants for pharmacological probing of the mSlo3 channel is problematic as, as our study shows, this mutation appears to be in the conserved quinoline binding site of K^+ channels and thus results in an increased apparent potency of these compounds. Therefore, the potencies of other intracellular pore blockers may also be affected by mutations in the S6 domain. Interestingly, extracellular pore blockers like Ba^{2+} are unaffected by the mutation as it does not affect their ability to access their binding site.

6.2 Slo2

This study suggests that *in vivo* the Na^+ activated hSlo2.2a channels are a component of the background K^+ conductance that can be activated under a variety of conditions to hyperpolarise or stabilise the resting membrane potential of the cell. This differs from previous studies that have focused on the rSlo2.2a and rSlo2.2b channels, as hSlo2.2a channels mediate a non rectifying K^+ current, rather than a voltage dependent outwardly rectifying K^+ current. This observation suggests that the physiological roles of Slo2.2 may be more important in humans than in rats. hSlo2.2a channels only require the presence of intracellular Na^+ rather than Na^+ and depolarisation, as required for rSlo2.2a activation, thus the hSlo2.2a channel will activate at all physiological potentials. However, we also suggest that the rectification observed in rSlo2.2 currents may be either due to application of a p/4-type leak subtraction protocol or the difference in the selectivity filter sequence. When we applied a p/4 protocol to our recordings currents became outwardly rectifying and thus similar to currents previously reported from rSlo2.2a channels. The previous studies do not state if any leak subtraction protocol, was used in the recording protocols (Brown *et al.*, 2008).

This study also found that bithionol, a compound that has been shown to activate rSlo2.2b channels, is also able to activate heterologously expressed hSlo2.2a channels. Our study of the cooperativity of bithionol activation with $[Na^+]_i$ over $[Cl^-]_i$ and the model of potential bithionol binding sites generated by Dr. Lippiat, suggest that bithionol activates these channels by binding to the large C-terminal domain near the Cl^- binding site. This model explains why bithionol activation was absent with the endogenous HEK cell Kv channels, as these channels lack the large C-terminal domain characteristic of Slo channels. This requirement for the large C-terminal domain seems to be contradicted by the inhibition of K_{ATP} mediated current by bithionol application however, we suggest that this may be due to inhibition of GDH in the upstream activation pathway for K_{ATP}.

These findings suggest that activators of Slo2.χ, may have clinical relevance as targets for novel analgesics in inflammatory pain. This is suggested by our finding that bithionol application causes a shift in the RMP and activation of a K^+ current in DRG neurons, including both the large and small nociceptive sub types. However, specificity of novel analgesics will have to be tested as whilst we were unable to determine if bithionol has specificity for hSlo2.2a over hSlo2.1. Bithionol may not be a viable novel analgesic for systemic application, as the side effects may include; cardiac arrhythmia (hSlo2.1

activation), hyperinsulinemia (K_{ATP} inhibition) and ototoxic effects (K_{NA} activation in MNTB). However, these potential side effects many not manifest as bithionol has been used clinically for a number of years to treat fasciolosis in humans with no observed contraindications (Farag *et al.*, 1988; Bassiouny *et al.*, 1991; Bacq *et al.*, 1991). Secondly bithionol activation of K_{Na} neurones MNTB neurons, *in vitro*, has been shown to only increase the AHP and increase the temporal fidelity of the signal rather than affecting the RMP resulting in silencing of these neurons (Yang *et al.*, 2007). However, it has yet to be shown if the increased fidelity of this signal is beneficial to the whole animal, or if it alters processing in the auditory pathway. There may also be a range of other side effects of bithionol application as unpublished results mentioned in the original study, suggest that Slo1 channels may also be activated by bithionol (Yang *et al.*, 2006). These side effects could be largely counteracted by localised application to the nociceptive neurons. Alternatively design of more selective K_{Na} channel activators, in particular with specificity for the Slo2.2 subtypes over Slo2.1, will also have reduced side effects in kidney and cardiac tissues where Slo2.2 is not currently thought to be expressed.

6.3 Final Conclusions

Thus in conclusion, Slo2 and Slo3 channels are under-researched members of the Slo channel sub-family. Our study has shown that both of these channels are viable targets for pharmacological modulation to treat inflammatory pain and infertility conditions respectively. However, the tools available that are used in this study are too non-specific for clinical use, and would result in a range of undesirable side effects.

Chapter VII: References

Altschul SF, Gish W, Miller W, Myers EW & Lipman DJ (1990). Basic local alignment search tool. *J Mol Biol* **215,** 403–410.

Amantea D, Russo R, Bagetta G & Corasaniti MT (2005). From clinical evidence to molecular mechanisms underlying neuroprotection afforded by estrogens. *Pharmacological Research* **52,** 119–132.

Armstrong CM & Taylor SR (1980). Interaction of barium ions with potassium channels in squid giant axons. *Biophys J* **30,** 473–488.

Arnold K, Bordoli L, Kopp J & Schwede T (2006). The SWISS-MODEL workspace: a web-based environment for protein structure homology modelling. *Bioinformatics* **22,** 195–201.

Austin C (1951). Observations on the Penetration of the Sperm into the Mammalian Egg. *Aust Jnl Of Bio Sci* **4,** 581–596.

Bacq Y, Besnier JM, Duong TH, Pavie G, Metman EH & Choutet P (1991). Successful treatment of acute fascioliasis with bithionol. *Hepatology* **14,** 1066–1069.

Barfield JP, Yeung CH & Cooper TG (2005*a*). The effects of putative K+ channel blockers on volume regulation of murine spermatozoa. *Biol Reprod* **72,** 1275–1281.

Barfield JP, Yeung CH & Cooper TG (2005*b*). Characterization of potassium channels involved in volume regulation of human spermatozoa. *Mol Hum Reprod* **11,** 891–897.

Bassiouny HK, Soliman NK, el-Daly SM & Badr NM (1991). Human fascioliasis in Egypt: effect of infection and efficacy of bithionol treatment. *J Trop Med Hyg* **94,** 333–337.

Berg AP, Sen N & Bayliss DA (2007). TrpC3/C7 and Slo2.1 are molecular targets for metabotropic glutamate receptor signaling in rat striatal cholinergic interneurons. *J Neurosci* **27,** 8845–8856.

Berkefeld H, Sailer CA, Bildl W, Rohde V, Thumfart J-O, Eble S, Klugbauer N, Reisinger E, Bischofberger J, Oliver D, Knaus H-G, Schulte U & Fakler B (2006). BKCa-Cav channel complexes mediate rapid and localized Ca2+-activated K+ signaling. *Science* **314,** 615–620.

Bezanilla F (2000). The voltage sensor in voltage-dependent ion channels. *Physiol Rev* **80,** 555–592.

Bhattacharjee A, Gan L & Kaczmarek LK (2002). Localization of the Slack potassium channel in the rat central nervous system. *J Comp Neurol* **454,** 241–254.

Bhattacharjee A, von Hehn CAA, Mei X & Kaczmarek LK (2005). Localization of the Na+-activated K+ channel Slick in the rat central nervous system. *J Comp Neurol* **484,** 80–92.

Bhattacharjee A, Joiner WJ, Wu M, Yang Y, Sigworth FJ & Kaczmarek LK (2003). Slick (Slo2.1), a rapidly-gating sodium-activated potassium channel inhibited by ATP. *J Neurosci* **23,** 11681–11691.

Bischoff U, Vogel W & Safronov BV (1998). Na+-activated K+ channels in small dorsal root ganglion neurones of rat. *J Physiol (Lond)* **510 (Pt 3),** 743–754.

Brenner R, Chen QH, Vilaythong A, Toney GM, Noebels JL & Aldrich RW (2005). BK channel beta4 subunit reduces dentate gyrus excitability and protects against temporal lobe seizures. *Nat Neurosci* **8,** 1752–1759.

Brenner R, Peréz GJ, Bonev AD, Eckman DM, Kosek JC, Wiler SW, Patterson AJ, Nelson MT & Aldrich RW (2000). Vasoregulation by the beta1 subunit of the calcium-activated potassium channel. *Nature* **407,** 870–876.

Brown MR, Kronengold J, Gazula V-R, Chen Y, Strumbos JG, Sigworth FJ, Navaratnam D & Kaczmarek LK (2010). Fragile X mental retardation protein controls gating of the sodium-activated potassium channel Slack. *Nat Neurosci* **13,** 819–821.

Brown MR, Kronengold J, Gazula V-R, Spilianakis CG, Flavell RA, von Hehn CAA, Bhattacharjee A & Kaczmarek LK (2008). Amino-termini isoforms of the Slack K+ channel, regulated by alternative promoters, differentially modulate rhythmic firing and adaptation. *J Physiol (Lond)* **586,** 5161–5179.

Budelli G, Hage TA, Wei A, Rojas P, Jong Y-JI, O'Malley K & Salkoff L (2009). Na+-activated K+ channels express a large delayed outward current in neurons during normal physiology. *Nat Neurosci* **12,** 745–750.

Butler A, Tsunoda S, McCobb DP, Wei A & Salkoff L (1993). mSlo, a complex mouse gene encoding "maxi" calcium-activated potassium channels. *Science* **261,** 221–224.

Caballero R, Pourrier M, Schram G, Delpón E, Tamargo J & Nattel S (2003). Effects of flecainide and quinidine on Kv4.2 currents: voltage dependence and role of S6 valines. *Br J Pharmacol* **138,** 1475–1484.

Chanda B, Asamoah OK, Blunck R, Roux B & Bezanilla F (2005). Gating charge displacement in voltage-gated ion channels involves limited transmembrane movement. *Nature* **436,** 852–856.

Chang MC (1951). Fertilizing Capacity of Spermatozoa deposited into the Fallopian Tubes. *Nature* **168,** 697–698.

Chemaxon (2011). Marvin, Calculator Plugin. Available at: http://www.chemaxon.com/marvin/sketch/index.php [Accessed August 12, 2011].

Chen H, Kronengold J, Yan Y, Gazula V-R, Brown MR, Ma L, Ferreira G, Yang Y, Bhattacharjee A, Sigworth FJ, Salkoff L & Kaczmarek LK (2009). The N-terminal domain of Slack determines the formation and trafficking of Slick/Slack heteromeric sodium-activated potassium channels. *J Neurosci* **29,** 5654–5665.

Chen X & Aldrich RW (2011). Charge substitution for a deep-pore residue reveals structural dynamics during BK channel gating. *J Gen Physiol* **138,** 137–154.

Choisy SCM, Hancox JC, Arberry LA, Reynolds AM, Shattock MJ & James AF (2004). Evidence for a novel K(+) channel modulated by alpha(1A)-adrenoceptors in cardiac myocytes. *Mol Pharmacol* **66,** 735–748.

Clark EN, Corron ME & Florman HM (1993). Caltrin, the calcium transport regulatory peptide of spermatozoa, modulates acrosomal exocytosis in response to the egg's zona pellucida. *J Biol Chem* **268,** 5309–5316.

Costa PF, Emilio MG, Fernandes PL, Ferreira HG & Ferreira KG (1989). Determination of ionic permeability coefficients of the plasma membrane of Xenopus laevis oocytes under voltage clamp. *The Journal of Physiology* **413,** 199–211.

Dai L, Garg V & Sanguinetti MC (2010). Activation of Slo2.1 channels by niflumic acid. *J Gen Physiol* **135,** 275–295.

Dean J (2007). The enigma of sperm-egg recognition in mice. *Soc Reprod Fertil Suppl* **63,** 359–365.

Doyle DA, Morais Cabral J, Pfuetzner RA, Kuo A, Gulbis JM, Cohen SL, Chait BT & MacKinnon R (1998). The structure of the potassium channel: molecular basis of K+ conduction and selectivity. *Science* **280,** 69–77.

Dryer SE (1994). Na+-activated K+ channels: a new family of large-conductance ion channels. *Trends in Neurosciences* **17,** 155–160.

Eisenbach M & Giojalas LC (2006). Sperm guidance in mammals - an unpaved road to the egg. *Nat Rev Mol Cell Biol* **7,** 276–285.

Elkins T, Ganetzky B & Wu CF (1986). A Drosophila mutation that eliminates a calcium-dependent potassium current. *Proc Natl Acad Sci USA* **83,** 8415–8419.

Farag HF, Salem A, el-Hifni SA & Kandil M (1988). Bithionol (Bitin) treatment in established fascioliasis in Egyptians. *J Trop Med Hyg* **91,** 240–244.

Franciolini F, Hogg R, Catacuzzeno L, Petris A, Trequattrini C & Adams DJ (2001). Large-conductance calcium-activated potassium channels in neonatal rat intracardiac ganglion neurons. *Pflügers Archiv European Journal of Physiology* **441,** 629–638.

Gao S-bang, Wu Y, Lü C-xia, Guo Z-hua, Li C-hong & Ding J-ping (2008). Slack and Slick KNa channels are required for the depolarizing afterpotential of acutely isolated, medium diameter rat dorsal root ganglion neurons. *Acta Pharmacol Sin* **29,** 899–905.

Gessner G & Heinemann SH (2003). Inhibition of hEAG1 and hERG1 potassium channels by clofilium and its tertiary analogue LY97241. *Br J Pharmacol* **138,** 161–171.

Gomora JC, Enyeart JA & Enyeart JJ (1999). Mibefradil potently blocks ATP-activated K(+) channels in adrenal cells. *Mol Pharmacol* **56,** 1192–1197.

Grunnet M & Kaufmann WA (2004). Coassembly of big conductance Ca2+-activated K+ channels and L-type voltage-gated Ca2+ channels in rat brain. *J Biol Chem* **279,** 36445–36453.

Gu N, Vervaeke K & Storm JF (2007). BK potassium channels facilitate high-frequency firing and cause early spike frequency adaptation in rat CA1 hippocampal pyramidal cells. *J Physiol (Lond)* **580,** 859–882.

Harrison RA. & Gadella BM (2005). Bicarbonate-induced membrane processing in sperm capacitation. *Theriogenology* **63,** 342–351.

Hashitani H & Brading AF (2003). Ionic basis for the regulation of spontaneous excitation in detrusor smooth muscle cells of the guinea-pig urinary bladder. *Br J Pharmacol* **140,** 159–169.

Hayashi Y, Shi S-H, Esteban JA, Piccini A, Poncer J-C & Malinow R (2000). Driving AMPA Receptors into Synapses by LTP and CaMKII: Requirement for GluR1 and PDZ Domain Interaction. *Science* **287,** 2262–2267.

Heginbotham L, Lu Z, Abramson T & MacKinnon R (1994). Mutations in the K+ channel signature sequence. *Biophys J* **66,** 1061–1067.

Hille B (2001). *Ion Channels of Excitable Membranes*. Sinauer Associates Inc.,U.S.

Ho H-C, Granish KA & Suarez SS (2002). Hyperactivated motility of bull sperm is triggered at the axoneme by Ca2+ and not cAMP. *Dev Biol* **250,** 208–217.

Hopper SH & Wood KM (1958). Development of a germicidal soap containing bithionol. *J Am Pharm Assoc Am Pharm Assoc (Baltim)* **47,** 317–318.

Hou S, Xu R, Heinemann SH & Hoshi T (2008). Reciprocal regulation of the Ca2+ and H+ sensitivity in the SLO1 BK channel conferred by the RCK1 domain. *Nat Struct Mol Biol* **15,** 403–410.

Jiang B, Sun X, Cao K & Wang R (2002*a*). Endogenous Kv channels in human embryonic kidney (HEK-293) cells. *Mol Cell Biochem* **238,** 69–79.

Jiang Y & MacKinnon R (2000). The Barium Site in a Potassium Channel by X-Ray Crystallography. *The Journal of General Physiology* **115,** 269–272.

Jiang Y, Lee A, Chen J, Cadene M, Chait BT & MacKinnon R (2002*b*). Crystal structure and mechanism of a calcium-gated potassium channel. *Nature* **417,** 515–522.

Jiang Y, Ruta V, Chen J, Lee A & MacKinnon R (2003). The principle of gating charge movement in a voltage-dependent K+ channel. *Nature* **423,** 42–48.

Joiner WJ, Tang MD, Wang LY, Dworetzky SI, Boissard CG, Gan L, Gribkoff VK & Kaczmarek LK (1998). Formation of intermediate-conductance calcium-activated potassium channels by interaction of Slack and Slo subunits. *Nat Neurosci* **1,** 462–469.

Kameyama M, Kakei M, Sato R, Shibasaki T, Matsuda H & Irisawa H (1984). Intracellular Na+ activates a K+ channel in mammalian cardiac cells. *Nature* **309,** 354–356.

Kiefer F, Arnold K, Künzli M, Bordoli L & Schwede T (2009). The SWISS-MODEL Repository and associated resources. *Nucleic Acids Res* **37,** D387–D392.

Kim EY, Ridgway LD, Zou S, Chiu Y-H & Dryer SE (2007). Alternatively spliced C-terminal domains regulate the surface expression of large conductance calcium-activated potassium channels. *Neuroscience* **146,** 1652–1661.

Kirichok Y, Navarro B & Clapham DE (2006). Whole-cell patch-clamp measurements of spermatozoa reveal an alkaline-activated Ca2+ channel. *Nature* **439,** 737–740.

Knaus HG, Folander K, Garcia-Calvo M, Garcia ML, Kaczorowski GJ, Smith M & Swanson R (1994). Primary sequence and immunological characterization of beta-subunit of high conductance Ca(2+)-activated K+ channel from smooth muscle. *Journal of Biological Chemistry* **269,** 17274–17278.

Knaus HG, Schwarzer C, Koch RO, Eberhart A, Kaczorowski GJ, Glossmann H, Wunder F, Pongs O, Garcia ML & Sperk G (1996). Distribution of high-conductance Ca(2+)-activated K+ channels in rat brain: targeting to axons and nerve terminals. *J Neurosci* **16,** 955–963.

Lee J-H, Kim H-J, Kim H-D, Lee B-C, Chun J-S & Park C-S (2009). Modulation of the conductance-voltage relationship of the BK(Ca) channel by shortening the cytosolic loop connecting two RCK domains. *Biophys J* **97,** 730–737.

Li M, Smith CJ, Walker MT & Smith TJ (2009). Novel Inhibitors Complexed with Glutamate Dehydrogenase. *Journal of Biological Chemistry* **284,** 22988–23000.

Li Y, Berke I, Chen L & Jiang Y (2007). Gating and inward rectifying properties of the MthK K+ channel with and without the gating ring. *J Gen Physiol* **129,** 109–120.

Lingle CJ (2007). Gating rings formed by RCK domains: keys to gate opening. *J Gen Physiol* **129,** 101–107.

Lippiat JD, Standen NB & Davies NW (2000). A residue in the intracellular vestibule of the pore is critical for gating and permeation in Ca2+-activated K+ (BKCa) channels. *J Physiol (Lond)* **529 Pt 1,** 131–138.

Lippiat JD, Standen NB, Harrow ID, Phillips SC & Davies NW (2003). Properties of BK(Ca) channels formed by bicistronic expression of hSloalpha and beta1-4 subunits in HEK293 cells. *J Membr Biol* **192,** 141–148.

Lishko PV, Botchkina IL & Kirichok Y (2011). Progesterone activates the principal Ca2+ channel of human sperm. *Nature* **471,** 387–391.

Lishko PV, Botchkina IL, Fedorenko A & Kirichok Y (2010). Acid Extrusion from Human Spermatozoa Is Mediated by Flagellar Voltage-Gated Proton Channel. *Cell* **140,** 327–337.

Liss B & Roeper J (2001). Molecular physiology of neuronal K-ATP channels (review). *Mol Membr Biol* **18,** 117–127.

Liu G, Zakharov SI, Yang L, Deng S-X, Landry DW, Karlin A & Marx SO (2008). Position and role of the BK channel alpha subunit S0 helix inferred from disulfide crosslinking. *J Gen Physiol* **131,** 537–548.

Lu S, Das P, Fadool DA & Kaczmarek LK (2010). The slack sodium-activated potassium channel provides a major outward current in olfactory neurons of Kv1.3-/- super-smeller mice. *J Neurophysiol* **103,** 3311–3319.

Ma Z, Lou XJ & Horrigan FT (2006). Role of charged residues in the S1-S4 voltage sensor of BK channels. *J Gen Physiol* **127,** 309–328.

MacKinnon R (2004). Nobel Lecture. Potassium channels and the atomic basis of selective ion conduction. *Biosci Rep* **24,** 75–100.

Malmberg AB, Brandon EP, Idzerda RL, Liu H, McKnight GS & Basbaum AI (1997). Diminished inflammation and nociceptive pain with preservation of neuropathic pain in mice with a targeted mutation of the type I regulatory subunit of cAMP-dependent protein kinase. *J Neurosci* **17,** 7462–7470.

Marsden RL, McGuffin LJ & Jones DT (2002). Rapid protein domain assignment from amino acid sequence using predicted secondary structure. *Protein Sci* **11,** 2814–2824.

Martínez-López P, Santi CM, Treviño CL, Ocampo-Gutiérrez AY, Acevedo JJ, Alisio A, Salkoff LB & Darszon A (2009). Mouse sperm K+ currents stimulated by pH and cAMP possibly coded by Slo3 channels. *Biochem Biophys Res Commun* **381,** 204–209.

Meech RW (1974). The sensitivity of Helix aspersa neurones to injected calcium ions. *J Physiol* **237,** 259–277.

Meech RW & Standen NB (1975). Potassium activation in Helix aspersa neurones under voltage clamp: a component mediated by calcium influx. *J Physiol (Lond)* **249,** 211–239.

Meera P, Wallner M, Song M & Toro L (1997). Large conductance voltage- and calcium-dependent K+ channel, a distinct member of voltage-dependent ion channels with seven N-terminal transmembrane segments (S0-S6), an extracellular N terminus, and an intracellular (S9-S10) C terminus. *Proc Natl Acad Sci USA* **94,** 14066–14071.

Meredith AL, Thorneloe KS, Werner ME, Nelson MT & Aldrich RW (2004). Overactive bladder and incontinence in the absence of the BK large conductance Ca2+-activated K+ channel. *J Biol Chem* **279,** 36746–36752.

Misonou H, Menegola M, Buchwalder L, Park EW, Meredith A, Rhodes KJ, Aldrich RW & Trimmer JS (2006). Immunolocalization of the Ca2+-activated K+ channel Slo1 in axons and nerve terminals of mammalian brain and cultured neurons. *J Comp Neurol* **496,** 289–302.

Mori K, Kobayashi S, Saito T, Masuda Y & Nakaya H (1998). Inhibitory effects of class I and IV antiarrhythmic drugs on the Na+-activated K+ channel current in guinea pig ventricular cells. *Naunyn Schmiedebergs Arch Pharmacol* **358,** 641–648.

Nanou E, Kyriakatos A, Bhattacharjee A, Kaczmarek LK, Paratcha G & El Manira A (2008). Na+-mediated coupling between AMPA receptors and KNa channels shapes synaptic transmission. *Proceedings of the National Academy of Sciences* **105,** 20941–20946.

Navarro B, Kirichok Y & Clapham DE (2007). KSper, a pH-sensitive K+ current that controls sperm membrane potential. *Proc Natl Acad Sci U S A* **104,** 7688–7692.

Navarro B, Kirichok Y, Chung J-J & Clapham DE (2008). Ion channels that control fertility in mammalian spermatozoa. *Int J Dev Biol* **52,** 607–613.

Nelson MT, Cheng H, Rubart M, Santana LF, Bonev AD, Knot HJ & Lederer WJ (1995). Relaxation of arterial smooth muscle by calcium sparks. *Science* **270,** 633–637.

Neyton J & Miller C (1988). Discrete Ba2+ block as a probe of ion occupancy and pore structure in the high-conductance Ca2+ -activated K+ channel. *J Gen Physiol* **92,** 569–586.

Nikpoor P, Mowla SJ, Movahedin M, Ziaee SA-M & Tiraihi T (2004). CatSper gene expression in postnatal development of mouse testis and in subfertile men with deficient sperm motility. *Hum Reprod* **19,** 124–128.

Nuwer MO, Picchione KE & Bhattacharjee A (2009). cAMP-dependent kinase does not modulate the Slack sodium-activated potassium channel. *Neuropharmacology* **57,** 219–226.

Nuwer MO, Picchione KE & Bhattacharjee A (2010). PKA-induced internalization of slack KNa channels produces dorsal root ganglion neuron hyperexcitability. *J Neurosci* **30,** 14165–14172.

Osterrieder W & Holck M (1989). In vitro pharmacologic profile of Ro 40-5967, a novel Ca2+ channel blocker with potent vasodilator but weak inotropic action. *J Cardiovasc Pharmacol* **13,** 754–759.

Peitsch MC (1995). Protein Modeling by E-mail. *Nat Biotech* **13,** 658–660.

Perchenet L & Clément-Chomienne O (2000). Characterization of mibefradil block of the human heart delayed rectifier hKv1.5. *J Pharmacol Exp Ther* **295,** 771–778.

Petkov GV, Bonev AD, Heppner TJ, Brenner R, Aldrich RW & Nelson MT (2001). β1-Subunit of the Ca2+-activated K+ channel regulates contractile activity of mouse urinary bladder smooth muscle. *The Journal of Physiology* **537,** 443–452.

Petrik D, Wang B & Brenner R (2011). Modulation by the BK accessory β4 subunit of phosphorylation-dependent changes in excitability of dentate gyrus granule neurons. *Eur J Neurosci*; DOI: 10.1111/j.1460-9568.2011.07799.x.

Posson DJ, Ge P, Miller C, Bezanilla F & Selvin PR (2005). Small vertical movement of a K+ channel voltage sensor measured with luminescence energy transfer. *Nature* **436,** 848–851.

Quirk JC & Reinhart PH (2001). Identification of a novel tetramerization domain in large conductance K(ca) channels. *Neuron* **32,** 13–23.

Raffaelli G, Saviane C, Mohajerani MH, Pedarzani P & Cherubini E (2004). BK potassium channels control transmitter release at CA3-CA3 synapses in the rat hippocampus. *J Physiol (Lond)* **557,** 147–157.

Rozen S. & Skaletsky HJ (2000). Primer3 on the WWW for general users and for biologist programmers. In *Bioinformatics Methods and Protocols: Methods in Molecular Biology.*, pp. 365–386. Humana Press, Totowa, NJ,.

Ruffin VA, Gu XQ, Zhou D, Douglas RM, Sun X, Trouth CO & Haddad GG (2008). The sodium-activated potassium channel Slack is modulated by hypercapnia and acidosis. *Neuroscience* **151,** 410–418.

Sambrook J & Russell D (2000). *Molecular Cloning: A Laboratory Manual*, 3rd edn. Cold Spring Harbor Laboratory Press,U.S.

Sănchez-Chapula JA, Ferrer T, Navarro-Polanco RA & Sanguinetti MC (2003). Voltage-dependent profile of human ether-a-go-go-related gene channel block is influenced by a single residue in the S6 transmembrane domain. *Mol Pharmacol* **63,** 1051–1058.

Sánchez-Chapula JA, Navarro-Polanco RA, Culberson C, Chen J & Sanguinetti MC (2002). Molecular Determinants of Voltage-dependent Human Ether-a-Go-Go Related Gene (HERG) K+ Channel Block. *Journal of Biological Chemistry* **277,** 23587–23595.

Santi CM, Butler A, Kuhn J, Wei A & Salkoff L (2009). Bovine and Mouse SLO3 K+ Channels. *Journal of Biological Chemistry* **284,** 21589–21598.

Santi CM, Ferreira G, Yang B, Gazula V-R, Butler A, Wei A, Kaczmarek LK & Salkoff L (2006). Opposite regulation of Slick and Slack K+ channels by neuromodulators. *J Neurosci* **26,** 5059–5068.

Santi CM, Martínez-López P, de la Vega-Beltrán JL, Butler A, Alisio A, Darszon A & Salkoff L (2010). The SLO3 sperm-specific potassium channel plays a vital role in male fertility. *FEBS Lett* **584,** 1041–1046.

Sausbier M *et al.* (2005). Elevated blood pressure linked to primary hyperaldosteronism and impaired vasodilation in BK channel-deficient mice. *Circulation* **112,** 60–68.

Sausbier U, Sausbier M, Sailer CA, Arntz C, Knaus H-G, Neuhuber W & Ruth P (2006). Ca2+ -activated K+ channels of the BK-type in the mouse brain. *Histochem Cell Biol* **125,** 725–741.

Schreiber M, Wei A, Yuan A, Gaut J, Saito M & Salkoff L (1998). Slo3, a novel pH-sensitive K+ channel from mammalian spermatocytes. *J Biol Chem* **273,** 3509–3516.

Seino S (2003). Physiology and pathophysiology of KATP channels in the pancreas and cardiovascular system: A review. *Journal of Diabetes and its Complications* **17,** 2–5.

Shen KZ, Lagrutta A, Davies NW, Standen NB, Adelman JP & North RA (1994). Tetraethylammonium block of Slowpoke calcium-activated potassium channels expressed in Xenopus oocytes: evidence for tetrameric channel formation. *Pflugers Arch* **426,** 440–445.

Sprossmann F, Pankert P, Sausbier U, Wirth A, Zhou X-B, Madlung J, Zhao H, Bucurenciu I, Jakob A, Lamkemeyer T, Neuhuber W, Offermanns S, Shipston MJ, Korth M, Nordheim A, Ruth P & Sausbier M (2009). Inducible knockout mutagenesis reveals compensatory mechanisms elicited by constitutive BK channel deficiency in overactive murine bladder. *FEBS J* **276,** 1680–1697.

Steidl JV & Yool AJ (2001). Distinct mechanisms of block of Kv1.5 channels by tertiary and quaternary amine clofilium compounds. *Biophys J* **81,** 2606–2613.

Steinberg MI & Molloy BB (1979). Clofilum--a new antifibrillatory agent that selectively increases cellular refractoriness. *Life Sci* **25,** 1397–1406.

Student (1908). THE PROBABLE ERROR OF A MEAN. *Biometrika* **6,** 1–25.

Suarez SS (2008). Control of hyperactivation in sperm. *Hum Reprod Update* **14,** 647–657.

Tamsett TJ, Picchione KE & Bhattacharjee A (2009). NAD+ activates KNa channels in dorsal root ganglion neurons. *J Neurosci* **29,** 5127–5134.

Tang Q-Y, Zhang Z, Xia J, Ren D & Logothetis DE (2010*a*). Phosphatidylinositol 4,5-bisphosphate activates Slo3 currents and its hydrolysis underlies the epidermal growth factor-induced current inhibition. *J Biol Chem* **285,** 19259–19266.

Tang Q-Y, Zhang Z, Xia X-M & Lingle CJ (2010*b*). Block of mouse Slo1 and Slo3 K(+) channels by CTX, IbTX, TEA, 4-AP and quinidine. *Channels (Austin)*. Available at: http://www.ncbi.nlm.nih.gov/pubmed/19934650.

Tao X, Lee A, Limapichat W, Dougherty DA & MacKinnon R (2010). A gating charge transfer center in voltage sensors. *Science* **328,** 67–73.

Tseng-Crank J, Foster CD, Krause JD, Mertz R, Godinot N, DiChiara TJ & Reinhart PH (1994). Cloning, expression, and distribution of functionally distinct Ca(2+)-activated K+ channel isoforms from human brain. *Neuron* **13,** 1315–1330.

Uchino S, Wada H, Honda S, Hirasawa T, Yanai S, Nakamura Y, Ondo Y & Kohsaka S (2003). Slo2 sodium-activated K+ channels bind to the PDZ domain of PSD-95. *Biochem Biophys Res Commun* **310,** 1140–1147.

Uebele VN, Lagrutta A, Wade T, Figueroa DJ, Liu Y, McKenna E, Austin CP, Bennett PB & Swanson R (2000). Cloning and functional expression of two families of beta-subunits of the large conductance calcium-activated K+ channel. *J Biol Chem* **275,** 23211–23218.

Visconti PE, Westbrook VA, Chertihin O, Demarco I, Sleight S & Diekman AB (2002). Novel signaling pathways involved in sperm acquisition of fertilizing capacity. *J Reprod Immunol* **53,** 133–150.

Wallén P, Robertson B, Cangiano L, Löw P, Bhattacharjee A, Kaczmarek LK & Grillner S (2007). Sodium-dependent potassium channels of a Slack-like subtype contribute to the slow afterhyperpolarization in lamprey spinal neurons. *J Physiol (Lond)* **585,** 75–90.

Wallner M, Meera P & Toro L (1999). Molecular basis of fast inactivation in voltage and Ca2+-activated K+ channels: a transmembrane beta-subunit homolog. *Proc Natl Acad Sci USA* **96,** 4137–4142.

Weiger TM, Holmqvist MH, Levitan IB, Clark FT, Sprague S, Huang WJ, Ge P, Wang C, Lawson D, Jurman ME, Glucksmann MA, Silos-Santiago I, DiStefano PS & Curtis R (2000). A novel nervous system beta subunit that downregulates human large conductance calcium-dependent potassium channels. *J Neurosci* **20,** 3563–3570.

Werman R & Grundfest H (1961). Graded and all-or-none electrogenesis in arthropod muscle. II. The effects of alkali-earth and onium ions on lobster muscle fibers. *J Gen Physiol* **44,** 997–1027.

Werman R, McCann FV & Grundfest H (1961). Graded and all-or-none electrogenesis in arthropod muscle. I. The effects of alkali-earth cations on the neuromuscular system of Romalea microptera. *J Gen Physiol* **44,** 979–995.

Williams SE, Brazier SP, Baban N, Telezhkin V, Müller CT, Riccardi D & Kemp PJ (2008). A structural motif in the C-terminal tail of slo1 confers carbon monoxide sensitivity to human BK(Ca) channels. *Pflugers Arch* **456,** 561–572.

Woodhull AM (1973). Ionic Blockage of Sodium Channels in Nerve. *J Gen Physiol* **61,** 687–708.

Wu RS, Chudasama N, Zakharov SI, Doshi D, Motoike H, Liu G, Yao Y, Niu X, Deng S-X, Landry DW, Karlin A & Marx SO (2009). Location of the beta 4 transmembrane helices in the BK potassium channel. *J Neurosci* **29,** 8321–8328.

Wu Y, Yang Y, Ye S & Jiang Y (2010). Structure of the gating ring from the human large-conductance Ca2+-gated K+ channel. *Nature* **466,** 393–397.

Xia J & Ren D (2009). The BSA-induced Ca2+ influx during sperm capacitation is CATSPER channel-dependent. *Reprod Biol Endocrinol* **7,** 119.

Xia XM, Ding JP & Lingle CJ (1999). Molecular basis for the inactivation of Ca2+- and voltage-dependent BK channels in adrenal chromaffin cells and rat insulinoma tumor cells. *J Neurosci* **19,** 5255–5264.

Xia X-M, Zhang X & Lingle CJ (2004). Ligand-dependent activation of Slo family channels is defined by interchangeable cytosolic domains. *J Neurosci* **24,** 5585–5591.

Yang B, Desai R & Kaczmarek LK (2007). Slack and Slick K(Na) channels regulate the accuracy of timing of auditory neurons. *J Neurosci* **27,** 2617–2627.

Yang B, Gribkoff VK, Pan J, Damagnez V, Dworetzky SI, Boissard CG, Bhattacharjee A, Yan Y, Sigworth FJ & Kaczmarek LK (2006). Pharmacological activation and inhibition of Slack (Slo2.2) channels. *Neuropharmacology* **51,** 896–906.

Yang C-T, Zeng X-H, Xia X-M & Lingle CJ (2009). Interactions between β Subunits of the KCNMB Family and Slo3: β4 Selectively Modulates Slo3 Expression and Function. *PLoS ONE* **4,** e6135.

Yeung CH & Cooper TG (2001). Effects of the ion-channel blocker quinine on human sperm volume, kinematics and mucus penetration, and the involvement of potassium channels. *Mol Hum Reprod* **7,** 819–828.

Yoo HY, Zheng H, Nam JH, Nguyen YH, Kang TM, Earm YE & Kim SJ (2008). Facilitation of Ca2+-activated K+ channels (IKCa1) by mibefradil in B lymphocytes. *Pflugers Arch* **456,** 549–560.

Yuan P, Leonetti MD, Pico AR, Hsiung Y & MacKinnon R (2010). Structure of the Human BK Channel Ca2+-Activation Apparatus at 3.0 Å Resolution. *Science* **329,** 182–186.

Yuan, Dourado M, Butler A, Walton N, Wei A & Salkoff L (2000). SLO-2, a K+ channel with an unusual Cl- dependence. *Nat Neurosci* **3,** 771–779.

Yuan, Santi CM, Wei A, Wang ZW, Pollak K, Nonet M, Kaczmarek L, Crowder CM & Salkoff L (2003). The sodium-activated potassium channel is encoded by a member of the Slo gene family. *Neuron* **37,** 765–773.

Yusifov T, Savalli N, Gandhi CS, Ottolia M & Olcese R (2008). The RCK2 domain of the human BKCa channel is a calcium sensor. *Proceedings of the National Academy of Sciences* **105,** 376–381.

Zeng X-H, Yang C, Kim ST, Lingle CJ & Xia X-M (2011). Deletion of the Slo3 gene abolishes alkalization-activated K+ current in mouse spermatozoa. *Proc Natl Acad Sci USA* **108,** 5879–5884.

Zeng Y, Oberdorf JA & Florman HM (1996). pH Regulation in Mouse Sperm: Identification of Na+-, Cl--, and[formula]Dependent and Arylaminobenzoate-Dependent Regulatory Mechanisms and Characterization of Their Roles in Sperm Capacitation. *Developmental Biology* **173,** 510–520.

Zhang H, Zhu B, Yao J-A & Tseng G-N (1998). Differential Effects of S6 Mutations on Binding of Quinidine and 4-Aminopyridine to Rat Isoform of Kv1.4: Common Site but Different Factors in Determining Blockers' Binding Affinity. *Journal of Pharmacology and Experimental Therapeutics* **287,** 332–343.

Zhang L, Sukhareva M, Barker JL, Maric D, Hao Y, Chang YH, Ma W, O'Shaughnessy T & Rubinow DR (2005). Direct binding of estradiol enhances Slack (sequence like a calcium-activated potassium channel) channels' activity. *Neuroscience* **131,** 275–282.

Zhang X, Zeng X & Lingle CJ (2006*a*). Slo3 K+ Channels: Voltage and pH Dependence of Macroscopic Currents. *J Gen Physiol* **128,** 317–336.

Zhang X, Zeng X, Xia X-M & Lingle CJ (2006*b*). pH-regulated Slo3 K+ channels: properties of unitary currents. *J Gen Physiol* **128,** 301–315.

Zhang Z, Rosenhouse-Dantsker A, Tang Q-Y, Noskov S & Logothetis DE (2010). The RCK2 domain uses a coordination site present in Kir channels to confer sodium sensitivity to Slo2.2 channels. *J Neurosci* **30,** 7554–7562.

Zhou Y, Morais-Cabral JH, Kaufman A & MacKinnon R (2001). Chemistry of ion coordination and hydration revealed by a K+ channel-Fab complex at 2.0 A resolution. *Nature* **414,** 43–48.